UNIVERSITY OF SOUTHAMPTON

FACULTY OF MEDICINE

Cancer Sciences Unit

Metabolism and Motility of Head and Neck Cancer: Characterisation, Prognostication and Novel Target Identification

By

Jason Fleming

MBBS BSc MRCS DOHNS MEd

Thesis for the degree of Doctor of Philosophy

September 2016

UNIVERSITY OF SOUTHAMPTON
ABSTRACT
FACULTY OF MEDICINE, CANCER SCIENCES UNIT
Thesis for the degree of Doctor of Philosophy

METABOLISM AND MOTILITY OF HEAD AND NECK CANCER: CHARACTERISATION, PROGNOSTICATION AND NOVEL TARGET IDENTIFICATION

By Jason Fleming

Head and neck cancer (HNSCC) worldwide affects over 500,000 new people each year and overall mortality has remained at 50% despite promising new treatments. Although FDG-PET imaging is in widespread clinical practice, the unique metabolic features of this disease and its subtypes remain poorly understood. We have previously identified C-terminal tensin-like (CTEN; *TNS4*), a member of the TENSIN gene family that encodes focal adhesion adaptor proteins, as being a likely target gene of a cell's metabolic sensors (CtBPs). CTEN is also emerging as a prognostic marker in many cancer types but its mechanism of action and clinical relevance in HNSCC was unknown.

Clinical relevance was examined through tissue microarray immunohistochemistry analysis of 260 consecutively treated oropharyngeal cancer patients, demonstrating CTEN expression to have a significant inverse correlation with disease-specific survival, as well as a determinant of chemoradiotherapy resistance. RNA sequencing analysis and *in vivo* results helped direct *in vitro* functional assays, utilising gene knockdown methods, resulting in discovery of a novel CTEN function promoting cell survival in HNSCC cell lines, potentially through a TGFβ-dependent pathway.

Linking tumour cell metabolism, we proposed a novel mechanism whereby increasing glycolytic stimuli could regulate CTEN expression via a CtBP2 dependent pathway. We revealed a binding site for the CtBPs on the CTEN promoter via chromatin immunoprecipitation analyses. Given the clinical relevance of the human papilloma virus (HPV) in clinical practice, we proceeded to classify the metabolic profiles of both HPV-positive and HPV-negative HNSCC and identified one potential metabolic target, the monocarboxylic acid transporter 1 (MCT1). Metabolic profiling confirmed HPV-negative HNSCC as an ideal candidate disease for targeting with a novel MCT1-inhibitor and *in vitro* treatment resulted in potentially beneficial effects on both metabolic activity and radiosensitivity of cells. We therefore highlighted the potential therapeutic benefits of metabolic agents in novel combination therapy strategies.

Table of Contents

List of Tables

List of Figures

DECLARATION OF AUTHORSHIP

I, JASON CHARLES FLEMING

declare that this thesis and the work presented in it are my own and has been generated by me as the result of my own original research.

Metabolism and Motility of Head and Neck Cancer: Characterisation, Prognostication and Novel Target Identification

I confirm that:

1. This work was done wholly or mainly while in candidature for a research degree at this University;
2. Where any part of this thesis has previously been submitted for a degree or any other qualification at this University or any other institution, this has been clearly stated;
3. Where I have consulted the published work of others, this is always clearly attributed;
4. Where I have quoted from the work of others, the source is always given. With the exception of such quotations, this thesis is entirely my own work;
5. I have acknowledged all main sources of help;
6. Where the thesis is based on work done by myself jointly with others, I have made clear exactly what was done by others and what I have contributed myself;
7. None of this work has been published before submission

Signed:

Date: 6th October 2016

Acknowledgements

Firstly I would like to thank my supervisors – Professor Gareth Thomas, Dr. Jeremy Blaydes and Mr. Dae Kim for their input in this project, both from before I made the decision to embark on this work, up to the submission of my thesis and beyond. Their initial enthusiasm stimulated my leap into the unknown and their knowledge, enthusiasm and experience played a huge role in my achievements to date.

None of this work would have been possible without funding and I would like to thank a number of institutions and individuals for making my project financially possible: Mr. Harries, Mr. Watts and the ENT Department at Royal Sussex County Hospital, the research team led by Professor Chauhan and the ENT Department at Queen Alexandra Hospital, The Halley Stewart Trust, the Royal College of Surgeons (England) and the generous Fellowship support from the Medical Research Council (MRC). Not only did the MRC fund my research at home, but also their additional support enabled me to visit MD Anderson, Texas. Consequently, I would like to thank in particular Professor Myers and his whole team for welcoming me into their group, giving me valuable feedback on my work, and introducing me to new techniques that I have been able to directly incorporate into my work. Dr. Sassan Hafizi at the University of Portsmouth has also given me vital input at important moments over the past few years and I am grateful to him for sharing his wealth of knowledge on Tensin biology.

There are too many people within the laboratory to thank personally as so many colleagues both inside and outside of the Experimental Pathology Group enriched my experience! However my utmost thanks to Veronika Jenei – you are a first rate (and very patient!) teacher and colleague and you gave me all the science fundamentals to follow my interests; Abbie Mead, Jo Tod, Hollie Robinson, Steve Frampton, Chris Hanley, Max Mellone, Kate Packwood, Caroline Barker, Charlie Birts, Matt Darley, Monette Lopez and last but by no means least, Karwan Moutasim – from classic Tuesday afternoon help, through to a friendly ear, Banterbury discussions or just supplying a cup of coffee at that perfect moment, thank you all for making PhD life so enjoyable.

Finally thank you to Mum, Dad and my fiancé Theresa for their unwavering support and helping me navigate the bad times, and celebrate the good!

Definitions and Abbreviations

3D	three-dimensional
2D	two-dimensional
ATP	adenosine triphosphate
BSA	bovine serum albumin
CO2	carbon dioxide
CTEN	tensin-4
Ctrl	control
DAPI	4’,6-diamidino-2-phenylindole
DMEM	Dulbecco’s Modified Eagle’s medium
DMSO	dimethyl sulphoxide
DNA	deoxyribonucleic acid
ECM	extracellular matrix
EGF	epidermal growth factor
EMT	epithelial-mesenchymal transition
FA	focal adhesion
FACS	fluorescent activated cell sorting
FAK	focal adhesion kinase
FBS	fetal bovine serum
GAP	GTPase activating protein
GEF	guanine exchange factor
HFFF2	human fetal foreskin fibroblasts
HIF-1α	hypoxia inducible factor 1 alpha
HNSCC	head and neck squamous cell carcinoma
KGM	keratinocyte growth medium
LAP	latency associated peptide of TGF-β
LLC	large latent complex
LTBP	latent TGF-β binding protein
Mins	minutes
MLEC	mink lung epithelial cells
MMP	matric metalloproteinases
mRNA	messenger ribonucleic acid

OSCC	oral squamous cell carcinoma
OPSCC	oropharyngeal squamous cell carcinoma
PBS	phosphate buffered saline
PCR	polymerase chain reaction
PET	positron emission tomography
PI3K	phosphoinositol 3 kinase
PIP2	phosphatidylinositol 4,5-bisphosphonate
PIP3	phosphatidylinositol 3,4,5-triphosphate
PTB	phosphotyrosine binding domain
PVDF	polyvinylidene fluoride
ROCK	rho-associated protein kinase
RNA	ribonucleic acid
RPMI	Roswell park memorial institute
SH2	SRC homology 2
siRNA	small interfering ribonucleic acid
SLC	small latent complex
SMA	smooth muscle actin
Tiam1	T-cell lymphoma invasion and metastasis 1
TGF-β	transforming growth factor beta
TMA	tissue microarray
TNS3	tensin-3
VEGF	vascular endothelial growth factor

Chapter 1: INTRODUCTION

1.1 Head and neck cancer

1.1.1 Introduction

Head and neck cancer is a collective name for a biologically similar group of cancers that originate from the nasal cavity and paranasal sinuses, oral cavity, pharynx and larynx. Over 90% of these derive from epithelial cells of mucosal linings and are termed head and neck squamous cell carcinomas (HNSCC). With over 500,000 new diagnoses each year and a mortality over 50% (Loyo et al., 2013), the disease burden is significant. In the UK, 2012 saw almost 9700 new cases accounting for 4% of the national cancer incidence (excluding skin) (Ferlay et al, 2012). Furthermore, survival rates have remained relatively unchanged over the past 3 decades yet the incidence continues to rise. From 1990-2006, oropharyngeal cancer incidence in the UK has risen by over 200%, oral by 30%, salivary by 37% and palatal by 66% (Price et al., 2010). The reasons for this trend are multifactorial. Although tobacco smoking and alcohol consumption remain the most important independent risk factors (Roland and Paleri, 2008), numerous other risk factors have now been proposed to explain international and regional changes of incidence. Indeed tobacco-related cancers are in fact decreasing in incidence (Leemans et al., 2011). For example immigration from the Indian subcontinent with the habit of betel chewing may contribute to the UK rise in oral cancer, and the rise of human papilloma virus-induced tumours in younger populations accounts for the increasing oropharyngeal cancer incidence (Cadoni et al., 2012).

Despite the heightened awareness of early symptoms, multimodal treatment and the reporting of new prognostic histological features, the 5-year survival rates for this disease have remained relatively static for the past three decades at around 50%, albeit with significant variability across tumour locations (Loyo et al., 2013). Surgery and radiotherapy, with or without concomitant chemotherapy, are the mainstays of treatment in HNSCC (Roland and Paleri, 2012). However both of these modalities can result in significant morbidity with aesthetic and/or functional deformities, especially concerning speech and swallowing. Treatment failure and locoregional recurrence occur in upto 30% of patients and account for the majority of disease-related mortality (Leemans et al., 1994).

1.1.2 Genetic alterations in HNSCC

Although HNSCC is genetically heterogeneous, a number of pathways are commonly implicated. In the epithelium of the head and neck mucosal surfaces, the primary genetic alterations are usually secondary to the carcinogenic effects of tobacco and alcohol, although in the oropharynx oncogenic subtypes of the human papilloma virus (HPV) are now a major aetiological factor (Curry et al., 2014); this disease has a distinct oncogenic mechanism and phenotype and will be considered separately.

The most commonly identified mutation in HPV-negative HNSCC is in the tumour suppressor gene *TP53*, which is present in around 50% of cases and has a 1-5 fold negative impact on survival (Loyo et al., 2013). *TP53* has a key role in causing cell cycle arrest in order to repair DNA damage, and ushering the cell into apoptotic or senescent pathways if said damage is irreparable. This function is exerted through the induction of the cell cycle regulator p21. *TP53* mutations have also been linked to altered tumour metabolism, increasing the aerobic glycolytic capacity through activation of a wide range of enzymes and glucose transporters (Cairns et al., 2011). Despite the prevalence of mutations and their important oncogenic effects, studies looking at the *TP53* biomarker potential have not yet reached sufficient sensitivity or specificity for widespread clinical use (Loyo et al., 2013).

The second most commonly mutated gene in HNSCC is *NOTCH1*, a gene with cancer-type dependent effects but in this disease, a tumour suppressor with a mutation incidence of approximately 15% (Tan et al., 2013). In this context the majority of mutations appear to affect the EGF-like ligand-binding domain or the Notch1 intracellular domain (NICD), suggesting loss of function (Loyo et al., 2013). Dual oncogenic and tumour suppressor function in different tumours means targeting thus far has been ineffective, even hazardous.

Although mutations in the *Ras family: HRAS* (Harvey)*, KRAS* (Kirsten) *and NRAS* (neuroblastoma) are implicated in over a third of human tumours, there was ongoing debate about their prevalence in HNSCC (Barbacid, 1987). However novel techniques such as deep sequencing have shown than in a U.S. cohort, *HRAS* mutations are one of the most common HNSCC mutations (Frederick et al., 2013). Mutations in these small GTPases cause the proteins to be constitutively active in the GTP-bound state, thus resulting in increased proliferation and survival signalling (Matthaios et al., 2011). This

signalling operates through numerous downstream pathways, most notably the Raf/MEK/ERK serine threonine pathway and the phosphatidylinositol 3-kinase (PI3K) pathway. In HNSCC, alterations of these pathways can also occur through mutations further downstream e.g. loss of PTEN resulting in PI3K over-activation (Castellano and Downward, 2011). Indeed there are a multitude of receptor tyrosine kinases that activate PI3K and the epidermal growth factor receptor (EGFR) is one such membrane bound receptor that is overexpressed in upto 90% cases, although mutations are only present in about 10% of cases (Curry et al., 2014). EGFR binding triggers a cascade of signals that activate many oncogenic effects including survival, proliferation and invasion (Kim et al., 2008; Sheu et al., 2009). It also stimulates angiogenesis by increasing interleukin 8 (IL-8) and vascular endothelial growth factor (VEGF) production (Kalyankrishna and Grandis, 2006; Koontongkaew, 2013). Overexpression of EGFR has frequently been shown to independently correlate with tumour stage, reduced radiation sensitivity and increased risk of recurrence (Numico et al., 2010; Rabinowits and Haddad, 2012; Song et al., 2004).

The product of the tumour suppressor gene cyclin-dependent kinase inhibitor 2A (*CDKN2A*), p16, regulates cell cycle progression through its interaction with Retinoblastoma (Rb) protein and is typically upregulated in hypoxia and other stress conditions (Horiguchi et al., 2012). It is often disrupted in HNSCC patients and overexpression, such as that occurring in virally induced tumours, correlates with improved prognosis (Bova and McGuinness, 2007; Bova et al., 1999; Koontongkaew, 2013). Rb binding to and inhibition of the senescence-promoting transcription factor E2F is reversed by the cyclin-dependent kinase-4 and -6 (CDK4 and CDK6) which phosphorylate Rb, allowing cell cycle progression (Morgan, 1995; Serrano et al., 1993; Sherr, 1994). P16 however inhibits these CDKs, allowing the Rb-E2F complex to stabilise and halt cell cycle progression. This is of particular relevance in human papillomavirus-positive HNSCC.

1.1.3 Human papilloma virus (HPV)

HPV has come to prominence as an independent risk factor for HNSCC in light of the reducing prevalence of tobacco smoking in Western countries. Indeed HPV is now a direct aetiological factor in upto 25% of HNSCC, most commonly in oropharyngeal squamous cell carcinoma (OPSCC) (Krupar et al., 2014). Tonsil tumours in particular have an HPV prevalence of 51 to 93% (Hammarstedt et al., 2006; Näsman et al., 2009; Rotnáglová et

al., 2011). The risk of infection is directly correlated with the number of lifetime orogenital contacts, although tobacco and alcohol exposure tend to be lower (Krupar et al., 2014). The patient demographic is also different with patients being on average 5 years younger than the typical HNSCC patient (Loyo et al., 2013). The high-risk subtype is HPV-16, whereas HPV-6 and-11 are low risk and normally associated with warts and laryngeal papillomatosis (Dickens et al., 1991). Two HPV vaccines, namely the bivalent Cervarix (serotypes 16 and 18; GlaxoSmithKline Biologicals) and quadrivalent Gardasil (serotypes 6, 11, 16, 18; Merck & Co. Inc.) were approved in 2009 and 2006 respectively. Given the young vaccine population and disease presentation predominantly in patients over 40, there will be a significant lag time before the effect on virally-induced HNSCC can be assessed.

The mechanism behind HPV-carcinogenesis centres on the transforming oncoproteins E6 and E7, which are produced in actively dividing cells. These proteins inactivate cellular p53 and Rb tumour suppressor proteins respectively (Loyo et al., 2013), resulting in loss of tumour suppressor function and disruption of cell cycle control (Krupar et al., 2014). HPV-positive disease is often distinguished from negative disease by the presence of p16, a regulator of Rb which, as already discussed, inhibits CDKs 4 and 6, allowing activation of the Rb pathway (Morgan, 1995; Serrano et al., 1993; Sherr, 1994). There is an increased incidence of lymph node metastases and advanced stage at presentation for HPV-positive disease but despite this, these patients have repeatedly been shown to have improved disease-free and overall survival (Fakhry et al., 2008; O'Rorke et al., 2012; Syrjänen, 2010). This is at least in part due to the improved disease response to radio- and chemotherapy (Krupar et al., 2014). There are however an 'intermediate' risk group of patients within the HPV-positive group, often associated with smoking history, and identifying patients in this group is of paramount importance (Ang et al., 2010).

1.1.4 Tumour microenvironment in HNSCC

The high rate of treatment failure and local recurrence in HNSCC has brought about the concept of 'field change' or 'condemned mucosa' (Slaughter et al. 1953), describing the irreversible changes of epithelial, stromal and immune cells surrounding a tumour which facilitates tumour growth and invasion, or new tumour foci development. This milieu, together with the surrounding matrix, describes the tumour microenvironment and

incorporates the model of a tumour representing a complex interplay between cancer cells and these surrounding supportive cells (Fig. 1-1).

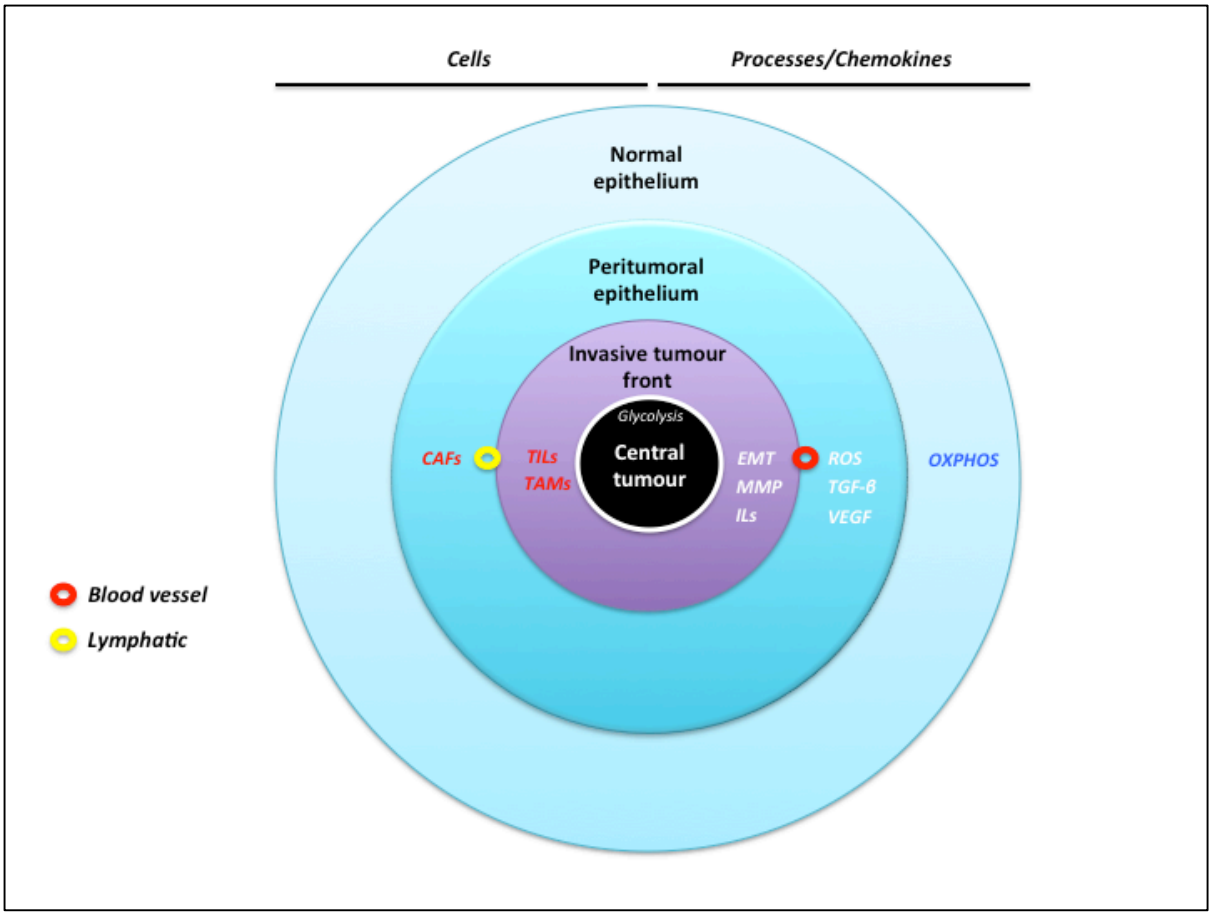

Figure 1-1. Simplified schematic representation of tumour microenvironment. Important example processes and chemokines involved in tumour progression are displayed on right of diagram and involved stromal cells on left. CAFs: cancer-associated fibroblasts, TILs: tumour infiltrating lymphocytes; TAMs: tumour associated macrophages; EMT: epithelial-mesenchymal transition; MMP: matrix metalloproteinases; ILs: interleukins; ROS: reactive oxygen species; TGF-β: transforming growth factor β; VEGF: vascular endothelial growth factor; OXPHOS: oxidative phosphorylation.

We have therefore moved away from the tumour being considered as a distinct clinical entity to its surroundings, to a model where the tumour microenvironment is considered as a vital, integrated component of the cancer. As alluded to in Fig. 1-1, the microenvironment contains a number of different cell types including myofibroblasts (or cancer-associated fibroblasts, CAFs) and their fibroblast precursors, smooth muscle cells, endothelial cells, pericytes and a range of immunological cells including neutrophils, basophils, eosinophils, mast cells, T- and B-lymphocytes, natural killer cells and antigen presenting cells (APCs) (Koontongkaew, 2013). Numerous studies have demonstrated important roles in promoting tumour progression for these associated cells, although

most notably for CAFs and endothelial cells. More recently evidence is growing about the role of a competent immune response on determining the prognosis of cancer with a variety of reports finding dysfunctional circulating and tumour infiltrating lymphocytes in HNSCC patients – potentially through defective T cell activation and/or function. A reduction in function or number of CD8+ effector T cells may thus be a target for tumours to exploit to evade host immunity (Pretscher et al., 2009). This ability to potentially alter the host immune response may have important implications in our attempts to categorise the differences in phenotype of HPV-positive disease. The presence of the oncogenic proteins E6 and E7 in virally-induced HNSCC prompts an increased host immune response and several studies report an increased number of tumour infiltrating lymphocytes (TILs) in HPV-positive disease (Kong et al., 2009; Näsman et al., 2012; Russell et al., 2013). More recently work from our group has demonstrated that TIL levels in the primary tumour correlate with improved survival within an HPV-positive disease cohort (Ward et al., 2014).

The mechanism behind this immunosuppressive effect is unclear. There are multiple pathways involved in regulating immune response although interestingly, tumour metabolism has been identified as a key player (Gottfried et al., 2012). For example, lactic acid derived from glycolysis in tumours has been shown to suppress CD8+ T cells and natural killer cell proliferation (Fischer et al., 2007; Mendler et al., 2012). Indeed proliferating lymphocytes exhibit a preference for aerobic glycolysis much akin to tumours and in a tumour's vicinity they are therefore in a competitive environment with the cancer cells for a glucose influx and lactate efflux (Fox et al., 2005). Krupar el al (2014) demonstrated that the distribution of the GLUT1 transporter in HPV-positive and – negative HNSCC correlated with CD8+ TIL patterns, adding further evidence to the relationship between immune response and metabolism.

Fibroblasts are the most abundant cells in the tumour microenvironment, responsible for secretion of a variety of structural proteins and cytokines. CAFs may differentiate from fibroblasts, or from circulating mesenchymal stem cells recruited to the tumour microenvironment (Xouri and Christian, 2010). They do in fact share many characteristics with activated myofibroblasts (Schäfer and Werner, 2008) and are therefore fixed in an 'active' state, playing a role in tumour progression, invasion and metastasis (Pavlides et al., 2009). They, like myofibroblasts, are defined by the accumulation of α-smooth muscle actin (α-SMA) (Kawashiri et al., 2009; Tomasek et al.,

2002) and in HNSCC are associated with dense collagen deposition and a desmoplastic stroma, which provides a permissive environment for tumour growth (Chen et al., 2001; Kunz-Schughart and Knuechel, 2002). As well as this influence on stromal composition, CAFs have been demonstrated to produce a range of cytokines important in promoting tumour cell motility including hepatocyte growth factor (HGF), CXCL12 and, notably, TGF-β - a pleiotropic cytokine that correlates with increased tumour invasion through the process of epithelial to mesenchymal transition (Leef and Thomas, 2013; Moustakas and Heldin, 2012). Indeed Gaggioli et al (2007) described evidence suggesting that CAFs enable remodelling of the extracellular matrix to lay pathways along which HNSCC tumour cells can follow to invade. This may be through their ability to secrete matrix metalloproteinases (De Wever et al., 2008; Orimo et al., 2005).

CAFs also have a potentially important role in tumour metabolism. Aerobic glycolysis is a particular metabolic feature of tumour cells, proliferating lymphocytes and myofibroblasts, with resulting production of lactate (Pavlides et al., 2009). An interdependent relationship has therefore been proposed whereby cancer cells may induce glycolysis in surrounding stromal cells such as CAFs/myofibroblasts (Vincent et al., 2008). The resulting pyruvate/lactate produced could then be used as a high-energy metabolite by the tumour cells via oxidative phosphorylation pathways. Curry et al (2013) recently published evidence that this may be occurring in HNSCC. The process of aerobic glycolysis and this inverse cancer-stromal metabolic hypothesis are known as the 'Warburg effect' and 'Reverse Warburg effect' respectively and will be discussed further in Chapter 1.2.

1.1.5 TGF-β signalling

TGF-β is a pro-inflammatory pleiotropic cytokine that is involved in a wide variety of biological functions. The cytokine has three known isoforms (TGF-β1, -β2, and -β3) (Patil et al., 2011) with significant redundancy and their action is mediated through two receptors (type I and type II) (Massagué and Gomis, 2006). The functions of TGF-β are diverse, with important roles in key cell processes such as proliferation, differentiation and extracellular matrix (ECM) production (Kaminska et al., 2005) and the TGF-β paradox is a reference to its ability to inhibit cell cycle progression in benign or early malignant cells but switch to a promoter role in tumour progression and metastasis in established cancer cells (Principe et al., 2014). This may be mediated either through reduced or

altered sensitivity to TGF-β signalling, or an increased production/activation effect (Wakefield and Roberts, 2002). Whilst deregulation of TGF- β expression or signalling has been implicated in a variety of diseases (Kaminska et al., 2005), only its role in cancer will be discussed here (Fig. 1-2).

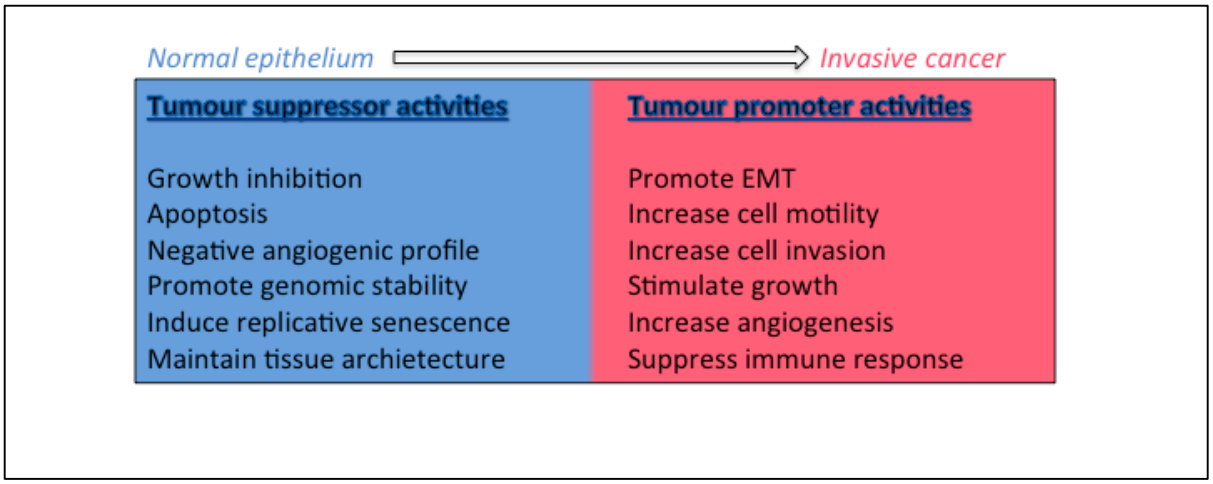

Figure 1-2. The TGF-β paradox. The multiple functions of the cytokine TGF-β illustrate both tumour suppressor and promoter activities. The switch in these functions, allowing a permissive environment for tumour invasion is poorly understood. Figure adapted from Wakefield et al (2002)

To understand the function of TGF-β *in vivo* we need to understand its mechanism of activation, as the mature form of the cytokine, bound to its propeptide the latency-associated peptide (LAP), is inactive (Gleizes et al., 1997). This complex, known as the small latent complex (SLC), usually combines with associated latent TGF-β binding proteins (LTBPs) to form the large latent complex (LLC) (Gleizes et al., 1997) which, via covalent cross-links to matrix proteins, can be incorporated into the ECM (Taipale et al., 1996). These bound complexes can therefore provide a pool of inactive TGF-β.

The mechanisms of release and therefore activation of the TGF-β molecule are multiple and varied, although a significant number of the more recognised activators are linked functionally to the ECM (Munger and Sheppard, 2011). Integrins, heterodimeric cell surface adhesion and signalling molecules are important such activators and will be discussed further in Chapter 1.4. LAP in the tumour stroma may therefore modulate tumour behaviour through its interaction with integrins expressed by tumour cells (Thomas et al., 2002). Upon activation of TGF-β, high affinity binding initially to TGF-βRII occurs, which then results in phosphorylation of TGF-βRI to form an activated TGF-β receptor complex. The activated TGF-β receptor (TGF-β R1/R2) phosphorylates and

activates the Smad2 and Smad3 proteins, which then bind to Smad4 before migrating to the nucleus to regulate transcription (Blobe et al., 2000). Non-canonical pathways include m-TOR, RhoA, Ras, MAPK, PI3K/AKT, PP2A/p70s6K, and JNK (Mu et al., 2012).
TGF-β1 signalling, via Smad recruitment and phosphorylation, has been shown to be a potent mediator of epithelial-mesenchymal transition (EMT) (Valcourt et al., 2005; Zavadil and Böttinger, 2005).

EMT is a process of cellular developmental transition from a polarised epithelial phenotype to a highly motile mesenchymal phenotype (Yu et al., 2011). It has been cited as a key process in embryogenesis, fibrosis as well as tumourigenesis (Huber et al., 2005; Thiery et al., 2009), where it may instigate the onset of cancer cell migration and invasion (Grünert et al., 2003; Thiery, 2002). The loss of E-cadherin is considered a crucial step in EMT and is regulated by various transcription factors including Snail (Batlle et al., 2000), Twist (Mani et al., 2008) and ZEB1 (Batlle et al., 2012; Sánchez-Tilló et al., 2011, 2010). A wide variety of growth factors, signalling pathways and microenvironment conditions such as hypoxia have been shown to induce EMT (Thiery et al., 2009). This cellular reprogramming results in a reorganisation of cell-cell junctions and adhesion sites, fundamentally affecting the cell's physical behaviour and priming it for detachment from an organised epithelial layer to ultimately migrate (Thiery et al., 2009). TGF-β1 signalling is therefore fundamental to changes in the interactions between tumour cells and their environment.

1.2 Tumour cell metabolism

Hanahan and Weinberg's (2000) famous six hallmarks of cancer were amended in 2011 to include deregulation of cellular energy metabolism and evasion of immune destruction. However altered tumour metabolism is not a new concept. In the 1920s Otto Warburg, a German physiologist and Nobel laureate, proposed that cancer cells metabolise more glucose to lactate than regular cells (Warburg et al., 1926). However the resurgence of interest in tumour metabolism has been encouraged, not only by the advance in research technologies, but by a number of scientific and clinical observations (Dell' Antone, 2012) including:

1) High sensitivity of ^{18}FDG-PET imaging, showing glucose uptake by tumours, to follow malignant disease progression.
2) Links demonstrated between cell death pathways and bioenergetic mechanisms.
3) Multiple metabolism genes affected by mutations in oncogenes.

Warburg's initial theory of impairment of mitochondrial oxidative phosphorylation as a cause for this effect has been shown to be an incorrect hypothesis (Kroemer and Pouyssegur, 2008), not least by the demonstration that inhibition of glycolysis in tumours allows for the restoration of mitochondrial oxidative phosphorylation (OXPHOS) (Jose et al., 2011; Smolková et al., 2011). However, the importance and reliance of cancer cells on aerobic glycolysis has endured. Often talked about in conjunction with Warburg's observations is the Crabtree effect – the glucose induced inhibition of cell respiration in proliferating tumour cells (Dell' Antone, 2012). Cells require energy in the form of adenosine triphosphate (ATP) molecules, derived from glucose. How this ATP is produced depends on a variety of different pathways but in normal cells, the more efficient respiratory, or OXPHOS pathway is employed, generating more ATP molecules (38) per glucose molecule than glycolysis (4). The tricarboxylic acid (TCA or Kreb's) cycle generates reduced nicotinamide adenine dinucleotide and flavin adenine dinucleotide (NADH and FADH2 respectively) from a pyruvate molecule. These are key electron donors that can transfer eight high-energy electrons to the electron transport chain in mitochondria, allowing the creation of an electrochemical proton gradient that ultimately results in ATP production. Glycolysis however diverts this pyruvate to lactic acid by the enzyme lactate dehydrogenase, generating NAD+ in the process (Kim et al., 2005). The cellular cytosolic NAD+/NADH ratio is a crucial relationship to regulate metabolic homeostasis and cellular redox state. Aberrations are often reflected by both normal physiological and pathological bioprocesses (Bakker et al., 2001; Lin and Guarente, 2003; Ying, 2008). With a free NAD+/NADH ratio of over 600 (Zhang et al., 2002) it is clear that small changes in NADH concentration can dramatically affect this redox state. Thus conditions that upregulate NADH levels by glycolysis will shift the NAD+/NADH balance significantly (Heiden, 2009) and although the conversion of pyruvate to lactate oxidises the reduced NADH, this is at a significantly slower rate than glycolysis.

In certain conditions such as hypoxia, or in specific locations such as brain, liver and muscle, cells can be driven into a glycolytic dominant phenotype (Zheng, 2012). In these situations, pyruvate is reduced to lactate by lactate dehydrogenase (LDH-A) in the

cytoplasm and lactate is then excreted extraceullularly by monocarboxylate transporters (MCTs) (Zheng, 2012). Cancer cells exhibit similar behaviour; they preferentially use glycolysis for energy production, even in the presence of oxygen, a phenomenon known as aerobic glycolysis. At first inspection this preference seems counterintuitive – reliance on a less efficient glucose metabolic pathway. A number of possible explanations have been proposed, attempting to explain this dependence on aerobic glycolysis, including:

1) highly efficient ATP production via OXPHOS would result in negative feedback of the rate-limiting enzyme of glycolysis (phosphofructokinase 1 [PFK1]), as well as pyruvate kinase 1, ultimately resulting in the inhibition of glycolysis (Zheng, 2012).
2) speed of ATP production in glycolysis is faster, which suits the rapid cell proliferation in tumours (Pfeiffer et al., 2001).
3) tumours often exhibit hypoxic foci, and glycolysis result in a selective growth advantage in these areas (Fantin et al., 2006)
4) the product of glycolysis, lactate, when released extracellularly results in acidification of the microenvironment. This has been shown to enhance both the invasion and metastasis of cancer cells (Gatenby and Gillies, 2008; Vaupel, 2010).
5) with reduction in OXPHOS, less cytotoxic reactive oxygen species are generated (Denko, 2008; Nogueira et al., 2008).

All the above likely contribute to the metabolic choice of cancer cells to varying degrees in a location and tumour-type specific way. However the most convincing hypothesis for the importance of aerobic glycolysis concerns a tumour's requirement for macromolecule biosynthesis. Both glycolysis and its associated pentose phosphate pathway (hexose monophosphate shunt) act as sources of precursors essential for the synthesis of RNA, DNA, phospholipids, fatty acids, cholesterol, and porphyrins (Pedersen, 2007) – all vital in rapidly growing and proliferating cells. This necessity therefore could potentially explain how such high biosynthetic demands of cancer cells are met (Heiden, 2009). An early criticism was that exploitation of these biosynthetic pathways could result in weakening and ultimately cessation of the TCA cycle but the recruitment and metabolism of glutamine has since been shown to support this function through a process called anapleurosis (Dell' Antone, 2012). Following conversion of glutamine to glutamate, its derivative α-ketoglutarate can then enter into the TCA cycle to propagate

the process and provide further metabolic intermediates (Zheng, 2012). This mechanism is supported by the finding that glutaminolysis is frequently elevated in cancer (DeBerardinis and Cheng, 2010; Wise et al., 2008). A summary of the above pathways is shown in Fig. 1-3.

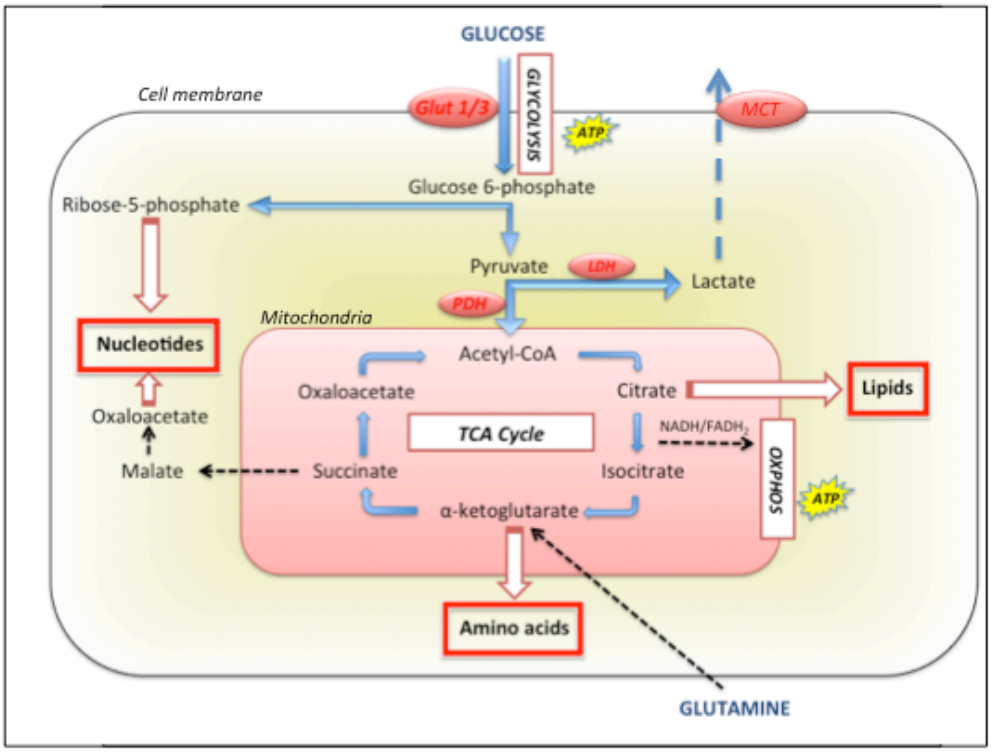

Figure 1-3. Glycolysis, the TCA cycle and biosynthesis. The key steps in ATP production in cells are shown. Macromolecule biosynthesis pathways are highlighted in red boxes, indicating the key precursors that can be exploited by a glycolytic dominant phenotype in tumour cells.

Despite a marked interest in potential metabolomics therapeutics, there have been failures in pharmacotherapeutic advances, not least due to the difficulty in translating metabolic signatures in targets and also the risk of catastrophic changes through off target alterations in metabolism of normal cells (D'Alessandro and Zolla, 2012). A greater appreciation of the effects that a tumour's metabolic preferences has on a cell's behaviour is therefore required, as well as identification of less diverse markers of a cell's metabolic profile that might lead to a more targeted approach for future therapeutic strategies.

1.3 COOH-terminal binding proteins

Cells are constantly reliant on the balance between key metabolic co-factors as well as their environment to direct their energy pathways. It is therefore vital that they are able to monitor these pathways and the cellular energy stores. We have already described the importance of the NAD+/NADH ratio and the impact that changes in metabolism have upon this redox state. It can therefore be considered as a readout of the metabolic state of a cell (Krejčí, 2012) and specific monitoring systems have evolved for a cell to detect and respond to these changes. The carboxy-terminal binding proteins (CtBPs) are key metabolic sensors and have been shown to have important functions in embryogenesis, development and tumourigenesis (Chinnadurai, 2002).

CtBP1 was recognised first due to its interaction the C-terminus of adenovirus E1A proteins (Boyd et al., 1993) and then later identified as a transcriptional repressor of multiple targets. Further evidence suggested that CtBP1 was an antagonist of the epithelial phenotype (Chinnadurai, 2009) and acted to suppress genes such as E-cadherin through interaction with Zeb, a zinc finger transcriptional repressor (Grooteclaes and Frisch, 2000). CtBP2 was discovered several years later by data bank sequence analysis (Schaeper, Boyd et al. 1995). Encoded by genes located on chromosomes 4 and 10 respectively, CtBP1 and 2 have a number of different isoforms due to alternative RNA splicing; for both CtBP1 and -2 these include long (CtBP1-L/CtBP2-L) and short (CtBP1-S/CtBP2-S) isoforms, all with a highly conserved structure across species, and an additional RIBEYE isoform for CtBP2 (Schmitz et al., 2000; Spanò et al., 1999).
CtBP1 and CtBP2 transcripts are widely expressed in both adult tissue and during development (Furusawa et al., 1999; Hildebrand and Soriano, 2002; Sewalt et al., 1999), and appear to function interchangeably in certain functions, not surprisingly as they share a reported 78% amino acid identity and 83% similarity (Katsanis and Fisher, 1998). Each protein has a significant degree of homology between domains, consisting of a central region with a NAD+-dependent dehydrogenase domain and a N-terminus containing PXDLS (proline-any amino acid-aspartic acid-leucine-serine) domain, which can bind to variety of transcriptional factors (Chinnadurai, 2002). The dehydrogenase domain has an important role in promoting dimerisation between CtBP1 and CtBP2, stimulated by NADH binding (Kumar et al., 2002; Nardini et al., 2003). NADH ligand binding has >100 fold stronger affinity than NAD+ which is critical to its function in sensing redox changes (Fjeld

et al., 2003; Zhang et al., 2002) and a homo or heterodimer has the potential to form a complex containing two PXDLS-containing proteins (Bergman and Blaydes, 2006).

Two main functions have been assigned to CtBP proteins, namely that of transcriptional regulation and also in regulating Golgi membrane maintenance (Bergman and Blaydes, 2006), although we will focus primarily on the former.

1.3.1 Transcriptional regulation by CtBPs

The CtBPs are able to act as transcriptional corepressors to alter target gene expression (Paliwal et al., 2006). Metabolic changes resulting from hypoxia, increased glucose transporter expression and the Warburg effect, stimulates glycolysis resulting in an accumulation of NADH. NADH ligand binding to the CtBP dehydrogenase domain triggers a conformational change resulting in activation and dimerisation. This dimerisation is crucial to the transcriptional repressive function, highlighted by a number of studies where mutations inhibiting this binding resulted in ineffectual transcriptional activity (Kumar et al., 2002; Kuppuswamy et al., 2008; Zhao et al., 2009). Homo- or heterodimers can then form the base of large complexes incorporating other chromatic modifying agents e.g. histone deacetylases [HDAC], histone demethylases [HDMs] and histone methyltransferases [HMTs] as well as over 30 different transcription factors which are required to link the CtBPs to their target gene promoters (Chinnadurai, 2009; Fig. 1-4). Zeb proteins Snail and Slug are examples of well known transcription factors that are able to recruit CtBPs to repress the expression of epithelial phenotype genes in mesenchymal cells (Grooteclaes and Frisch, 2000; Peinado et al., 2004; Tripathi et al., 2005).

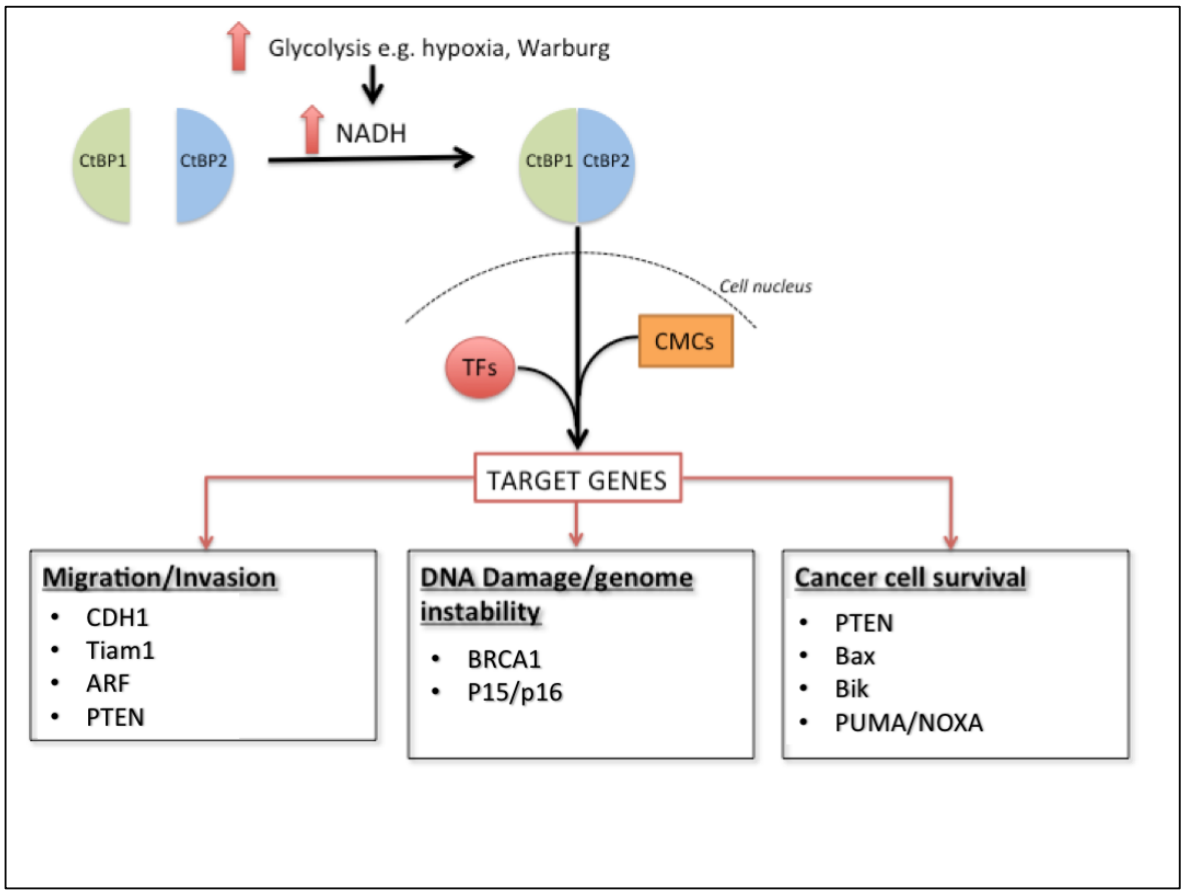

Figure 1-4. CtBP targets in tumourigenesis. NADH-responsive CtBPs respond to increasing glycolysis by dimerising and translocating to the cell nucleus for gene targeting. Actual locations of monomers are more complex than illustrated due to differential localisation between isomeric variants. The grouped targets shown have all been demonstrated to be targets for transcriptional repression. Tiam1 however has been shown to be activated by CtBP2 to promote tumour cell migration (Paliwal et al., 2012)**; TFs – transcription factors; CMCs – chromatic modifying complexes.**

1.3.2 CtBPs and cancer

With tumour cells exhibiting the Warburg effect to varying degrees, the response of the metabolic sensors CtBPs to increasing NADH from glycolysis will play an important role in regulating transcription. Little is known about the relevance of CtBP expression in tumours although a recent genome-wide study has identified overexpression of CtBP1 and CtBP2 in colon, breast, and prostate cancers (Thomas et al., 2008). Similarly, elevated nuclear CtBP levels have been shown to correlate with tumour progression in a variety of malignancies, including breast (Di et al., 2013), head and neck and oesophageal cancers (Deng et al., 2010; Guan et al., 2013).

CtBPs may have an important role in promoting EMT and an invasive cell phenotype by repressing important epithelial adhesion molecules such as E-cadherin (Chinnadurai, 2009; Thiery, 2002), and hypoxia plays a key role through this mechanism *in vitro* with poor vascularisation, high glycolysis and increased free NADH enhancing recruitment of CtBP to the E-cadherin promoter (Zhang et al., 2006). CtBP-mediated control of cell migration can also function through the PI3K/Akt signalling pathway by regulation of the tumour suppressor PTEN (Paliwal et al., 2007). The same group also demonstrated a link between CtBP2 and T-cell lymphoma invasion and metastasis (Tiam1), a GTP exchange factor promoting active GTPase state (i.e. activating Rac1, cdc42, Rho) (Paliwal et al., 2012). This was notable in that CtBP2 was shown to co-activate, not repress Tiam1 expression, recruiting to the Tiam1 promoter by the basic Kruppel-like factor 8 (KLF8) transcription factor and accelerating colon cancer cell migration *in vitro*.
However CtBPs are not simply regulators of epithelial behaviour and motility; expression profiling has revealed a number of other pro-apoptotic target genes such as Bax and Noxa (Grooteclaes et al., 2003). Other tumour suppressor targets have also been identified most notably the cell cycle inhibitors p16Ink4a, p15Ink4b, which function through the Rb pathway, and Ink4a/Arf (p14ARF) that stabilises p53 (Chinnadurai, 2009). Knockdown experiment results indicating a CtBP1/2 repression of p16 have been confirmed by demonstration of enhanced occupancy of CtBP at the p16 promoter in hypoxic conditions (Mroz et al., 2008). Similarly, CtBP has been suggested to play a role in p15 repression, most likely through a Zeb1-dependent repressor complex system (Liu et al., 2008). A final notable target presented in the literature is BRCA1, whose protein product has important cellular functions in DNA repair and cell cycle regulation. Evidence points to CtBP-directed complexes playing a key role in BRCA1 transcriptional regulation in response to environmental stimuli (Di et al., 2010).

CtBPs, through their function as redox and metabolic sensors, are able to link cellular metabolic status to transcriptional regulation (Fjeld et al., 2003) and the wide array of targets, especially the new evidence of involvement in EMT regulation, provide potential mechanisms of how a cancer cell's metabolism can directly affect the way the cell moves and interacts with its environment. This means that targeting of this pathway can potentially have a direct impact on tumour cell behaviour and indeed early work has been promising with small cyclic peptide inhibition of CtBP dimerisation resulting in

impaired mitotic fidelity and reduced proliferation of tumour cells *in vitro* (Birts et al., 2013).

1.4 Integrins

The extracellular matrix (ECM) has an important role in the context of providing a reservoir of bound proteins for the cell to exploit when appropriate stimuli are supplied. The most important receptors used by cells to adhere to the ECM are integrins - transmembrane structures that form both cell-cell and cell-matrix adhesion (Hynes, 2002).

1.4.1 Structure

There are 24 known integrins and they exist in a heterodimeric structure, composed of an α- (18 types) and β-subunit (8 types). The specific combination of these subunits determines the binding specificity; important ligands include laminins (α2β1, α3β1, α6β1, α7β1), fibrillar collagens (α1β1, α2β1, α3β1, α10β1, α11β1), fibronectin (a5b1, avb3, a4b1) and LAP (αvβ1, αvβ5, αvβ3, αvβ6 αvβ8) (Ludbrook et al., 2003; Takada et al., 2007). The transmembrane structure of integrins means that they can link the ECM with the intracellular actin cytoskeleton which, when considered with the binding specificity of the extracellular domains, has important functional consequences. Integrins can adopt low-, moderate- and high-affinity conformations, the latter of which is termed 'activation' and can be mediated either by signals from inside the cell (inside-out signalling) or by extracellular factors (outside-in signalling) (Margadant et al., 2011). This level of control allows both intra- and extracellular signalling cascades to result in profound changes to a cell's behaviour and interactions with the ECM. For example, ligand binding to integrins can result in their recruitment and clustering with the formation of an adhesion complex, effects on cell adhesion and migration, and activation of a variety of proliferative and survival cascade reactions (Campbell and Humphries, 2011). These clusters of integrins are integral to the formation of adhesion complexes which mature in a stepwise manner but include focal complexes, focal adhesions and fibrillar adhesions, the type determined by time of formation/maturation and specificity of both integrins and recruited adaptor focal proteins (Geiger and Yamada, 2011). Indeed integrins are unusual cell receptors as they possess no inherent enzymatic activity but instead rely on spatial aggregation and

recruitment of adaptor proteins at adhesion sites, which are able to propagate other signalling pathways (Zaidel-Bar et al., 2004). Important ancillary functions such as angiogenesis are also reliant on appropriate integrin signalling – for example αv integrins are overexpressed on endothelial cell surfaces and promote growth and survival of newly formed vessels (Weis and Cheresh, 2011). With important roles in cell-cell adhesion and cell-matrix interactions, it is not surprising that integrins have been implicated in tumourigenesis and metastatic potential.

1.4.2 The role of integrins in cancer

Abnormal cell migration is a characteristic feature of metastatic cells (Clainche and Carlier, 2008). Migration however depends on complex, dynamic interactions between adhesion sites and the ECM – with adhesion formation and protrusion at the leading edge and release of adhesions at the rear (Cox and Huttenlocher, 1998). Rate of formation or release at each of these sites can therefore become rate-limiting to speed of migration (Jay et al., 1995; Marks et al., 1991; Wessels et al., 1994).

In 2D assays, cell migration is often referred to as occurring in a biphasic pattern with optimal migration occurring at moderate adhesion strengths – sufficient to allow new adhesion formation but not rate limiting on release of rear adhesion sites (Huttenlocher et al., 1996). Therefore integrin-ligand binding affinity and the strength of ECM-cytoskeletal linkages through transmembrane integrin receptors will play a key regulatory role in cell migration dynamics (Huttenlocher et al., 1996). Thus although integrins in themselves are not oncogenic, elevated expression of certain heterodimers or their activation are often associated with tumour growth, invasion and metastasis through various mechanisms (Weis and Cheresh, 2011). For example αvβ3 expression is associated with disease progression and poor prognosis in a range of cancers including melanoma (Danen et al., 1994; Nip et al., 1992), pancreatic (Hosotani et al., 2002) and breast (Felding-Habermann et al., 2001), potentially through angiogenic or matrix metalloproteinase production (Bauer et al., 2007; Baum et al., 2007; Kikkawa et al., 2002). Elevated αvβ5 signalling similarly promotes an invasive tumour cell phenotype (Klemke et al., 1994; Ricono et al., 2009). Integrin αvβ6 has received significant attention in recent years due to its relatively restricted expression to cells involved in remodelling and healing, including most notably in malignant cells (Breuss et al., 1995; Clark et al., 1996). For example Thomas et al (2001) found increased expression of this integrin in malignant

keratinocytes and this promoted invasion in an MMP9-dependent manner; upregulation of αvβ6 has also been shown in both pre-malignant and oral tumour samples (Hamidi et al., 2000). Indeed increased αvβ6 expression has now been reported in multiple tumour types including oral, colon, breast and cervical carcinomas (Arihiro et al., 2000; Elayadi et al., 2007; Hazelbag et al., 2007; Sipos et al., 2004). β1 integrins have also shown relevance in tumour progression, with studies demonstrating inside-out activation of β1 integrins promotes tumour cell extravasation and colonization (Kato et al., 2012) and upregulated β1 expression in HNSCC has been reported by a number of authors (Koivisto et al., 2000; Van Waes et al., 1995; Wang et al., 2012). Whether this is subunit dependent is less clear, as Dos Santos et al (2012) recently presented that poorer prognosis in breast cancer patient is associated with overexpression of all β1 integrins rather than a particular heterodimer class. This observation is likely tumour type dependent.

1.4.3 Focal adhesions

Adhesion complexes are heterogeneous and complex structures with a variety of sizes, morphologies, locations and components and have an important role in determining cell behaviour (Geiger and Yamada, 2011). Integrins play a central role in their formation and structure and mediate the formation of a structural link between the ECM and cytoplasmic actin cytoskeleton (Hynes, 1992). However the recruitment of focal adhesion adaptor proteins are also a vital part of the 'adhesome' providing either mechanical strength or mediating intracellular signalling (Critchley, 2000). By studying the components and integrin specificity of different focal contacts, as well as their location, it has been shown that adhesion sites can be broadly divided into different groups (Zaidel-Bar et al., 2004; Fig. 1-5). Along the cell periphery, usually associated with motile cells that exhibit protrusions and lamellipodia, small adhesions to the ECM form known as focal complexes. By their nature they are transient connections but the aggregation of β3-integrins are a key component, as well as variable accumulation of other actin binding proteins (e.g. vinculin, paxillin). They also mediate signals that promote actin polymerization (Alexandrova et al., 2008). At these peripheral sites, Rho activation or mechanical tension results in maturation of the adhesion sites into focal adhesions (Ballestrem et al., 2001; Galbraith et al., 2002; Rottner et al., 1999), although as they mature they can be found increasingly at central sites as well. These sites are highly

tyrosine phosphorylated but contain the same integrin and adaptor protein constituents as their precursors (Zamir et al., 1999). However, in keeping with their more mature and active role, there is recruitment of Talin – an adaptor protein crucial for integrin activation that has been shown correlate with an aggressive disease phenotype in HNSCC (Lai et al., 2011) and prostate cancer (Sakamoto et al., 2010). There is also variable recruitment of focal adhesion kinase (FAK) and integrin-linked kinase (ILK), which mediate intracellular signalling cascades e.g. PI3K. The regulation of signalling pathways through focal adhesions is an interesting area of current research. Finally at central cell locations fibrillar adhesions form, associated with recruitment of α5β1 integrin and fibronectin fibrils and the protein Tensin. Both Tensin and Talin bind to β-integrin tails although their recruitment is temporally distinct, mirroring the temporal relationship between focal adhesion and fibrillar adhesion formation (Legate and Fässler, 2009) – Talin's major role as previously mentioned is with the early activation of integrins (Zaidel-Bar et al., 2003) whereas Tensin is only found at very mature focal adhesions and fibrillar adhesions where it has been proposed to have a more important signalling role (Katz et al., 2000; Legate and Fässler, 2009). The relationship between Talin or Tensin binding, through phosphorylation of β integrins, has prompted the hypothesis that a regulatory switch therefore exists between a structural/activating complex or signalling complex (Mccleverty et al., 2007).

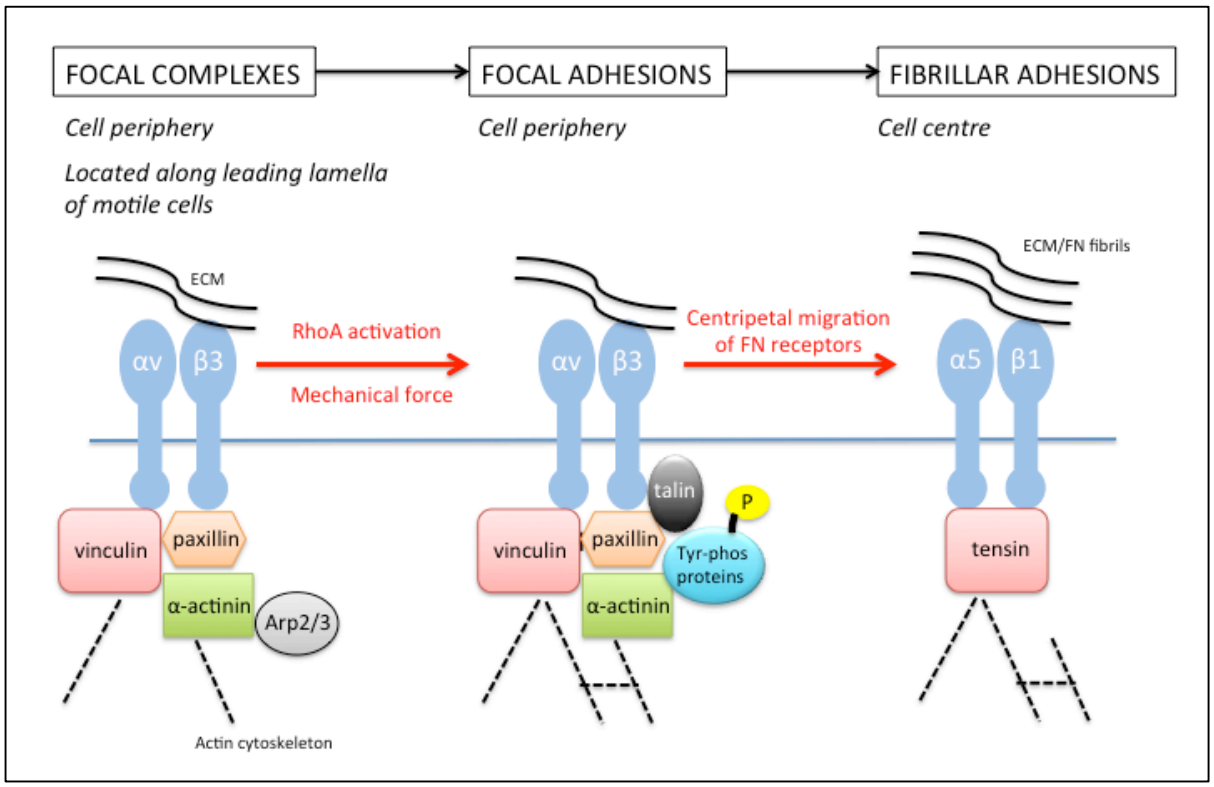

Figure 1-5. Types of adhesion site complexes. The stages illustrated demonstrate a general left to right maturation process, although recruitment of different adaptor proteins confers important structural and signalling properties to the adhesion sites. (FN = fibronectin; ECM = extracellular matrix; Tyr-phos = tyrosine phosphorylated; Arp2/3 = actin-related protein 2/3; P = phosphate group).

It is therefore evident that the different types of focal adhesions provide not only a base for structural adhesion to the ECM to provide traction forces, so important in migrating cells, but temporal recruitment of important proteins such as Tensin provide a key role in mature focal adhesion formation and signalling pathways. These adhesions therefore are critical to allow a cell to move and interact with its environment and are therefore likely to have an important role in tumourigenesis.

1.5 Tensin

1.5.1 Structure and function

The first Tensin cDNA sequence was isolated from chicken by Davis et al. (1991) and allowed characterisation of the protein's structure and function. Evidence has since emerged to suggest that the Tensins are an important protein family linking the ECM, the actin cytoskeleton, and signal transduction. Tensins are recruited to fibrillar adhesions associated with β1 integrins, and also with mature focal adhesions in association with αvβ3 integrin (Katz et al., 2000; Zaidel-Bar et al., 2003). The integrin interaction does not appear to require tyrosine phosphorylation (Katz et al., 2007). Both Tensin and Talin have also been shown to bind to β3-, β5- and β7-integrin tails (Calderwood et al., 2003, 1999; Mccleverty et al., 2007). Indeed these studies suggested that the phospho-tyrosine binding (PTB) domain of Tensins bind to the cytotails of β3 and β5 far better than to the β1 cytotail in vitro. Tensins broadly comprise three important functional sites: an N-terminus with actin binding sites to connect with the cytoskeleton, a central domain with F-actin barbed end capping function (in Tensin-1), and a C-terminus containing both a Src homology 2 (SH2) domain mediating binding to a wide range of signalling proteins e.g. PI3K, p130Cas, FAK (Auger et al., 1996) and a phosphotyrosine binding domain (PTB) which recognises ligands that possess an NPxY motif e.g. β-integrin tails (Chen and Lo, 2003). In the case of p130Cas, this has been shown to be affected by Src activity (Qian et al., 2009). Indeed there is growing evidence that many focal adhesion adaptor proteins, including Tensins, are not just structural proteins but play an important role in mediating inside-out and outside-in signal transduction pathways (Chan et al., 2015).

Four members of Tensin family have now been identified – Tensin-1, -2 and -3 (TNS1, 2 and 3) as well as Tensin-4 (TNS4 or CTEN). TNS1-3 possess high sequence homology of both their N and C terminals. CTEN however lacks the actin binding domain which has important proposed consequences on its function (Chen et al., 2002; Lo and Lo, 2002) (Fig. 1-6). The *TNS4* gene localizes to chromosome 17q21, a region frequently deleted in prostate cancer (Gao et al., 1995; Williams et al., 1996). The promoter region of 327-bp around exon 1 has been identified, containing a p63 binding site (Chen et al., 2013).

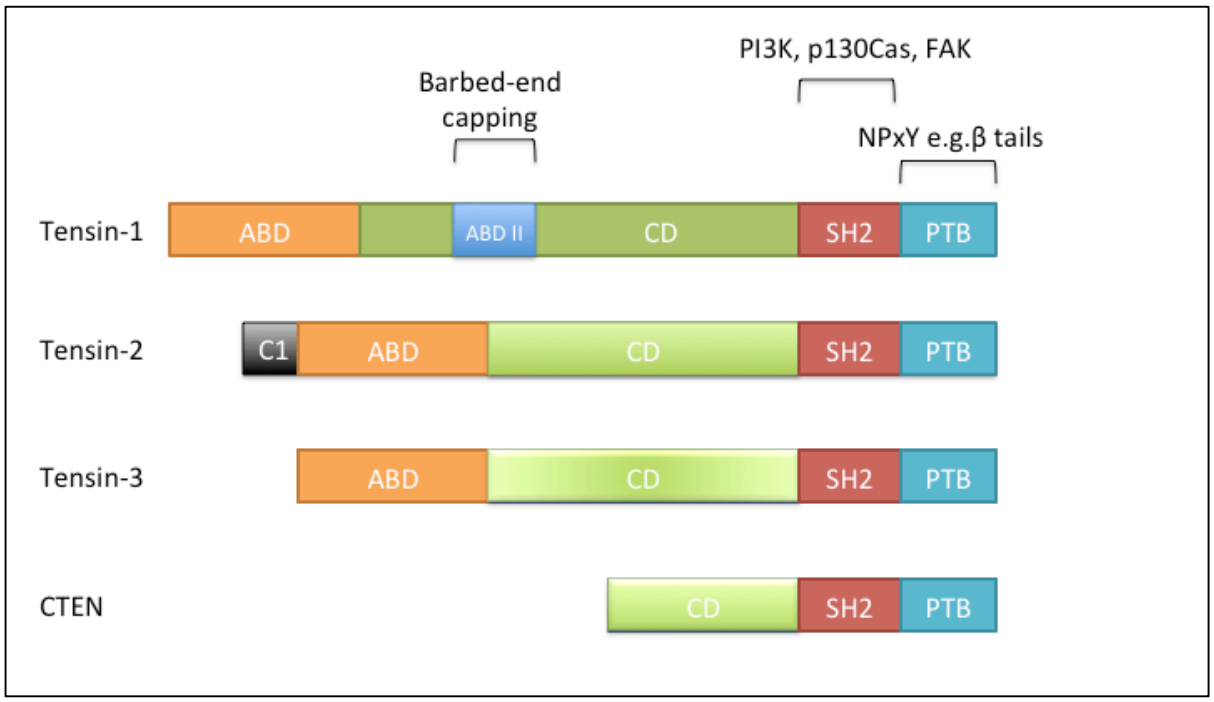

Figure 1-6. Functional organisation of Tensins. A non-homologous central domain (CD), Src homology 2 (SH2) domain and phosphotyrosine-binding (PTB) domain are conserved between proteins. The SH2 domain permits binding to tyrosine-phosphorylated proteins, examples of which are illustrated. The PTB domain permits binding to any structures containing an NPxY motif. Barbed-end capping function is unique to Tensin-1 whereas a protein kinase C conserved region 1 (C1) is unique to Tensin-2. (Adapted from Lo, 2004)

Knockout mice have been developed for TNS1 indicating that it is important for normal renal function, with Tensin-null mice developing severe nephronophthisis and tubular disease (Lo et al., 1997). A TNS2 deletion mutant exhibits severe proteinuria and glomerulosclerosis (Cho et al., 2006) whereas inactivation of TNS3 in mice resulted in growth retardation and postnatal lethality in one third of the homozygous mutants, with incomplete development of small intestine, lung, and bone highlighted at a histological level (Chiang et al., 2005). The authors proposed that TNS3 might play an important role in cell adhesion at a specific early developmental stage in these tissues. The tissue distribution and knockout phenotype of CTEN has not yet been reported. Both TNS3 and CTEN demonstrate minimal expression in normal tissues including breast, heart, lung, liver, pancreas, ovary, and colon with CTEN in particular having highly restricted expression to the prostate and placenta (Lo and Lo, 2002; Maeda et al., 2006). However, expression profiles in tumour tissue have demonstrated important features.

1.5.2 The role of Tensins in cancer

When considering both the localisation of Tensins to focal adhesions as well as their constituent binding sites to both integrins (via PTB domain) and oncogenic ligands (SH2 domain), it is not surprising that they have been shown to have an important role in the tumour phenotype. Although the dysregulation of focal adhesion complexes is one recognised mechanism behind the ability of cancer cells to metastasise (Liao et al., 2007), a clear role or mechanism of action in oncogenesis for Tensins has not been elucidated and findings appear tumour type-specific. For example, although TNS1 overexpression promotes cell migration (Chen et al., 2002), it was not expressed in either breast or prostate cancer cell lines (Chen et al., 2000). Similarly, splice variants of TNS2 exhibited opposite effects on cell growth and transformation (Yam et al., 2006). TNS3 has had similarly variable experimental results in vitro; in melanoma cell lines TNS3 has been shown to both increase (Qian et al., 2009) and decrease (Martuszewska et al., 2009) cell migration. In addition the former cited paper also demonstrated that TNS3 maintained the oncogenic growth properties in cell lines from non-small cell lung carcinoma and breast cancer in a range of cell assays where as Martuszewska et al (2009) showed in vivo reduced expression of TNS3 in renal tumours.

CTEN has been more extensively investigated as a potential tumour marker in the literature, even though early reports demonstrated down-regulation in the majority of prostate cancer cell lines (Lo and Lo, 2002), paclitaxel resistance increased following knockdown (Li et al., 2010) and forced expression in a breast cancer cell line had no significant effect on cell behaviour (Lo et al., 2005). Katz et al's (2007) seminal paper demonstrating a reciprocal switch between the two proteins TNS3 and CTEN in an EGF-driven mammary cell model has formed the basis of many of the recent hypotheses behind the pro-oncogenic effects of CTEN. This group initially identified TNS3 and CTEN as potentially key proteins in cell migration and adhesion from a reciprocal expression change in a geneset analysis following EGF stimulation, with TNS3 mRNA expression reducing and CTEN increasing significantly. Indeed they reproduced the displacement of TNS3 from focal adhesion sites by forced expression of CTEN and, together with Tensin's ability to bind the cytoplasmic tail of β1 integrins, they hypothesised that the lack of actin binding domain in CTEN would result in this Tensin switch breaking the link between the ECM and actin cytoskeleton, facilitating cell movement (Fig. 1-7). In addition, *in vivo*

relevance was demonstrated by showing positive correlations between CTEN expression and both breast tumour grade and lymph node metastases. However the evidence for this switch has not been consistent across different cell lines. For example in colorectal cancer cell lines, variable expression of TNS3 tended to reflect the co-expression levels of CTEN at the protein level. (Thorpe et al., 2015).

More recently the CTEN-SH2 domain has also been shown to interact with and stabilise phosphorylated MET, an upregulated tyrosine kinase receptor signalling pathway in the majority of solid cancers, as well as stabilising β1 integrins (Muharram et al., 2014). Chan et al. (2015) also demonstrated a progressive up-regulation of CTEN expression following EGF treatment and this resulted in a morphological change to a mesenchymal-like elongated shape, although a direct causative role of CTEN to this effect was only suggested. Their results indicated that in hepatocellular carcinoma, CTEN was a downstream target of ERK kinase and promoted cell proliferation and migration. EGF is not the only growth factor implicated in the regulation of Tensin expression. Other factors and cytokines including fibroblast growth factor (FGF2), nerve growth factor (NGF), insulin-like growth factor (IGF-1), transforming growth factor β (TGF-β) and interleukins 6 and 13 (IL6, IL13) induced CTEN expression in human prostate and colon cell lines (Hung et al., 2014). The inconsistencies and numerous proposed CTEN signalling pathways and mechanisms of action suggest diverse roles in different tissue types and support an organ/system based focus for further investigation.

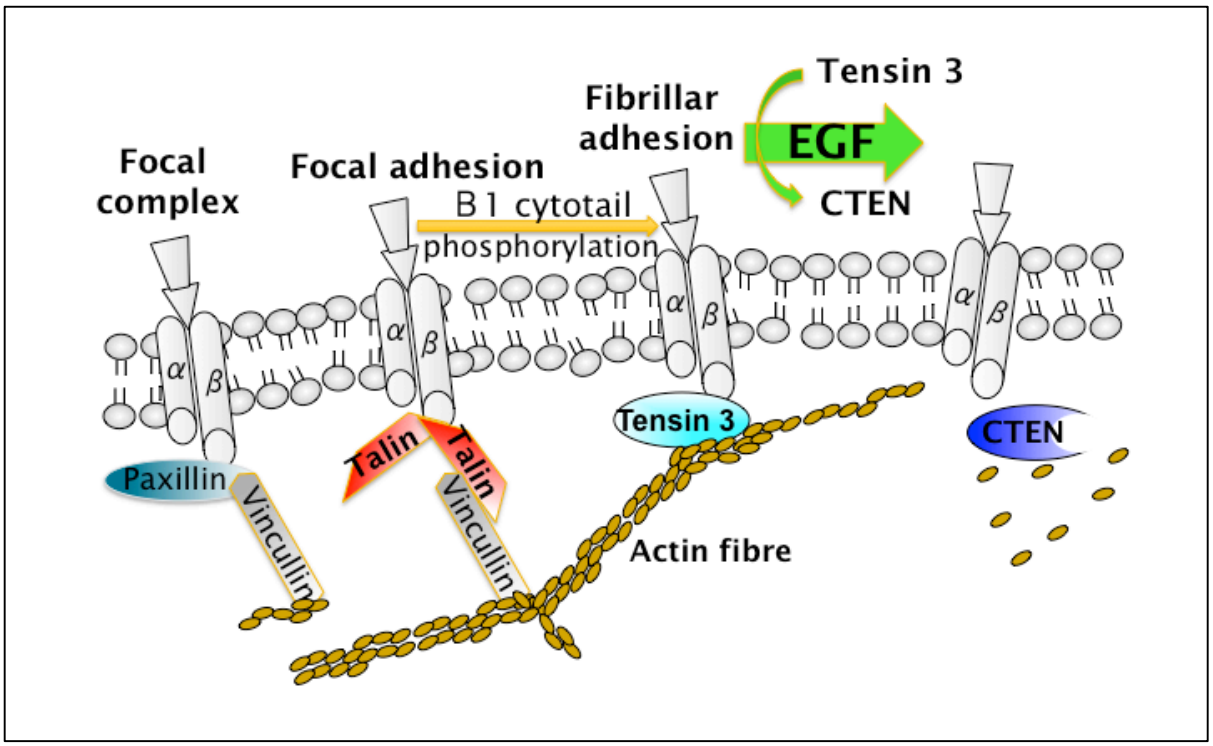

Figure 1-7. Reciprocal Tensin switch. In a mammary cell model, EGF stimulation resulted in displacement of Tensin-3 by CTEN. The latter protein's absent actin binding domain disrupts ECM-cytoskeletal linkage, which has important implications for cell migration. Adapted from Katz et al (2007)

Over the past few years CTEN has been shown to positively regulate cell migration in a variety of cell lines and increased expression has been demonstrated in a large number of tumour types including gastric, colorectal, lung, skin, thymoma and pancreatic, associated in the majority of cases with advanced stage and aggressive disease (Al-Ghamdi et al., 2013, 2011; Albasri et al., 2011a; Albasri et al., 2011b; Li et al., 2010; Liao et al., 2009; Sakashita et al., 2008; Sasaki et al., 2003; Sjoestroem et al., 2013). The importance of CTEN expression in head and neck cancer has not been studied and the mechanism of its oncogenic role has not been clarified.

The relevance of CTEN as either a marker for, or causative of tumour development is still under debate. A variety of cytokines upregulated by the RAS-Raf-Mek, PI3K-Akt and Stat3 pathways result in increased CTEN expression, including EGF, FGF2, PDGF, TGF-β and interleukins-6 and -13 (Al-Ghamdi et al., 2011; Barbieri et al., 2010; Hung et al., 2014). Interestingly hypoxia also resulted in upregulation of CTEN in a peripheral blood lymphocyte study (Brooks et al., 2009), although no link has yet been established between Tensin expression and cancer cell metabolism. However, a number of mechanisms for CTEN-induced pro-oncogenesis have also been proposed. CTEN both up-

regulates ILK (integrin linked kinase) (Albasri et al. 2011b) and reduces E-cadherin expression at the post-transcriptional level, positively regulating cell migration (Albasri et al., 2009). The SH2 domain of Tensins binds to the Rho GTPase-activating proteins (RhoGAPs) deleted in liver cancer 1 (DLC1) and DLC3, to the kinase PDK1, to the adaptor Dok2 (Qian et al., 2007; Wavreille and Pei, 2007) and potentially also to PI3K, although there is debate about whether this is through an indirect mechanism (Legate and Fässler, 2009; Wavreille and Pei, 2007). The localisation of DLC1 to focal adhesions has been investigated recently; the rhodopsin (Rho) family of small GTPases (RhoA, Rac1 and Cdc42 being the most studied) vary between activation states depending in turn on the activity of guanine nucleotide exchange factors (GEFs) or GTPase activating proteins (GAPs) which promote an active or inactive form respectively. DLC1 is one such GAP which is recognised as a tumour suppressor (Durkin et al., 2007) and therefore loss of expression is often found in solid tumours (Wong et al., 2003; Yuan et al., 2003). In mammary cell lines, both TNS3 and CTEN were shown to have distinct opposite effects on RhoA activity with TNS3 activating DLC1 GAP function whereas CTEN had the converse effect, positively regulating RhoA activity and cell migration (Cao et al., 2012). However although hemizygous deletions of the DLC1 locus are observed in HNSCCs, sequencing studies of a cancer cohort revealed that this gene is unlikely to be primary target for inactivation in this disease (Hewitt et al., 2004).

1.6 Summary and aims

Head and neck cancer is genetically heterogeneous but a number of pathways and components of the tumour microenvironment have been shown to be important in tumour progression. The rise of virally induced tumours has further complicated the tumour landscape. Tumour stage and locoregional spread at disease presentation are critically important to prognosis and therefore studies of cell migration, focal adhesions and integrin signalling are vital to further our understanding of this disease. Despite potential involvement in all of these cellular processes, CTEN is under researched and its biological functions unclear, despite the growing evidence for overexpression in a variety of human cancers.

In addition, tumour cell metabolism is receiving increasing research attention due to the clinical impact made by surrogate markers of glycolysis such as FDG-PET; the potential for both novel biomarkers and targets for pharmacological interventions however at present remain largely unanswered. Evidence is starting to emerge that cancer cells not only direct metabolic pathways to optimise both energy production and macromolecule production, but also that this unique metabolism may fundamentally affect how a cell behaves, moves and interacts with the microenvironment. We will therefore explore any potential links between cell metabolism and cell motility.

1.6.1 Hypothesis

CTEN overexpression plays an important role in the tumour potential and behaviour of head and neck cancer cells.

1.6.2 Aims

1) Determine the clinical relevance of CTEN in a large HNSCC tumour database with clinicopathological parameters.
2) Explore the effect of CTEN on *in vivo* models and utilise next generation sequencing to identify biological processes of relevance to help direct functional *in vitro* investigations.
3) Identify any potential links between CTEN and tumour metabolism
4) Investigate the metabolic profile of HNSCC in both HPV-positive and HPV-negative disease to help identify any potentially novel therapeutic targets in this disease.

Chapter 2: MATERIALS AND METHODS

2.1 Cell culture

2.1.1 Cell culture

Cell culture techniques were performed in a laminar flow hood, routinely sterilised prior to use with 70% ethanol. Gloves and laboratory coat were worn at all times as standard. All tissue culture reagents and media were stored at either 4°C or -20°C and sterilised using a 0.22µm filter system (Millipore) with a vacuum driver pump, and are listed in Appendix A. Reagents were warmed to 37°C in a water bath prior to cell culture use.

2.1.2 Cell lines

All cell lines utilised in this work are mammalian cell lines, predominantly from head and neck origin. All cell lines were regularly tested for mycoplasma contamination using PCR – no contaminated cell lines were identified or included; cells were grown in a humidified environment with 5-10% CO_2 at 37°C.

The following cell lines were used in this study:

Head and neck:

5PT - cisplatin-resistant subline derived from a tumour of supraglottis (primary site).

BICR6 - adherent keratinocyte cell line derived from a squamous cell carcinoma of the hypopharynx of a Caucasian male.

DETROIT 562 - derived from pleural fluid of an adult female with primary carcinoma of the pharynx. The cells have the type B glucose-6-phosphate dehydrogenase.

H357 - established from a squamous cell carcinoma (SCC) of the tongue (20mm) of a 74 year-old male patient.

IC6pr - H357 retrovirally transfected with two empty vectors (a negative control for VB6 cell line).

SCC25 – Immortalised cell line derived from a tongue squamous cell carcinoma in a 70-year old male patient. Stably resistant to cisplatin.

UD-SCC-2 and UPCI:SCC90 – immortalised cell lines derived from the upper aerodigestive tract from suspected HPV-derived tumours. Kindly supplied by Susanne M. Gollin (University of Pittsburgh, USA; shortened to SCC2 and SCC90 respectively in results)

VB6 - H357 retrovirally transfected with αv and then with β6 cDNA.

Other:

BxPC3 – immortalised human primary pancreatic epithelial adenocarcinoma cell line derived from a 61-year-old female with a primary pancreatic adenocarcinoma

Capan-1 – immortalised human primary pancreatic epithelial adenocarcinoma cell line derived from a 40-year-old male with a primary pancreatic adenocarcinoma

DLD1 – epithelial cell line derived from a Dukes' type C colorectal adenocarcinoma in an adult male patient

Flo1 - FLO-1 was established from a distal oesophageal adenocarcinoma in a 68 year-old Caucasian male in 1991.

OE21 - OE21, also known as JROECL21, was established in 1993 from a squamous carcinoma of mid oesophagus of a 74 year-old male patient. The tumour was identified as pathological stage IIA (UICC) and showed moderate differentiation.

Panc0403 – immortalised human pancreatic epithelial adenocarcinoma cell line derived from a primary tumour removed from the head of the pancreas of a male with pancreatic adenocarcinoma.

MCF7 - Breast adenocarcinoma cell line derived from metastatic deposit.

MLEC – mink lung epithelial cells are stably transfected with an expression construct containing a truncated plasminogen activator inhibitor type-1 (PAI-1) promoter fused to the firefly luciferase reporter gene resulting in TGF-β responsive dose-dependent luciferase activity.

HFFF2 – human fetal foreskin fibroblasts derived from a 14-18 week old human fetus.

A full alphabetically listed inventory of cell lines can be found in Table 2-1 together with their culture media conditions. All cell lines are human origin unless otherwise stated. All media contains 10% fetal bovine serum and 2mM L-Glutamine. Medium does not include antibiotics or antifungals unless otherwise stated.

Cell line	Origin (reference)	Medium
5PT	Cisplatin- resistant subline derived from a tumour of supraglottis (larynx, primary site). (Bauer et al., 2005)	KGM
BICR6	Hypopharyngeal squamous cell carcinoma (Edington et al., 1995)	KGM
BxPC3	Pancreatic adenocarcinoma (Loor et al., 1982)	KGM
Capan-1	Pancreatic ductal adenocarcinoma (Fogh et al. 1977)	DMEM
DETROIT 562	Derived from pleural fluid of an adult female with primary carcinoma of the pharynx. The cells have the type B glucose-6-phosphate dehydrogenase. (Peterson et al., 1971)	DMEM
Flo1	Oesophageal adenocarcinoma (Hughes et al., 1997)	KGM
H357	Squamous cell carcinoma of tongue (Prime et al., 1990)	KGM
HFFF2	Foreskin fetal fibroblast derived from a 14-18 week old human foetus	DMEM
IC6pr	H357 retrovirally transfected with two empty vectors (a negative control for VB6 cell line) (Thomas, Lewis et al. 2001)	KGM

MCF7	Breast adenocarcinoma cell lines (derived from metastatic site) (Soule et al., 1973)	DMEM
MLEC	*Mink origin*: Lung epithelium (Abe et al. 1994)	DMEM + 400g/ml Geneticine
OE21	Oesophageal squamous cell carcinoma (Rockett et al., 1997)	RPMI
Panc0403	Pancreatic adenocarcinoma (Thu et al., 2014)	RPMI + sodium pyruvate (1mM), insulin (0.2units/ml),
SCC25	Oral keratinocytes derived from an SCC of the tongue (Rheinwald and Beckett 1981)	HAM's F12: DMEM (1:1)
UD-SCC-2/ UPCI:SCC90	Upper aerodigestive tract, HPV-positive SCC (Nagel et al. 2013)	DMEM
VB6	H357 retrovirally transfected with αv and then with β6 cDNA (Thomas, Lewis et al. 2001)	KGM

Table 2-1. Description of cell lines used and growth media requirements.

2.1.3 Subculturing cell lines

Cells were maintained as an adherent monolayer in sterile tissue culture flasks (Falcon) in 5-10% CO_2 humidified incubators at 37^{o}C. At 80-90% confluency existing culture medium was aspirated and the monolayer was washed with Phosphate Buffered Saline (PBS; Sigma Aldrich) to remove any residual serum. After removal of PBS wash, 0.05% trypsin/ 5mM EDTA solution (PAA) was added and flasks were returned to the incubators for a cell line-dependent period of time to allow for detachment. At this point serum-containing medium was added to inactivate trypsin and cell suspension aliquots were then added to a new flask containing fresh medium at a ratio of 1:3-1:10, dependent on growth rate.

Subculturing was performed twice weekly. Media and solutions used in this study are listed in Appendix A.

2.1.4 Mycoplasma screening

All reconstituted cell stocks were routinely tested for mycoplasma contamination. Following a minimum of two cell culture passages, supernatant (10mls) from cells was collected and centrifuged at 4500rpm for 10min. Excess supernatant was discarded and mycoplasma PCR detection was performed on the remaining 500µl sample. A 1µl representative sample was used as the template for the PCR. Details of primers, master mix composition and cycling conditions are described in Appendix F.

2.1.5 Maintenance and recovery of cell stocks

2.1.5.1 Cryopreservation

For stock maintenance, cells (approximately $1x10^6$/ml) were stored in liquid nitrogen in the presence of a cryopreserving agent (dimethyl sulfoxide [DMSO]) to prevent formation of ice crystals and preserve cell integrity. Cells in log phase were pelleted and re-suspended in normal growth medium containing 10% DMSO (Sigma Aldrich). Cell suspension was then pipetted into labelled cryovials (1ml/vial) and placed in an insulated polycarbonate freezing container ("Mr. Frosty, Nalgene®) prior to overnight storage at -80^{o}C. Vials were transferred the next day to -196^{o}C vapour phase of liquid nitrogen for long-term storage.

2.1.5.2 Thawing (reconstitution) of cell stocks

Cryovials were removed from the liquid nitrogen freezer and rapidly placed in a water bath at 37°C until almost fully thawed. Following transfer to a laminar flow hood, the cell suspension was then pipetted into a 15ml falcon tube containing pre- warmed medium and centrifuged at 1250rpm for 3 minutes at room temperature. The supernatant was aspirated, cell pellet re-suspended in fresh medium and transferred into a $25cm^3$ tissue culture vessel. Once cells had adhered, medium containing dead cells was removed the following day and fresh medium replaced to allow an adherent monolayer to develop prior to routine sub-culturing. Cells were allowed to grow for at least a week and

passaged twice before routine mycoplasma screening was performed and before they were used in experiments.

2.1.6 Cell counting

Cell counting was performed utilising a CASY automated low voltage counting system (Innovatis AG, UK/Roche Diagnostics GMBH). Following trypsinisation and preparation of a cell suspension for counting, 20µl of this suspension was added to 10ml of filtered isotonic buffer Casyton (Roche Diagnostics). By comparison, in functional experiments (e.g. migration, invasion assays) for the end-assay count, 500µl suspension was added to 9.5mls Casyton. A measuring capillary was then immersed in this new diluted sample and drawn up automatically to pass through two platinum electrodes, which create a low voltage field. The resistance created by an intact cell membrane passing through this field is converted to an electric signal, and distinct from damaged/dead cells which were excluded. This recorded signal is then converted to a cell count, adjusted for cell aggregation and original cell suspension dilution to give a cell count. This is automatically repeated three times resulting in the software supplying a final average cell count. All cell counts were performed using this method.

2.2 Protein expression

2.2.1 Western blotting

2.2.1.1 Cell Lysis

Cell lysis was performed on ice in NP40 lysis buffer (Appendix A) containing protease inhibitor cocktail (protease inhibitor cocktail set I; Calbiochem, Merk Chemicals). For cells plated in 6-well plates or dishes, cells were washed twice with ice-cold PBS, 40µl-100µl of NP40 buffer mix was added and cells collected with a cell scraper and transferred into an eppendorf. If in a cell suspension, cells were centrifuged into a pellet, excess medium was removed and lysis buffer was added directly to this tube. Forceful pipetting was used to thoroughly mix buffer and cells and the resulting lysate was left to incubate on ice for 5 minutes. A 10-minute 13,000rpm centrifugation at 4^{o}C was then performed before the supernatant was transferred into a new microcentrifuge tube for immediate analysis or storage for short (-20^{o}C) or long-term (-80^{o}C) basis.

2.2.1.2 Protein quantification

Protein concentration was measured using the Bio-Rad DC protein assay kit (Bio-Rad) according to the manufacturers instructions. This colorimetric assay is based on the Lowry assay and depends on a protein-copper tartrate reaction in alkaline solution, and the subsequent reduction of Folin reagent by the products of this reaction over the course of 10-15 minutes. The resulting degree of blue colour can then be read on a spectrophotometer at 650nm absorbance.

Bovine serum albumin (BSA, Sigma-Aldrich©) protein standards were made in NP40 buffer to create a standard curve and this was performed prior to every assay. 5µl of BSA standard or protein sample were added to separate wells of a 96 well plate. 20µl reagent S (surfactant solution) and 980µl reagent A (alkaline copper tartrate) were combined and 25µl of this new 'reagent A*' was added to each well. Finally 200µl of reagent B (Folin) was added to the wells and a 10-15 minute room temperature incubation was performed before the plate was read on a spectrophotometer (BD Biosciences) at 650nm absorbance. Plotting the standard curve gradient allowed extrapolation and determination of the unknown protein sample concentrations on Excel (Microsoft® Excel® for Mac, 2011).

2.2.1.3 Sodium dodecyl sulphate polyacrylamide gel electrophoresis (SDS-PAGE)

Samples with equal protein concentrations as determined by the prior assay were separated under reducing conditions in SDS-PAGE. Cellular proteins were separated according to their molecular weight using a polyacrylamide gel mounted in a vertical gel electrophoresis apparatus system (Mini Trans-Blot® Cell, Bio-Rad, UK). Polyacrylamide gel mixture of a desired percentage (Appendix A) was hand-cast by pouring in between a glass and a spacer plate (1.5mm thick), locked into a casting stand, and allowed to polymerase for 30-40 minutes at room temperature. A water layer was added to avoid dehydration, which was removed prior to casting of the stacking gel component. This involved adding 2ml of a 4% stacking gel on top of the polymerised resolving gel and inserting a 10 well comb for the second polymerisation stage (20-30 minutes). At this point, the combs were removed and the gels were placed in an electrophoresis tank, which was filled with a running buffer (Appendix A). Cell lysates were boiled at 95^{o}C for 10 mins in the presence of Laemmli buffer containing 5% β-mercapthoethanol then centrifuged and loaded into the individual wells of the stacking gel using capillary

disposable pipette tips. A pre-stained protein ladder (Fermentas) was loaded in parallel wells. The gel was then run for approximately 90 minutes at 150 volts until sufficient protein migration has occurred, indicated by the visible migration of the molecular weight marker. Following completion the gels were carefully removed in preparation for transfer and the apparatus disassembled and cleaned.

2.2.1.4 Immunoblotting

This involved transferring proteins from the gel to a specialised polyvinylidene difluoride (PVDF) membrane. The membrane facilitates high binding efficiency of electroblotted material in the presence of SDS in transfer buffer. Protein transfer was performed using Mini PROTEAN® Tetra electrophoresis system (BIO RAD). Firstly PVDF membrane (Millipore) was activated with 100% methanol, washed in distilled water and then incubated at room temperature in transfer buffer (Appendix A). After running, the gel was removed from the glass plates and together with the membrane it was sandwiched between two stacks of filtered 100% cotton paper (Whatman) and fibre pads in a gel holding cassette, all soaked in transfer buffer. The cassette was placed in direct contact with plate electrodes in a transfer chamber filled with transfer buffer, together with an intra-chamber icebox, and peri-chamber ice packing to prevent over-heating. The protein transfer process was run at 80 volts for 80 minutes.

After completion, the membrane was incubated at room temperature on a rocking plate in blocking solution (5% non-fat dry milk, 0.1% PBS-Tween) for 1 hour to prevent non-specific binding. Following a 5 minute wash in PBS-Tween solution (0.1%), the blots were incubated in primary antibody overnight at 4°C. The following day, the membrane was washed three times for 10 minutes in 0.1% PBS-Tween and then incubated with HRP - conjugated secondary antibody (Invitrogen) raised against the corresponding host primary antibody species in a blocking solution for 1 hour at room temperature. After a final triplicate wash in 0.1% PBS-Tween a chemiluminiscent substrate (SuperSignal West Pico Chemiluminiscent Substrate; Thermo Scientific) was added onto the membrane. Detection was performed using ChemiDoc™ software (BIO RAD). If required, re-blotting was preceded by a 15-20 minute incubation with stripping buffer prior to further antibody incubation. HSC70 was routinely utilised as a loading control. A range of antibodies used in this study are listed in Appendix A.

2.3 Gene silencing

2.3.1 siRNA interference

All siRNAs used in this study are listed in Appendix A. All commercially available siRNAs were resuspended upon delivery in DEPC (diethylprocarbonate)-treated water to a 20µm stock solution, aliquoted and stored at -20^{o}C until use. For the transfection process, cells were initially plated in 6-well plates (Falcon) at 5x10^{4}/ well in standard growth medium and allowed to adhere for 24 hours. Oligofectamine 2000 reagent (Invitrogen/Life Technologies Ltd.) was used for all transfections, in the absence of serum.
Prior to transfection, cells were washed once with OptiMEM® reduced-serum medium (GIBCO™, Invitrogen, Life Technologies Ltd.) and then 800µl of OptiMEM was added into each well. The required amount of siRNA was diluted in OptiMEM® to form a duplex solution (solution A; total volume 203µl). 3µl Oligofectamine™ reagent was diluted in 13µl OptiMEM® to form a 16µl transfection solution (solution B, vortexed after mixing). After 10 minutes incubation at room temperature, these solutions were combined and mixed prior to a further incubation at room temperature for 20 minutes (total volume 219µl [solution C]). Following this final incubation period, 200µl of solution C was pipetted drop-wise to each well of the 6-well plate. Culture plates were returned to humidified incubators for 4 hours prior to the addition of 500µl of cell line specific culture medium, supplemented with 30% serum. Transfected cells were used in functional assays at varying time points post-transfection and knockdown was confirmed by Western blotting or PCR.

siRNA optimisation was performed for TNS3 and CTEN sequences (Appendix B). Briefly, cells were transfected as per the above protocol using different siRNA formulations. Cells were lysed at 24 hours and 48 hours post transfection and subsequent immunoblotting was performed to determine optimal protein knockdown.

2.3.2 Generation of stable knockdown cell line

As a more durable alternative to transient siRNA transfection and to minimise the potential for off-target effects, stable CTEN knockdown cells were created by the introduction of small hairpin RNA (shRNA) into our cells of interest. The introduction of shRNA using viral vectors into our cells of interest allowed analysis and comparison of the

effects of long-term CTEN gene knockdown and was also employed for the *in vivo* methods. SCC25 cell line was used for all shRNA work and subsequent functional analysis.

2.3.2.1 Determining sensitivity of target cells to Polybrene®:

SCC25 cells were initially plated in 6-well plates (Falcon) at $5x10^4$/ well in standard growth medium and allowed to adhere for 24 hours; On day 2, 1000x stock concentration of Polybrene® (Santa Cruz) was diluted in standard growth media to make 4 concentrations (2, 4, 6 & 8 ug/ml) and a standard growth media control was also included. 1ml of each concentration was added to relevant cell wells and cells were returned to a 10% CO_2 humidified incubator at 37^oC. Cell viability was observed for 72 hours by microscopic examination. No change in cell viability, conformation, or confluency between different concentrations was observed and 8ug/ml was therefore selected for subsequent use in shRNA introduction.

2.3.2.2 Puromycin kill curve:

SCC25 cells were initially plated in 6-well plates (Falcon) at $5x10^4$/ well in standard growth medium and allowed to adhere overnight. The following day culture medium was replaced with medium containing varying concentrations of puromycin (control, 0.25, 0.5, 1, 2, 4ug/ml). Media was replenished every 3 days and wells were observed microscopically for viability and the percentage of cell death. The most appropriate puromycin concentration killing cells within 5-10 days after addition of antibiotic was selected (2ug/ml), and this was in keeping with previously published protocols in the SCC25 cell line (Le et al., 2000).

2.3.2.3 Target cell infection

To produce a stable CTEN knockdown cell line, human shRNA lentiviral particles (4 unique 29mer target-specific shRNA, 1 scramble control; see Appendix A for individual sequences) were purchased from Origene. The shRNA expression cassette (Fig. 2-1) consists of a 29 bp target gene specific sequence, a 7 bp loop, and another 29 bp reverse complementary sequence, all under human U6 promoter together with a GFP tag.

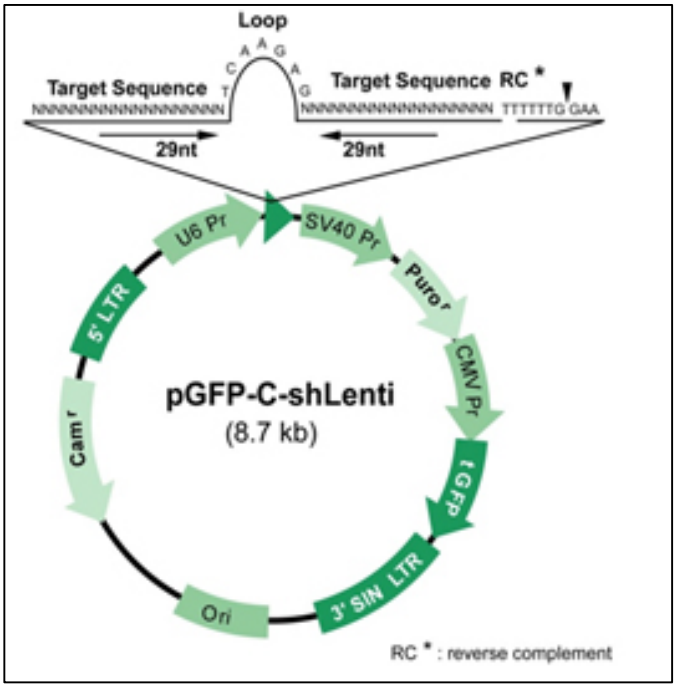

Figure 2-1. Map of shRNA expression cassette used to create stable cell line. Figure reproduced from Origene (http://www.origene.com/shRNA/vector_information.aspx).

SCC25 cells were seeded at $6x10^5$/ $25cm^2$ flask (1 flask per infection plus one for mock infection to determine adequate selection) in standard growth medium to aim for 50% confluency the following day. Following overnight incubation, medium in each flask was replaced with 3mls of the virus particle mixture comprising: DMEM, 10% FCS, 1% L-Glutamine, 8 μg/ml Polybrene® and viral particles at a MOI (multiplicity of infection) of 2. Transduction units (TU/ml) for each sequence were supplied on purchase to enable accurate MOI calculation. The following day, the particle-containing medium was removed and disposed of using standardised viral precautions and normal culture medium was put on all cells. Later that day, this medium was replaced with puromycin-containing medium at the pre-determined concentration (2ug/ml). Over the next 2-3

weeks, cell cultures were fed with fresh puromycin-containing medium and a pooled cell culture was grown for further experiments. At this point successful gene silencing was confirmed both by examination of GFP expression in monolayer cell cultures and by examination of protein levels with Western blotting (Appendix B) as previously described.

2.4 DNA/ RNA analysis

2.4.1 TaqMan® Real Time Polymerase Chain Reaction (RT-PCR)

The real-time TaqMan® quantitative assay is based on florescence resonance energy transfer (FRET) principle. The TaqMan® probe has a fluorescent reporter dye at its 5' terminus and a quencher located at its 3' end. The quencher is free to interact with the reporter dye in an intact probe, and this interaction inhibits the release of a fluorescent signal. However, in the presence of a target sequence, the probe anneals downstream from one of the primer sites during hybridisation and the 5'-3' exonuclease activity of Taq polymerase results in cleavage of the dual-labelled probe. This permits the release of a fluorescent signal and forms the basis of the fluorophore-based detection system, with the resulting signal allowing quantitative measurements of the accumulation of the target sequence. During the PCR run the computer software constructs amplification plot using the fluorescent emission data.

TaqMan® RT-PCR was performed as a two-stage procedure. First, RNA was extracted from samples to be analysed using RNAeasy Kit (Qiagen) according to manufacturer instructions. Resulting RNA was re-suspended in RNAse–free water, quantified on a spectrophotometer and used immediately or stored at -70C°. Collected RNA was then used to synthesize cDNA using a qScript™ cDNA SuperMix (Quanta Biosciences, VWR) according to manufacturer instructions. In the second step, the TaqMan® assay was performed. Briefly, 5µl of cDNA (10ng/µl) was added in duplicates to a 96- well PCR plate (Applied Biosystems) on ice. A reaction mix was prepared by combining PerfeCTa FastMix II (Quanta Biosciences, VWR), an advanced qPCR reagent system for fast PCR cycling protocols, with 20X TaqMan® MGB probes (Applied Biosystems) and nuclease-free water. Then 15µl of the reaction mix was added to each well and a cover with a lid. The plate was centrifuged at 3000rpm for 1 minute to ensure

the reaction mix and cDNA were mixed at bottom of the wells and air bubbles excluded. The plate was then placed in a 7900HT Fast- Real Time PCR System (Applied Biosciences). The assay was performed using the comparative C_T method, wherein the amount of target DNA was normalized to a housekeeping control (β-actin) to derive relative C_T values.

2.5 Functional assays

2.5.1 Coating with ECM Proteins

As described in Chapter 1.4, integrins mediate attachment of cells to extracellular matrix (ECM) proteins. To study these interactions therefore requires the use of a range of ECM proteins in functional assays to both select and observe the relative activity of different integrins. This requires the coating of working surfaces involved in these assays with specific ECMs, primarily for both adhesion and migration assays.

The ECM proteins utilised are demonstrated in Table 2-2. Whilst the amount used to coat surfaces in different assays was variable, the protocol for coating surfaces always involved a 1-hour incubation of the surface immersed in the ECM mixture at the stated concentrations at 37^{o}C. Heat-inactivated bovine serum albumin (BSA; 0.1%) was used as control for non-specific binding. Surfaces were then blocked with migration buffer (the corresponding serum- and growth factor-free medium for each cell line supplemented with 2mM L-glutamine and 0.1% heat-inactivated BSA) for 30 minutes.

ECM protein	**Concentration**	**Source**
Human recombinant fibronectin	20µg/ml	Sigma Aldrich
TGFβ Latency- associated peptide (LAP)	0.5µg/ml	Sigma Aldrich
Rat tail collagen type I	10µg/ml	Millipore

Table 2-2. List of extracellular matrix (ECM) proteins used in functional assays (Transwell® migration and XCELLigence adhesion assays).

2.5.1.1 Adhesion/Proliferation Assays

The XCELLigence Real Time Cell Analyser (RTCA) (Roche) allows researchers to measure cell adhesion and proliferation in real time in a label-free environment, thus providing a more physiologically relevant assay than traditional end-point assays. The technology uses microelectrodes, incorporated onto the under-surface of custom E-16 View plates (Roche). Cell contact and adherence to the bottom of the well results in an increased electrical impedance across the electrode/solution interface which can then be recorded and displayed graphically as relative change (Cell Index).

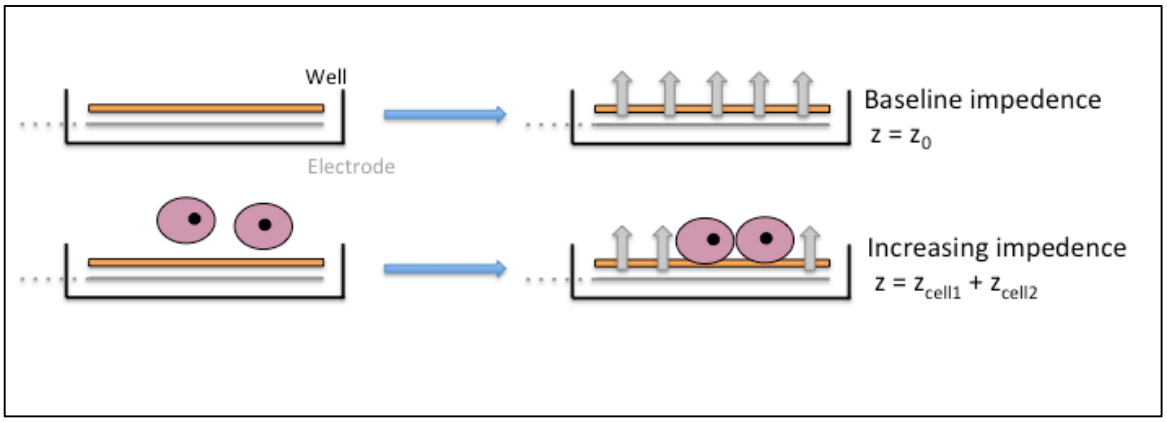

Figure 2-2. Principle of XCELLigence assay detection. In the absence of cells microelectrodes detect baseline impedance. When cells attach to the electrode and spread there is an increase in electrical impedance. Adapted from Urcan *et al* (Urcan et al., 2010)

For adhesion assays, the bottom of the E-16 plate was coated with a desired ECM-protein (80µl/ well) as described previously. Following the 1h incubation, the ECM solution was carefully aspirated and replaced with 100µl of cell line-specific migration buffer at room temperature for 30 minutes. The E-plate plate was then inserted into the analyser and baseline readings and plate connections were checked using the manufacturers software. Once connections were confirmed and correct, the plates were carefully removed and a 100µl cell suspension ($2x10^4$) was seeded on the top of 100µl of migration buffer, and the plate was then placed back in the XCELLigence analyser at 37°C. Proliferation assays, were performed in the same manner without the coating step and with normal serum containing medium. Electrical impedance was measured every 2min for 4-8h (adhesion) or every 10min for 48-72h (proliferation assays).

In addition to the XCELLigence automated form of proliferation analysis, simple well-based proliferation counts were also performed on both transient (siRNA) and stable (shRNA) CTEN knockdown cells to verify results. Briefly, cells were plated in wells of a 24

well plate $5x10^4$ in triplicates in serum-containing medium. Cells were left to proliferate for 48 hours and then trypsinised and counted on the CASY counting system (Innovatis AG, UK/Roche Diagnostics GMBH).

2.5.2 3-dimensional proliferation assays

In order to analyse the effects of CTEN on cell proliferation in a more physiological 3D environment, prolonged assays to count cell proliferation of cells suspended in a collagen gel were performed. Briefly, collagen gels were prepared on ice, comprising 7 volumes of rat tail collagen type I (Millipore), 1 volume of 10x DMEM (Sigma Aldrich), 1 volume of serum and 1 volume of SCC25 cells (control/CTEN siRNA transfected or shRNA transduced) suspended at final concentration of $5x10^4$ cells/ml. The mixture was neutralised by addition of 0.1M sodium hydroxide with gentle mixing. 1 ml of this mixture was pipetted into each well of a 24-well plate and allowed to polymerize for 1 hour at 37°C. Subsequently, 1ml of 10% DMEM was added on the top of each gel to prevent dehydration, and incubated at 10% CO_2 and 37°C until assay completion. At each desired time point for proliferation count, media was aspirated from the control and knockdown cell containing gels and replaced with 10% collagenase (Sigma). The gels were placed on a 37°C heating plate and left on a plate shaker for 1-2 hours until complete gel digestion had occurred. Cell counts were then determined using the previously described CASY automated cell counter.

2.5.3 Transwell® migration assay

Haptotactic cell migration was measured using Corning Transwell® inserts (Costar®, Sigma Aldrich), a specialised insert containing a porous polyethylene tetraphthallate membrane (6.5mm diameter and 8µm pore size) which divides a well into an upper and lower chamber (Fig. 2-3).

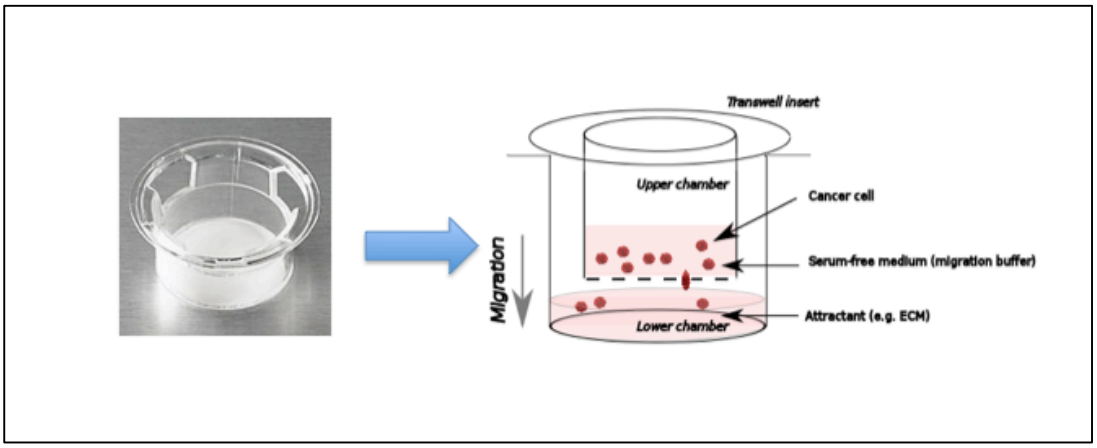

Figure 2-3. Schematic representation of a Transwell ® migration assay. The bottom of each Transwell® has a porous membrane (pore size 8µm), which is coated with an ECM protein. Cells are plated in the top chamber, in the presence of migration buffer, and allowed to migrate across into the bottom chamber.

Cells plated in the top chamber migrate stimulated by an ECM protein towards the bottom chamber and are counted on the automated cell counter at the end of the assay. Alternatively serum-containing medium was used as a chemoattractant in the lower chamber to observe non-integrin specific migration. Each experimental condition is repeated in triplicate and wells were coated with ECM specific to the experiment as previously described. To determine non-specific migration, the under-surfaces of control wells were coated solely with migrating (serum-free) buffer. Cells resuspended at equal concentrations in migration buffer were seeded at $5x10^4$/well into the upper chamber and allowed to migrate at 37^{o}C overnight into the lower chamber. For blocking experiments, cells were incubated with appropriate blocking concentrations of antibodies (αυβ6 (63G9) or α5β1 (12G10)) at 4^{o}C for 30 minutes prior to seeding into the Transwell inserts. Surplus cells not used in the assay were lysed to confirm protein knockdown.

The following day cells which had migrated into the bottom chamber were washed with PBS, detached by addition of 0.5ml trypsin to the bottom chamber with inserts still in place, and incubated at 37°C for 60 minutes. Subsequently, 0.5ml of trypsin/cell solution was added to 9.5ml of filtered CASYton solution and counted using CASY counter as described previously.

2.5.4 Matrigel® invasion assay

Cell invasion was measured in a similar fashion to migration assays i.e. using Transwell® inserts, but a protein gel used at the upper/lower chamber interface. This protein gel comprised a 70µl mixture of alpha MEM and Matrigel® (BD Biosciences) at 2:1 ratio and allowed to polymerise at 37°C for 1h. 500µl of serum-containing medium was added to the bottom chamber of Transwell® act as an attractant for cell invasion. Cells ($5x10^5$) re-suspended in 200µl of alpha MEM (GIBCO) were added into the top chamber, on the top of Matrigel®, and incubated for 72 hours at 37°C to allow sufficient cell invasion (Fig. 2-4). After this time cells from the bottom chamber were washed once with PBS and detached with 0.5ml trypsin and counted on CASY counter in standard fashion.

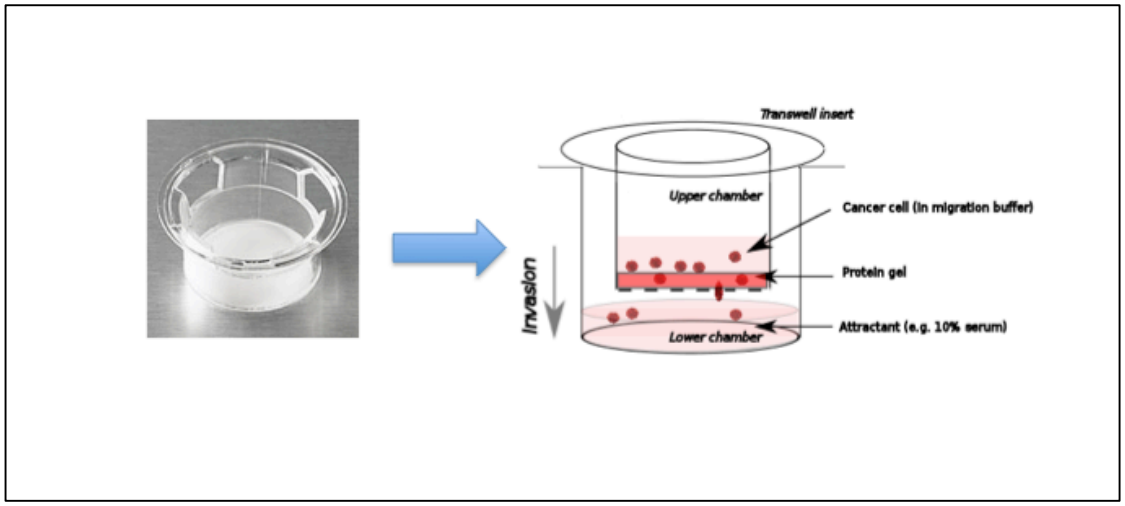

Figure 2-4. Schematic representation of a Transwell® invasion assay. The bottom of each Transwell® contains an alpha MEM/Matrigel gel layer. Cells must invade through this gel towards a serum-containing medium in the bottom chamber

2.5.5 Scratch wound assay

A scratch or wound-closing assay allows analysis of individual cell and collective cell migration under the stimulation of a scratch in a confluent cell monolayer. This technique utilised time-lapse microscopy to take serial image captures to allow real time analysis of the wound closure progress.

Cells were plated at $8x10^5$/well in a 6-well plate and allowed to adhere to form a confluent layer overnight. The next day a scratch along the centre of the well was introduced with a sterile P200 pipette tip and ruler guide. All wells were washed with

migration buffer to remove any detached cells, and finally 1ml of migration buffer was added to each well.

The 12- well plate was then placed on a heated stage (37°C) in an environmental chamber connected to Olympus IX81 microscope (located in the Bio-imaging Unit, Southampton General Hospital). The CO_2 flow was connected to the plate using a 0.8mm needle. The Cell^P software was set up to image two different fields within each well over 12-48h, taking a picture every 5min using a 20X objective of Zeiss AxioCam MRm camera, together with automatic focussing. Collected images were processed using ImageJ software. To track individual cells from both sides of the wound a Manual Tracking plugin was employed, while directionally of cell movement was determined with Chemotaxis Tool plugin.

2.5.6 Organotypic culture assays (HNSCC)

Organotypic cultures were prepared based on the principles and techniques described by Nystrom et al (2006).

Gel preparation

Organotypic gels were prepared on ice, comprising 3.5 volumes type I rat tail collagen (Millipore), 3.5 volumes Matrigel (Becton-Dickinson), 1 volume 10x DMEM, 1 volume fetal calf serum and 1 volume of 10% DMEM containing $2.5x10^5$/ml HFFF2 cells. The mixture was neutralised by addition of 0.1M sodium hydroxide with gentle mixing. 1 ml of this mixture was pipetted into each well of a 24-well plate and allowed to polymerize for 1 hour at 37°C. Subsequently, 1ml of 10% DMEM was added on the top of each gel to prevent dehydration, and left overnight at 10% CO_2 and 37°C.

Cell seeding and nylon sheets

24h after gel polymerization, medium was aspirated from the gel and a mixture of HNSCC ($5x10^5$) cells and HFFF2 fibroblasts ($25 x10^4$) in a combined volume of 1ml of DMEM was added drop- wise onto top of the gel. The gels were then left for a further 24 hours at 37^oC. Concurrently, autoclaved nylon sheets (pore diameter 100µm) were coated with a solution containing 7 volumes of rat-tail collagen type I (Millipore), 10x DMEM, serum and 10% DMEM (1 volume each). The coating solution was neutralised when necessary, and incubated with nylon sheets for 30 minutes at 37°C. Then, coated sheets were fixed with

10% glutaraldehyde (Sigma Aldrich) in PBS for 1 hour at 4°C and then washed three times with PBS and once with 10% DMEM. The nylon sheets were stored in 10% DMEM at 4°C.

Assembly

24h after cell seeding (day 3 of experiment) the organotypic cultures were assembled in a 6-well plate. An autoclaved stainless steel grid (2.5cm^2), with its sides bent down to form 4-5mm 'legs', was placed in the bottom of a single well. A coated nylon sheet was positioned carefully on the centre of the grid. To transfer the organotypic gel, first medium was aspirated off the gel, and a sterile spatula was used to carefully detach it from the sides of the 24-well plate. The gel was the lifted with the spatula, and raised on the top of nylon sheet. Finally 4.8ml of growth medium was added to bottom of the well. The media was thus just reaching the undersurface of the grid, forming a liquid-air interface at this lower gel level. Where radiation exposure of the gels was required, assembled organotypic grids and cultures were transferred to the radiation chamber and exposed to 1x2 Gray clinical radiation dose. The assembled organotypic culture was then placed in the incubator (10% CO_2, 37°C) and grown for 7 days. Medium in the bottom of the plate was replaced every 2 days. After 7 days the gels were bisected, fixed in formal-saline and processed to paraffin. Sections (4 µm) were stained for H&E +/- pan-cytokeratin.

2.6 Flow cytometry

Flow cytometry was utilised to study cell surface integrin changes following manipulation of Tensin proteins. Cells to be labelled with appropriate antibodies were trypsinised, washed in cell-specific migration buffer and counted on the automated CASY cell counter. Cells were resuspended at a concentration of 1x10^5 cells/150 µl equally in a 96-well plate in 1ml FACS buffer (Appendix A). Subsequent steps were performed on ice with centrifugation performed at 4°C. Cells were pelleted by centrifugation at 1250rpm for 3 minutes. Supernatant was poured off and cells were then incubated with 100µl 10% human serum (Thermo Scientific) for 30 minutes, ensuring adequate mixing by pipetting. After this time, a further 100µl FACS buffer was added and another centrifugation at 1250rpm was performed. Cell were then re-suspended in 50µl primary antibody conjugated to an appropriate flourochrome, and incubated for 15 minutes on ice in the

dark. FACS buffer alone was used for control, non-stained cells. After the incubation, cells were washed twice with 150 µl FACS buffer and pelleted by centrifugation for 3 minutes at 2000 rpm in between washing steps. Labelled cells were then scanned on a BD FACS Canto II cytometer (BD Biosciences™) by acquiring $1x10^4$ events. Compensation if required was performed before sample acquisition using single stained populations. Voltage, forward and side scatter settings were also manually adjusted to optimise cell population visualisation prior to sample acquisition and recording. Analysis was performed using FlowJo Version X.0.7 (Treestar, OR). Data was then plotted as median fluorescence (arbitrary units) intensity.

2.7 Functional TGFβ assays

2.7.1 TGFβ activation assay

The effect of Tensins on TGF-β1 activation was studied using an MLEC luciferase assay (Abe et al. 1994), which relies on the ability of active TGFβ1 to induce expression of plasminogen activator inhibitor type-1 (PAI-1). The MLEC cells used stably express a construct containing a TGFβ1 responsive PAI-1 promoter fused to the firefly luciferase reporter gene. Thus stimulation with active TGFβ causes a luminometrically measureable increase in the luciferase enzyme activity. Previous studies have confirmed that the truncated PAI-1 promoter is highly specific for TGFβ1 and is minimally influenced by other known PAI-1 inducers (Abe et al., 1994b; van Waarde et al., 1997).

MLEC cells were seeded in 96-well plates at a concentration of $5x10^4$ cells/well and cultured at 37°C, 10% CO_2 for 24 hours. Following this, our transfected cells of interest were trypsinised from their plates and seeded at $8x10^4$ cells/well on top of the MLEC monolayer, which is serum-starved for 4 hours prior to co-culturing. Each well is plated with 6 repeats. This co-culture is allowed to incubate overnight. After a minimum of 20 hours, all cells are prepared for the assay using the luciferase assay kit (Promega) according to manufacturers instructions. Briefly, 25µl of reporter lysis buffer (Promega) was added to each well and the plate was transferred to -80°C for a minimum of 30 minutes. The plate was then defrosted at room temperature, each well scraped with a 10µl pipette tip and the plate was centrifuged at 2600rpm for 10 minutes at 4°C. 20µl of supernatant was then transferred to a white bottom 96-well plate, 50µl of luciferase assay substrate (Promega) was added and luminescence measured using a Varioskan

plate reader. A standard curve to known TGFβ concentrations (human recombinant) was produced in triplicate for each experiment. For inhibitor experiments using monoclonal blocking antibodies, the cancer cells were incubated with the specific antibody for 30minutes at 4^{o}C prior to their plating on top of the MLEC cells.

2.7.2 Co-culture

To examine the importance of Tensins on myofibroblast differentiation, co-culture experiments were performed utilising transfected knockdown cells and HFFF2 fibroblast cell cultures. 1x10^{5} HFFF2s were plated in 6-well plates and 5x10^{4} HFFF2s were plated on 13mm glass coverslips and allowed to adhere overnight. The following day, the same number of transfected cancer cells, following trypsinisation, were plated on top of the HFFF2s. Control wells of just HFFF2s and cancer cells individually were included alongside all experiments. Once the cancer cells had adhered, the medium was changed for serum-free medium on the cells and for one of the HFFF2 alone control wells, 2μg/ml TFGβ1 was added as a positive control. All plates were then incubated at 37^{o}C for a further 24 hours. At this point cells on cover slips were fixed and stained for immunofluorescent analysis or collected from the 6-well plates for immunoblotting/PCR analysis.

2.7.3 Immunofluorescence

Glass coverslips (13mm) were placed in 24-well plates and coated with collagen I (10μg/ml) before incubation at 37^{o}C for 1 hour. Excess collagen mixture was then aspirated and the cover slips washed in situ with 250μl serum-free media appropriate to the cell line to be used. The cancer cells to be analysed were then counted as previously described and 7x10^{4} cancer cells were plated on top of the cover slips. A variable incubation time at 37^{o}C was then performed depending on whether adherent or spreading cells were to be used (range 1-6 hours). Cells were then fixed with 4% paraformaldehyde (Sigma Aldrich) in PBS for 10 min and then permeabilised using 0.1% Triton X-100/PBS for 20 min. Blocking was performed for 30 min in 3% bovine serum albumin/PBS, and then samples were incubated with primary antibody for 2 h in 0.6% bovine serum albumin/PBS, followed by species-specific secondary antibody. The secondary antibodies comprised Alexa Fluor 594-conjugated anti-mouse or anti-rat immunoglobulin G (Molecular Probes). Cells were counterstained with 1 μg/ml DAPI

(4',6'-diamidino-2-phenylindole; Sigma Aldrich) +/- TRITC-conjugated Phalloidin (Merck Millipore, USA) at a dilution of 1:1000 for 15 minutes at the end of the secondary-antibody incubation. A final 3 wash cycle comprising 2 x PBS and 1 x water wash was completed and coverslips were carefully mounted on slides with fluorescent mounting medium (Dako Cytomation) and allowed to dry overnight before imaging. The following day, all cells were visualized using a Zeiss Axiovert 200 fluorescence microscope with a 40x or 100x oil objective, and images were collected using an Orca-ER digital camera (Hamamatsu) and processed using Openlab 3.5.1 Software (Improvision). Identical exposure times were applied for different images within the same experiment.

2.8 Metabolic assays

2.8.1 Glucose assay

The glucose assay (Sigma) runs on the principle that following glucose oxidation to gluconic acid and hydrogen peroxide, the latter reacts with o-dianisidine in the presence of peroxidase to form a colorimetrically measureable product. Reagents were prepared according to manufacturers instructions and a standard curve was created by diluting glucose standard to a range of concentrations. At the start of the assay, 2ml of Assay Reagent was added to each tube and mixed. Each tube was incubated at 37^{o}C for exactly 30 minutes at which time the absorbance was read on a rapid read protocol by a Varioskan™ (Thermoscientific) plate reader at 540nm.

2.8.2 Seahorse Extracellular Flux (XF) Analyser

Seahorse XF Analyser (Seahorse Bioscience) measures mitochondrial respiration and glycolysis and allows for real-time environment alterations through the use of injection ports. Stress test kits were used to determine *in vitro* oxygen consumption rate (OCR) and extracellular acidification rate (ECAR) as a measure of glycolysis. Seahorse uses cartridges, each containing 96 probes with two fluorophores, which are quenched by oxygen or free protons, providing information about cellular respiration and extracellular acidification, respectively (Fig. 2-5)

One day before the experiment, cells ($2x10^4$) were plated in 80µl of growth medium in a XF96 culture plate (Seahorse), while the probes were immersed in XF Calibrant Solution (Seahorse; lacking sodium bicarbonate and FCS) overnight at 37°C in non-CO_2 incubator. Running medium was prepared using glucose-free DMEM (Sigma Aldrich) supplemented with 10% serum, 2mM L- glutamine (PAA) and 1mM sodium pyruvate (PAA), and the pH was adjusted to 7.4 at 37°C. The following day, drugs from mitochondrial and glycolysis stress kits (Seahorse) were diluted in running medium to desired concentrations, and loaded into injection ports of the probe cartridge. Medium used for washes and injections was kept in water bath at 37°C throughout the experiment. Cells were washed twice with 200µl of running medium, and the plate was placed in a non-CO_2 37°C incubator. A protocol was designed based on the desired investigations but briefly, OCR and ECAR were measured over a 3 minute period, followed by 3 min mixing and re-oxygenation of the media. Once the experiment protocol had been designed on the custom Seahorse software, the assay cartridge was placed first into the instrument to allow automatic calibration of optical probes. When this process was complete, the cells had a final wash and 180µl of running medium was added into each well. This was allowed to warm for 5 minutes prior to insertion into the flux analyser.

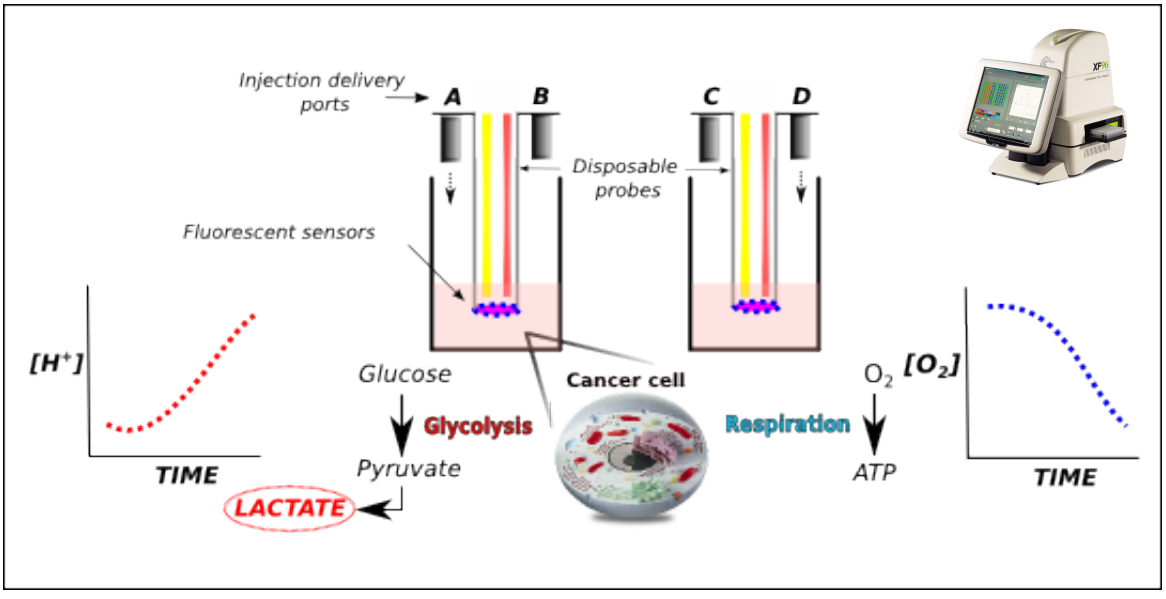

Figure 2-5. Principles of Seahorse XF Analyser. Cancer cells generate ATP preferentially through aerobic glycolysis, to produce lactic acid. Mitochondria can also use oxygen to generate ATP through respiration. Oxygen and free protons excreted by cells into their medium are detected by special probes and recorded as oxygen consumption rate (OCR) and extracellular acidification rate (ECAR) respectively. Readings are then sent via fibre-optic channels to the Analyser. In between measurements, probes are lifted up to allow proper mixing of the

medium. Up to four different drugs can also be loaded into the drug ports located within the probe cartridge. Adapted from Seahorse Bioscience (www.seahorsebio.com).

Measurements of OCR and ECAR were taken at 2-minute intervals by placing the probes in the culture medium, just above the cell monolayer. In between readings, probes were lifted up to ensure mixing of the medium. Drugs (20µl/well) were injected at scheduled intervals and the results were analysed using Seahorse software.

2.9 Chromatin Immunoprecipitation (ChIP)

Chromatin immunoprecipitation (ChIP) is a powerful and rigorous technique to investigate the association between proteins and DNA in a cell of interest. DNA-binding proteins play a fundamental role in the regulation of key cellular processes and this technique enables analysis of the DNA regions in the genome where chromatin-associated proteins bind. This method was performed using the MAGnify™ Chromatin Immunoprecipitation System from (Invitrogen by Life Technologies, NY) and followed according to manufacturers instructions. Fig. 2-6 represents a workflow summary of the procedure steps.

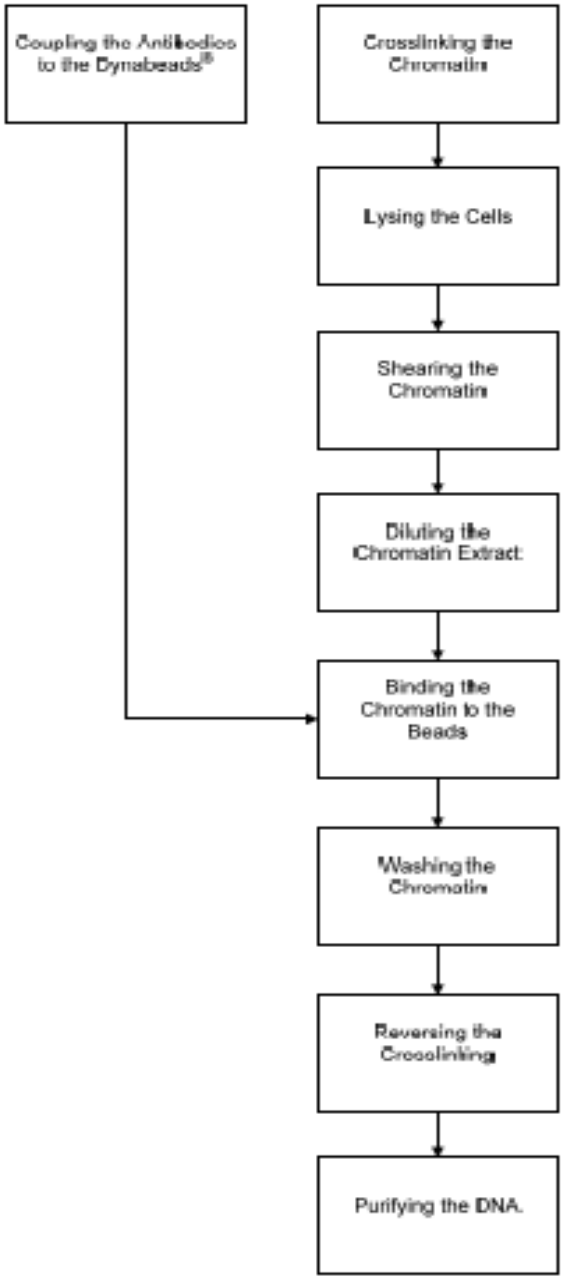

Figure 2-6. System Workflow Diagram for the MAGnify chromatin immunoprecipitation kit, reproduced from product user guide (Publication Number MAN0001631)

ChIP assays were performed using the MAGnify system according to the manufacturer's protocol with a few modifications. Briefly, 3 x 10^6 cells of utilised cell lines at 1x10^5/ChIP reaction were collected and resuspended in 500 µl of phosphate-buffered saline (PBS) at room temperature (RT). Fixation was the performed with 13.5 µl of 37% formaldehyde (RT on a rotator, 10 min) and the reaction was stopped with 57 µl 1.25 M glycine.

Following two washes with ice-cold PBS, 50 µl/1x10^6 cells of supplied lysis buffer (Life Technologies) was added (min. volume 200 µl) to resuspend and the samples immediately prepared for sonication. Focussed-ultrasonication was optimised and then performed on ice at the following settings: (Intensity 3.5, microtip, 5x15 seconds on, 20 seconds off) to reduce DNA length to approximately 100-400bp. Following confirmation of DNA size on a 2% agarose gel (Appendix D), sheared chromatin was aliquoted and snap frozen followed by -70^{o}C storage for later use.

When ready to proceed, the chromatin was thawed on ice and adjusted to 100 µl with dilution buffer and then immunoprecipitated on a rotator overnight at 4^{o}C with magnetic protein A/G beads pre-bound with either rabbit IgG (Life Technologies) or CtBP antibody previously validated for ChIP (E-12 (Santa Cruz); PhD thesis University of Southampton, M. Chrzan, 2014). An aliquot of unbound chromatin was also kept separate as input control and included in all steps subsequent to the immunoprecipitation. The beads were subsequently washed 3 times with IP1 buffer and twice with IP2 buffer before immune complex elution (55 °C, 30 min) and then reverse crosslinking (65 °C, 1 h) was performed in the presence of proteinase K. Finally, DNA purification was performed again utilising magnetic beads and purification buffer wash repeats before final DNA elution (55 °C, 20 min) was performed and collected DNA stored at -20^{o}C until use.

2.9.1 Design of primers

The potential target gene for CtBP transcriptional co- suppressor investigated in this study was CTEN. The CTEN promoter was recently identified by Chen et al. (Chen et al., 2013) through analysis of a 2kb genomic DNA region upstream of the first CTEN exon and from this, they were able to identify the most functionally active 327-bp region (Appendix D). This region therefore was used as the template for primer design using Primer 3 software (version 4.0.0). Utilising an optimal primer size of 20, there were 10 primer pairs designed spanning the sequence of interest with overlapping sequences (Appendix D).

2.9.2 End- point PCR

DNA collected after ChIP was then analysed using end-point PCR and primers design for CTEN promoter, run on a 2% agarose gel. Thermocycler settings were optimised prior to

final ChIP analysis (Table 2-3). The reaction was set up on ice using a PCR master mix (Megamix-blue (Microzone, Sussex, UK)). All reagents were thawed on ice, and the reaction solution containing 18 µl master mix, and 0.5 µl of both forward and reverse primer were prepared in 0.5ml PCR tubes. Finally 1 µl of sample DNA was added to the side of the tub and then the solution was spot centrifuged immediately prior to heating. Using a pre-heated block, cycling conditions were as follows:

1 cycle	95°C	30 seconds
36 cycles	95°C	30 seconds
	57°C*	30 seconds
	72°C	30 seconds
1 cycle	72°C	1 minute
1 cycle	4°C	infinite

Table 2-3. Cycling conditions used for ChIP end point PCR reactions. The annealing temperature (*) was optimised prior to final settings

2.10 AZD3965 concentration response optimisation

AZD3965 (AstraZeneca, Waltham, MA) was reconstituted according to the manufacturers instructions to a working stock concentration of single use aliquots at 1uM solution in DMSO. These were stored at −20°C. SCC25 cells ($5x10^5$) were plated into 10cm dishes the day prior to initiation of treatment with AZD3965. A full range of treatment concentrations were tested from 0.01nM through to 1000nM and a DMSO control was also included. Media was replaced after 24 hours. At 48 hours the cells were trypsinised and counted prior to the proliferation assay preparation step.

For this proliferation assay, the E-16 plate wells were filled with 100µl of cell line-specific medium at room temperature for 30 minutes. The E-plate plate was then inserted into the analyser and baseline readings and plate connections were checked using the manufacturers software. Once connections were confirmed and correct, the plates were carefully removed and a 100µl cell suspension ($2x10^4$) was seeded on the top of the warmed medium, and the plate was then placed back in the XCELLigence analyser at

37°C. Electrical impedance was measured every 10min for 48 hours and kill curves were then analysed for the full range of AZD3965 concentrations. From this analysis, 10nM inhibitor concentration was selected as the most appropriate functional dose for drug analysis, consistent with recent publications using the same compounds (Polański et al., 2014). Cells were exposed to AZD3965 for 48 hours prior to use in functional assays.

2.10.1 Clonogenic survival assay

SCC25 cells were treated with 10nM and 100nM AZD3965 or a DMSO control for 48 hours prior to the start of the survival assay. Following prior optimisation of optimal cell density, treated SCC25 cells were then trypsinised, counted and seeded in 6-well plates at 2000 cells/well. AZD3965/DMSO containing media was replaced after 24 hours and then left in situ for 10 days until conclusion of the experiment. Cells were then fixed in a 3% crystal violet/10% formalin solution. Following collation of scanned images, the 'ColonyArea' plugin of Image J (Rasband, 1997), allowing automated thresholding and analysing was used and this enabled calculation of both % area and intensity of colonies.

2.11 Immunohistochemistry

Immunohistochemistry staining for CTEN was initially optimised on whole thyroid tissue sections (papillary, follicular, colloid goitre). Slides were first deparaffinised in clearane (2x10 minutes) and then rehydrated through graded alcohols. Endogenous peroxidases were then blocked using a 0.5% solution of hydrogen peroxide in methanol (10 minutes). The sections were then washed in Tris-buffered saline prior to antigen retrieval. Citrate buffer was made from 2.1g sodium citrate crystals in 1litre water together with titrated NaOH to obtain a pH of 6. The slides were then heated for 20 minutes in a microwave in this 0.01M citrate buffer. After 3 x 2 minute TBS washes, Avidin (20 min) and Biotin (20 min) blocking solutions were used on the slides to quench non-specific binding sites and the primary antibodies applied at a range of dilutions (1:100, 1:200, 1:500) to find the best ratio. Negative controls using incubation buffer with no primary antibody was used to observe non-specific staining. The slides were left to incubate overnight at 4^{o}C.

The following day the slides were returned to room temperature before three further TBS 5 minute washes. Biotinylated secondary antibodies against the appropriate primary antibodies were then applied at a dilution of 1:400 for 30 minutes. Another 3x5

minute TBS wash cycle was performed and the slides were then exposed to the streptavidin-biotin-peroxidase complex at a dilution of 1:200 again for 30 minutes. After a final wash cycle, the sections were covered using diaminobenzidine as a chromogen for 5 minutes. This was rinsed off and the slides then washed in running tap water for 5 minutes, before being counterstained for 1 min exactly in Mayer's haematoxylin (1% w/v haematoxylin, 0.11M ammonium aluminium sulphate, 0.001M sodium iodate, 0.0048M citric acid, 0.3M chloral hydrate). Having been returned to the running tap water for another 5 minutes the sections were dehydrated back through graded alcohols (2 mins each) and cleared in clearane (5 mins). DPX mounting medium was used to mount the slides in perspex with cover slips and the slides were left to dry at room temperature. Once optimal antibody staining dilutions had been determined, automated immunostaining (Ventana XT, Ventana, Tucson, AZ, USA) was performed in a CPA-accredited clinical cellular pathology department for HNSCC tissue samples.

2.12 Tissue microarray

A previously constructed TMA library was used for archived tissue IHC analysis(Ward et al., 2014). This library consisted of 260 patients who had archived pathological material available, out of a total cohort of 442 consecutively treated patients with oropharyngeal squamous cell carcinoma from University Hospital Southampton (2000-10), Poole NHS Foundation (2000-6) and Bart's and the London NHS Trust (2000-6). Patients had been excluded from this cohort if they had a duration of follow up under 6 months, had received either no treatment or treatment without curative intent, or had an unknown cause of death. Full demographic and clinicopathological data had been collated from these patients including: age, set, site, smoking status, alcohol intake, T stage, N stage, treatment modality, treatment failure, tumour recurrence, date and cause of death. This study was approved under ethics codes: UKCRN 8130, ISRCTN 71276356; and REC references 09/H0501/90 and 07/Q0405/1. Tissue microarrays (TMAs) were constructed using triplicate, randomly selected, paraffin-embedded 1-mm tumour cores (Aphelys Minicore 2, Mitogen, Harpenden, UK) by Toby Mellows and Maria Lopez. Following a trial staining of a number of tissue sections utilising the automated system and independent review of the stained slides by GT and KM, a 1:200 concentration of CTEN antibody was utilised with a high pH (Tris-EDTA buffer (pH 9.0)) antigen retrieval protocol. TMA Scoring

was performed by KM and JF independently blinded to the clinical outcome variables as 'absent-low' [Low] or 'moderate-high' [High]. For analysis, tumours confirmed as HPV-positive had to be positive for both p16 immunohistochemistry and HPV ISH (Robinson et al., 2010).

2.13 RNA sequencing data

2.13.1 SCC25 cell line CTEN knockdown analysis

In order to identify potential target genes and pathways involved in CTEN signalling, RNA sequencing was employed on paired samples on which CTEN expression had been silenced. Three separate paired experiments were performed on SCC25 cells from different batches at similar passages. Each experiment involved siRNA transfection with control or CTEN siRNA as previously described and collection of cells at 24 hours. RNA was extracted from samples to be analysed using RNAeasy Kit (Qiagen) according to manufacturer instructions. Resulting RNA was re-suspended in RNAse–free water, quantified on a spectrophotometer and RNA quality was determined using Bioanalyser analysis (Agilent Technologies Inc.) to obtain RNA integrity numbers prior to downstream processing. Following confirmation of CTEN knockdown by PCR as previously described, 250-300ng of total RNA at a minimum concentration of 25ng/ul was sent to Expression Analysis Genomic Services (Durham, USA). RNA sequencing was performed using Illumina Truseq Stranded protocol, with paired end sequencing and 20 million reads per sample. Reads were mapped to the human genome (hg19) with Tophat 2.0.13 (Trapnell et al., 2009), indexed and sorted with Samtools -1.2 (Li et al., 2009) and counted using HTSeq (Anders et al., 2014) to allow normalisation and differential gene expression analysis.

2.13.2 Clinical patient data

RNA had previously been isolated from HNSCC tumour samples from 10 HPV-positive and 13 HPV- negative subjects. Clinical HPV status determined by both p16-positivity and *in situ hybridization* (*ISH*) was concordant with the RNAseq read data for CDKN2A. Reads were mapped to the human genome (hg19) with Tophat 2.0.13 and counted using HTSeq.

Raw counts were normalized through trimmed mean of M-values (TMM) method and differential expression analysis performed using DESeq (Anders and Huber, 2010).

2.14 *In vivo* orthotopic model

Male athymic nude Ncr-nu/nu mice, 6–8 weeks of age, were purchased from Charles River (UK) and housed in a pathogen-free animal facility. All animal procedures were performed in accordance with a previously published protocol for oral orthotopic models (Myers et al., 2002) and under a local project license for orthotopic models (Project license holder: Professor Alex Mirnezami). Stable CTEN knockdown SCC25 cell line and their transduced controls were used and following collection and counting, 50,000 cells/30ul additive free DMEM were prepared. Mice were put into two groups of 10 for control or CTEN knockdown cell injection. All of the mice were anaesthetised with an inhalational agent (isoflurane/O_2 mix) and underwent submucosal tongue injection of the allocated cell line directly into the anterior tongue using a 100ul Hamilton syringe (Hamilton Co.; Fig. 2-7) with a 30 gauge hypodermic needle. Injections were performed in batches of 5, alternating between control and knockdown groups to minimize any potential bias for altering injection technique. Mice were examined once weekly for the development of tongue tumours and sacrificed when they had lost >20% of their preinjection body weight. Soft diet was instigated once any tumour was visible. Following termination, mice were imaged on fluorescence imager (IVIS, Perkin Elmer) to identify those with potential cervical metastasis and help direct dissection. All tongue tumours and pathological cervical lymph node specimens were then processed for histopathological examination. Tumour volume (V) was calculated using the volume formula: ($V=½ (LxW^2)$), where L= length and W= width (Dhani et al., 2014).

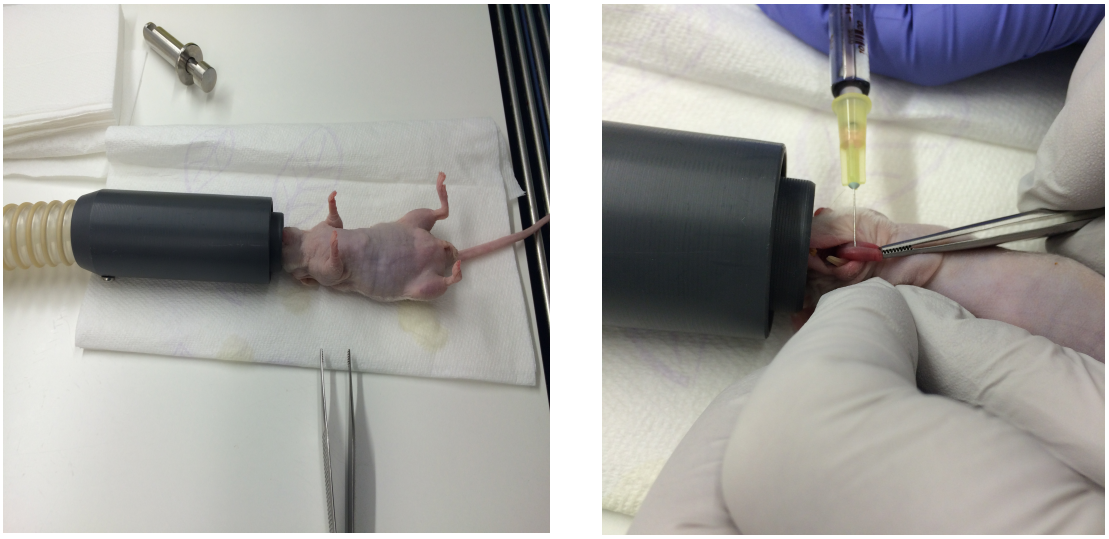

Figure 2-7. Orthotopic tongue injection. Mice were individually sedated with inhalation isoflurane/O_2 and then underwent submucosal tumour cell injection following gentle tongue protrusion. Tongue manipulation was relaxed prior to needle withdrawal to minimise tumour cell extrusion.

2.15 Statistical analysis

For comparisons between experimental groups in functional assays, a Student's T-test was utilised employed (Prism v6 for Mac, Graphpad Software). Statistical significance was taken at $p<0.05$ and on graphs was annotated as follows: * = $p<0.05$; ** = $p<0.01$; *** = $p<0.001$; **** = $p<0.0001$. Errors correspond to standard deviation unless otherwise stated.

For TMA/database analysis, SPSS Statistics (v21 for Mac, IBM) was used. The primary endpoint was death from OPSCC (i.e., disease-specific survival (DSS)). An OPSCC-specific survival time was measured from the date of diagnosis until date of death from OPSCC or date last seen alive. Death from other causes or loss to follow up was marked as censored for analysis. Patients with an unknown cause of death or who only received palliative treatment were excluded from survival analysis. Kaplan–Meier plots (with log-rank tests) and both unadjusted and adjusted Cox proportional hazards models were used to analyse the survival data.

Chapter 3: Clinical relevance of CTEN expression in head and neck cancer

3.1 Introduction

The vast majority of head and neck cancer disease comprises squamous cell carcinoma (HNSCC; >95%) but despite a lack of significant change in the 5-year overall survival rate, patients presenting with early stage disease (I and II) actually have a 60-90% chance of cure with current treatment modalities, depending on anatomical location (Brockstein et al., 2004). However prognosis is highly dependent on lymph node and distant metastasis and late presentation of disease (III and IV) accounts for over 60% of new diagnoses (Duray et al., 2014). Whilst there is promise with new large genomic studies in identifying potential novel disease markers (Lawrence et al., 2015), there has been a dearth of clinical studies translating promising pre-clinical work to the oncology clinic to adequately address prognostic factors in this diverse disease. Human papillomavirus (HPV) status remains the most robust and important disease marker for HNSCC (Cardesa and Nadal, 2011). Given the impact of late disease stage on prognosis, the inability to molecularly screen and identify early disease together with the lack of accurate prognostic biomarkers remains a significant hurdle to improving overall survival. With recent developments in large data genomic characterisation of HNSCC, the focus is now shifting towards identifying clinically relevant genomic and proteomic alterations that can be examined in HNSCC clinical studies to assess validity.

Tensins are focal adhesion adaptor proteins that have recently been implicated in a variety of cancer types and CTEN (or Tensin-4) in particular has been the most investigated to this point. As well as exhibiting a relatively restricted pattern of expression in normal human tissues (Lo, 2014), CTEN appears to be the prime candidate member of the Tensin family mediating an oncogenic effect, although there are conflicting reports in which tumour suppressor functions have been reported (Albasri et al., 2011; M. Katz et al., 2007; Y. Li et al., 2010; Martuszewska et al., 2009; Sjoestroem, Khosravi, Zhang, Martinka, & Li, 2013). The mechanism of biological action is also unclear, with studies implicating integrin-mediated effects on cell motility (Katz et al., 2007), a signalling role through activation of kinase pathways (Albasri et al., 2011b), regulation of molecular switches involving Rho GTPase-activating proteins (Liao et al., 2007), EGFR signalling activity (Hong et al., 2013) and interaction with β-catenin (Liao et al., 2009).
The function and clinical importance of CTEN in HNSCC has not previously been investigated but given the importance of direct tumour invasion and locoregional

recurrence in this disease, CTEN is a prime candidate gene for further study. To this end, we performed immunohistochemistry analysis of a large head and neck cancer patient cohort, corroborated clinical findings with true orthotopic *in vivo* models and employed next generation RNA sequencing to identify potential implicated biological pathways.

3.2 Clinical correlation of CTEN expression in oropharyngeal cancer

To examine clinical relevance we investigated the expression of CTEN in a large cohort of HNSCC patients related to clinicopathological features and survival. Patients for this analysis were taken from a cohort of consecutively treated patients (n=442) with oropharyngeal squamous cell carcinoma (OPSCC) from University Hospital Southampton (2000-10), Poole NHS Foundation (2000-6) and Bart's and the London NHS Trust (2000-6), collated by Mr. Matthew Ward (Ward et al., 2014). 260 patients from this cohort had archived pathological material available and were therefore included in the analysis. Tissue microarrays (TMAs) were constructed using triplicate, randomly selected, paraffin-embedded 1-mm tumour cores (Aphelys Minicore 2, Mitogen, Harpenden, UK) by Toby Mellows and Maria Lopez and staining/scoring performed as outlined in Chapter 2.12. Tumours confirmed as HPV-positive had to be positive for both p16 immunohistochemistry and HPV ISH (Robinson et al., 2010). In order to examine the prognostic relevance of CTEN expression, we scored CTEN levels in the TMA samples as absent/weak or moderate/strong staining. Scoring was performed by two independent blinded scorers (JF, KM), the latter a Specialty Registrar in Pathology. Patient demographics for the study population are shown in Table 3-1, including clinicopathological details at the time of diagnosis and subsequent primary treatment.

Of the 260 patients included in the study, 146 (56%) were classified with HPV-positive disease. Median follow-up was 58 months with a minimum follow-up of 8 months. Overall disease stage tended to be more advanced (Stage III/IV) in HPV-positive (92.4%) compared to HPV-negative disease (69.9%). Despite this, distant metastatic disease was rarer in the HPV-positive disease group (0.7%) compared to the HPV-negative group (2.6%). There was a trend for stronger CTEN staining scores in HPV-negative (73.7% of cases) compared to HPV-positive disease (41.4%). HPV-positive OPSCC patients in this cohort had a mean estimated survival of 9.04 years (CI 9.246-9.831; non-parametric

median not available in this model) and a 78% 5-year survival (SE 0.038). HPV- negative patients on the other hand a mean estimated survival of 5.293 (CI 4.334-6.253) and a median survival of 3.5 years (CI 1.662-5.338) and a 46% 5-year survival, which is comparable with other published reports (Ang et al., 2010; Fakhry et al., 2008; Marur et al., 2010).

Table 3-2 shows the univariate and multivariate hazard ratios (HR) for OPSCC mortality for each factor individually, together with associated P-values. In agreement with previous studies, patients with HPV-negative tumours had significantly worse disease-specific survival compared with HPV-positive disease (HR 3.11 (2.00-4.86)). Worse prognosis was significantly associated with HPV-negative tumours, an older age at diagnosis (>70 years), heavy smokers (defined as >10 pack year history (Ang et al, 2010; Gillison et al, 2012)) and advanced T-stage tumours (T3/4). Importantly, reduced survival was also significantly associated with a high CTEN staining score. A multivariate analysis was performed adjusting HRs for age, T-stage and smoking status, which were all significant variables in univariate analysis. CTEN remained a statistically significant marker of OPSCC mortality. These analyses however only demonstrated grouped OPSCC disease and Table 3-3 demonstrates the multivariate analysis repeated, but subdivided into HPV-positive and –negative patients, which is of greater clinical relevance. An enter method for Cox regression analysis was performed and CTEN score remained a significant prognostic value on both univariate and multivariate analysis for both HPV-negative and HPV-positive disease. In order to determine the prognostic performance of a high CTEN score, we analysed the sensitivity, specificity and resulting likelihood ratio for this metric, related to the chance of death from OPSCC disease. In HPV-negative disease, a high CTEN score has a resulting sensitivity of 79%, specificity of 31.6% and the positive likelihood ratio was therefore 1.15. In HPV-positive disease in comparison, sensitivity of CTEN score was 63.3%, with a specificity of 64.7% and a likelihood ratio of 1.79.

Consistent with these findings, analysis using Kaplan-Meier curves with Log Rank analysis to compare the survival distributions by CTEN score, demonstrated high CTEN scoring to be associated with reduced disease-specific survival compared to tumours exhibiting a low CTEN score in overall OPSCC disease and HPV-positive disease (log-rank = 0.001; Fig. 3-1). There was similar trend in survival distribution between high and low CTEN scoring in HPV-negative patients although this did not quite reach significance (log-rank = 0.062).

	All OPSCC		HPV-positive OPSCC		HPV-negative OPSCC	
	Frequency	%	Frequency	%	Frequency	%
Final HPV status						
Negative	114	*43.8*	-	-	-	-
Positive	146	*56.2*	-	-	-	-
Gender						
Female	68	*26.2*	36	*24.7*	32	*28.1*
Male	192	*73.8*	110	*75.3*	82	*71.9*
Age at diagnosis						
<50	54	*20.8*	39	*26.7*	15	*13.2*
50-69	157	*60.4*	88	*60.3*	69	*60.5*
70+	49	*18.8*	19	*13.0*	30	*26.3*
Smoking						
Non smoker/Ex-smoker	103	*48.8*	78	*62.9*	25	*28.7*
Current smoker	108	*51.2*	46	*37.1*	62	*71.3*
Alcohol						
Non-drinker/Ex drinker	31	*16.0*	18	*16.1*	13	*15.9*
Current drinker	163	*84.0*	94	*83.9*	69	*84.1*
Overall stage						
I/II	45	*17.4*	11	*7.6*	34	*30.1*
III/IV	213	*82.6*	134	*92.4*	79	*69.9*
Tumour stage						
Tis/T1/T2	157	*64.3*	99	*69.2*	58	*57.4*
T3/T4	86	*35.2*	43	*30.1*	43	*42.6*
Tx	1	*0.4*	1	*0.7*	0	*0.0*
Nodal metastases						
No	51	*21.0*	12	*8.5*	39	*38.6*
Yes	192	*79.0*	130	*91.5*	62	*61.4*
N stage						
N0-N2a	82	*33.7*	33	*23.2*	49	*48.5*
N2b-N3	161	*66.3*	109	*76.8*	52	*51.5*
Distant Mets at presentation						
No	240	*98.8*	141	*99.3*	99	*98.0*
Yes	3	*1.2*	1	*0.7*	2	*2.0*
Tumour grade						
Well/moderately differentiated	89	*34.2*	29	*19.9*	60	*52.6*
Poorly differentiated	171	*65.8*	117	*80.1*	54	*47.4*
Primary Treatment						
Surgery	103	*39.6*	56	*38.4*	47	*41.2*
Chemo-RT or RT alone	141	*54.2*	86	*58.9*	55	*48.2*
None/Palliative	16	*6.2*	4	*2.7*	12	*10.5*
CTEN score						
Absent/weak	116	*50.4*	86	*58.9*	30	*26.3*
Moderate/strong	114	*49.6*	60	*41.1*	84	*73.7*

Table 3-1. Clinicopathological features of oropharyngeal cancer (OPSCC) patient database. Frequencies along with % are listed, for total patient cohort, and divided by human papillomavirus (HPV) status.

	All OPSCC			
	Univariate HR (95% CI)	*P*-value	Multivariate HR (95% CI)	*P*-value
Age				
For each additional year	1.03 (1.02-1.05)	***<0.0001***	1.04 (1.01-1.06)	***0.001***
HPV status				
HPV +ve	1		1	
HPV-ve	3.11 (2.00-4.86)	***<0.0001***	3.04 (1.67-5.53)	***<0.0001***
Gender				
Female	1		1	
Male	1.36 (0.82-2.25)	*0.23*	1.20 (0.67-2.17)	*0.54*
Smoking				
Non smoker/Ex smoker/<10 pack year	1		1	
>10 pack years	2.34 (1.41-3.87)	***0.001***	2.09 (1.25-3.49)	***0.005***
Alcohol				
Non-drinker/Ex drinker	1		1	
Current drinker	0.64 (0.35-1.16)	*0.14*	0.56 (0.29-1.06)	*0.076*
Overall stage				
I/II	1		1	
III/IV	1.29 (0.71-2.32)	*0.4*	0.01 (0.23-1.61)	*0.31*
Tumour stage				
Tis/T1/T2	1		1	
T3/T4	2.83 (1.82-4.40)	***<0.0001***	2.87 (1.75-4.71)	***<0.0001***
Nodal metastases				
No	1		1	
Yes	1.13 (0.65-1.95)	*0.675*	1.20 (0.645-3.17)	*0.72*
N stage				
N0-N2a	1		1	
N2b-N3	1.28 (0.79-2.06)	*0.32*	1.14 (0.67-1.94)	*0.62*
Treatment				
Surgery +/- radiotherapy	1		1	
Radiotherapy	1.64 (0.91-2.94)	*0.1*	1.13 (0.52-2.42)	*0.76*
Chemoradiotherapy	0.96 (0.55-1.69)	*0.89*	0.90 (0.45-1.83)	*0.78*
Cten score				
Absent/weak	1		1	
Moderate/strong	3.13 (1.93-5.06)	***<0.0001***	2.80 (1.62-4.86)	***<0.0001***

Table 3-2. Univariate and multivariate analysis of all OPSCC patients. Hazard ratios (HR) are displayed together with the 95% confidence intervals. Multivariate analysis adjusted for age, T stage, and smoking status. Significant P-values (<0.05) are shown in bold type. CTEN scoring remained significant on multivariate analysis.

	HPV +ve OPSCC			HPV-ve OPSCC		
	Univariate HR (95% CI)	Multivariate HR (95% CI)	*P*-value	Univariate HR (95% CI)	Multivariate HR (95% CI)	*P*-value
Age						
For each additional year	1.03 (0.98-1.00)	1.02 (0.98-1.06)	0.37	1.03 (1.00-1.05)	1.03 (1.00-1.05)	***0.04***
Gender						
Female	1	1		1	1	
Male	1.63 (0.66-3.99)	1.70 (0.56-5.16)	*0.35*	1.34 (0.73-2.45)	1.24 (0.57-2.67)	*0.59*
Smoking						
Non smoker/Ex smoker/ <10 pack years	1	1		1	1	
>10 pack years	4.79 (1.87-12.26)	5.73 (2.16-15.23)	***<0.0001***	0.52 (0.28-0.95)	0.61 (0.33-1.13)	*0.115*
Alcohol						
Non-drinker/Ex drinker	1	1		1	1	
Current drinker	0.66 (0.25-1.78)	0.43 (0.13-1.48)	*0.18*	0.61 (0.29-1.28)	0.69 (0.30-1.55)	*0.364*
Overall stage						
I/II	1	1		1	1	
III/IV	2.45 (0.33-17.98)	0.30 (0.03-3.40)	*0.33*	2.13 (1.12-4.04)	1.09 (0.36-3.31)	*0.883*
Tumour stage						
Tis/T1/T2	1	1		1	1	
T3/T4	4.07 (1.94-8.53)	4.98 (2.10-11.82)	***<0.0001***	1.93 (1.11-3.34)	1.73 (0.94-3.19)	*0.076*
Nodal metastases						
No	1	1		1	1	
Yes	1.41 (0.33-5.94)	2.27 (0.29-18.02)	*0.44*	2.27 (1.22-4.20)	1.51 (0.48-4.72)	*0.483*
N stage						
N0-N2a	1	1		1	1	
N2b-N3	1.27 (0.51-3.12)	1.11 (0.36-3.42)	*0.86*	2.31 (1.30-4.12)	1.67 (0.88-3.16)	*0.115*
Treatment						
Surgery +/- radiotherapy	1	1		1	1	
Radiotherapy	1.82 (0.63-5.23)	1.06 (0.25-4.46)	*0.94*	1.46 (0.72-2.93)	1.41 (0.57-3.44)	*0.456*
Chemoradiotherapy	1.08 (0.43-2.68)	0.84 (0.26-2.72)	*0.77*	1.40 (0.67-2.91)	1.20 (0.47-3.04)	*0.709*
CTEN score						
Absent/weak	1	1		1	1	
Moderate/strong	3.33 (1.57-7.03)	2.46 (1.02 -5.95)	***0.045***	1.81 (0.95-3.44)	2.21 (1.06-4.62)	***0.035***

Table 3-3. Univariate and multivariate analysis results for OPSCC patients subdivided by HPV status. Hazard ratios (HR) are displayed together with the 95% confidence intervals. Multivariate analysis was performed adjusted for those parameters found to be significant factors on univariate analysis (age, T stage and smoking status; P values for univariate analysis not shown). P-value for multivariate analyses are shown and significant values are highlighted in bold type. CTEN scoring remained significant on multivariate analysis for both HPV-positive and HPV-negative disease.

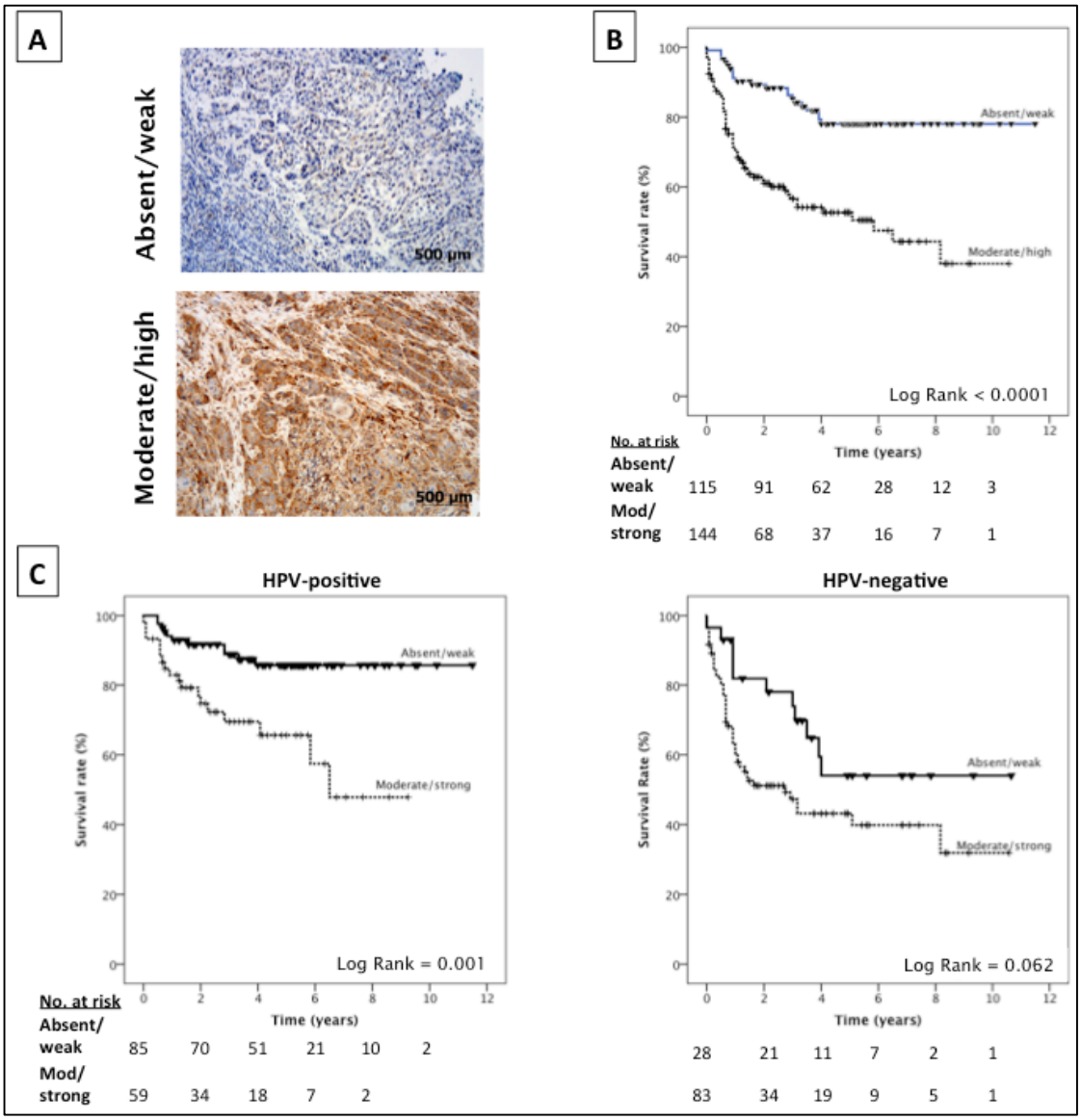

Figure 3-1. Survival analysis for OPSCC dataset. A, example immunohistochemical scoring for CTEN protein is demonstrated following optimisation; two independent raters scored slides as either absent/low or moderate/strong staining. Kaplan-Meier curves were then produced using SPSS Statistics (v21 for Mac, IBM) with disease specific survival as an end-point. Analysis was performed for all OPSCC patients (B), as well as cases split by HPV status (C). Significant log rank scores were obtained for the overall OPSCC dataset, HPV-positive cases and in the subset treated by chemoradiation (chemo/DXT).

3.3 CTEN depletion reduces tumour growth *in vivo*

We have demonstrated through examination of a large OPSCC dataset that CTEN has an important potential clinical relevance in HNSCC. We performed an *in vivo* experiment to test whether CTEN expression would confer a protective effect over the aggressive tumour phenotype of an effective orthotopic oral HNSCC model. In order to study the effect of CTEN expression on cancer cell function we created a stable shRNA-transduced CTEN knockdown cell line with an oral HNSCC cell line (SCC25; see Fig. 4-5A (right panel) or 7.2 (Appendix B) for knockdown confirmation). SCC25 cells treated with either shControl or shCTEN RNA containing a GFP tag were injected into the tongues of nude mice as previously described. The effects of CTEN expression on tumour growth over time were measured using callipers, together with immediate post-mortem fluorescence imaging on a small animal imaging system (IVIS, Perkin Elmer). Specimens were then fixed in formalin for pathological processing and examined by a Consultant Head and Neck pathologist (GT; Fig. 3-2A, left panel). Due to the occasional difficulties distinguishing injection trauma from tumour, for inclusion in volume analysis tumour had to be evident in 2 of 3 modalities (clinical examination, GFP imaging, pathology). Dubious specimens where tumour was only suspected in 1 of the above examinations were excluded from statistical analysis. Due to the difficulty in detecting micro-metastases in cervical lymph node specimens obtained, subtraction fluorescence imaging alone was utilised to determine the presence and number of micro metastases.

Histopathological examination of dissected tumours supported that the model represented an accurate model of head and neck SCC with a classic pathological appearance, as well as features of intralymphatic and perineural invasion (Fig. 3-2A, right panel). No distinct differences in primary tumour morphology between shControl and shCTEN cells were observed. Weekly prospective tumour measurements as well as post-mortem GFP expression analysis revealed a consistent and significant reduction of tumour growth in CTEN depleted tumours. In addition there was an objective reduction in the presence of micro metastases in the CTEN knockdown tumours, although these deposits were not pathologically confirmed. Interestingly there was no significant difference in the tumour formation rate between the two groups.

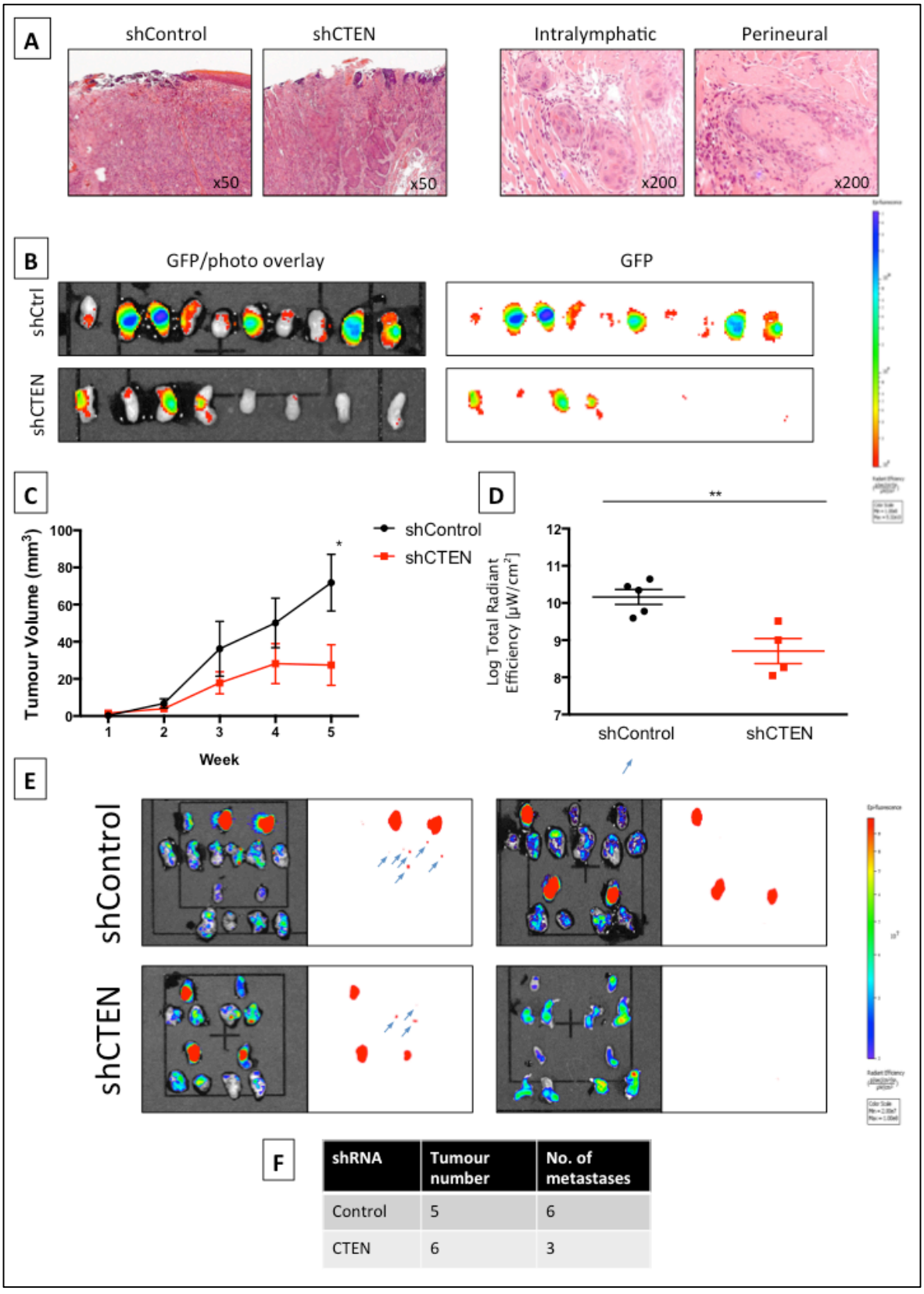

shRNA	Tumour number	No. of metastases
Control	5	6
CTEN	6	3

Figure 3-2. CTEN depletion reduces tumour growth in an orthotopic mouse model of oral cancer. A, xenograft tumours were made by orthotopically injecting shCtrl or shCTEN treated SCC25 cells, allowed to grow for 6 weeks with microcalliper measurement weekly and then dissected and pathologically examined. The orthotopic tumours mimicked the pathological appearance of human HNSCC accurately, including other features of aggressive tumour invasion such as lymphatic and perineural invasion. B, C, D, post-mortem tongue specimens were

dissected and imaged on a small animal imager utilising a GFP tag included with the shRNA vectors. Microcalliper tumour volumes performed prospectively throughout the experiment were then compared with automated radiation efficiency measurements and both corroborated a significant tumour growth reduction in CTEN knockdown tumours (Student *t* test, * p<0.05, ** p<0.01). E, tongue specimens (top specimen in each double row) and bilateral cervical lymph node chains (bottom specimens (2 per animal) in each row) were surgically dissected and imaged for GFP expression. The subsequent image overlays then underwent digital image subtraction to identify tumour deposits in the cervical lymph node biopsies. Suspected micro metastases were labelled (blue arrows) and counted (F). Note – two mouse specimens were not included in the final imaging analysis due to their demise in the week prior to experiment completion. Their results upto the point of death have been included in the growth analysis.

These results support our clinical findings that CTEN is a relevant biological target in HNSCC with both translational and functional relevance, supporting tumour growth and invasion in established tumours. Our clinical correlation between CTEN expression and disease specific survival in a large OPSCC dataset has provided evidence of the potential utility of CTEN as a prognostic marker; however our *in vivo* results also indicate that CTEN may be an exciting target for therapeutic intervention.

3.4 RNA sequencing to study the *in vitro* role of CTEN in HNSCC

There have been a number of recent studies that have explored functional geneset databases in an attempt to identify the genomic landscape of HNSCC (Kaddi and Wang, 2015; Lawrence et al., 2015; Pavón et al., 2015), and profiling of 279 HNSCC samples collected through The Cancer Genome Atlas has helped to provide insights into new pathways and targets of potential therapeutic importance (Lawrence et al., 2015). We have demonstrated the functional importance of CTEN in HNSCC. However, despite the increase in recent publications on CTEN and Tensin biology, the mechanism behind these effects, as well as other potential functions of the protein remain unclear. We performed high-throughput RNA sequencing analysis on control or CTEN siRNA treated cells in order to give us the opportunity to explore the functional role of this protein and direct further experiments.

A standardised sequencing pipeline (Chapter 2.14) was utilised for analysis of the raw data to obtain a matrix of differential gene expression affected by CTEN knockdown. Determination of RNA quality by the University of Southampton Bioanalyser facility

together with confirmation of knockdown by PCR is shown in Appendix C. A total of 349 differentially expressed genes (DEGs) were identified by comparing control with CTEN-knockdown SCC25 cells, with 234 up-regulated and 115-down regulated genes (logFC>1, p<0.05). A heat map was produced showing the relative expression of all DEGs, demonstrating clustering between control and CTEN knockdown cells (Fig. 3-3A). This unsupervised clustering method reassuringly showed separate grouping of Control and CTEN siRNA-treated cells. The GoTermFinder server (http://go.princeton.edu/cgi-bin/GOTermFinder) was utilised to identify shared gene ontology (GO) terms from all significant differentially expressed genes (P<0.05) and REViGO tool (http://revigo.irb.hr/) was utilised to remove redundant terms and visualise them in a Treemap, which is a two-level hierarchy of GO terms (Fig. 3-3B). As expected, we observed a large number of terms related to regulation of cell motility and migration. However, there were also a large number of related enriched GO terms appearing more prominently in the analysis, including terms related to signal transduction (e.g. 'positive regulation of signal transduction'), cellular metabolism (e.g. 'regulation of primary metabolic process') as well as cell proliferation and apoptosis (e.g. 'cell death', 'apoptotic process'). These results raise the possibility that previously published CTEN-dependent effects on cell motility may have been affected by functional effects on alternate cell signalling pathways and cell survival.

The GeneMANIA server (Warde-Farley et al., 2010) was used to predict network interactions between the DEGs, using the top 20 related genes and the inbuilt weighting system. Networks were visualised using Cytoscape for Mac (v3.3.0; http://www.cytoscape.org/index.html). From the 234 up-regulated and 115 down-regulated genes, GeneMANIA recognised 234 and 103 genes respectively. GO enrichment terms over-represented in the constructed networks for both up- and down-regulated genesets were extracted and listed (Fig. 3-4A&B), and the full lists were used to create corresponding interaction networks (Fig. 3-5A&B). DEG lists were then combined and graphically represented and validated using the Reactome webserver (Croft et al., 2014; Milacic et al., 2012), which uses a 'reaction' as the central class, with biological events as subclass classifications (Fig. 3-5C). Whilst all these analyses encompass a large number of GO terms, there are a number of interesting and novel findings. There is corroboration between these terms and the previous GO enrichment from all DEGs with the inclusion of a number of cell death and proliferation terms. However collating both GO sets, there is

notable inclusion of cell differentiation, extracellular matrix assembly and epithelial-mesenchymal transition as well as response to viral infection.

In addition to this network analysis, we also performed an MCODE clustering algorithm (Bader and Hogue, 2003) which detected a total of 8 and 4 clusters in the up-regulated and down-regulated DEG networks. Using a cut-off of clusters containing >10 nodes and a minimum MCODE score of 5.0, only 6 in the former and 1 clusters in the latter were selected and these are displayed in Appendix C (Figure 7-3). In order to examine potential protein interaction networks, our DEG groups were then mapped separately into the Search Tool for the Retrieval of Interacting Genes (STRING) database (Jensen et al., 2009), which contains functional links between proteins based on both published experimental evidence as well as predictive genomics. For our purpose, a confidence score of >0.4 was used for interaction analysis. Protein-protein interaction (PPI) networks for both up- and down-regulated DEGs were then visualised on Cytoscape (v3.3.0). A total of 229 nodes and 102 nodes were incorporated into the up- and down-regulated networks respectively. In addition, the network was further analysed by MCODE and a total of five sub-network clusters were identified. This highest scoring cluster from up- and down-regulated PPI networks is shown in Fig. 3-6. The functions of these clusters were mainly correlated with TGFβ1 pathway and ECM formation, as well as the immune response to a viral infection.

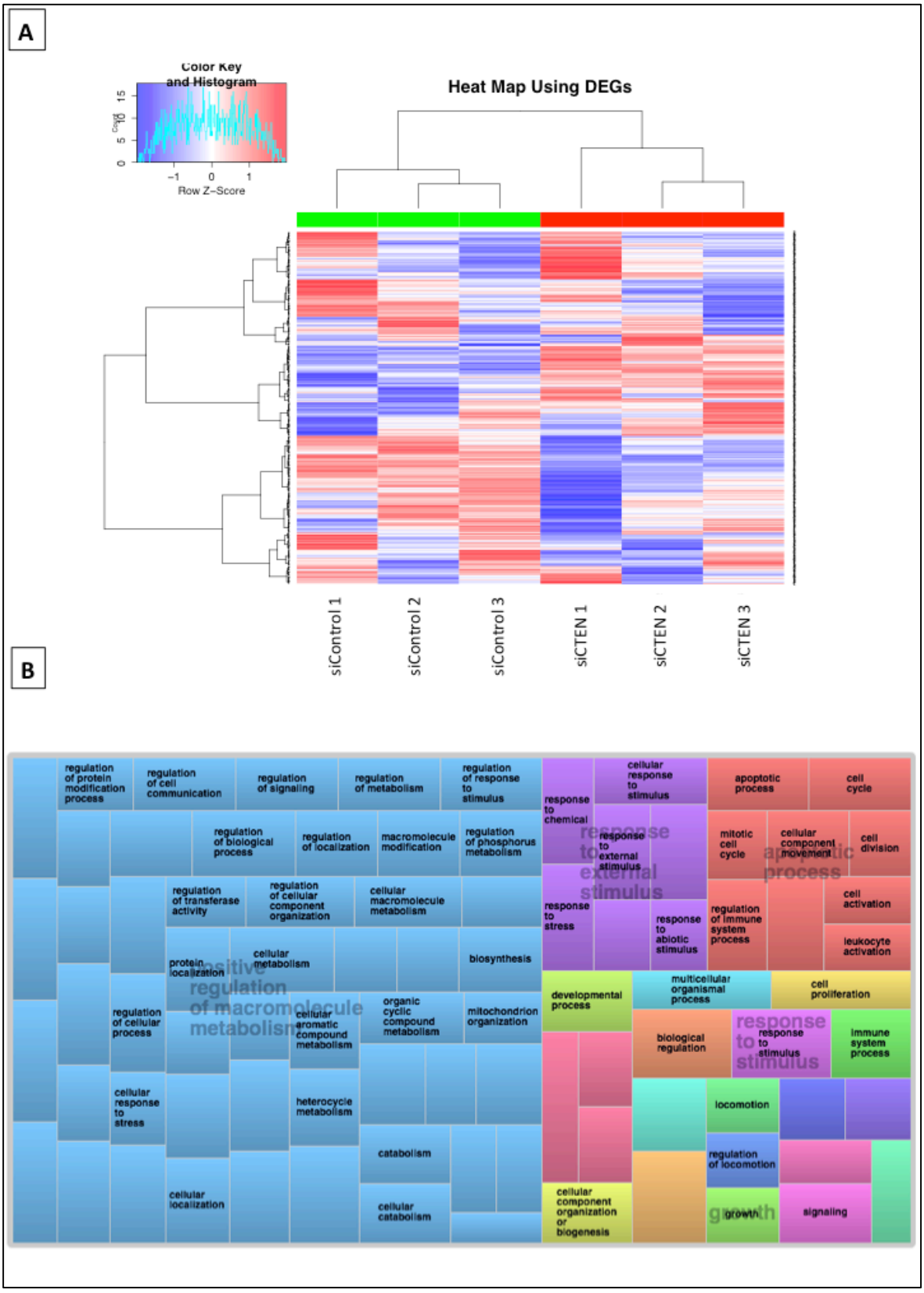

Figure 3-3. A, Heat map showing hierarchical unsupervised clustering analysis of siRNA Control and siRNA CTEN treated SCC25 cells (Abs logFC>1, p<0.05). Red, upregulation, blue downregulation. Heat map produced with aid of Bioinformatics Core, University of Southampton. B, TreeMap visualisation obtained from REVIGO analysis (http://revigo.irb.hr/) of the summary of GO terms for all DEGs (p<0.01) between control and treated samples. Related GO terms with semantic similarity are

grouped in the same colours and the dimensions of the coloured areas are proportional the direction of the impact. Not all terms are shown due to space constraints.

A. Up-regulated

GO id	Description	q-value	Occurrences in Sample	Occurrences in Genome
GO:0090114	COPII-coated vesicle budding	0.0478	4	13
GO:0085029	extracellular matrix assembly	0.0478	4	11
GO:0048207	vesicle targeting, rough ER to cis-Golgi	0.0478	4	13
GO:0060317	cardiac epithelial to mesenchymal transition	0.0478	4	12
GO:0048208	COPII vesicle coating	0.0478	4	13
GO:0007219	Notch signaling pathway	0.0478	9	111
GO:0060419	heart growth	0.0478	5	26
GO:0007178	transmembrane receptor protein serine/ threonine kinase signaling pathway	0.0544	12	218
GO:0031058	positive regulation of histone modification	0.0544	5	28
GO:0043525	positive regulation of neuron apoptotic process	0.0580	4	15
GO:0045596	negative regulation of cell differentiation	0.0580	13	266
GO:0007184	SMAD protein import into nucleus	0.0580	4	16
GO:1901216	positive regulation of neuron death	0.0580	4	16
GO:0030855	epithelial cell differentiation	0.0580	13	263
GO:0035265	organ growth	0.0660	5	33
GO:0060840	artery development	0.0660	5	33
GO:0090100	positive regulation of transmembrane receptor protein serine/threonine kinase signaling pathway	0.0660	6	53
GO:0014855	striated muscle cell proliferation	0.0704	4	18
GO:0060038	cardiac muscle cell proliferation	0.0704	4	18
GO:2001252	positive regulation of chromosome organization	0.0864	5	36
GO:0004674	protein serine/threonine kinase activity	0.0898	13	290
GO:0001704	formation of primary germ layer	0.0899	5	37
GO:0045445	myoblast differentiation	0.0980	5	38
GO:0060389	pathway-restricted SMAD protein phosphorylation	0.0984	5	39
GO:0001706	endoderm formation	0.0984	4	21
GO:0055017	cardiac muscle tissue growth	0.0984	4	21

B. Down-regulated

GO id	Description	q-value	Occurrences in Sample	Occurrences in Genome
GO:0034340	response to type I interferon	6.09E-17	16	75
GO:0009615	response to virus	6.09E-17	22	205
GO:0060337	type I interferon signaling pathway	6.09E-17	16	74
GO:0071357	cellular response to type I interferon	6.09E-17	16	74
GO:0051607	defense response to virus	6.05E-11	14	116
GO:0045071	negative regulation of viral genome replication	8.35E-11	10	38
GO:0098542	defense response to other organism	1.37E-10	16	188
GO:0045069	regulation of viral genome replication	1.58E-09	10	51
GO:0019079	viral genome replication	1.56E-08	10	64
GO:0048525	negative regulation of viral process	1.65E-08	10	65
GO:0043901	negative regulation of multi-organism process	1.12E-07	10	79
GO:0050792	regulation of viral process	1.27E-06	11	134
GO:0043900	regulation of multi-organism process	1.41E-06	13	215
GO:0034341	response to interferon-gamma	1.54E-06	10	105
GO:0043903	regulation of symbiosis, encompassing mutualism through parasitism	1.89E-06	11	142
GO:0071346	cellular response to interferon-gamma	5.53E-06	9	89
GO:0003725	double-stranded RNA binding	1.34E-05	7	45
GO:0060333	interferon-gamma-mediated signaling pathway	3.94E-04	7	73
GO:0035455	response to interferon-alpha	0.0014	4	14
GO:0048738	cardiac muscle tissue development	0.0150	6	85
GO:0035456	response to interferon-beta	0.0180	3	9
GO:0098586	cellular response to virus	0.0425	3	12
GO:0039528	cytoplasmic pattern recognition receptor signaling pathway in response to virus	0.0425	3	12
GO:0055021	regulation of cardiac muscle tissue growth	0.0831	3	15

Figure 3-4. Gene ontology (GO) enrichment terms over-represented in network analysis of both up-regulated (upper) and down-regulated (lower) differentially expressed genesets. Network interactions from RNAseq differentially expressed genes between siControl and siCTEN treated SCC25 cells were discovered using GeneMANIA

(Warde-Farley et al., 2010). GO enriched terms for each visualised network were then extracted in Cytoscape for Mac (v3.3.0).

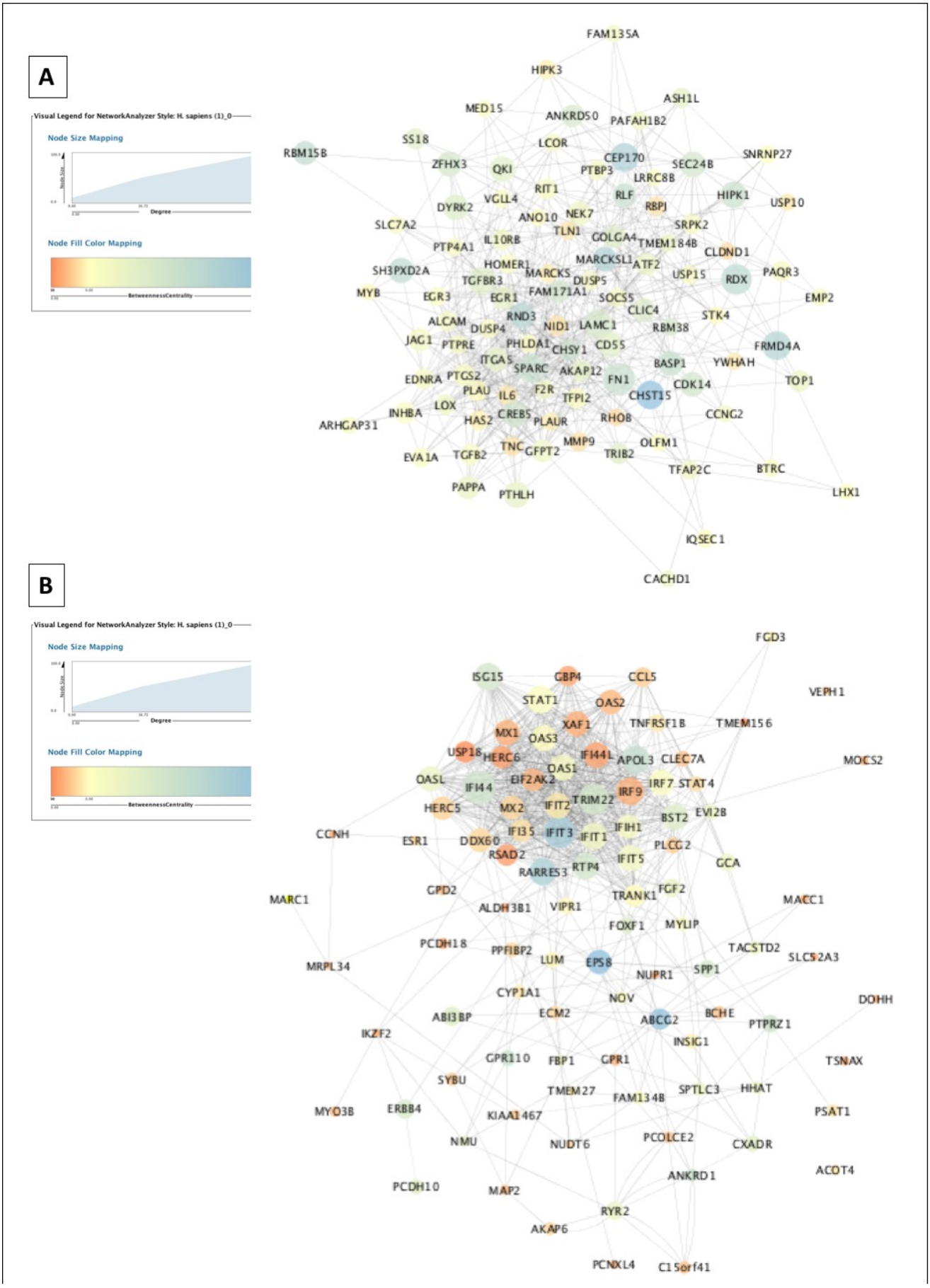
A
Visual Legend for NetworkAnalyzer Style: H. sapiens (1)_0
Node Size Mapping
Degree
Node Fill Color Mapping
BetweennessCentrality
FAM135A
HIPK3
ASH1L
MED15
ANKRD50
PAFAH1B2
SS18
LCOR
RBM15B
ZFHX3
QKI
CEP170
SEC24B
SNRNP27
PTBP3
LRRC8B
RIT1
RLF
HIPK1
USP10
VGLL4
DYRK2
RBPJ
ANO10
NEK7
SRPK2
SLC7A2
TLN1
GOLGA4
TMEM184B
IL10RB
PTP4A1
CLDND1
HOMER1
MARCKSL1
ATF2
SH3PXD2A
MARCKS
USP15
RDX
PAQR3
TGFBR3
DUSP5
MYB
EGR3
EGR1
FAM171A1
SOCS5
EMP2
CLIC4
STK4
ALCAM
RND3
DUSP4
NID1
LAMC1
RBM38
JAG1
PTPRE
PHLDA1
CHSY1
CD55
FRMD4A
ITGA5
SPARC
AKAP12
BASP1
YWHAH
EDNRA
PTGS2
FN1
CDK14
TOP1
PLAU
IL6
F2R
TFPI2
CHST15
LOX
INHBA
HAS2
CREB5
PLAUR
RHOB
CCNG2
ARHGAP31
TNC
MMP9
OLFM1
EVA1A
TGFB2
GFPT2
TRIB2
TFAP2C
BTRC
PAPPA
PTHLH
LHX1
IQSEC1
CACHD1
B
Visual Legend for NetworkAnalyzer Style: H. sapiens (1)_0
Node Size Mapping
Degree
Node Fill Color Mapping
BetweennessCentrality
FGD3
ISG15
GBP4
CCL5
VEPH1
STAT1
OAS2
XAF1
TNFRSF1B
TMEM156
MX1
OAS3
USP18
HERC6
IFI44L
APOL3
CLEC7A
MOCS2
OAS1
OASL
EIF2AK2
IRF7
STAT4
IFI44
IRF9
HERC5
MX2
IFIT2
TRIM22
BST2
EVI2B
CCNH
IFI35
IFIT3
IFIT1
IFIH1
ESR1
DDX60
PLCG2
RSAD2
IFIT5
GCA
RARRES3
RTP4
GPD2
TRANK1
FGF2
MARC1
MACC1
ALDH3B1
VIPR1
FOXF1
MYLIP
PCDH18
TACSTD2
PPFIBP2
SLC52A3
LUM
EPS8
MRPL34
NUPR1
SPP1
CYP1A1
NOV
DOHH
ABI3BP
ECM2
ABCG2
BCHE
PTPRZ1
IKZF2
INSIG1
GPR110
FBP1
GPR1
TSNAX
SYBU
TMEM27
SPTLC3
HHAT
FAM134B
MYO3B
ERBB4
KIAA1467
PSAT1
NMU
NUDT6
PCOLCE2
CXADR
ANKRD1
ACOT4
PCDH10
MAP2
RYR2
AKAP6
PCNXL4
C15orf41

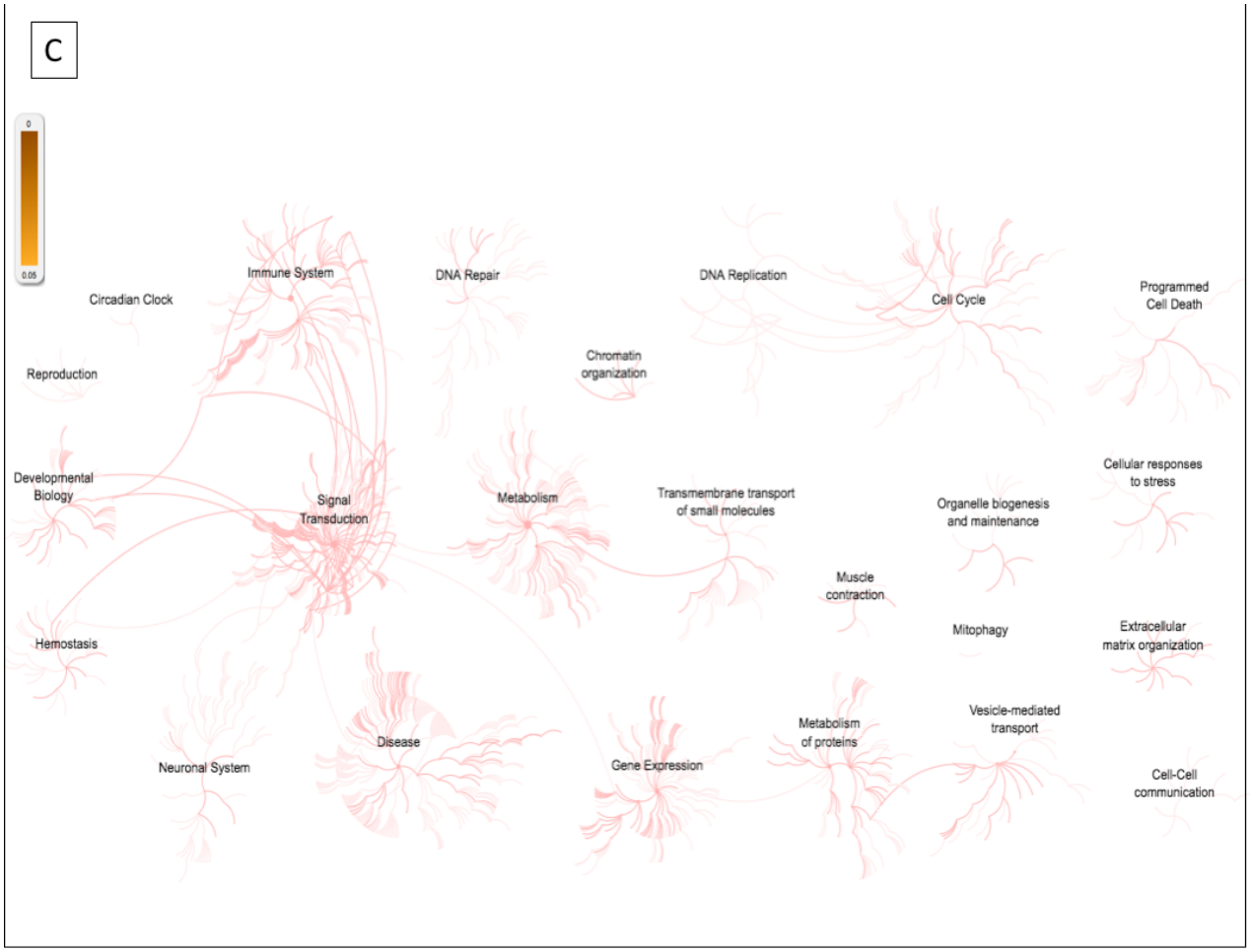

Figure 3-5. Gene network interactions following CTEN knockdown. Network interactions were constructed from 234 up-regulated (A) and 115 down-regulated genes (B; Log2FC>1, P<0.05) following siControl or siCTEN treatment of SCC25 cells using the GeneMANIA server (Warde-Farley et al., 2010). Networks were visualised using Cytoscape for Mac (v3.3.0; http://www.cytoscape.org/index.html). The GeneMANIA force directed layout was employed and network complexity was reduced through utilisation of an in-built filter based on node degree. C, differentially-expressed genes were grouped together and used as input for the Reactome server (Croft et al., 2014; Milacic et al., 2012) **for alternative representation of involved biological pathways. Each node represents a pathway, with the size of the node reflecting the number of entities (proteins, small molecules, genes etc.) belonging to that pathway.**

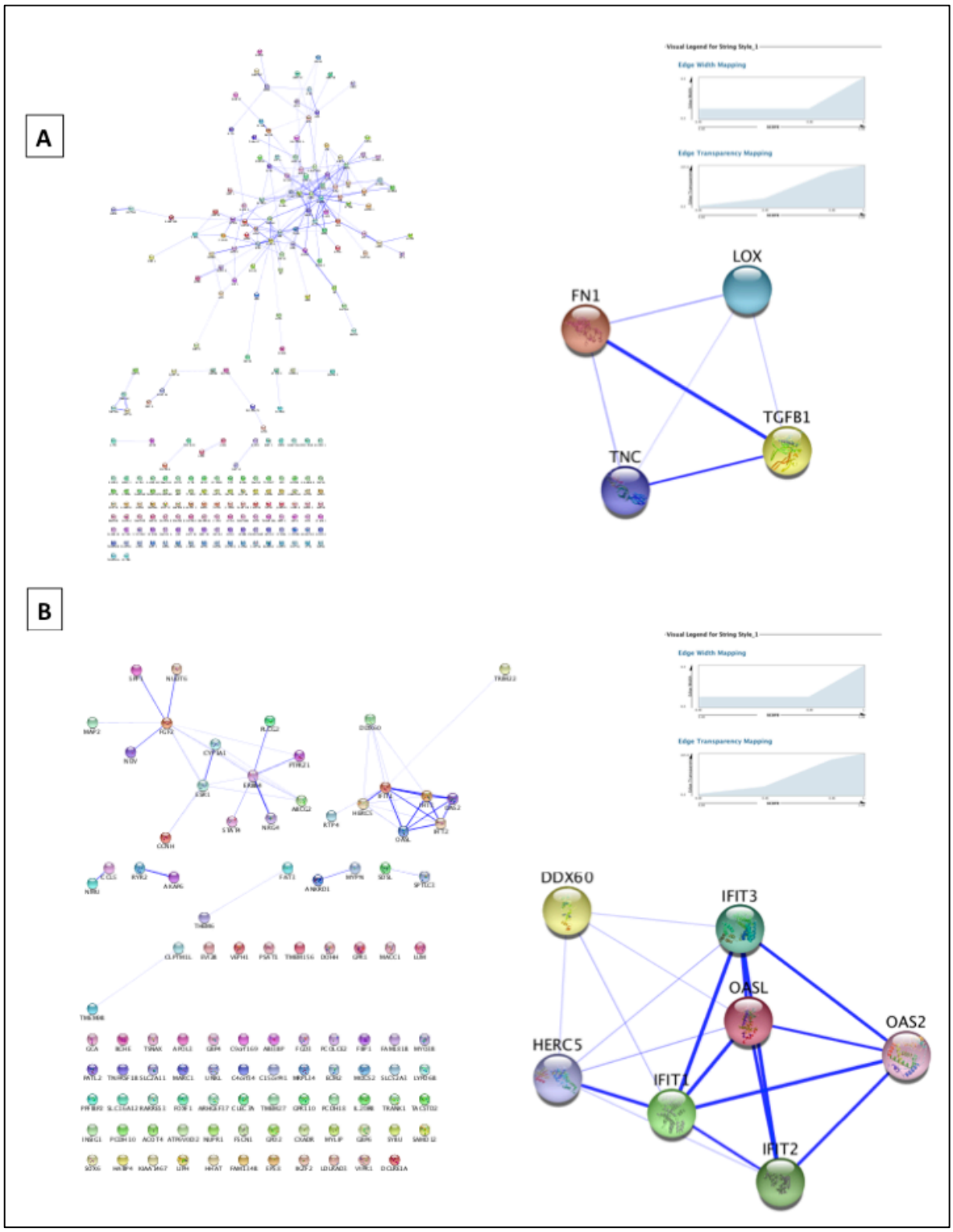

Figure 3-6. Protein-protein interaction (PPI) clusters following siRNA knockdown of CTEN. PPI data was obtained from the Search Tool for the Retrieval of Interacting Genes STRING database (Jensen et al., 2009), using our up- (A) or down-regulated (B) genesets (confidence score >0.4). Each global network is illustrated in the left panel. For each global network, MCODE (Bader and Hogue, 2003) **analysis was performed to identify significant clusters. The highest scoring cluster for both up- (A) and down-regulated (B) genes is displayed in the right panel.**

3.5 Discussion

Survival rates for HNSCC have remained relatively unchanged in the past 3 decades with 5-year survival remaining approximately 50% (Loyo et al., 2013). Locoregional recurrence and associated treatment failure can occur in up to 30%, depending on tumour stage at presentation, and accounts for the majority of deaths with 50-60% mortality resulting from failed locoregional control (Curry et al., 2014). Human papillomavirus is now an important causative factor in HNSCC disease and routinely investigated, particularly in the workup of oropharyngeal disease; as well as a reduced association with a smoking and alcohol history, HPV-positive disease patients have a better overall and progression-free survival than those with HPV-negative disease. Indeed a number of clinical trials are currently in progress investigating de-escalation protocols for those tumours with a viral origin e.g. De-ESCALaTE (**De**termination of **E**pidermal growth factor receptor inhibitor (cetuximab) versus **S**tandard **C**hemotherapy (cisplatin) early **A**nd **L**ate **T**oxicity **E**vents in **H**uman **P**apilloma**v**irus positive oropharyngeal squamous cell carcinoma), and PATHOS (**P**ost-operative **a**djuvant **t**reatment for **H**PV-p**os**itive tumours). There is also no current mechanism of identifying those HPV-positive patients who are likely suffer a more aggressive disease course before treatment. This alternate clinical profile likely reflects a host of genetic and mechanistic biological alterations compared to non-viral disease.

Similar to all tumours arising from the squamous lining of mucosal surfaces, the basement membrane provides a biological barrier to tumour degradation. The degradation of the basement membrane and subsequent invasion of tumour cells is the key to understanding metastasis. To metastasise, cancer cells must develop motility, alter their cell-cell adhesions and remodel the extracellular matrix. Following its identification in 2002, CTEN has been identified as an important focal adhesion adaptor protein, which has a restricted expression pattern in normal tissues, concentrated particularly in the prostate (Lo and Lo, 2002). It has, however, been found to have significantly increased expression in many cancer types including thymoma (Sasaki et al., 2003), gastric (Sakashita et al., 2008), colorectal (Albasri et al., 2011b), breast (Albasri et al., 2011a; Katz et al., 2007), lung (Hong et al., 2013; Sasaki et al., 2003), skin (Sjoestroem et al., 2013) and pancreatic cancer (Al-Ghamdi et al., 2013). It has never previously been investigated in HNSCC but could have potentially important clinical impact if the findings from other tumour types were replicated.

Katz et al (2007) analysed 272 archived samples of invasive breast carcinomas and found a strong correlation between CTEN and high tumour grade and local lymph node involvement, implicating CTEN as an important player in breast cancer progression as well as a marker of aggressive disease. Expression was also associated with high EGFR expression. These results were replicated in a separate dataset of breast cancer patients (Albasri et al., 2011a). Similar associations were found in gastric cancer, with CTEN overexpression associated with poor grade, metastasis, and poor prognosis (Sakashita et al., 2008). Sjoestroem et al (2013) analysed a large TMA dataset of melanocytic lesions and similarly found an significant association with overall and disease-specific 5-year survival for primary melanoma patients, which was maintained on univariate analysis. Albasri et al. (2011a) similarly showed in a univariate analysis that high CTEN correlated with shorter disease-free survival, although significance was lost when undergoing multivariate analysis controlling for disease stage and vascular invasion.

We demonstrated a predominantly cytoplasmic and heterogeneous staining pattern, in keeping with other immunohistochemistry studies (Albasri et al., 2011a). We similarly found high CTEN expression to be a significant marker of OPSCC mortality on univariate analysis for both overall OPSCC disease, and stratified by HPV involvement. Importantly, CTEN remained a significant marker on multivariate analysis controlling for age, T stage, and smoking status. On survival analysis, there was a highly significant difference between the Kaplan-Meier plots for both all OPSCC and HPV-positive disease according to CTEN score ($P \leq 0.001$), with the plots in HPV-negative disease demonstrating a strong trend that did not quite reach significance ($P=0.062$). These plots did not control for treatment modality. There was a significant correlation between higher CTEN expression and HPV-negative status ($P<0.0001$) but we found no correlation between CTEN expression and tumour grade or lymph node involvement, unlike previous studies in other cancer types. We also found no association with EGFR expression. It will be necessary to validate these findings on another large tumour dataset but this study demonstrated an important potential clinical relevance for CTEN as an independent, significant clinical marker of disease prognosis independent of other disease variables. Although there are knockout mice models for a number of the other Tensin family members, there has been relatively little *in vivo* work studying CTEN. One study did utilise intrasplenic injections in mice with colorectal cancer cells overexpressing CTEN, resulting in a significantly increased local and metastatic tumour burden, together with shortened

survival (Albasri et al., 2011b). Following our positive findings of clinical relevance in HNSCC, we confirmed that CTEN has functional relevance in an orthotopic model of HNSCC. Although CTEN depletion did not result in a histological or morphological change in tumour appearance, absence of this protein did abrogate tumour growth, measured by both calliper and fluorescence emission, as well as reduce the number of micrometastases. The latter result must be interpreted with caution given that deposits were detected by fluorescence detection and there was a lack of similar association in our previous clinicopathological tumour database.

Despite the increasing evidence for an significant cancer promoting role for CTEN in a variety of tumour types, and now our evidence for its potential importance in HNSCC, the involved biological pathways remained unclear. RNA sequencing technology allowed us to identify potential CTEN functions to help guide future investigations. Whilst gene ontology analysis resulted in a long list of pathway biological process terms implicated in changes resulting from CTEN silencing, the clustering algorithm utilised demonstrated an interesting representation of semantically similar terms, with particular highlighting of cell metabolism, cell signalling, growth and proliferation and finally the apoptotic process (Fig. 3-3). Whilst cell locomotion is a term pulled out of the treemap analysis, and an extracellular matrix specific gene ontology process is near the top of the individual term lists, in keeping with previous reports of focal adhesion activity of Tensins, it is noticeable that a cell movement global domain is not highlighted in this analysis. Similarly when interrogating gene network interactions, it is signal transduction, metabolism, cell cycle and programmed cell death that are notably prominent (Fig. 3-5). This is not the first discovery of an association of Tensins with apoptosis. Lo at al. (2005) noticed a human specific interaction between caspase 3 and CTEN, with the resulting fragment able to induce apoptosis in prostate epithelial cells. Our *in vivo* work however suggests that this could be a highly clinically relevant mechanism of action.

Another interesting finding was elucidated when focussing on protein interaction networks. MCODE (Bader and Hogue, 2003) analysis helps find highly interconnected clusters in these networks and the highest scoring up-regulated cluster involving TGF-β1 signalling sheds new light onto the role of Tensins with the extracellular environment. TGF-β1 is a prominent stimulator of myofibroblast transdiffentiation, and therefore the finding of this cytokine pathway in a high impact cluster raises interesting possibilities on

how CTEN may be involved in modulating the tumour microenvironment and 'inside-out' cell signalling.

Considering CTEN has been shown to be have a highly clinically relevant association of CTEN with HNSCC disease, as well as supporting *in vivo* tumour growth, it is worth engaging in efforts to further define its biological function *in vitro* in this disease. Despite its localisation in previous work to focal adhesions, there are a number of uncertain areas regarding its function. We have demonstrated that this may extend beyond a pure structural or focal adhesion role and further investigation may help us further understand the role of CTEN, paving the way towards justification of its use as a prognostic marker or therapeutic target.

Chapter 4: Functional confirmation of CTEN activity in HNSCC

4.1 Introduction

The ability of tumour cells to invade and metastasise is one of the key hallmarks of cancer (Hanahan and Weinberg, 2011) but despite this the underlying mechanisms are still poorly understood (Bacac and Stamenkovic, 2008). There is however a greater appreciation of the multistep nature of this process and the ability of carcinoma cells to invade the basement membrane and surrounding stroma in order to migrate to blood or lymph vessels is widely acknowledged as a key first step in this metastatic cascade.

The transmembrane glycoprotein family of integrins have been prime suspects for investigation in this process due to their ability to modulate the majority of cellular functions required for metastasis, namely migration, invasion, proliferation and survival (Desgrosellier and Cheresh, 2010; Felding-Habermann, 2003). Whilst many of these functions are utilised in normal physiological processes such as development and wound healing, it is the recruitment of these functions by cancer cells that is believed to facilitate tumour progression. Many of these processes have a direct effect on cell migration, which is fundamental to the process of invasion (Condeelis et al., 2005). Aberrant expression and/or activation of cell surface integrins are therefore highly implicated in many of the hallmarks of cancer (Weis and Cheresh, 2011). The interaction between a cell and its substrate environment is critical to understanding cell migration as this process involves the dynamic protrusion of the leading edge of a cell and formation of a stabilising adhesive complex (Huttenlocher et al., 1996). It is the strength of this complex which allows the generation of sufficient traction force which, together with release of adhesion sites at the trailing edge, allows directional cell movement (Lee et al., 1994). Integrins act in these adhesion sites as a structural link between the extracellular matrix and the actin cytoskeleton (Hynes, 1992) and it is the unique integrin ligand specificity that can control the formation and strength of these focal adhesions (Burridge et al., 1988). The link with the actin cytoskeleton is mediated through actin binding proteins (Zaidel-Bar et al., 2004) which aggregate in situation- and temporally-specific patterns.

Tensins are translocated to assembling adhesion sites upon integrin ligation, although the fact that in some cell types Tensins are detected only at mature focal adhesions and fibrillar adhesions indicates that the pattern of binding protein recruitment at these adhesion sites is tightly regulated (Katz et al., 2000; Legate and Fässler, 2009; Zamir et al., 1999).

Although four Tensin proteins have been identified (TNS1-3 & CTEN), the middle regions of the proteins are highly divergent, suggesting unique functions. Integrin biology *per se* has been the subject of significant research efforts over the past decades, and realisation of their importance for mediating tumour interactions with the extracellular environment have culminated in both translational diagnostic trials and, more recently, therapeutic interventions in the form of monoclonal antibodies (Moore et al., 2014). However when considering adaptor proteins that are integral to integrin-focal adhesion complex formation, significantly less is known. Indeed despite the apparent key functions of Tensins in supporting mechanisms including cell motility, epidermal growth factor receptor expression, tumourigenicity and integrin stability (reviewed in Lo, 2014), little is known about their translational relevance or potential as therapeutic targets. In the previous chapter we demonstrated an important clinical association between CTEN expression and HNSCC disease prognosis and confirmed these findings with *in vivo* tumour models, supporting CTEN as having an important tumour promoting role. Novel data was obtained from RNA sequencing work in a human HNSCC cell line implicating pathways involved in cell movement, cell signalling, cell proliferation and apoptosis as being important for CTEN function. There was also an association with cell metabolism which will be discussed in a Chapter 5. Finally protein analysis highlighted a TGF-β1 signalling cluster as an important interacting network in CTEN biology, highly relevant given the published investigations into the role of Tensins with focal adhesions and interactions with the extracellular matrix.

This chapter introduces the expression and functional roles of CTEN in HNSCC cell lines, focussing on integrin-dependent functions vital for tumourigenicity. Highly relevant physiological models were then employed to more accurately predict the role of CTEN in 3D environments and validate our previous clinical findings.

4.2 CTEN is widely expressed in human cancer cell lines

In order to determine the functional role of CTEN *in vitro* in HNSCC, a range of cell lines were firstly screened by Western blotting for protein expression including cell lines derived from tumours with published high CTEN expression: MCF7 (breast), Capan1,

BxPC3 and Panc0403 (pancreatic); Flo1 and OE21 (oesophageal)] as well as head and neck cell lines [SCC25, 5PT (laryngeal); Detroit 562 (metastatic HNSCC); BICR6 (hypopharynx); H357 (oral) and H357 derivatives genetically manipulated to express varying levels of αvβ6 integrin (VB6 high αvβ6; C1 low αvβ6; IC6pr αvβ6 negative (Moutasim et al., 2010) (Fig. 4-1A). Two (virally derived) HPV-positive HNSCC cell lines were also included (SCC2, SCC90). CTEN expression was found to be ubiquitous, with variable expression between cell lines. Whilst no positive control cancer cell line was identified from the existing literature, there is significant evidence for CTEN upregulation in breast cancer (Katz et al., 2007) and we therefore included MCF7 for this purpose. It is worth noting that in almost all HNSCC cell lines CTEN levels were increased compared to the breast line and CTEN therefore appears to be highly expressed in this cancer type *in vitro*. An interesting finding was the apparent reciprocal expression between CTEN and integrin β6, highlighted by examining the β6-positive cell line VB6, and its controls (IC6pr and C1).

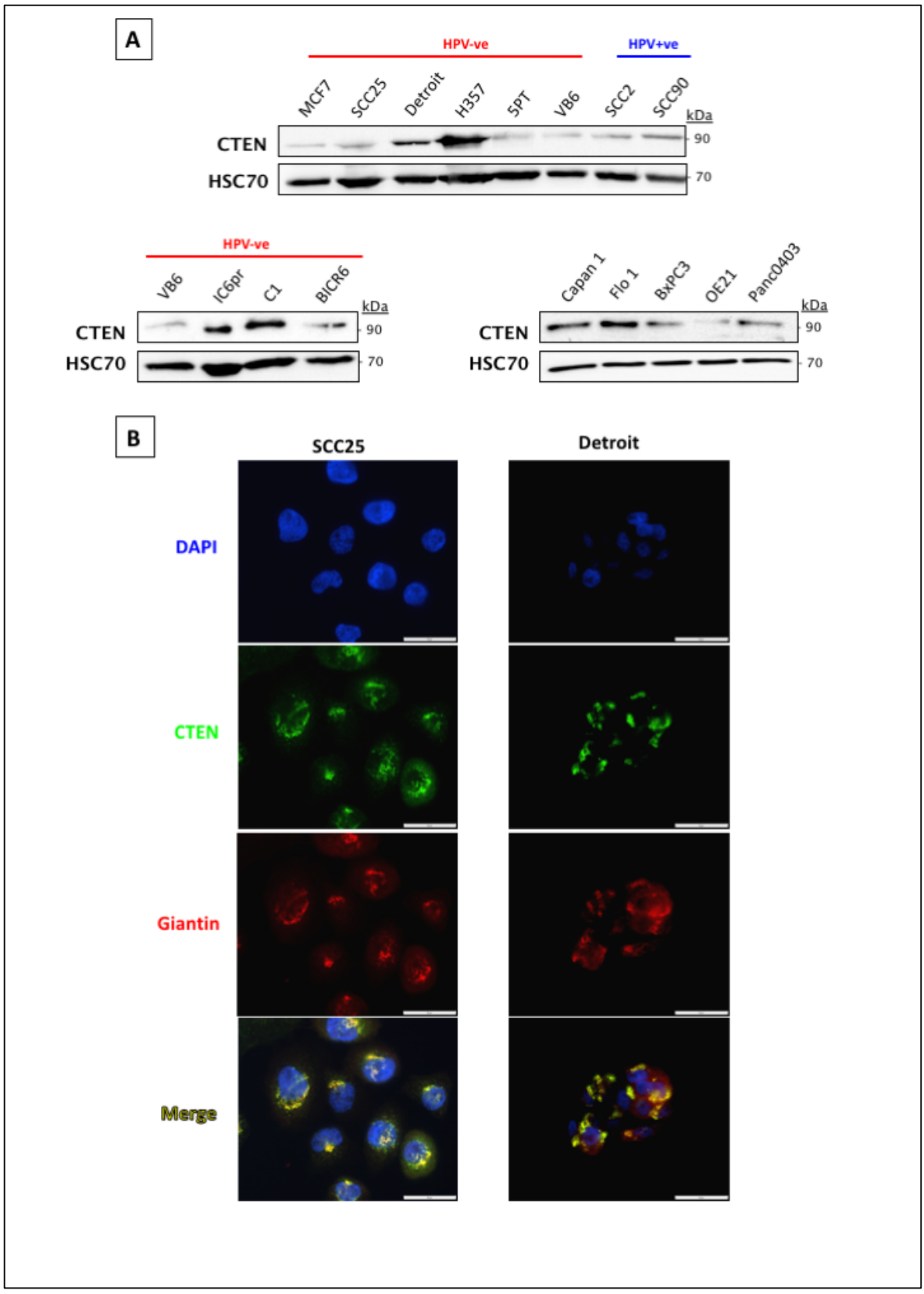

Figure 4-1. Expression and localisation of CTEN in a range of human cancer cell lines. A, Western blot results showing CTEN expression in a range of cancer cell lines, including HNSCC (SCC25, Detroit 562, H357, 5PT, VB6, IC6pr, C1 and BICR6), pancreatic (Capan1, BxPC3 and Panc0403) and oesophageal (Flo1 and OE21) cell lines. All cell lines were cultured and harvested at 80-90% confluency for lysis. A breast cancer cell line MCF7 was used as a positive control. HSC70 was used as loading control. B, Immunofluorescence of SCC25 and Detroit 562 cells stained for Giantin (red) and

CTEN (green). Cell nuclei are stained with DAPI (blue). Photomicrographs were taken at 100x magnification using identical exposure times and camera settings (scale bar = 50μm). Co-localisation of Giantin and CTEN was demonstrated in both cell lines, identifying Golgi bodies as the most prominent location of CTEN in both cell lines.

Immunofluorescence was then performed on fully adherent cancer cells (SCC25 derived from a primary tumour and Detroit 562 from a metastatic deposit; Fig 4-1B). The initial observation of a perinuclear localisation of CTEN prompted a repeat concurrent stain with the Golgi protein Giantin and this confirmed accurate co-localisation of CTEN to Golgi bodies in both cell lines.

4.3 CTEN and the TGF-β1 activation pathway in oral cancer cells

RNA sequencing analysis highlighted the involvement of a number of biological pathways previously unrecognised in CTEN biology. The upregulation of a network involving transforming growth factor beta-1 (TGF-β1) in response to CTEN depletion (Fig. 3-6A) is of particular interest. TGF-β1 is an important regulator of tumour progression (Hazelbag et al., 2004; Kaminska et al., 2005; White et al., 2010), and plays a key role in functions linked to CTEN biology e.g. cell motility (Giampieri et al., 2009). As well as a direct effect on cancer cells, TGF-β1 also modulates a variety of interactions between tumour cells and their microenvironment, not least through functional links to the ECM (Munger and Sheppard, 2011), stimulation of epithelial-mesenchymal transition (EMT) (Valcourt et al., 2005; Zavadil and Böttinger, 2005) and activation of integrins (Hynes, 1992; Munger and Sheppard, 2011; Thomas et al., 2002). Given their close functional association, we wanted to determine whether a direct biological relationship existed between these two proteins and therefore we conducted a number of experiments to investigate whether CTEN affected functional TGF-β1 activation in HNSCC cell lines (Fig. 4-2). We conducted mink lung epithelial cell (MLEC) assays in two HNSCC cell lines that have previously been shown to activate this cytokine in our group (Munger et al., 1999; Thomas et al., 2001a, 2001b) (Fig. 4-2A, left panel). Importantly, both cell lines demonstrated significantly increased TGF-β1 activation following transient CTEN knockdown. Given that both these HNSCC cell lines highly express αvβ6 (Munger et al., 1999; Thomas et al., 2001a, 2001b), it was important to consider the effect that cell surface integrins may be having on the TGF-β1

pathway. As heterodimeric cell membrane receptors, integrins do not function simply as adhesion molecules, but also act as receptors for the activation of complex inside-out and outside-in signalling pathways, which regulate cell function. Integrin αvβ6 is of particular importance here not only due to its multiple regulatory functions in tumour progression (Hazelbag et al., 2007), but also due to its ability to activate TGF-β through binding to latency associated peptide (LAP), allowing mature TGF-β1 to bind to its receptors (Munger et al., 1999; Thomas et al., 2002). To test whether the TGF-β1 activation we detected was occurring in an αvβ6 integrin-dependent manner, we measured TGF-β1 activation in Control and CTEN siRNA-transfected cells, which were treated with an αvβ6-specific blocking antibody, 63G9. Indeed, blocking αvβ6 integrin resulted in a significant inhibition of TGF-β1 activation (Fig. 4-2A, middle panel). This is consistent with the aforementioned role of αvβ6 in TGF-β1 activation (Munger et al., 1999; Munger and Sheppard, 2011). Surface integrin expression was analysed by flow cytometry on a BD FACSCanto™ II system, utilising an unconjugated β6 antibody (620W) with Alexa Fluor® 647 secondary. The APC/Alexa Fluor® 647 flourochrome was selected to avoid any spill over from the GFP expression incorporated into the shRNA construct. Analysis demonstrated that depletion of CTEN resulted in a reproducible 33% increase in surface β6 expression (Fig. 4-2B).

The desmoplastic stromal response to tumours and alterations in the microenvironment have been shown to significantly modulate tumour cell behaviour (Rosenthal et al., 2004). Cancer-associated fibroblasts (CAFs or myofibroblasts) are the predominant cell in the stroma and therefore likely play a key role in this remodelling. Various cytokines and growth factors have been shown to induce fibroblast-to-myofibroblast transdifferentiation, but the most potent of these is TGF-β1. To determine whether CTEN affected the ability of cancer cells to induce myofibroblast differentiation in concordance with our MLEC assay results, we carried out co-culture experiments with SCC25 oral cancer cells and HFFF2 fibroblasts (Fig. 4-2C&D). There are several markers that can be used to monitor myofibroblast transdifferentiation. The most commonly accepted features of myofibroblasts, however, are increased expression of alpha smooth muscle actin (αSMA), and a dense, contractile αSMA-positive stress fibre network (Eyden, 2005; Kawashiri et al., 2009).

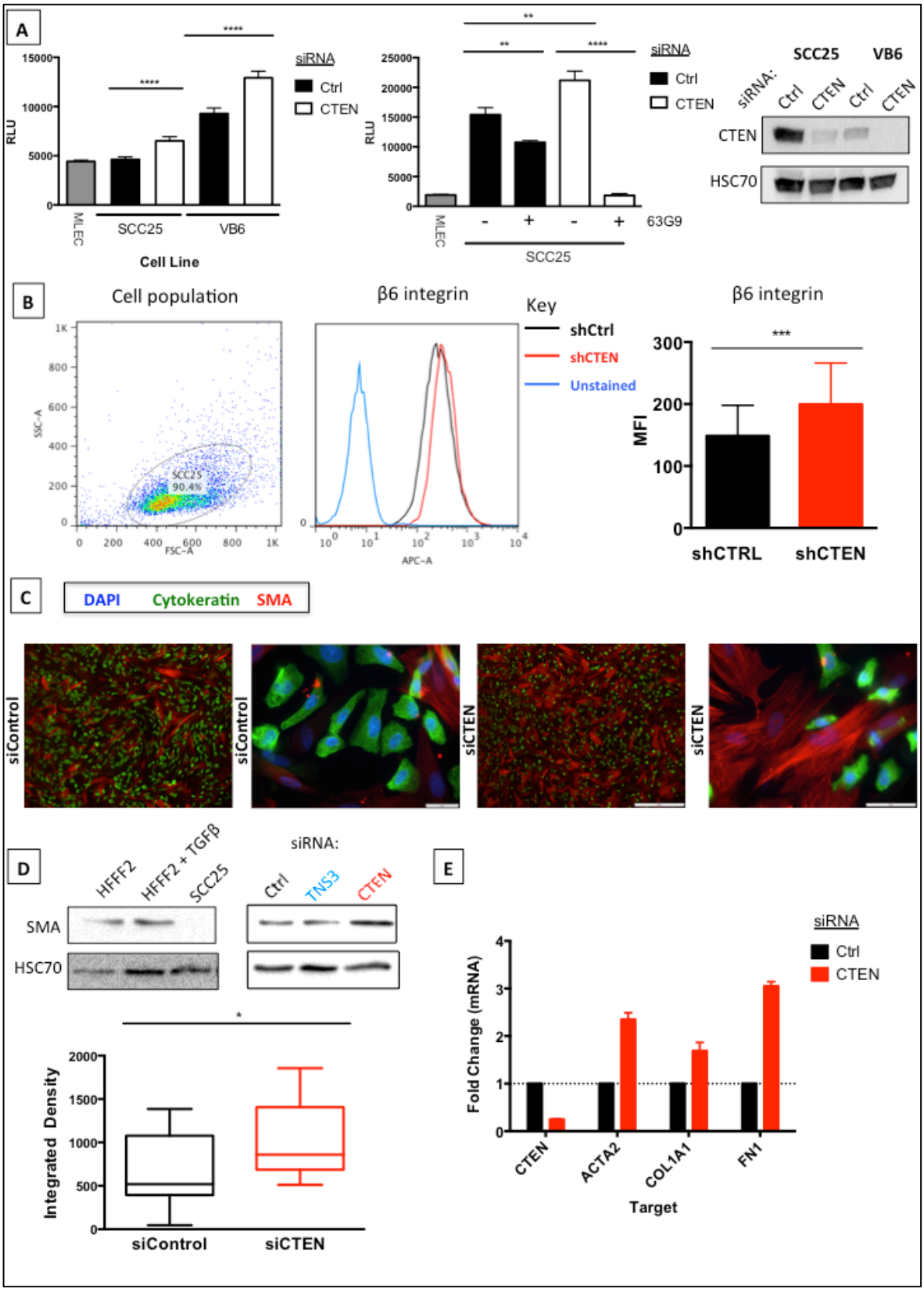

Figure 4-2. CTEN knockdown results in β6-mediated TGF-β1 activation. A, TGF-β1 activation was measured using a mink lung epithelial cell (MLEC) assay; these cells contain a truncated, specific TGF-β1 responsive PAI-1 promoter fused to the firefly luciferase reporter. SCC25 and VB6 cells were included, as known β6-expressing TGF-β1 activating HNSCC cell lines. CTEN siRNA resulted in a significantly increased activation of TGF-β1 compared to control siRNA-transfected cells in both cell lines (**P<0.0001; left panel). MLEC cells alone represent basal luciferase expression.**

The αvβ6-specific 63G9 was then included in the SCC25 assay and this blocking antibody reduced both control and CTEN knockdown-induced TGF-β1 activation confirming that TGF-β1 activation in SCC25 cells is dependent on the integrin αvβ6 (**P<0001; middle panel). Western blot confirms CTEN knockdown (right panel) and HSC70 was used as a loading control. B, flow cytometry analysis of surface integrin expression was performed on stable CTEN knockdown SCC25 cells using a BD FACSCanto™ II system with a non-conjugated primary (620W) and Alexa Fluor® 647 secondary antibody for β6. Cell population gating was performed to exclude outliers and included over 90% of the tested population. Blocking was performed with 10% human serum prior to staining. 10,000 events were captured and following acquisition, analysis was performed with FlowJo Version 7.6 (Treestar, OR). Representative histograms (n=2) are shown for each integrin, including an unstained negative control, as well as grouped median fluorescence (MFI) which demonstrated a significant increase in surface β6 expression in knockdown cells (P<0.001; ratio paired T-test). C, D, co-culture was performed of siRNA treated SCC25 and fibroblasts (HFFF2). Co-culture immunofluorescence was performed (C) with nuclear DAPI staining (blue), cytokeratin (green) and SMA (red) staining and representative micrographs are demonstrated (x10 (left) and x40 (right) for each siRNA condition). D, co-cultures were collected and Western blots performed, including protein collected from a sole negative fibroblast control (HFFF2), positive TGF-β1 stimulated HFFF2 control and cancer cells only (SCC25) negative control (upper panel). CTEN siRNA transfected cells demonstrated increased myofibroblast SMA expression (n=2); TNS3 was included on this immunoblot to confirm a CTEN specific response; HSC70 used as a loading control). Further quantification verification of SMA expression is demonstrated in (D, lower panel) – a box plot of SMA expression in co-culture was calculated from automated red (TRITC) measurement using ImageJ software. 12 random high power (x40) fields were photographed and RGB colour images were split. Auto thresholds of the red image were applied and integrated density measured in the resulting image as a product of mean grey value and area. Horizontal line indicates median value and whiskers show the 95% confidence intervals. E, co-cultured cells were collected at 48 hours for RNA extraction. Results indicate relative RNA expression following Taqman® qPCR (2 stage). Results were normalised to GAPDH control. CTEN fold change confirms adequate knockdown in co-culture. Analysis demonstrates significant increase in multiple markers of myofibroblast differentiation in CTEN knockdown cells including SMA (ACTA2), α-1 type-1 collagen (COL1A1) and fibronectin (FN1).**

As shown in Fig. 4-2D, when HFFF2 fibroblasts were co-cultured with CTEN siRNA-transfected SCC25 cells there was a significant increase in αSMA expression. By performing immunofluorescent staining of our co-cultures, we confirmed that CTEN not only upregulated expression of αSMA but it also induced the development of an αSMA-positive stress-fibre network, a known marker of myofibroblasts (Fig. 4-2C). To further confirm the effect of CTEN knockdown on fibroblast-to-myofibroblast transdifferentiation, we measured the expression of a number of target genes associated with this myofibroblast phenotype such as ACTA2 (αSMA), COL1A1 (type I collagen) and FN1 (fibronectin) using Taqman qRT-PCR. For all these markers of myofibroblast

differentiation, a large upregulated RNA expression fold change was demonstrated in CTEN knockdown cells (Fig. 4-2E).

4.4 Regulation of the apoptosis pathway in HNSCC is related to CTEN expression

Normal cells require a degree of adhesion to a substrate, or the extracellular matrix, for survival and loss of these contracts or inadequate interaction with the extracellular environment can result in cell death through the triggering of apoptosis (also known as anoikis), thus ensuring cell survival is anchorage-dependent (Frisch and Screaton, 2001). Cancer cells however are known to be resistant to programmed cell death, including anoikis, and are able to thrive with the loss of anchorage dependent growth and metastatic spread to new environments (Frisch and Screaton, 2001; Huang and Ingber, 1999). The protease family of caspases are the key regulators of the apoptosis process (Riedl and Shi, 2004) and whether the process is initiated by the intrinsic or the extrinsic pathway, both pathways converge upon the common execution phase, comprising a series of caspase reactions (Wong, 2011). Caspase-3 is the key effector molecule here and once its precursor zymogen has been cleaved, the activated protease propagates the cell to apoptotic death.

Several lines of evidence suggested to us that CTEN may have a role in suppressing cancer cell apoptosis; most notably there was enrichment of apoptotic pathways in Gene Ontology terms following CTEN siRNA treatment of SCC25 cells. We performed immunohistochemistry staining of organotypic culture sections with activated caspase-3 antibody (Fig. 4-3A). In both SCC25 and Detroit 562 cell lines, we observed markedly increased expression of activated caspase-3 in the CTEN deplete cultures compared to control siRNA treated paired samples. CTEN-knockdown in flat monoculture had produced no effect on cell growth, so we specifically examined the effect in 3D-suspended culture. Control and shRNA-transduced CTEN knockdown cells were suspended in a collagen gel and, at set time points over a time course of one week, gels were dissolved with collagenase and live cells counted (Fig. 4-3B). This revealed a significant reduction, and levelling off, of proliferation in the CTEN-knockdown cells from Day 2 ($P<0.01$). This was also repeatable when performed with siRNA treated cells (data

not shown). Following H&E staining processed gels revealed single cell suspensions only in the CTEN-depleted cultures, with an absence of the colony clusters clearly visible in the control gels (Fig 4-3B, right panel).

Following the observed protective effect of CTEN upon cell survival in suspended culture models, we hypothesised that the apoptotic effect of ionising radiation may result in more pronounced cell death in CTEN-depleted cells compared to normal controls. We conducted clonogenic assays in SCC25 cells to ascertain this fact, exposing siRNA-treated SCC25 cells (control and CTEN) to varying doses (0-6Gy) of ionising radiation and observing their subsequent ability to form colonies and proliferate (Fig. 4.3C). Significantly reduced growth in colony area was observed with increasing doses of radiation, with an exaggerated apoptotic response to radiation-induced damage in CTEN knockdown cells ($P<0.01$).

Transforming growth factor-β (TGFβ) is a complex pleiotropic molecule that is involved in a diverse array of biological processes including metabolism, cell growth, differentiation and notably, apoptosis (Molinolo et al., 2009). A potential link between TGF-β signalling and apoptosis in HNSCC would be of functional relevance as we have already demonstrated both through RNA sequencing and TGFβ activation assays that CTEN depletion results in an up-regulation of TGFβ and TGFβ-dependent pathways. TGFβ has a paradoxical role in a variety of tumour types including HNSCC – a tumour suppressor during early tumour development (Engle et al., 1999) but a tumour promoter in larger established tumours (Piek and Roberts, 2001; Tang et al., 2003). Based on data to this point, we proposed that the apoptosis susceptibility mediated by a loss of CTEN might be mediated through a TGFβ-dependent pathway. We conducted preliminary work exploring this relationship and subjected siControl and siCTEN transfected SCC25 cells to 0 or 2Gy doses of ionising radiation with or without addition of a TGFβ RI kinase inhibitor (ALK5). The protein levels of activated caspase-3 were then examined by Western blot (Fig. 4-3D). As well as confirming a rise in activated caspase-3 levels in CTEN knockdown cells confirming CTEN depletion leads to a rise in the common apoptosis pathway at the protein level, addition of a TGFβ inhibitor (Alk5) abrogated the previously observed increase of activated caspase-3 in knockdown cells following ionising radiation exposure (Fig. 4-3D, arrow).

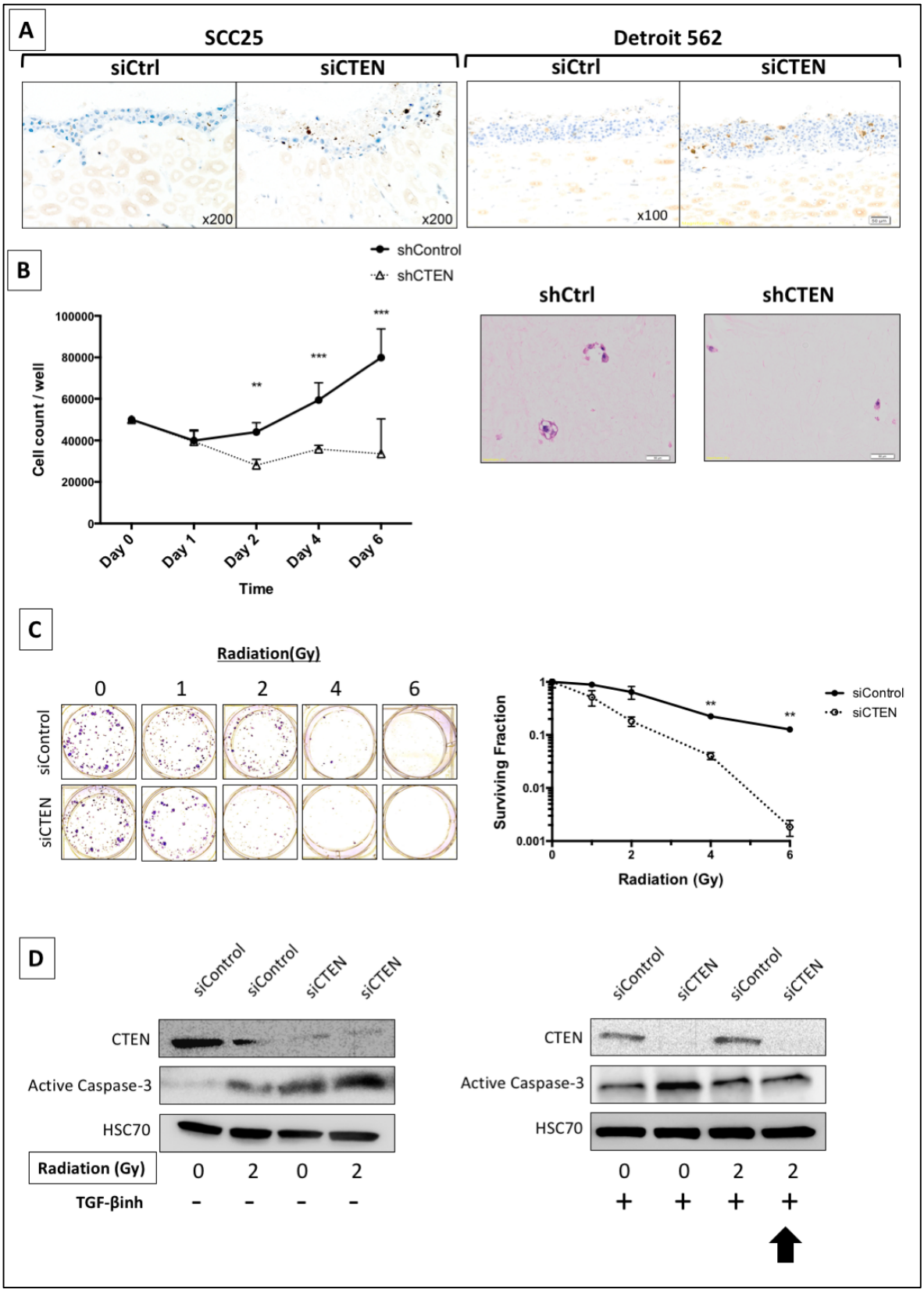

Figure 4-3. Apoptosis pathway activated in CTEN knockdown cells. A, organotypic culture sections from transient CTEN knockdown SCC25 and Detroit 562 assays were stained for activated caspase-3. Representative micrographs for SCC25 and Detroit 562 are demonstrated (x200 and x100 magnification respectively). Increased staining is evident across cell lines in CTEN knockdown cells (see Fig. 3.3 for knockdown confirmation). B, 3D collagen gel proliferation assays were performed by plating control shRNA transduced or stable CTEN knockdown cells at $5x10^4$

cells/ml suspended in a gel comprising collagen type I (Millipore), 10x DMEM (Sigma Aldrich) and FCS. After polymerisation, 10% DMEM was placed on top of the gel and then incubated at 37°C for a one week time course. At each time point 10% collagenase (Sigma) was used to digest the gels and then cell counts determined using a CASY automated cell counter. This demonstrated a significant increase in proliferation in the control cells compared to CTEN knockdown cells (P<0.01, ***P<0.001; Student's T-test). A gel from each condition at Day 6 was fixed and processed for staining with H&E demonstrating no 3D cell-cell contracts or cell groupings in the knockdown cultures. C, clonogenic assay are represented for control or CTEN knockdown SCC25 cells with a significant reduction in survival fraction at higher doses of radiation in the CTEN deplete cells (**P<0.01; n=2). Representative well photographs are displayed (min. 2 biological replicates) and log scale of survival fraction is used for survival curve. D, western blot results showing activated caspase-3 expression increases in CTEN knockdown cells, and this difference is exaggerated following exposure to ionising radiation (2Gy). Addition of a TGF-β RI kinase inhibitor (ALK5) in the cell suspension for 15 minutes prior to radiation exposure resulted in an abrogation of this caspase-3 increase (arrow). HSC70 was used as loading control. Blot represents single experiment.**

Following our observation of a protective effect on cell survival in cells expressing CTEN following radiation exposure, together with the clinical effects of radiotherapy in inducing activation of apoptotic cell pathways, we returned to our TMA database to examine for any correlation between CTEN and survival when stratified by treatment modality (Fig.4-4).

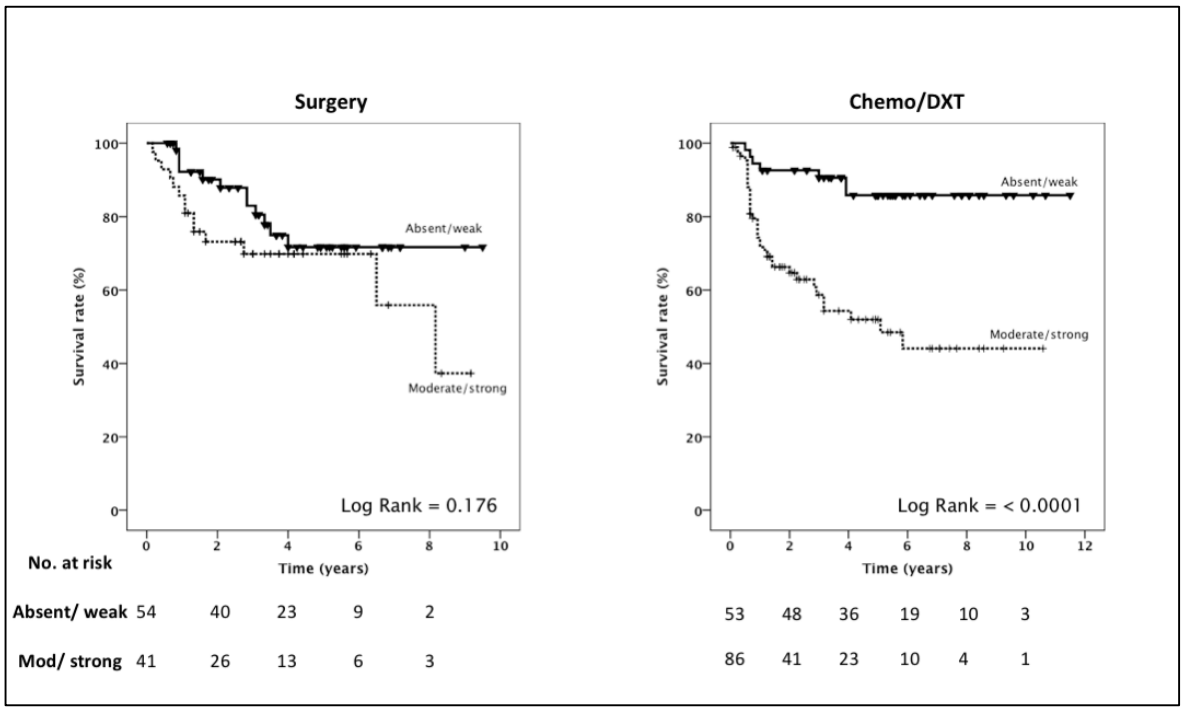

Figure 4-4. Survival analysis for OPSCC dataset by primary treatment modality. Kaplan-Meier curves were then produced using SPSS Statistics (v21 for Mac, IBM) with disease specific survival as an end-point and classified by CTEN expression as 'Absent/weak' or 'Moderate/strong'. Analysis was performed for all OPSCC patients split by treatment modality. Significant log rank scores were obtained for the population subset treated by chemoradiation (chemo/DXT).

We observed a clinical correlation with our *in vitro* results demonstrating that in tumours expressing high CTEN expression, there is a significant reduction in overall disease-specific survival when chemoradiation was the primary treatment modality. No associated correlation was evident in the group treated with surgery. This pattern was maintained when controlling for HPV status.

4.5 CTEN expression levels have a significant effect on tumour cell motility

The previously published localisation of Tensins to focal adhesion complexes, together with their recently documented association with integrin tails (Katz et al., 2007), has implicated these proteins as potential regulators of cell motility and interactions with the extracellular matrix. Despite our localisation of CTEN in adherent HNSCC cells to Golgi, cell locomotion was an over-represented term in our treemap analysis following RNA sequencing analysis in CTEN knockdown cells, and extracellular matrix interactions were

also highlighted in specific gene ontology processes (Chapter 3.4). We therefore investigated CTEN effects on cell locomotion by performing haptotactic migration assays, using our stable CTEN knockdown SCC 25 HNSCC cells (Fig. 4.5A, left panel). SCC25 cells have previously been demonstrated as αvβ6-positive (Coughlan et al., 2009; Nystrom et al., 2006), therefore the TGF-β1 Latency Associated Peptide (LAP), a ligand for αvβ6, was used as a ligand to study αvβ6-dependent migration. CTEN knockdown resulted in significantly reduced migration towards the ligand (P=0.037) and we performed concurrent proliferation assays to prove that this was not a result of reduced cell survival (Fig. 4-5A, middle panel). Haptotactic Transwell cell migration is dependent on the protrusion of the cell front through the microfilter pore, contact with the ECM ligand resulting in adhesion, and then mechanical traction/tension to allow movement of the cell body and rear through the pore (Huttenlocher et al., 1996). Adhesion to ECM is primarily integrin-mediated and critically regulated during directional cell migration (Huttenlocher and Horwitz, 2011). To investigate whether the effect on migration resulted from changes in cell adhesion, we performed adhesion assays utilising the xCELLigence real-time analyser in a range of HNSCC cell lines following siRNA knockdown of CTEN (Appendix E). There was no consistent significant difference in cell adhesion across cell lines between control and CTEN siRNA-transfected cells, and even where a trend approached significance, the direction of change varied between the cell lines.

Studies in a number of different tumour types have demonstrated a role for CTEN protein in promoting both cell motility and invasion (Al-Ghamdi et al., 2011; Albasri et al., 2009; Katz et al., 2007). All of our investigation on cell motility to date involved monoculture or 2D assays but *in vivo*, cancer cells invade in a 3D environment with important differences to simple migration, including altered ECM-cell interactions, as well as the formation of specialised cell structures e.g. invadopodia (Yamaguchi and Condeelis, 2007). It is therefore important to study the effect of CTEN depletion in more realistic physiological assays to determine its role in cell invasion, especially given our previous proliferation results. We conducted invasion assays using our previously utilised Boyden chamber technique with a layer of Matrigel at the bottom of the inner well, requiring digestion for cells to invade and pass through to the lower well. In order to ensure we have not been studying a cell line specific effect, transient CTEN knockdown with siRNA oligonucleotides was utilised to study both SCC25 and Detroit 562 HNSCC cell lines. CTEN knockdown resulted in a significant reduction of both SCC25 ($P<0.05$) and Detroit 562

cells ($P<0.01$; Fig. 4.5B, left panel). We repeated proliferation studies in these transient knockdown cells, which again showed no significant change in cell survival (Fig. 4-5B, right panel).

To corroborate these findings regarding cell motility effects, we used an alternative assay technique of scratch assays with time-lapse microscopy. In this assay, a wound was created in a cell culture monolayer of either control or stable CTEN knockdown SCC25 cells and then subsequent wound closure photographed over the course of the subsequent 24 hours. At the end of this assay, images were collated and Tscratch software (Gebäck et al., 2009) was used to measure the wound area remaining throughout the assay (Fig. 4-5D). This demonstrated a significantly faster closure of the wound in the control compared to the CTEN knockdown cells, and illustrative examples of wound appearance at 18 hours are demonstrated (Fig. 4-5E). Samples of leading edge cells in each group were also tracked and analysed using Chemotaxis plugin for ImageJ (Ibidi GmbH). No significant difference was observed in directionality (Fig. 4-5C) or overall velocity of cell movement (data not shown) between control and knockdown cells.

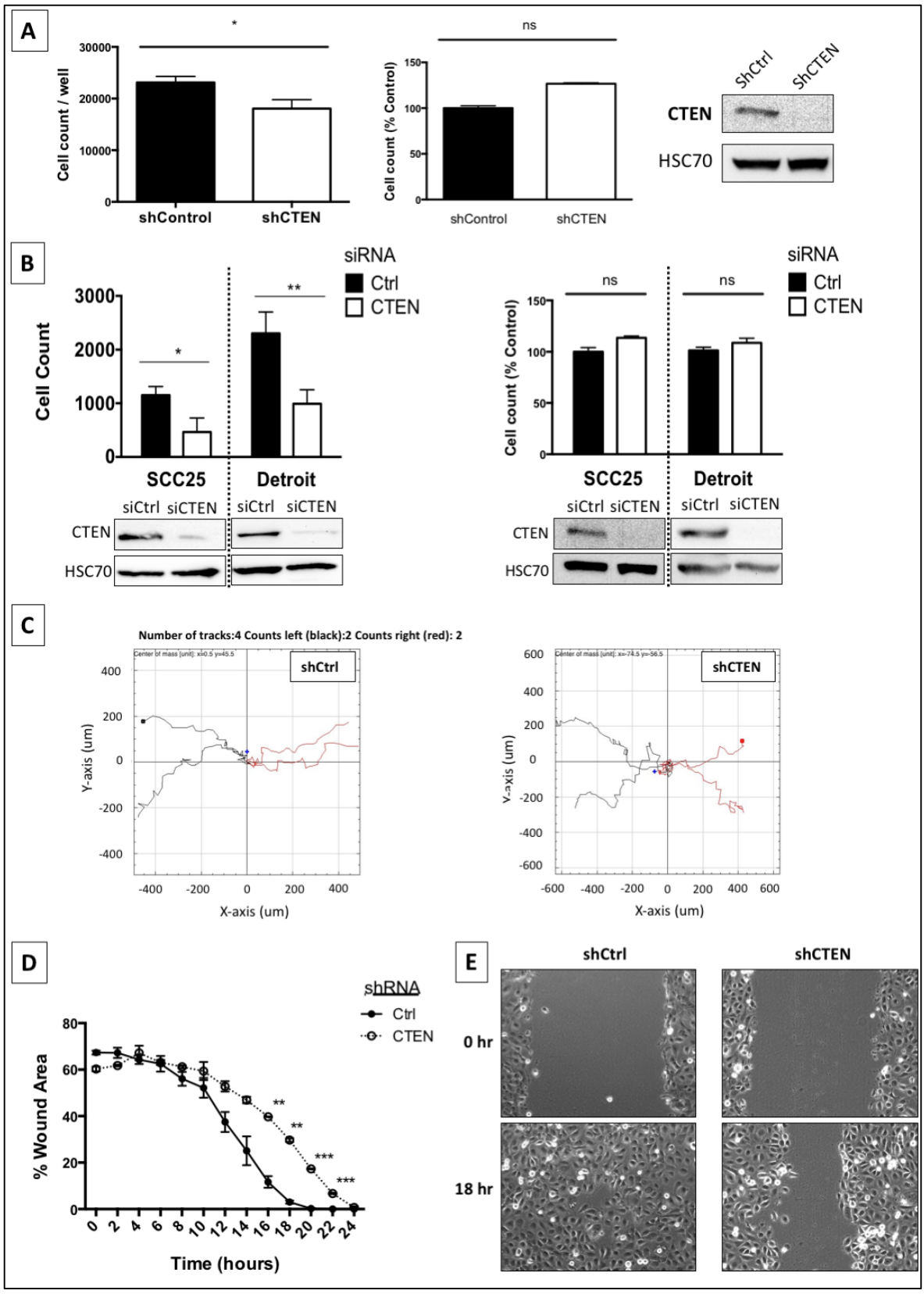

Figure 4-5. Suppression of CTEN expression reduces tumour cell motility. A, cell migration of CTEN deplete SCC25 cells was measured using Transwell migration assays (left panel). Bottom wells and inserts were coated with latency associated peptide (LAP; 0.5µg/ml) or bovine serum albumin (BSA; 0.1%) as a control and migrated cells counted after 24 hours. CTEN knockdown resulted in reduced cell migration (Student's t-test, two-tailed; *P<0.05). Cell proliferation was examined by plating Control and CTEN shRNA-transduced SCC25 cells in triplicate in 24-well plates and

cells counted on a Casy automated cell counter after 48 hours culture (middle panel). No significant difference was noted between cell proliferation. Western blots confirming complete knockdown are presented in the right panel together with HSC70 for loading control. B, two HNSCC cell lines (SCC25 and Detroit 562) were transfected with CTEN siRNA oligonucleotides and then plated at $5x10^4$ in the inner well of a Transwell inserts, with a Matrigel® protein layer at the upper/lower chamber interface (left panel). Cells that invaded through this gel towards serum-containing medium in the bottom chamber were counted after 72 hours on a Casy automated cell counter. CTEN depletion resulted in significantly reduced invasion in both SCC25 (*P<0.05; Student's T test) and Detroit 562 (P<0.01). Western blots confirming knockdown are presented underneath corresponding cell lines (lower panel) and HSC70 was used to confirm equal loading. The count-based proliferation assay was repeated with the siRNA-transduced cell lines and again no significant difference was found between final counts comparing siCtrl and siCTEN treated cells (right panel).**
C, D, E, time-lapse microscopy reveals an inhibition of SCC motility in CTEN-deplete cells on wound healing assay. Control and CTEN shRNA-transduced cells were plated at $8x10^5$ in 6-well plates and the following day a linear scratch was made in the cell monolayer using a P200 pipette tip. After washing, plates were transferred to a microscopy plate in a tank with 5% CO_2 insufflation and 37°C warming plate and time laps photomicrographs taken at 5-minute intervals with automatic focus function. Subsequent images were analysed on ImageJ using manual tracking, Tscratch software (Gebäck et al., 2009) and the Chemotaxis plugin for ImageJ (Ibidi GmbH). This demonstrated a significant delay in wound closure in CTEN knockdown cells (Student's t-test, two-tailed; **P<0.01; ***P<0.001; D, F), despite no difference in directionality (C).

Finally we proceeded to perform organotypic cultures in SCC25 cells. Organotypic cultures study invasion of cancer cells in a Matrigel/collagen gel in the presence of stromal cells, most commonly represented by fibroblasts and for these assays we used HFFF2 cells which are known to support HNSCC invasion models successfully and reliably (Marsh et al., 2008). Assays were performed using both transient CTEN knockdown and stable CTEN knockdown SCC25 cells (Fig. 4-6). Despite cultures lasting for 7 days, a reduction of CTEN levels were still observed at assay completion even with the use of siRNA, as demonstrated by Western blot. In both CTEN deplete cell cultures, invasion was significantly reduced (P<0.05; Fig. 4-6A). Initial inspection of H&E and pancytokeratin sections of the gels demonstrated reduced tumour cell invasion in CTEN knockdown cells. However closer inspection revealed that there also appeared to be significant cell loss within the surface layer in the CTEN deplete cells, most notable in the siRNA transfected cells (Fig. 4-6B, left panels), suggesting an additional effect on cell proliferation or survival that was not observed in 2D culture, consistent with our previous apoptotic study assays.

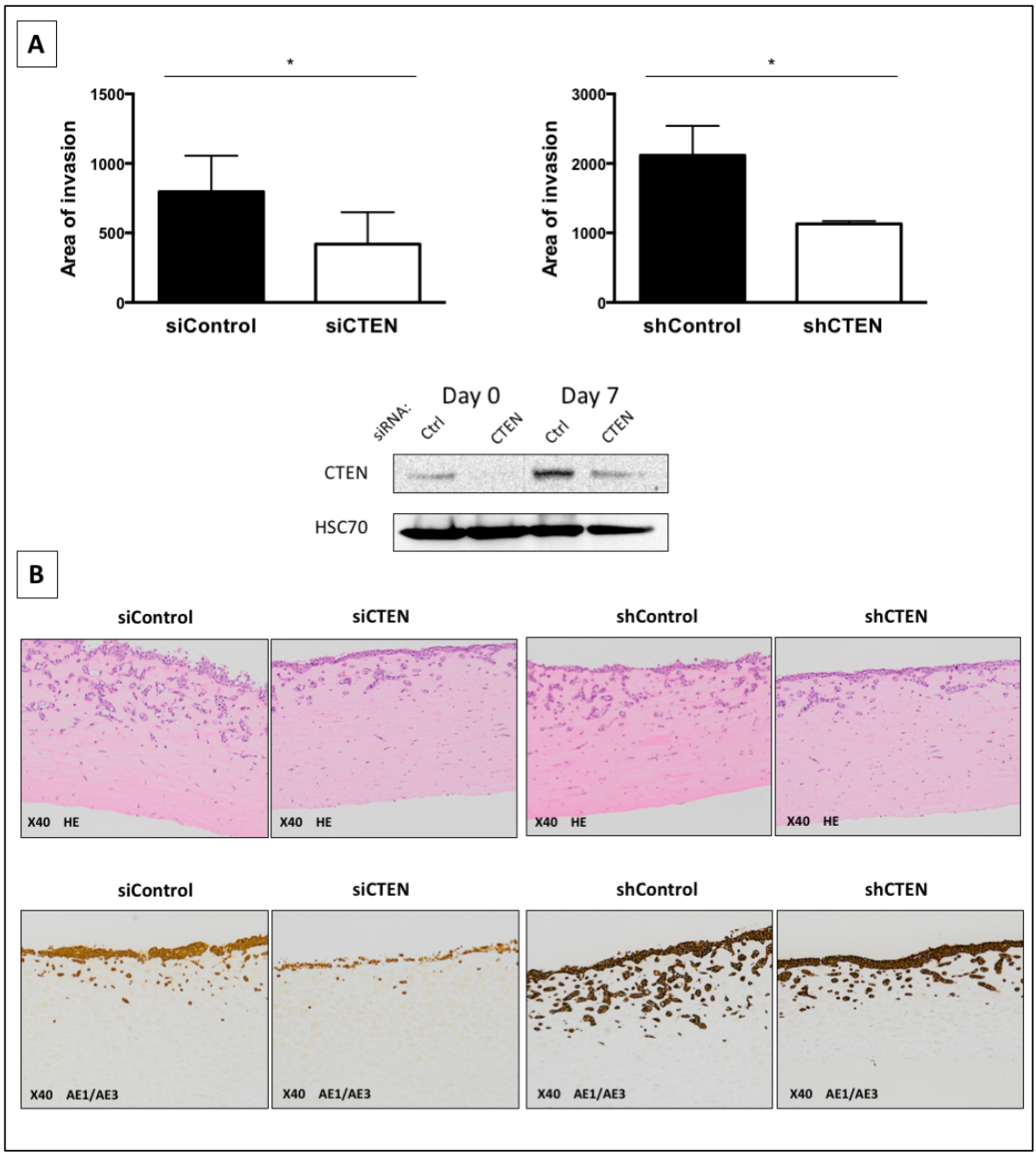

Figure 4-6. CTEN depletion results in reduced cancer cell invasion in 3D models. A, B, organotypic cultures were performed using either transient or stable CTEN knockdown SCC25 cells (siRNA, shRNA respectively). A gel mixture containing HFFF2 cells, Matrigel® and Collagen Type I was made after polymerisation, SCC25 cells were mixed with HFFF2 cells and added to the top of the gels, which were then incubated for 24 hours at 37°C. Gels were then raised onto nylon sheets and cells were allowed to invade for 7 days, utilising the principle of a liquid-air interface. After this time gels were bisected, fixed in formal-saline and processed to paraffin. Representative H&E and pancytokeratin stained sections (4 µm) are demonstrated with 40x magnification. Slide images were analysed in ImageJ for average area of invasion. There was significant reduction in cell invasion area in both cell lines ($P<0.05$; Paired T-test). Western blots demonstrating day 0 and day 7 CTEN protein expression for siRNA transfected cells are shown (A, lower panel).

4.6 Discussion

The aim of this chapter was to explore the cellular functions of CTEN in HNSCC cell lines. Broad cancer cell line screening showed that CTEN was expressed across a wide range of different cancer cell lines and indeed HNSCC lines demonstrated a greater level of protein expression compared to previously considered high CTEN expressing cells (MCF7). The proteins of Tensin-1, -2 and -3 differ from CTEN in that they contain an N-terminal actin binding domain (Lo and Lo, 2002) and it is this ability to disrupt the structural link between the ECM and actin cytoskeleton that has been suggested to explain the resulting cell motility effects (Katz et al., 2007; Mouneimne and Brugge, 2007). However, the factors governing the dynamics and maturation of cell-ECM contacts are poorly understood and a more detailed understanding of the 'adhesome' is required to fully integrate the regulation and consequence of multiple proteins and signalling pathway interactions.

Whilst more detailed analysis of the precise Golgi localisation was not performed, CTEN's colocalisation with giantin, a conserved Golgi membrane protein, provides an interesting insight into the protein's function in HNSCC cells. This may indicate that CTEN is undergoing modification as a result of significantly increased expression. However it may also indicate that CTEN is playing an important role in the cell's secretory and signalling pathway, as Golgi is a key structure in cell signalling by spatially regulating kinases, phosphatases and GTPases (Farhan et al., 2010). Indeed, the Golgi apparatus has also been implicated in the cell's apoptotic signalling pathway (Machamer et al., 2003) and TGF beta signalling (Annes et al., 2003). RNA sequencing analysis presented in the previous chapter importantly highlighted both of these signalling pathways when studing the effect of CTEN silencing in HNSCC cells.

The mechanisms of release, and therefore activation of the TGF-β molecule are multiple and varied, although a significant number of the more recognised activators are linked functionally to the ECM (Munger and Sheppard, 2011). The importance of αvβ6 integrin in HNSCC invasion has already been described in the literature whereby αvβ6 has been shown to induce migration and invasion of normal keratinocytes and OSCC cell lines (Thomas et al., 2001a, 2001b). HNSCC is usually characterised by a vigorous desmoplastic response, but the contribution of tumour integrin expression profile, or the reasons causing this are poorly understood (Rosenthal et al., 2004). This remodelling of the

tumour microenvironment is believed to modulate tumour cell proliferation and invasion and. αvβ6 has demonstrated the ability to directly activate both TGF-β1 and TGF-β3 through an αvβ6-dependent, protease-independent activation process and most activators of TGF-β are functionally and structurally linked to the ECM (Annes et al., 2002; Munger et al., 1999).

A biological relationship between TGF-β and CTEN was initially hinted at with our head and neck cancer cell line screen with the finding of low CTEN in high β6 expressing VB6 compared to its negative controls IC6pr and C1 which had corresponding high CTEN expression. From our RNA sequencing analysis we have demonstrated that TGF-β1 levels were upregulated following CTEN depletion and TGF-β activation following CTEN knockdown was confirmed in MLEC activation assays, likely through the upregulation of surface αvβ6 integrin expression. Further evidence of an αvβ6-mediated effect was demonstrated by both an increase in cell surface expression following CTEN knockdown, as well as the pronounced effect in this cell population by an αvβ6 blocking antibody (Fig. 4.2A, middle panel).

The importance of the tumour microenvironment to the behaviour of tumours is now well recognised and reviewed by Koontongkaew (2013), but the most important stromal cell contributing to this behaviour and playing a key role in the tumour modulating function is likely the cancer-associated fibroblasts (CAF or myofibroblast). A prominent stimulator of myofibroblast transdiffentiation is TGF-β1, and therefore the finding of this cytokine as a key component of a prominent up-regulated protein raised interesting possibilities on how CTEN may be involved in modulating the tumour microenvironment and 'inside-out' cell signalling.

However, the importance of a biological CTEN - TGF-β link may lie outside the immediate functional consequences of surrounding stromal cells in the microenvironment but in fact involve important downstream regulatory effects on the tumour cells themselves. The effect and dominant phenotype induced by TGF-β signalling in carcinogenesis is highly depending on the presence and stage of tumour growth – there is a paradoxical role of this cytokine with an early stage tumour suppressor role, switching to a tumour promoting effect in latter stages (Inman, 2011). In HNSCC there has been more focus on the tumour suppressor role of TGF-β with a number of studies reporting an association of inactivating mutations and deletions of the TGF-β receptors with disease progression (Pasche et al., 2005; Xie et al., 2003), a finding supported by the recent

genome-wide analysis performed on The Cancer Genome Atlas (Lawrence et al., 2015). TGF-β is recognised as a potent growth inhibitor and stimulator of differentiation for epithelial cells (Massagué and Gomis, 2006) but although TGF-β has been reported to induce apoptosis in a variety of cell types under varying physiological conditions, the molecular mechanisms and pathways involved remain poorly defined (Meulmeester and Ten Dijke, 2011). Following the supporting observation of increased cell death in both 3D proliferation and related organotypic assays in our CTEN knockdown cells, we subsequently demonstrated that CTEN depletion resulted in activation of apoptosis. Pilot experiments suggested that this was in a TGF-β dependent manner by the reversal of activated caspase-3 upregulation in the presence of a TGF-β inhibitor (representative of activation of the final common apoptosis pathway). Whilst the pro-apoptotic or pro-survival influence of TGF-β depends on a complex interplay of signalling pathways, there is a large body of evidence demonstrating pro-apoptotic responses in prostate (Chipuk et al., 2001), ovarian (Lafon et al., 1996), cervical (Kim et al., 1998), breast (Tobin et al., 2001) and gastric cancer cells (Yanagihara and Tsumuraya, 1992).

We have demonstrated a novel mechanistic pathway linking CTEN with apoptosis, potentially mediated through a TGF-β pathway. However the suggestion of a relationship between CTEN and apoptosis is not in itself a completely novel concept; apoptosis is stimulated by any disruption in cell adhesion and spreading, implicating a critical role for focal adhesions in cell survival and in 2005, Lo et al. demonstrated an association between caspase-3 and CTEN, with the subsequent CTEN-cleaved fragments significantly affecting cellular growth.

Despite the growing evidence of the oncological importance of Tensins *in vivo* there are a number of contradictory results in the literature when considering their effect on cancer cell behaviour. Overexpression of TNS3 in human kidney cells and one melanoma cell line has been shown to reduce cell migration in a fibronectin-mediated haptotactic migration assay (Martuszewska et al., 2009). Another study showed contrasting results, demonstrating that TNS3 knockdown (but not other genes) resulted in a reduction of migration in three non-squamous lung carcinoma cell lines and three melanoma cell lines. However, these results were obtained from random, non-integrin specific migration assays. Similarly, CTEN has been shown to promote migration in a variety of cancer cell lines including colorectal cell lines (Al-Ghamdi et al., 2011; Albasri et al., 2009) although no mention was made of the chemoattractant used. Two other studies using non integrin-

specific migration assays demonstrated that EGF-induced cell migration in mammary epithelial cells was largely abolished with the knockdown of CTEN and depletion of TNS3 resulted in dramatic increases in cell migration even in the absence of EGF (Cao et al., 2012; Katz et al., 2007). Although CTEN has been demonstrated to promote tumour cell motility in a variety of cancers (Al-Ghamdi et al., 2013, 2011; Albasri et al., 2009), its function in relation to head and neck cancer cell has not previously been investigated. There is however growing evidence that CTEN supports tumour growth and a number of recent publications on prognostic biomarker potential support this fact (Al-Ghamdi et al., 2013; A. Albasri et al., 2011; Hong et al., 2013; Katz et al., 2007; Sakashita et al., 2008; Sasaki et al., 2003; Sjoestroem et al., 2013).

We also observed a CTEN mediated affect on cell motility and invasion but these results must be interpreted with caution, given our findings of cell survival effects. CTEN depletion conferred an anti-migratory and anti-invasive behaviour across HNSCC cell lines, without an obvious effect on concurrent cell proliferation studies, and this phenotype was corroborated in scratch and organotypic assays. However, the increased expression of activated caspase-3 in cells from organotypic cultures suggests a pro-apoptotic effect in HNSCC cells following CTEN knockdown, supported by 3D gel proliferation studies demonstrating a clear reduction in cell survival in the absence of CTEN. Cell culture within a gel structure appeared to highlight a prominent CTEN-mediated tumour promoting effect. The reduction of invasion and motility seen in CTEN deplete cells in our Transwell assays may also have been an early cellular response to a this pro-apoptotic effect, although the end point of these shorter assays may have been too soon to observe a significant reduction in cell counts at the assay end point. Future work could examine the morphology of cells at this time point to identify early changes consistent with induction of apoptotic pathways. It is also possible that the mechanical stress on cells of being in suspended culture in a 3D environment, with the changes in cell-cell contacts, interactions and subsequent integrin signalling, is important in the more prominent apoptotic response to CTEN knockdown. These changes may induce replicative stress upon cells which are sensitised to apoptosis induction in the absence of CTEN expression.

Furthermore, we hypothesised that the cellular stress induced by radiation would result in a similar radiosensitive phenotype in CTEN deplete cells and this was confirmed in clonogenic assays. What we did not anticipate was such a striking clinical correlation

with our patient dataset whereby the high expression of CTEN appeared to similarly confer a dramatic radioprotective effect on HNSCC tumours, as evidenced by reduced disease specific survival.

In summary, these findings suggest important new functional roles for CTEN. Whilst the involvement of biological processes including cell migration and ECM formation support other published evidence of the impact of CTEN expression on cancer cell motility, manipulating CTEN expression appears to heavily impact on TGFβ1 mediated pathways, apoptosis and programmed cell death. Exploring the mechanism of CTEN-induced resistance to apoptosis and its relationship to TGFβ signalling may provide important insights into the regulating factors behind the TGFβ switch from tumour suppressor to tumour promoter, and importantly, shed new light on pathways involved in radiotherapy resistance of HNSCC tumours.

Chapter 5: Tumour metabolism in head and neck cancer

5.1 Introduction

There has been widespread resurgent scientific interest in metabolism, and particular that specific to cancer cells, despite the Warburg effect being first described in the 1920s (Warburg et al., 1926). Recent identification of ubiquitous links between oncogenes and important regulators of metabolism has fuelled this interest, as well as the common use of positron emission tomography in the head and neck clinic for identification, staging and follow up of tumours.

In hypoxia, glucose is converted to lactate through the activity of glycolytic enzymes and lactate dehydrogenase A, known as glycolytic metabolism. However although many cancer cells utilise the physiological responses to hypoxia, many tumours develop an oxygen-independent reprogramming of metabolism whereby aerobic glycolysis becomes the predominant form of metabolism even when oxygen levels are normal (Semenza, 2009). The combination of reduced pO_2 and increased lactate production through aerobic glycolysis are both independent predictors for the most aggressive tumours (Semenza, 2009). Despite this however, aerobic glycolysis produces only net 2 ATPs per molecule of glucose compared to that of 36 ATPs from oxidative phosphorylation [OXPHOS] (Lehninger et al., 1982). A number of hypotheses have been proposed to explain this energy deficit but the greater requirement of rapidly proliferating cells for biosynthetic precursors, which can be obtained via glycolytic intermediates, is currently the most popular theory proposed (Heiden, 2009). Acidification of the microenvironment, which has numerous advantages for tumours including immunosuppression (Fischer et al., 2007), MMP activation (Robey et al., 2009) and enhanced metastases (Rofstad et al., 2006) are also well researched theories.

Head and neck squamous cell carcinoma (HNSCC) is a highly heterogeneous disease but apart from anatomical site, the most commonly used and clinically relevant classification is based on the presence or absence of a human papillomaviral (HPV) origin, often referred to through the surrogate marker p16 (INK4A) (Ang et al., 2010; Chung et al., 2014). HPV-related cancers, although tending to present at a more advanced stage, paradoxically have a better prognosis than HPV-negative tumours (Chung et al., 2014; Lawrence et al., 2015). In contrast HPV-negative tumours have a stronger association with the more traditional risk factors of tobacco and alcohol use, as well as having a specific genotype with an overexpression of EGFR (Vainshtein et al., 2014).

HPV types 16 or 18 are the most likely to cause a persistent viral infection, which occurs in approximately 10% of all new HPV infections (Lévy and Bartosch, 2015) and they are therefore the most likely types to result in carcinogenesis. This effect occurs through the encoding of two proteins – E6 and E7, which result in the degradation of the tumour suppressors p53 and Rb respectively (Hu et al., 2015). P53 is integral to the cell's energy metabolism regulation and has been shown to lower rates of glycolysis and increase mitochondrial respiration (Kruiswijk et al., 2015) through its transcriptional repression of a variety of glycolytic markers including GLUT1 and GLUT4 (Zhang et al., 2013), glucose-6-phosphate dehydrogenase (Jiang et al., 2011) and phospho-glycerate mutase (PGM) (Kondoh et al., 2005). It is also able to induce TIGAR (TP53-inducible glycolysis and apoptosis regulator), which indirectly negatively regulates the rate-limiting step in glycolysis through phosphofructokinase 1 (PFK1) (Bensaad et al., 2009, 2006).

The effect of E7 oncoprotein on tumour metabolism is slightly more convoluted but likely results in inhibition of the lower parts of the glycolytic chain through targeting of the tumour version of pyruvate kinase (M2), helping to channel intermediate metabolites into nucleic acid synthesis, consistent with highly proliferating cells (Zwerschke et al., 1999). It would therefore appear that the presence of the E6 and E7 oncoproteins should likely have a significant effect on the metabolic signature of virally derived tumours, with the loss of p53 in particular resulting in a metabolism favouring energy production through glycolysis rather than oxidative phosphorylation (OXPHOS). However there are certain circumstances *in vitro* where p53 has actually been shown to promote glycolysis (Ruiz-Lozano et al., 1999) and therefore it is highly likely that the clinical situation is more complex.

Positron emission tomography (PET) is an imaging modality that uses a glucose analogue, fluorine-18- fluorodeoxyglucose (18F-FDG), to identify tissue with rapid glucose uptake, therefore exhibiting an ideal clinical use for the Warburg effect (Heiden, 2009). PET combined with CT imaging is an important tool used clinically for imaging both HPV-positive and –negative HNSCC before treatment, as well as post-treatment in surveillance protocols. Given the improved prognosis of HPV-positive disease, confirmation of viral involvement is now routinely sought in HNSCC but requires tissue for diagnosis. PET imaging measures have already been shown to have prognostic value with high pre-treatment standard uptake values (SUV) associated with worse outcome (Allal, 2002; Inokuchi et al., 2011) and negative follow-up scans predictive for improved disease free

survival (Martin et al., 2009; Zhang et al., 2011). The question therefore of whether PET activity can help to differentiate HPV-positive or –negative disease is therefore highly relevant and so far has had variable outcomes in the literature. This is despite recent evidence that high GLUT1 expression is associated with p16 negative, non-oropharyngeal, and EGFR positive tumours (Baschnagel et al., 2015). There have been reports indicating an association of HPV-negative tumours with higher SUV values (Joo et al., 2014; Tahari et al., 2014) and conversely, reports have suggested that high nodal FDG uptake should raise suspicion for positive HPV status in the evaluation of the primary lesion (Clark et al., 2015; Kendi et al., 2015). The effect therefore of HPV-induction on the metabolic reprogramming on a tumour is currently unclear and with a host of new metabolic inhibitors now entering early stage trials in other cancer types, further research is urgently required to clarify the metabolic features of HNSCC in these two groups.

There is also now increasing focus on the potential link between a tumour's metabolic phenotype and its ability to move and interact with the tumour microenvironment. The majority of these findings have been through studying the functions of key metabolic sensors – the C-terminal binding proteins (CtBP1 and CtBP2). NADH-dependent CtBP monomer dimerisation results in activation of their transcriptional repression function (Bergman and Blaydes, 2006; Chinnadurai, 2009) and a number of tumour suppressor genes involved in tumour cell motility, invasion and survival have recently been implicated. For example, activated CtBPs have been shown to repress E-cadherin expression (Zhang et al., 2006), promoting an EMT-phenotype in hypoxic tumours. CtBP1 has shown a close inverse correlation with E-cadherin expression in malignant breast cancer samples (Deng et al., 2012). CtBP2 has also been implicated in regulation of cell motility through its observed ability to repress PTEN expression with resulting increased phosphatidylinositol 3-kinase (PI3K) activity and Rac-dependent migration (Paliwal et al., 2007). More recently, CtBP2 has been identified as a positive regulator of T-cell lymphoma invasion and metastasis 1 (Tiam1), a GTP exchange factor (GEF) or activator for Rho-like GTPases (Paliwal et al., 2012). Indeed, to identify potential CtBP-dependent effectors, our group previously performed a gene expression array in an oral SCC cell line (SCC25) following CtBP knockdown (Rucka et al; unpublished). CTEN was identified as a previously unreported candidate gene for CtBP2 targeting, as it was found to be upregulated following CtBP2 knockdown. In support of this biological link, we also

noted an upregulation of gene ontology terms relating to cell metabolism on RNA sequencing analysis between control and CTEN siRNA treated samples.

In this chapter we explore the metabolic profiles of both HPV-negative and HPV-positive HNSCC. We have previously demonstrated the important functional and prognostic role of CTEN both *in vitro* and *in* vivo in HNSCC and we present novel evidence linking metabolism, through the metabolic sensors CtBPs, with the regulation of CTEN. CTEN is demonstrated as a previously unknown target of CtBP2 and therefore one potential downstream mediator of a cancer cell's complex glycolytic phenotype.

5.2 Glucose concentration in metabolism-dependent assays

To perform a range of metabolically sensitive assays, careful manipulation of the glucose concentration throughout the assay is required. Due to glucose uptake by cells, the glucose concentration in media will inevitably decrease. Cells left without glucose substrate could adversely affect outcomes. We therefore screened a representative HNSCC cell line (SCC25) in medium containing different concentrations of glucose to determine the rate of glucose consumption, which could help us to maintain suitable glucose concentration in future assays (Fig. 5-1).

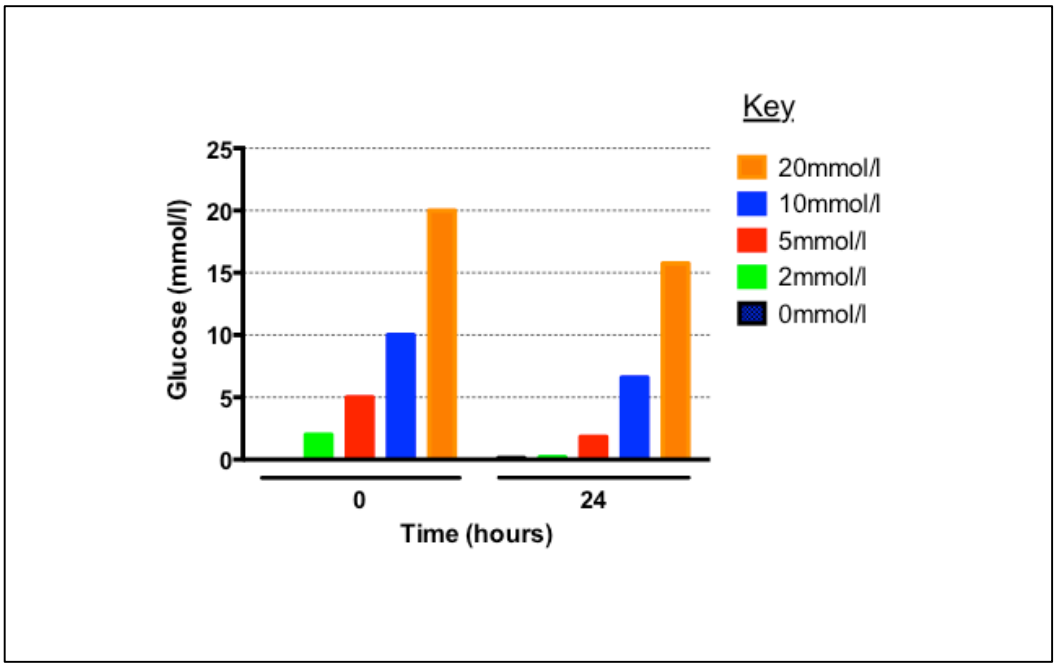

Figure 5-1. Glucose concentration after 24 hours in cell culture medium. **SCC25 cells were incubated in glucose free DMEM, supplemented with 10% fetal bovine serum and**

2mM L-glutamine. Glucose supplementation was performed at time-point 0 to give a set concentration range. Media was collected after 24 hours of cell culture and a glucose assay was utilised to analyse the residual glucose concentration.

As expected, glucose concentrations diminished such that 2 mmol/l glucose supplementation had all been used by the 24-hour time point. Due to this result, glucose was replaced at 24 hours of all assays where set glucose supplementation was required and glucose supplemented media for specific assays used 5 mmol/l as the lowest starting concentration, mirroring the normal physiological blood levels.

5.3 Glucose concentration affects cell glycolysis and respiration

In order to stimulate cancer cells *in vitro* to increase their glycolytic rate, a commonly used laboratory technique is to increase the concentration of available glucose in the cell media (Birts et al., 2013). To confirm that this did indeed result in an increased glucose uptake and glycolytic rate, we tested a highly glycolytic head and neck cancer cell line (H357) in an extracellular flux analyser, measuring oxygen consumption rate (OCR) and extracellular acidification rate (ECAR) (Fig. 5-2). From these two outputs we are able to extrapolate a cell's mitochondrial respiration (OCR) and glycolysis (ECAR). After stabilisation of the cell's bioenergy pathways, variable injections were used to study different metabolic capacities; 5mmol/l glucose was initially injected to observe for any response in glycolysis, followed by oligomycin A, which inhibits proton flow through ATP synthase and therefore blocks mitochondrial respiration. This allows us to observe maximal glycolytic rate and the difference is the glycolytic capacity of a cell line. Finally glycolysis was inhibited with the glucose analogue 2-deoxyglucose (2-DG) which has the 2-hydroxyl group replaced by hydrogen.

This powerful analytical technique demonstrated that the addition of glucose to cell medium indeed resulted in increased glycolysis with a higher ECAR exhibited by cells exposed to greater glucose concentrations, reflective of lactic acid production through the glycolytic pathway. This was supported by a reciprocal reduction in respiration (OCR). The basal respiration shown in Figure 5-2C is calculated from the last rate measurement before oligomycin injection minus the non-mitochondrial respiration rate. The OCR at 20mmol/l was inconsistent and did not demonstrate the continued trend for a respiration

to glycolysis switch evident at lower glucose concentrations but may reflect the increased need for greater ATP production in this highly metabolically stimulated population, therefore requiring significant contributions to metabolic demands from both the respiratory and glycolytic pathways. Oligomycin is an ATP synthase inhibitor, an enzyme integral for OXPHOS. As would be expected, addition of this antibiotic halts OXPHOS, with a drop and rise in the OCR and ECAR respectively. The ECAR results following injection indicate a glucose-responsive effect not only on the active glycolytic rate, but also on glycolytic capacity; cells supplemented with 20mM glucose have the greatest glycolytic capacity. Finally following 2-DG injection we observed a cessation of aerobic glycolysis indicated by a drop in ECAR to basal levels. Some residual basal glycolysis is evident in the highest glucose concentration (20mM). These results confirm that additions of variable glucose-supplemented medium are an appropriate stimulus in metabolic assays to increase the cellular glycolytic rate.

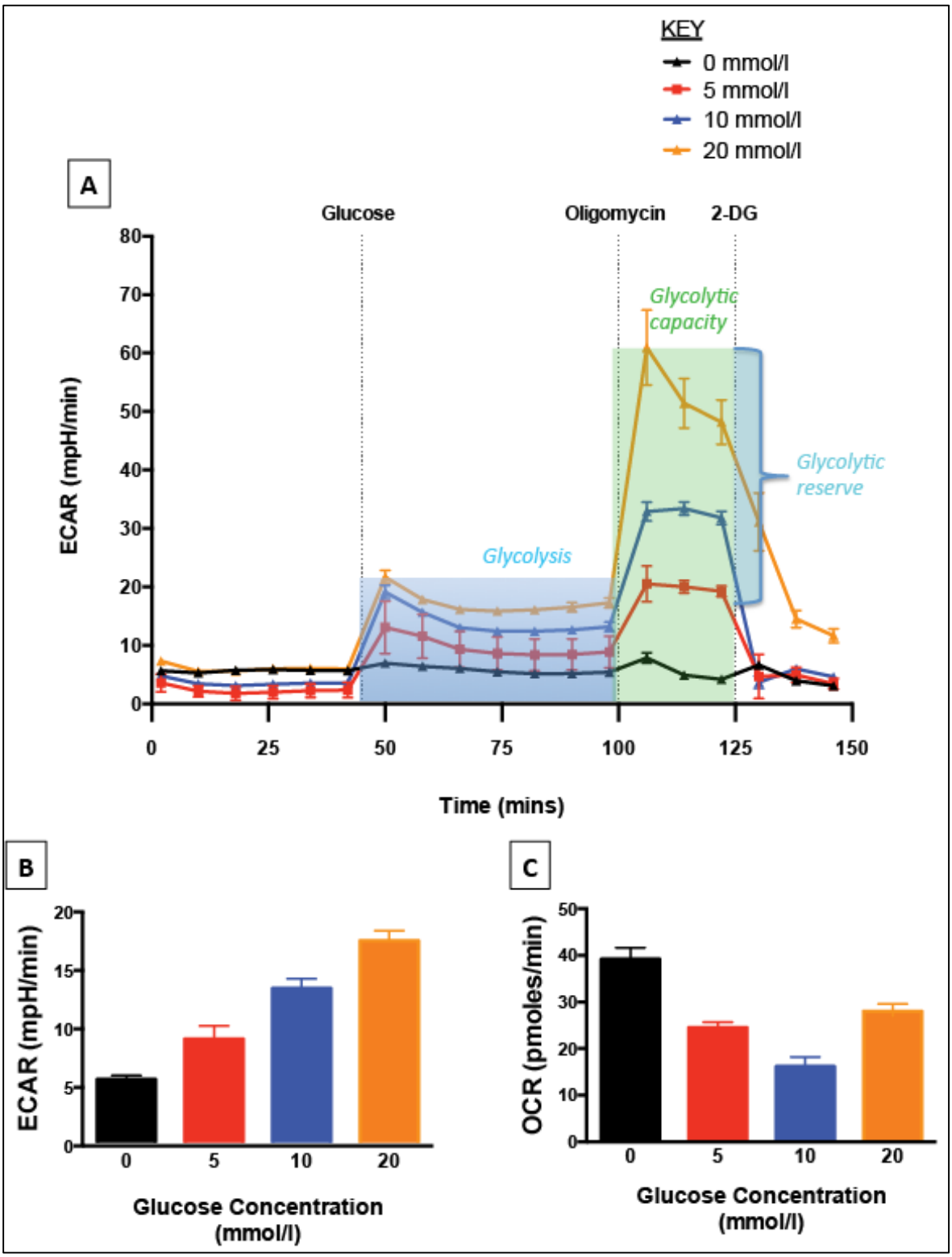

Figure 5-2. Metabolic flux analysis of increasing glycolysis in a HNSCC cell line (H357). A metabolic flux analyser (Seahorse®) was used to measure extracellular acidification rate (ECAR), a correlate of glycolysis, in real time following addition of various compounds. Higher glucose concentration supplementation resulted in an increased glycolytic rate (A). Glycolytic capacity and glycolytic reserve, as demonstrated for 20 mmol/l results, were also increased by higher glucose addition. B, bar chart representation at 98 minutes, prior to oligomycin injection, demonstrates the final basal glycolytic rate and was highly significant for multiple comparisons between groups (ANOVA test, P<0.0001). C, a reciprocal reduction in the basal respiration (OCR) was also observed with increasing glucose

concentrations below 20mmol/l, indicating that glucose is resulting in an increasing reliance on glycolysis for the cell's energy demands. Results are representative of two biological repeats with six replicate wells.

5.4 Real-time extracellular flux analysis

We hypothesise that the HPV status of HNSCC results in a distinct glycolytic profile dependent on the tumour origin. However in order to detect changes in the major energy-producing pathways of HNSCC cell lines, we require accurate analysis techniques operating in real time. The Seahorse XF96 Extracellular Flux Analyzer (Seahorse Bioscience, North Billerica, MA) was used for this purpose and enabled us to accurately contrast and compare the bioenergetic phenotypes of HPV-positive and HPV-negative cell lines. As previously the outputs of oxygen consumption rate (OCR) and extracellular acidification rate (ECAR) enable us to extrapolate a cell's mitochondrial respiration and glycolysis respectively. After stabilisation of the cell's bioenergy pathways, the first injection used was 5mmol/l glucose to represent a physiological concentration and allow observation of a cell's utilisation of the substrate. The antibiotic oligomycin A was then injected which inhibits proton flow through ATP synthase and therefore blocks mitochondrial respiration. Finally in half the cell cultures we stimulated maximal respiration by injecting carbonylcyanide-ptrifluoromethoxyphenyl hydrazone (FCCP), which absolves potential across the mitochondrial membrane leading to rapid O_2 use, and in the other half used the glucose analogue 2-deoxyglucose (2-DG) to inhibit glycolysis. Following completion, all results were normalised to total protein count following Bradford assay analysis to account for any variable cell line proliferation rates (Fig.5-3). Real time concurrent reading of cell lines in this technique allows a direct comparison of bioenergetic profiles and response to the various injections reveals key components of both oxidative phosphorylation and glycolytic pathways. The HPV-negative cell lines had significantly higher basal ECAR and OCR compared to the HPV-positive cell lines. The difference between maximal and basal ECAR is considered the glycolytic reserve capacity of cells and calculation (Fig.5-3D) demonstrates that HPV-negative cells have the potential for much higher glycolytic rates than their virally derived counterparts, and from the OCR/ECAR ratio these cell lines of SCC2 and SCC90 were indeed relying more on mitochondrial respiration for their energy requirements. Interestingly despite their

increased reliance on glycolysis, the respiratory capacity of SCC25 and SCC89 were also greater than the HPV-positive group indicating that these cell lines have greater potential for ATP production and could in theory switch between OXPHOS and glycolysis to satisfy greater bioenergy demands depending on various tumour factors such as blood supply, hypoxia and the surrounding microenvironment.

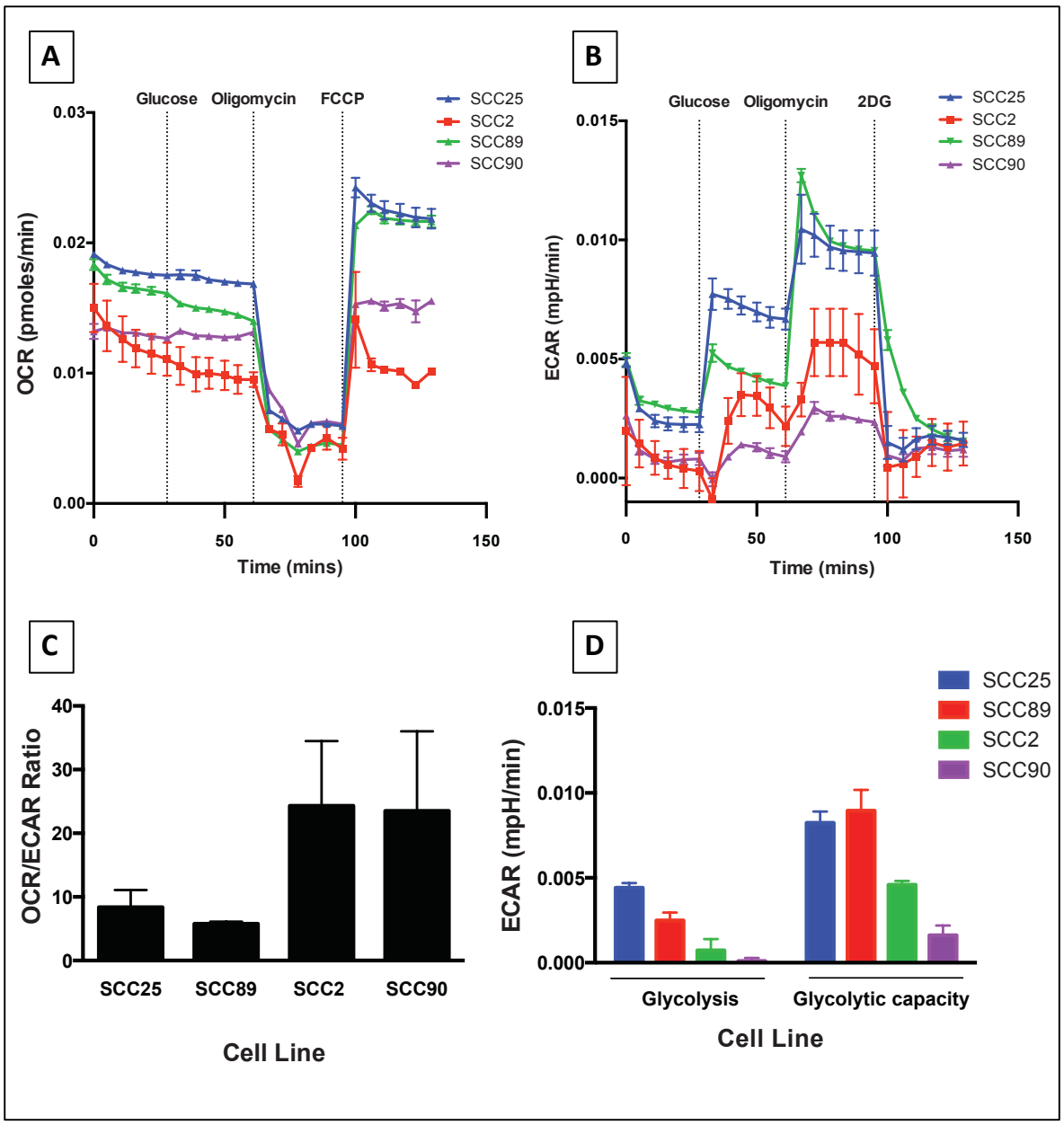

Figure 5-3. Bioenergetic profile of HPV-positive and HPV-negative cell lines. The extracellular acidification rate (ECAR) and oxygen consumption rate (OCR) were measured using an extracellular flux analyser (Seahorse Bioscience) to estimate glycolysis and mitochondrial respiration respectively. Two HPV-negative (SCC25, SCC89) and two HPV-positive (SCC2, SCC90) HNSCC cell lines were studied with a minimum of four replicate wells per experimental run. Data from one representative experiment is shown (n=2). Port injections as indicated in (A) & (B) included glucose (5mmol/l), the ATP synthase inhibitor oligomycin A and finally FCCP to uncouple mitochondria or 2-DG to cease glycolysis. HPV-negative cell lines demonstrated globally elevated OXPHOS and glycolytic rates with increased respiratory capacity (A) and glycolytic capacity (B, D). C, The OCR/ECAR ratio was calculated to determine the determination reliance on respiration vs glycolysis for a cell's bioenergetic requirements. This demonstrated a significantly reduced OCR/ECAR ratio in HPV-negative compared to HPV-positive cell lines, indicating the latter are more reliant on oxidative phosphorylation for ATP requirements than glycolysis (ANOVA, Tukey's multiple comparisons, P<0.01 for all comparisons HPV-ve vs HPV+ve cell

lines). D, ECAR values between cell lines were utilised to calculate the glycolytic rate (maximum rate measurement before oligomycin injection – last rate measurement before glucose injection) and glycolytic capacity (maximum rate measurement after oligomycin injection – last rate measurement before glucose injection), expressed as mpH/min.

Both HPV-positive cell lines appeared to be operating closer to their maximal respiratory capacity under standard cell culture conditions.

5.5 In vitro expression of metabolic markers

Whilst the high-affinity glucose transporter GLUT1 allows rapid uptake of glucose to accommodate an increase in glycolytic rate in response to, for example, hypoxia, it is part of a co-ordinated transcriptional response to such conditions (Burrows et al., 2010) and therefore a number of other targets can be analysed to get a global picture of a cancer cells metabolic phenotype. Lactate dehydrogenase A (LDHA) is one of the enzyme's subtypes favouring the production of lactate from pyruvate and has been found to be upregulated in a number of tumour types (Lewis et al., 1997; Shim et al., 1997). Furthermore this end by-product of glycolysis, lactate, requires close control within a cell's homeostatic capabilities and a number of different transporters have been implicated in maintaining this balance such as the monocarboxylate transporters (MCT1-4), of which MCT1 and MCT4 are the most researched due their localisation to the cell membrane. We obtained two cell lines of presumed HPV+ve origin: SCC2 and SCC90 (courtesy of Susanne Gollin, UPMC, PA). Polymerase chain reaction (PCR) was performed to confirm the presence of E6/E7 oncoprotein RNA at an expected DNA band of ≈300bp and following confirmation of the cell lines' HPV origin, we analysed a panel of both HPV-negative and HPV-positive cells for expression of the above proteins of interest (Fig. 5-2). The results of this protein expression analysis indicate an *in vitro* pattern with a distinct expression of metabolic markers between HPV-positive and –negative cell lines. This was most demonstrable for MCT1 expression, which will be investigated further in Chapter 6, but the data supported the hypothesis of a different metabolic signature existing between these two subgroups of HNSCC cell lines.

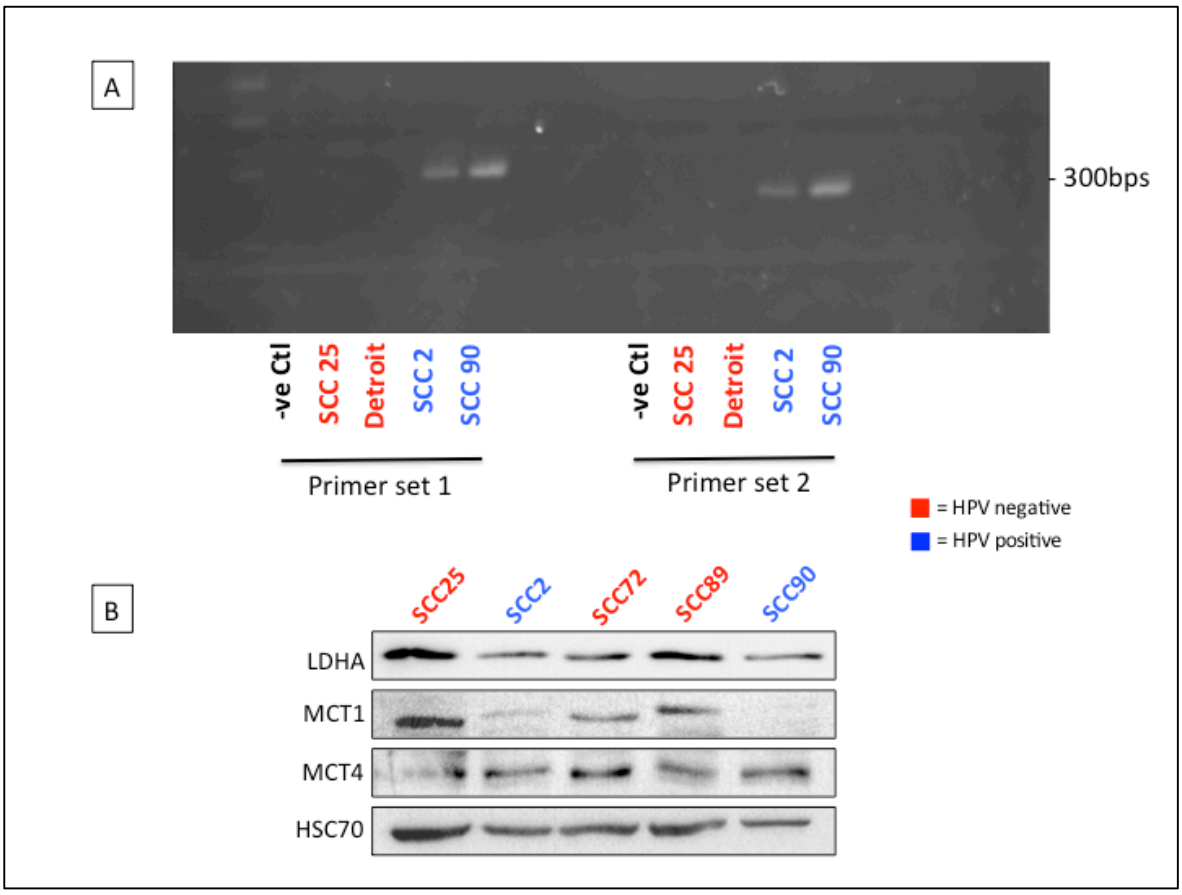

Figure 5-4. The presence of an HPV origin of cancer cell lines results in a distinct protein expression profile of glycolytic markers. A, Custom E6/7 primers were designed (KM; Appendix A) and RNA extracted from presumed HPV-positive cells lines (SCC2, SCC90) was compared with that from known HPV-negative cell lines (SCC25, Detroit 562) following amplification by PCR, run on a 2% agarose gel. RNA-ase free water was included as a negative control in the PCR. HPV origin of SCC2 and SCC90 was confirmed following observation of bands at approximately 300bp. B, A panel of HPV-negative (SCC25, SCC72, SCC89) and confirmed HPV-positive cell lines (SCC2, SCC90) were analysed for protein expression of key metabolic markers of LDHA, MCT1 and MCT4 by Western blotting. HSC70 was used as a loading control.

5.6 GLUT1 expression in HNSCC

Tumour cells exhibit a preference for glycolytic metabolism through the Warburg effect and many of the features common to tumours such as hypoxia, result in an upregulating glucose transporter (GLUT) expression (Heiden, 2009). GLUT1 in particular has been shown to strongly correlate with tumour growth and poor prognosis (Szablewski, 2013) and is a common reference target used when discussing the promotion of glucose uptake supporting the Warburg effect in tumour cells (Rigo et al., 1996). The correlation between GLUT1 and FDG accumulation is still unclear but the glucose transporter has been found

to be upregulated in HNSCC in a number of studies (Kunkel et al., 2003; Mellanen et al., 1994; Reisser et al., 1999; Tian et al., 2004).

GLUT1 is therefore a useful initial marker for the characterisation of tumour metabolism. We re-analysed a previously stained TMA slide library for GLUT1. As previously, patients for this analysis had been taken from a large cohort of combined OPSCC patients from University Hospital Southampton (2000-10), Poole NHS Foundation (2000-6) and Bart's and the London NHS Trust (2000-6) and collated by Mr. Matthew Ward (M. J. Ward et al., 2014; See Table 3-1 for patient demographics). The purpose of this re-analysis was to compare HPV-positive and HPV-negative HNSCC for GLUT1 scoring and thus start our comparison of the metabolic profile of these two tumour groups (Fig. 5-5). An established GLUT1 stained library was stratified as either high (moderate/strong staining) or low (absent/weak staining) and we found that high GLUT1 scoring was significantly associated with HPV-negativity ($P<0.0001$). Interestingly we found no significant association between GLUT1 score and prognosis in the two groups (Fig 5-5 B&C), although there was a strong trend in the HPV-positive cohort.

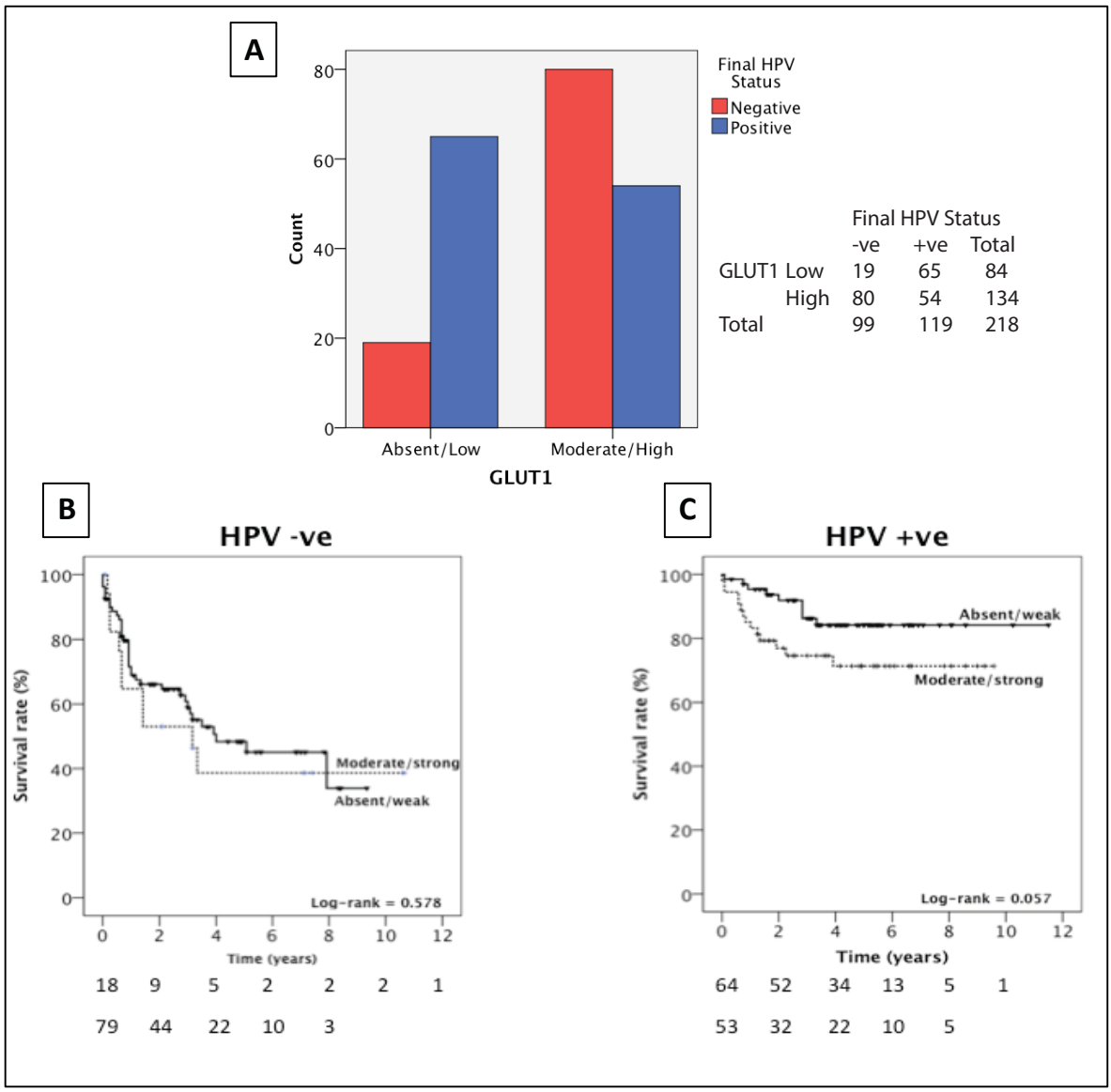

Figure 5-5. Clinicopathological data for GLUT1 scoring in HNSCC TMA. A, Cross-tabulation comparison of GLUT1 scoring (Low vs. High) by HPV status. Significantly higher GLUT1 scoring was observed in HPV-negative tumours compared with HPV-positive tumours (P<0.0001). B, C, Kaplan-Meier curves for HPV-negative (left) and HPV-positive OPSCC (right). On log-rank testing, no significant correlation was observed between GLUT1 scoring and disease specific survival irrelevant of HPV status although a trend approaching significance was observed in HPV-positive tumours.

By itself, an increase in GLUT1 expression may represent a variety of intra-tumoural features such a hypoxia, or a preference of alternative glucose transporters to mediate the glycolytic pathway. However, the increase preponderance of GLUT1 expression in HPV-negative tumours suggests that this tumour group has an increased glycolytic rate requiring an increase in these high affinity glucose transporters, in keeping with our previous *in vitro* metabolic flux analysis.

5.7 RNA expression panel of metabolic markers in HNSCC

Our initial screen of GLUT1 expression in an HNSCC TMA and subsequent cell line screen of important enzymes/transporters involved in lactate homeostasis suggested a significantly altered glycolytic profile between HPV-positive and –negative disease. Our real time extracellular flux analysis confirmed a higher glycolytic rate and reserve in HPV-negative cell lines. We utilised a previously collated local RNA database from a prospective patient cohort including 10 HPV-positive and 13 HPV-negative subjects (Woods et al, in press). Only tumours with a positive RNA signature for both oncoproteins E6 and E7 together with clinical correlation from p16 staining were classed as HPV positive (Robinson et al., 2010). Sequencing data was generated using PolyA selected RNA extracted from whole tumour tissue from each patient. Reads were mapped to the human genome (hg19) with Tophat 2.0.13 and then counted using HTSeq. The raw count data were normalised for library size between samples using the trimmed mean of M-values (TMM) method followed by applying a negative binomial model to obtain dispersion estimates. Genes were excluded that had less than 2 read counts per million (CPM) in 25% of samples, giving a total of 14,528 genes. From this dataset, we extracted read counts in both tumour groups of key genes involved in glycolytic and mitochondrial respiration gene in order to validate our previous protein work and *in vitro* cell line analysis. Therefore as well as investigating differences in expression of previously investigated genes including GLUT1, LDHA, MCT1 and MCT4, we also added LDHB, PDK1, HIF1A, PKM2, SDHD, NDUFA13 and TOMM20 to the panel (Fig. 5-6). We have already discussed the association of LDHA and tumour growth, but LDHB has also been associated with several cancer types, although the association is more complex (Doherty and Cleveland, 2013). Hypoxia-inducible factor 1 (HIF1A) increases the expression of a number of glycolytic markers and enzymes including GLUT1 and pyruvate dehydrogenase kinase 1 (PDK1), which phosphorylates and inactivates pyruvate dehydrogenase and therefore blocks entry of pyruvate into the tricarboxylic acid cycle (TCA), essentially decoupling glycolysis and OXPHOS (Kim et al., 2007, 2006). Another key enzyme regulating glycolysis and the Warburg effect in highly proliferating cells is pyruvate kinase M2 (PKM2), which determines the conversion of pyruvate to lactate (Christofk et al., 2008). PKM2 slows the metabolic passage through glycolysis and this allows the diversion of intermediates into macromolecule and NADPH production through the pentose phosphate pathway; a vital

component of rapidly dividing cells (Cairns et al., 2011). To give representation to OXPHOS genes we selected genes from Complex I and II in the respiratory chain, including NDUFA13 (Complex I) and succinate dehydrogenase (SDHD, Complex II) as well as mitochondrial import receptor subunit TOM20 homolog (TOMM20), which correlates with mitochondrial mass and OXPHOS metabolism. NDUFA13 is integral to the enzymatic activity of complex I and loss has been reported in several cancer types (Gong et al., 2007; Kalakonda et al., 2007) and SDH oxidizes succinate to fumarate in the TCA cycle and mutational effects on function have been implicated in hereditary paragangliomas and phaeochromocytomas (Baysal et al., 2000).

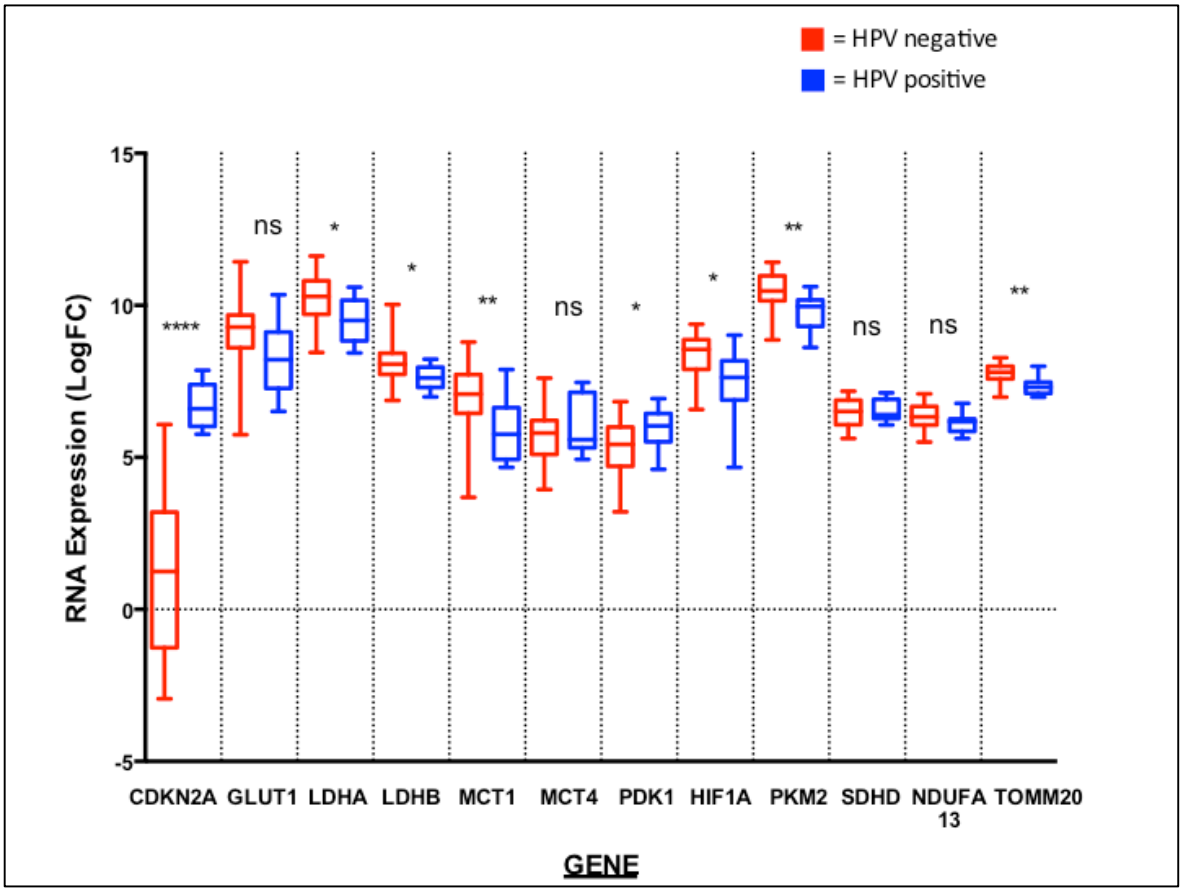

Figure 5-6. RNA expression panel of key metabolic genes comparing HPV-positive (n=10) with HPV-negative (n=13) HNSCC. mRNA levels are expressed as log2 gene expression. CDKN2A ($p16^{INK4a}$) is included as validation for determination of HPV positivity as clinically corroborated with IHC. Read counts compared with non-parametric Mann-Whitney test following graphical confirmation of non-normalised data distribution. Significantly increased expression levels in HPV-negative tumours are observed for LDHA (P=0.0143), LDHB (P=0.0143), MCT1 (P=0.0075), HIF1A (P=0.0213), PKM2 (p=0.0022) and TOMM20 (P=0.0013) whilst PDK1 alone was

elevated in HPV-positive tumours (P=0.0452). No difference between groups was observed for GLUT1 (P=0.0843), MCT4 (P=0.586), SDHD (P=0.863) or NDUFA13 (P=0.202).

This expression panel broadly supports our previous *in vivo* and *in vitro* data although such detailed RNA expression data raises some extra interesting points of discussion. Overall there is widespread elevation of RNA expression of genes associated with glycolysis including LDHA, HIFIA and PKM2 in the HPV-negative group. This trend was also present for GLUT1, although it did not reach significance (P=0.0843). The OXPHOS target RNA for components of complex I and II showed no significant difference between groups but TOMM20, a protein found in the outer mitochondrial membrane that correlates with OXPHOS (Wurm et al., 2011), was highly expressed in HPV-negative tumours, consistent with our flux analysis data where both ECAR and OCR were elevated in these non-virally derived cell lines. Interestingly there was an elevation in PKM2 in HPV-negative tumours, suggesting that there is more diversion of glycolytic intermediates into biosynthetic pathways such as the pentose phosphate pathway for macromolecule production. This was also consistent with our cell line data showing that HPV-negative cancer cells are globally metabolically more active with greater energy requirements in keeping with the requirement for redox balance in the presence of rapid cell division. It may also help to explain why our HPV-negative cell lines demonstrated a greater glycolytic capacity *in vitro*, with their full glycolytic potential moderated by elevated PKM2 to allow for intermediate shuttling for nucleotide and NADPH production.

RNA expression data alone doesn't necessarily fully explain the clinical picture. The phenotypic effect of these changes depends on protein expression, post-transcriptional regulation, duration of protein action and levels of activated protein, especially important when considering enzymatic processes. However analysis of this dataset supports previous results demonstrating that when considering glucose metabolism, HPV-negative tumours exhibit greater glycolytic rates and glycolytic capacity.

5.8 Metabolic signature from RNASeq data

The immunohistochemistry, clinical imaging and RNASeq data presented thus far have provided evidence in multiple different patient cohorts and cell lines of a glycolytic

signature in HPV-negative tumours. This raises the question however of whether other metabolic pathways differ between the two patient groups or whether the unique phenotype is confined to glucose metabolism pathways. This could have important implications for diagnosis, target identification and metabolic treatments in HNSCC and therefore warrants further investigation. To examine all metabolism related genes, we collected ID codes for all metabolism-related sub-pathways from the KEGG PATHWAY database (http://www.genome.jp/kegg-bin/get_htext#B1). MetabolicMine (http://www.humanmine.org/) was then utilised to perform a gene query for all genes involved in the identified pathways. Non-human species results were excluded and all gene symbols were converted into ensemble IDs. All genes were matched to related IDs apart from 3 genes which were lost in cross conversion (GALNTL2, GALNTL4, PTPLA). 111 metabolism-related genes were identified in the differentially expressed genes (DEG) between HPV+ve and –ve tumour samples (Fig. 5-7A) using the same RNASeq Poole Hospital patient dataset from Fig.5-6. The top up- and down-regulated genes were pulled from the dataset and are listed in Fig. 5-7B. Pearson's correlation analysis metric was used to produce a heat map of these 111 common genes coded for DEG values (Fig. 5-7C; performed together with Dr. J. Woo [Bioinformatics core, University of Southampton]).

A brief inspection of the global DEGs between the two patient groups indicated involvement of a large group of genes both inside and outside of carbon metabolism pathways. A closer analysis of the top differentially expressed genes certainly indicates a sizeable down regulation of genes involved in glycolysis in the HPV-positive group (Fig. 5-7B). For example, phospholipase A2, significantly down-regulated in the HPV-positive cohort, is an important enzyme involved in accelerating glucose utilization (Miwa et al., 1993) and similarly the significantly reduced expression of the glycolytic enzyme hexokinase in this group, a glycolytic enzyme that supports rapid proliferation (Wolf et al., 2011), is supportive of this hypothesis. It is also interesting to note the appearance of glutaminase as being up-regulated in the HPV-positive group, raising the suggestion that a reduction in the glycolytic flux rate here is resulting in an increase in glutaminolysis to balance energy production.

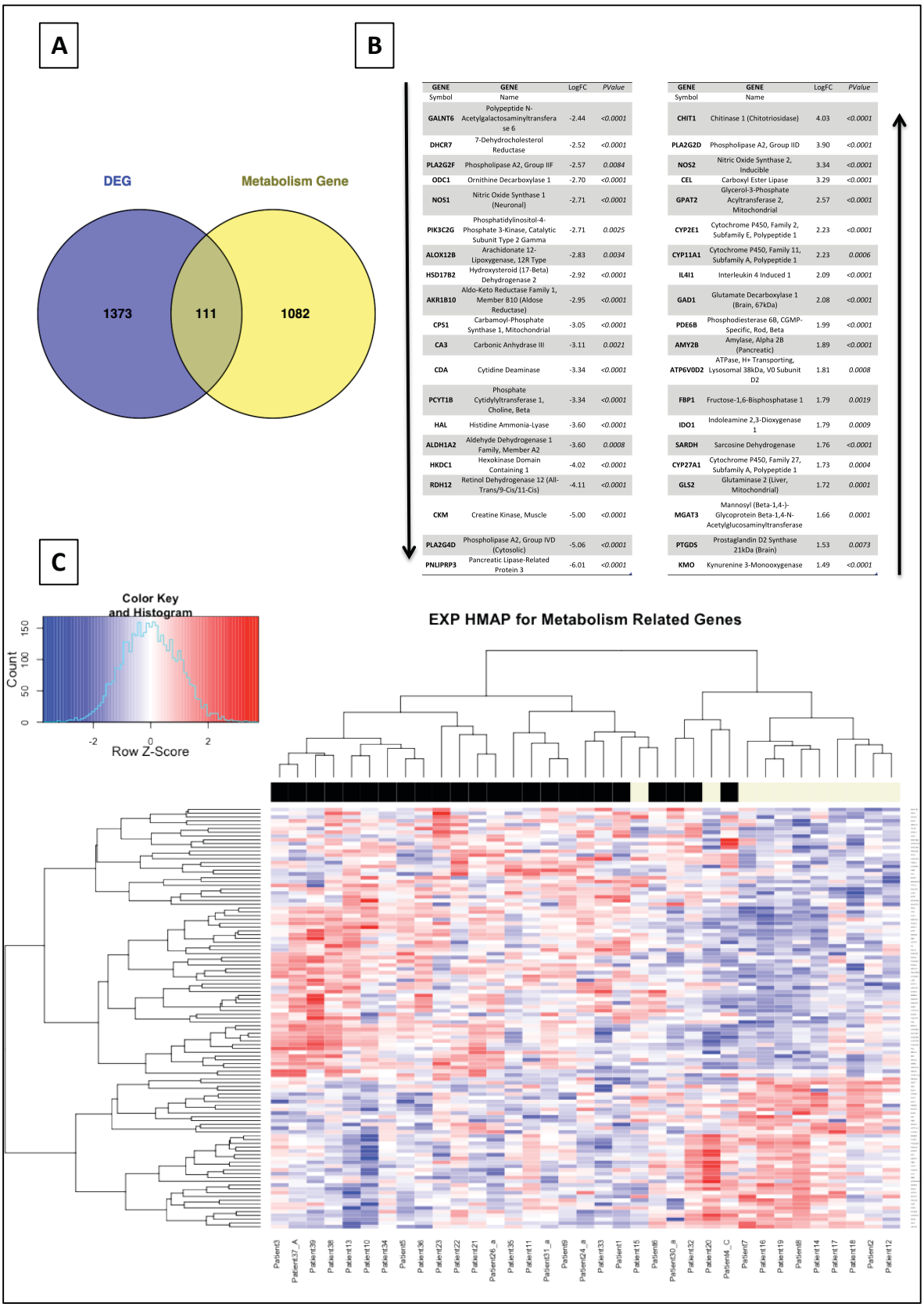

GENE Symbol	GENE Name	LogFC	PValue
GALNT6	Polypeptide N-Acetylgalactosaminyltransferase 6	-2.44	<0.0001
DHCR7	7-Dehydrocholesterol Reductase	-2.52	<0.0001
PLA2G2F	Phospholipase A2, Group IIF	-2.57	0.0084
ODC1	Ornithine Decarboxylase 1	-2.70	<0.0001
NOS1	Nitric Oxide Synthase 1 (Neuronal)	-2.71	<0.0001
PIK3C2G	Phosphatidylinositol-4-Phosphate 3-Kinase, Catalytic Subunit Type 2 Gamma	-2.71	0.0025
ALOX12B	Arachidonate 12-Lipoxygenase, 12R Type	-2.83	0.0034
HSD17B2	Hydroxysteroid (17-Beta) Dehydrogenase 2	-2.92	<0.0001
AKR1B10	Aldo-Keto Reductase Family 1, Member B10 (Aldose Reductase)	-2.95	<0.0001
CPS1	Carbamoyl-Phosphate Synthase 1, Mitochondrial	-3.05	<0.0001
CA3	Carbonic Anhydrase III	-3.11	0.0021
CDA	Cytidine Deaminase	-3.34	<0.0001
PCYT1B	Phosphate Cytidylyltransferase 1, Choline, Beta	-3.34	<0.0001
HAL	Histidine Ammonia-Lyase	-3.60	<0.0001
ALDH1A2	Aldehyde Dehydrogenase 1 Family, Member A2	-3.60	0.0008
HKDC1	Hexokinase Domain Containing 1	-4.02	<0.0001
RDH12	Retinol Dehydrogenase 12 (All-Trans/9-Cis/11-Cis)	-4.11	<0.0001
CKM	Creatine Kinase, Muscle	-5.00	<0.0001
PLA2G4D	Phospholipase A2, Group IVD (Cytosolic)	-5.06	<0.0001
PNLIPRP3	Pancreatic Lipase-Related Protein 3	-6.01	<0.0001

GENE Symbol	GENE Name	LogFC	PValue
CHIT1	Chitinase 1 (Chitotriosidase)	4.03	<0.0001
PLA2G2D	Phospholipase A2, Group IID	3.90	<0.0001
NOS2	Nitric Oxide Synthase 2, Inducible	3.34	<0.0001
CEL	Carboxyl Ester Lipase	3.29	<0.0001
GPAT2	Glycerol-3-Phosphate Acyltransferase 2, Mitochondrial	2.57	<0.0001
CYP2E1	Cytochrome P450, Family 2, Subfamily E, Polypeptide 1	2.23	<0.0001
CYP11A1	Cytochrome P450, Family 11, Subfamily A, Polypeptide 1	2.23	0.0006
IL4I1	Interleukin 4 Induced 1	2.09	<0.0001
GAD1	Glutamate Decarboxylase 1 (Brain, 67kDa)	2.08	<0.0001
PDE6B	Phosphodiesterase 6B, CGMP-Specific, Rod, Beta	1.99	<0.0001
AMY2B	Amylase, Alpha 2B (Pancreatic)	1.89	<0.0001
ATP6V0D2	ATPase, H+ Transporting, Lysosomal 38kDa, V0 Subunit D2	1.81	0.0008
FBP1	Fructose-1,6-Bisphosphatase 1	1.79	0.0019
IDO1	Indoleamine 2,3-Dioxygenase 1	1.79	0.0009
SARDH	Sarcosine Dehydrogenase	1.76	<0.0001
CYP27A1	Cytochrome P450, Family 27, Subfamily A, Polypeptide 1	1.73	0.0004
GLS2	Glutaminase 2 (Liver, Mitochondrial)	1.72	0.0001
MGAT3	Mannosyl (Beta-1,4-)-Glycoprotein Beta-1,4-N-Acetylglucosaminyltransferase	1.66	0.0001
PTGDS	Prostaglandin D2 Synthase 21kDa (Brain)	1.53	0.0073
KMO	Kynurenine 3-Monooxygenase	1.49	<0.0001

Figure 5-7. RNA sequencing analysis of HPV positive vs HPV-negative tumours in previously collected prospective HNSCC patient cohort. Genes in involved in global metabolism pathways were extracted from KEGG and compared against differentially expressed genes (DEG) from patient samples. A, 111 metabolism-related genes were identified in the differentially expressed genes (DEG) between HPV+ve and –ve tumour samples. B, Top 20 DEG based on up

or down-regulated log2 fold changes were extracted for inspection together with significant P-values. All fold changes represent changes in HPV-positive group compared to HPV-negative. C, Heat map of 111 common genes coded for DEG values as illustrated. Patients clustered in accordance with HPV status (black HPV-ve (left), grey HPV+ve (right)) for metabolism genes except for two outliers (patient15, patient20), both of whom exhibited unique histopathological features.

The observed clustering between HPV+ve and HPV-ve samples validates our hypothesis of a unique metabolic signature beyond simply glycolysis and OXPHOS genes separating these two groups as this heat map relates to all metabolism related genes. There were two noticeable outliers in the heat map and representative pathological slides were inspected by a Consultant Pathologist (GT) to identify any abnormal features: one (Patient15) was histologically confirmed as basaloid subtype, a particularly aggressive subtype, and the other (Patient20) had unusual keratinization normally associated with HPV-negative disease although in all other metrics it was classified as HPV-positive. In order to corroborate this unsupervised clustering, we performed principal component analyses (PCA; Fig. 5-8A). The commonly used definition for PCA is “a mathematical algorithm that reduces the dimensionality of the data while retaining most of the variation in the data set” (Ringnér, 2008) but essentially it is of most use as a data visualisation technique to reveal the internal structure of the data. However it is a linear and parametric method and therefore a new technique of t-Distributed Stochastic Neighbour Embedding (t-SNE) was also used as it is particularly adept at visualising high-dimensional datasets (Maaten and Hinton, 2008) (Fig. 5-8B).

Both of these unsupervised clustering techniques, which help in visualisation of our expression matrix dataset, clearly demonstrate separation of our two patient groups with near complete partition. The t-SNE technique of dimensionality reduction is gaining increased popularity in the literature due to its avoidance of co-ordinate crowding but the separation of the two groups on both different algorithm techniques based on all metabolism-related genes adds strong evidence to the hypothesis that the presence of an HPV-origin in tumours transforms a variety of different metabolic pathways.

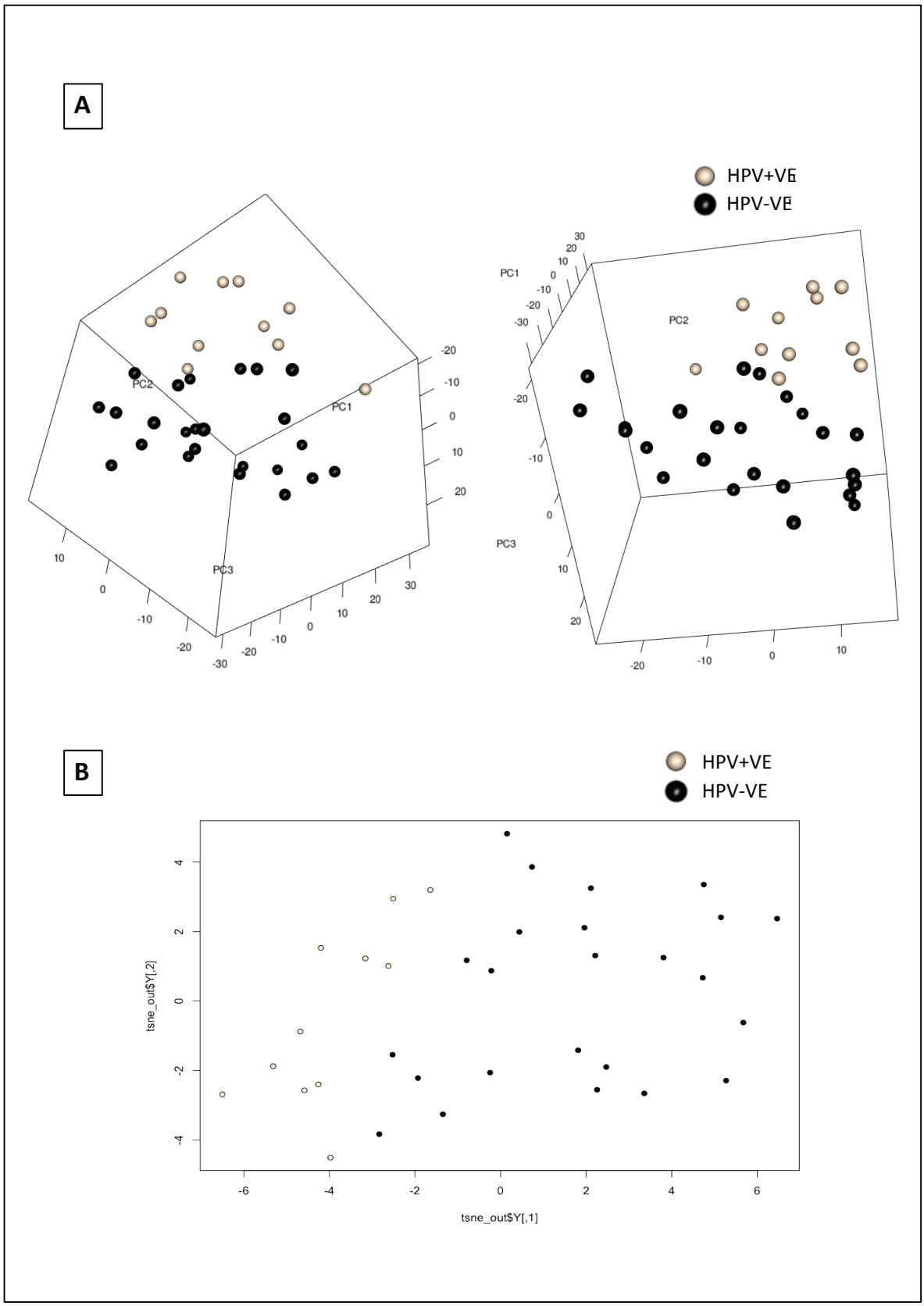

Figure 5-8. Unsupervised Clustering of 1205 Metabolism related genes. A, Principal Component Analysis (PCA plot), which visualizes our dataset as a set of coordinates in a high-dimensional space. As a technique to summarise our gene expression matrix, this technique identifies a smaller number of uncorrelated variables, or principal components (PC) in order to map our data, reducing the dimensionality whilst retaining the sample variance. B, t-Distributed Stochastic Neighbour Embedding (t-

SNE) is an alternative technique for visualising high-dimensional data by giving each datapoint a location in a two (or three) dimensional map allowing dimensionality reduction whilst avoiding datapoint crowding.

Finally to identify the involved pathways involved by these global metabolism changes between the two different tumour groups, we performed ontology analysis with the 111 differentially expressed genes (GO analysis performed in ToppGene (Chen et al., 2009)) and results were summarized in REVIGO(Supek et al., 2011) (Fig. 5-9).

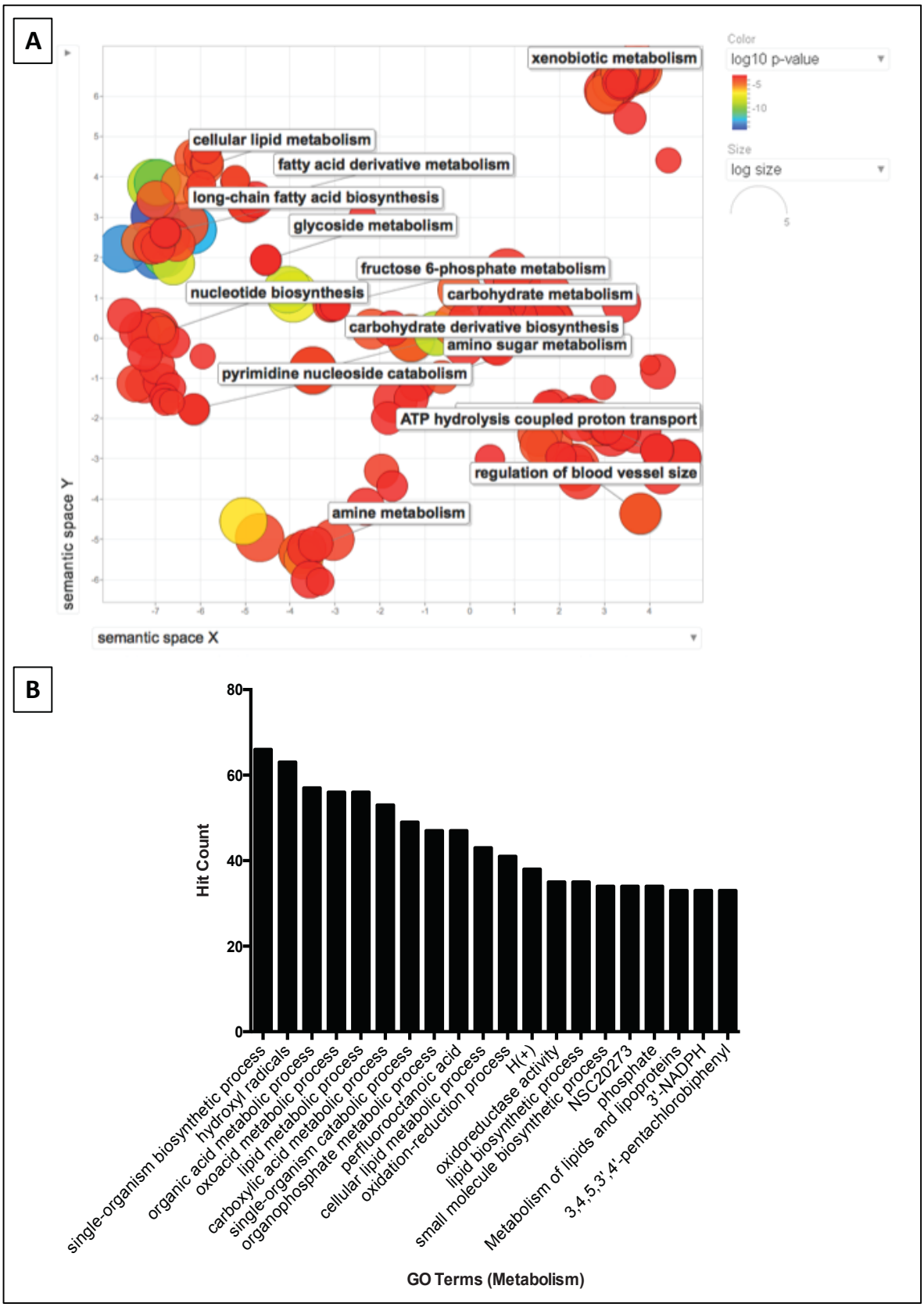

Figure 5-9. Gene ontology analysis of 111 common genes. A, Analysis was performed in ToppGene and summarised as a scatterplot of cluster representative terms in REVIGO based on semantic similarity. Bubble colour indicates the user-provided p-value and bubble size indicates the frequency of the GO term in the underlying database. Clusters with the largest and most significant values have been

highlighted with text descriptions. B, Top 20 GO terms based on hit counts in the query term have been extracted and represented graphically.

This pathway analysis and visualization technique allows a clear summarisation of involved gene ontology lists by reducing functional redundancies whilst allowing a two-dimensional plot of results (Fig. 5-9A). The illustrated scatterplot demonstrates that a diverse set of metabolism pathways are enriched between HPV-negative and –positive tumours including some of those we would expect in highly proliferating cells, such as nucleotide biosynthesis and carbohydrate metabolism, but also a variety of other pathways including, for example, fatty acid biosynthesis, lipid metabolism and amine metabolism. For further clarity the top 20 GO terms based on significantly enriched hit counts have been extracted and displayed (Fig. 5-9B), highlighting again that there a diverse array of different metabolic pathways between the two groups of tumours.

5.9 Correlation of glycolytic phenotype with FDG PET imaging

FDG-PET combined with computed tomography (CT) imaging is now a mainstay in clinical practice in head and neck oncology following repeated studies demonstrating its accuracy and sensitivity (Davison et al., 2010; Imsande et al., 2011; Isles et al., 2008; Subramaniam et al., 2010). Prior research has often been limited by HPV-negative sample size due to the emerging dominance of HPV-related tumours in the oropharynx and the previous relatively confined use of this imaging modality to this anatomical site. However, widespread reporting of glycolytic parameters in these comparative studies enables us to produce a virtual data-series combining these studies. There is wide variation of reported glycolytic parameters across studies and indeed a number of metrics can be obtained from original FDG-PET scans including, but not limited to, mean standardised uptake value (SUV(mean)), maximum standardised uptake value (SUV(max)), total lesion glycolysis (TLG) and metabolic tumour volume, the latter two requiring further volume of interest calculations. The relative tissue uptake of FDG is the most important factor and therefore the standardised uptake value is the best relative measure, compensating for patient size and amount of injected ^{18}FDG (Thie, 2004). Whilst there are inherent variations in physical and biological characteristics between scans including variable image acquisition and analysis parameters, SUV(max) has been proposed as a more

accurate estimate of the true SUV than SUV(mean) and also has improved reproducibility (Kinahan and Fletcher, 2010).

The following search strategy was utilised on Medline: ((FDG OR PET) AND (HPV OR papillomavirus)), with all fields included and including dates 1946-present. Titles and abstracts were scrutinized and full texts of relevant and related articles were retrieved. Only English language articles analysing the direct comparison between FDG-PET results in HPV-positive and HPV-negative HNSCC were selected. Reference lists of key articles were cross-referenced to identify additional articles. A total of 85 were identified with this search strategy and 71 were excluded following initial screening. Full articles for the remaining 14 papers were reviewed and from this, 7 were eligible for inclusion. However, there was a variation in the reporting of median versus mean SUV(max) scores between the two patient groups across these studies. To enable direct comparison, we utilised a published, validated approximation method for estimating the mean and standard deviation from the reported median, minimum and maximum values and study size (Wan et al., 2014). We also collected our own primary database of SUV(max) scores from two larger tertiary referral centres: Portsmouth Hospitals NHS Trust (2014-2015) and St Georges University Hospitals NHS Trust (2011-current). All patients with oropharyngeal disease who had undergone both PET-CT imaging and P16 immunotyping were eligible but due to the use of external imaging equipment and radiology reporting, there was limited data available for the majority of patients (N = 26; Age range 42-87 years). Our results indicated a mean SUV(max) score of 11.7 in the HPV-negative cohort (n=7, SD = 9.59) and 11.3 in the HPV-positive group (n=19, SD = 7.36). Similar data was collected from all relevant papers, where stated. Due to the lack of numbers of studies examining this subject we included all papers, where appropriate results statistics had been presented, in a meta-analysis. We also included our own collated data in this analysis (Fig. 5-10). A mean difference approach was utilised whereby the standard deviations (SD) are used together with sample size to calculate the study weight due to the variations between studies likely related to outcome measure reliability rather than significant differences between the study populations. Summary statistics show there to be moderate heterogeneity between studies (I^2 statistic = 0.42).

A

PAPER	HPV NEGATIVE		HPV POSITIVE	
	Sample size	SUV(max)	Sample size	SUV(max)
Baschnagel et al. 2015	45	*17.3*	52	*16.3*
Clark et al. 2015	n/k	13.7	n/k	10.3
Fleming et al 2016*	7	11.7	19	11.3
Garsa et al. 2013	18	*11.95*	25	13.25
Huang et al. 2015	49	17.7	30	17.5
Joo et al. 2014	50	*9.72*	28	*9.1*
Schouten et al. 2014	28	*13.53*	17	*8.57*
Tahari et al. 2014	98	*6.43*	25	*5.13*

B

	HPV-ve			HPV+ve				Mean Difference
Study or Subgroup	Mean [SUV(max)]	SD [SUV(max)]	Total	Mean [SUV(max)]	SD [SUV(max)]	Total	Weight	IV, Fixed, 95% CI [SUV(max)]
Baschnagel 2015	17.3	6.86	45	16.3	7.08	52	25.3%	1.00 [-1.78, 3.78]
Fleming 2016	11.7	9.59	7	11.3	7.36	19	3.2%	0.40 [-7.44, 8.24]
Garsa 2013	11.95	6.97	18	13.25	5.14	25	13.5%	-1.30 [-5.10, 2.50]
Joo 2014	9.72	4.55	28	9.1	5.13	50	40.2%	0.62 [-1.59, 2.83]
Schouten 2014	13.53	5.98	17	8.57	4.61	28	17.8%	4.96 [1.64, 8.28]
Total (95% CI)			**115**			**174**	**100.0%**	**1.22 [-0.18, 2.62]**

Heterogeneity: Chi² = 6.93, df = 4 (P = 0.14); I² = 42%
Test for overall effect: Z = 1.71 (P = 0.09)

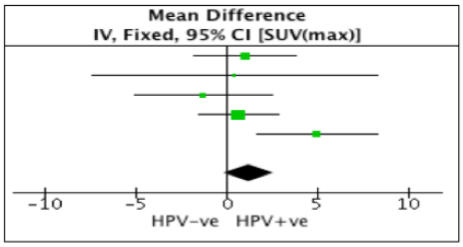

Figure 5-10. Combined FDG-PET derived SUV(max) scores from literature review (1946 – present) between HPV-negative and HPV-positive tumours. A, Table of collated mean SUV(max) scores alongside sample numbers for all relevant studies (* = own data, unpublished). Where mean SUV(max) was not reported, Indicated mean values were estimated from reported median, range and sample size as per Wan et al. (2014; italics)) (n/k = not known). B, C Table and Forest plot of comparison of SUV(max) for HPV-negative vs HPV-positive patients (mean difference, fixed effect analysis). Difference in means was + 1.22 (-0.18-2.62 [95% CI]), indicating a strong trend for higher SUV(max) scores in HPV-negative disease although no overall difference in SUV(max) scores between the two groups.

Overall summary statistics show there to be no overall difference between SUV(max) scores based on viral status, although there is a strong trend for higher SUV(max) scores in the HPV-negative populations (Z statistic = 1.71 (P=0.09; mean difference = 1.22 (95% CI -0.1 – 2.62). This result supports the important clinical decision that this PET output marker does not exhibit a significant enough differential accuracy

alone to determine the viral status of primary tumours. However, the strong trend for higher SUV(max) scores in the HPV-tumours is consistent with immunohistochemistry, protein and RNA screens of related glycolytic markers.

5.10 CtBP2 represses CTEN expression in HNSCC cell lines

We have previously shown that both glycolysis and CTEN expression are both tumour promoting and associated with poor disease-specific prognosis. Our group has also produced evidence that CTEN is a target for metabolic sensors based on gene microarray results in HNSCC (Chrzan et al, 2014; unpublished). We therefore examined for a possible transcriptional relationship between CTEN and the CtBPs, important cell metabolic sensors that regulate a network of gene transcription in response to metabolic stimuli. Western blotting analysis demonstrated that CTEN expression was increased 2.8 fold in SCC25 cells following CtBP2 knockdown and an increase was also noted in other HNSCC cell lines (BICR56 (tongue) and BICR6 (hypopharynx); Fig. 5-11A&B). CTEN mRNA levels following CtBP2 knockdown were similarly increased, upto 3-4 fold ($P < 0.05$) over control siRNA-treated cells across HNSCC cell lines (Fig. 5-11C), albeit significance was not reached in the additional cell lines due to large error bars. A subsequent time–course analysis was performed in SCC25 cells and demonstrated that this mRNA abundance change occurred as early as 24 hours following siRNA transfection (Fig. 5-11D), which would be consistent with a transcriptional level response.

The effect of CtBP2 knockdown on CTEN expression was also evident on immunofluorescent staining (Fig. 5-11E). Interestingly we also observed a change in localisation of CTEN following CtBP2 knockdown, as well as a change in cell morphology.

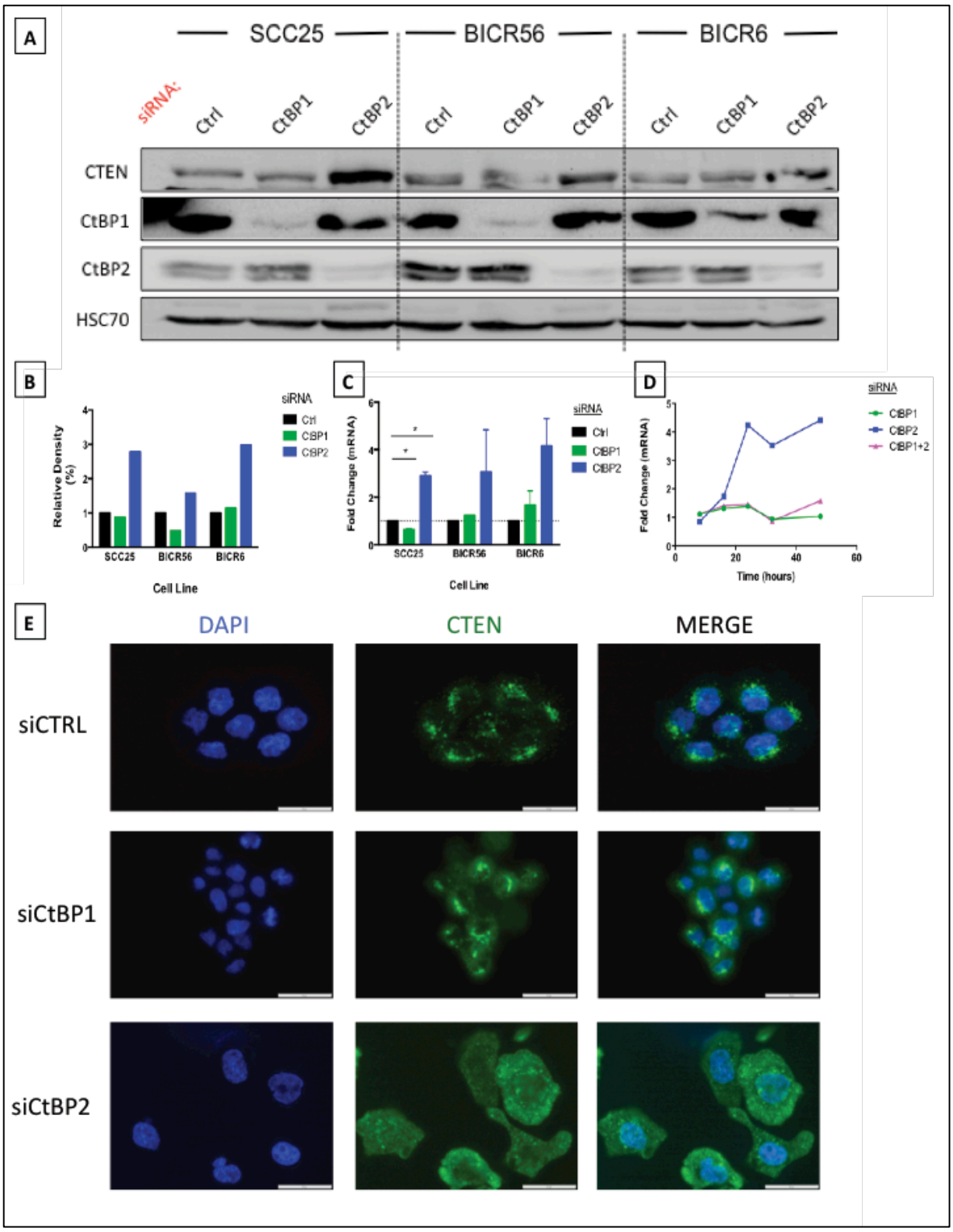

Figure 5-11. CTEN expression upregulated in CtBP2 knockdown cells across head and neck cell lines. A, SCC25 cells transfected with non-targeting control, CtBP1 or CtBP2 siRNA were harvested at 48 hours and then screened for TNS3 and CTEN expression by Western blotting. Following confirmation of a repressive effect of CtBP2 on CTEN expression at the protein level, two other head and neck cancer cell lines were screened for CTEN expression following CtBP2 knockdown to confirm the effect across cell lines. HSC70 was used as a loading control. The relative densitometry normalised to HSC70 controls is presented in B. C, Real-time Taqman® PCR assay of CTEN target was performed to confirm results at RNA level across cell lines. Results were normalised to a β-actin control. D, Time course repeat of PCR was performed

in SCC25 cells and CTEN expression fold change is illustrated. E, Cells were cultured on cover slips in preparation for immunofluorescence staining at 48 hours post-transfection. Nuclear (DAPI) and CTEN (Alexa Flour® 488) staining was performed and identical exposure times and camera settings were used for each image capture. 40x high-power images captured. Representative captured images are shown.

While in Ctrl siRNA-treated cells, CTEN demonstrated a peri-nuclear pattern in keeping with previous findings of Golgi localisation (Fig. 4-1), following CtBP2 knockdown a diffuse cytoplasmic staining pattern became evident, potentially in keeping with a global induction of transcription and translation. Although a reciprocal reduction in CTEN RNA expression was observed with CtBP1 knockdown in SCC25 cells (Fig. 5-11C), this was not observed at the protein level and not reproduced in other cell lines.

As previously described, CtBP1 and 2 are transcriptional repressors with the ability to detect elevated free nuclear NADH and then modify their activity to regulate expression of multiple genes (Zhang et al., 2002). Given our novel findings that CTEN is potentially a previously unreported target of CtBP2, we wanted to confirm that there was indeed a true repressive effect on CTEN expression and not an off-target effect from a single siRNA sequence. Therefore a new set of siRNAs targeting different sequences for CtBP1 and CtBP2 was utilised and CTEN expression was again measured at both translational (Fig. 5-12A) and transcriptional (Fig. 5-12B) level, simultaneously comparing the effect with that obtained using the original siRNA sequences. This screen indicated that the mechanism of CTEN control exhibited by CtBPs was potentially not specific to one isoform and both siRNA sequences may result in increased CTEN expression.

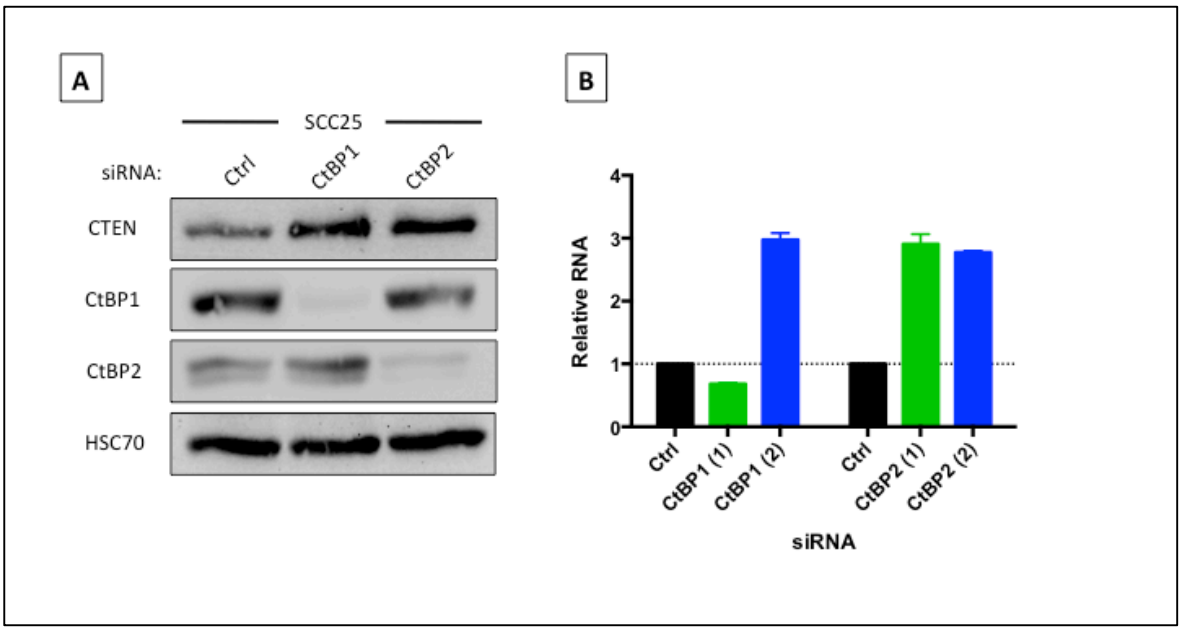

Figure 5-12. Elevation of CTEN expression following CtBP2 knockdown is consistent across siRNA sequences. SCC25 cells were transfected with either CTRL, CtBP1 or CtBP2 siRNA. A, siRNA oligo label (1) corresponds to the custom siRNA used for assays to this point in our laboratory whereas label (2) corresponds with the newly tested sequences. All siRNA sequence information can be found in Appendix A. CTEN protein and RNA expression was analysed at 48 hours following collection, by Western blotting (A, sequence 2 only) or Real-time Taqman® PCR assay respectively (B). HSC70 was used as a loading control in Western blots and C_T values from PCR replicates were normalised to β-actin control.

5.11 Regulation of CTEN expression by *in vitro* stimulation of glycolysis

Using various environmental stimulants as previously demonstrated, we can promote a tumour cell's glycolytic pathway and by inducing metabolic sensor activation secondary to NADH generation, we can observe the effect on protein expression (Kim et al., 2005). For example, cancer cells will take up glucose at a high rate for aerobic glycolysis with a corresponding glucose induced inhibition of cell respiration, known as the Crabtree effect (Dell' Antone, 2012). Similarly, simulated hypoxic conditions will activate hypoxia-inducible factor 1 (HIF1A) to amplify the transcription of genes encoding glucose transporters and most glycolytic enzymes, increasing the glycolytic capacity (Semenza, 2000). An increased glycolytic rate resulting in an increased reduction of NAD^+ to NADH, reducing the $[NAD^+]/[NADH]$ ratio, is a key activator of CtBP function and likely

differentially regulates CtBP-mediated repression (Chinnadurai et al., 2007). We have provided evidence suggesting that CTEN may be a novel transcriptional target for CtBP2 and that this may have a functional effect on a tumour cells phenotype. We therefore investigated whether this relationship had direct clinical relevance by attempting to replicate CTEN repression in response to glycolysis-promoting conditions that may be encountered by tumours *in vivo* through NADH-mediated activation of CTBP2 and dimerisation. These conditions included exposing SCC25 cells to increasing concentrations of glucose (Fig. 5-13A, B, C), as well as culture within a hypoxic chamber (Fig. 5-13D) and CTEN expression was examined at the 48-hour time point. Reduction of CTEN protein expression upon exposure to increased glucose availability was reproducible across cell lines. Change in CTEN mRNA level exhibited a downward trend but was only significant at the extremes of glucose concentrations ($P<0.05$). Similarly, hypoxic culture conditions resulted in reduction of CTEN protein expression. Whilst the glycolytic conditions produced in this experiment would be expected to induce global transcriptional repressive activity of the CtBPs, these findings do closely reproduce the expected effect of a direct CtBP2 repression of CTEN and provide further evidence that glycolysis may contribute to functional effects through transcriptional regulation of CTEN.

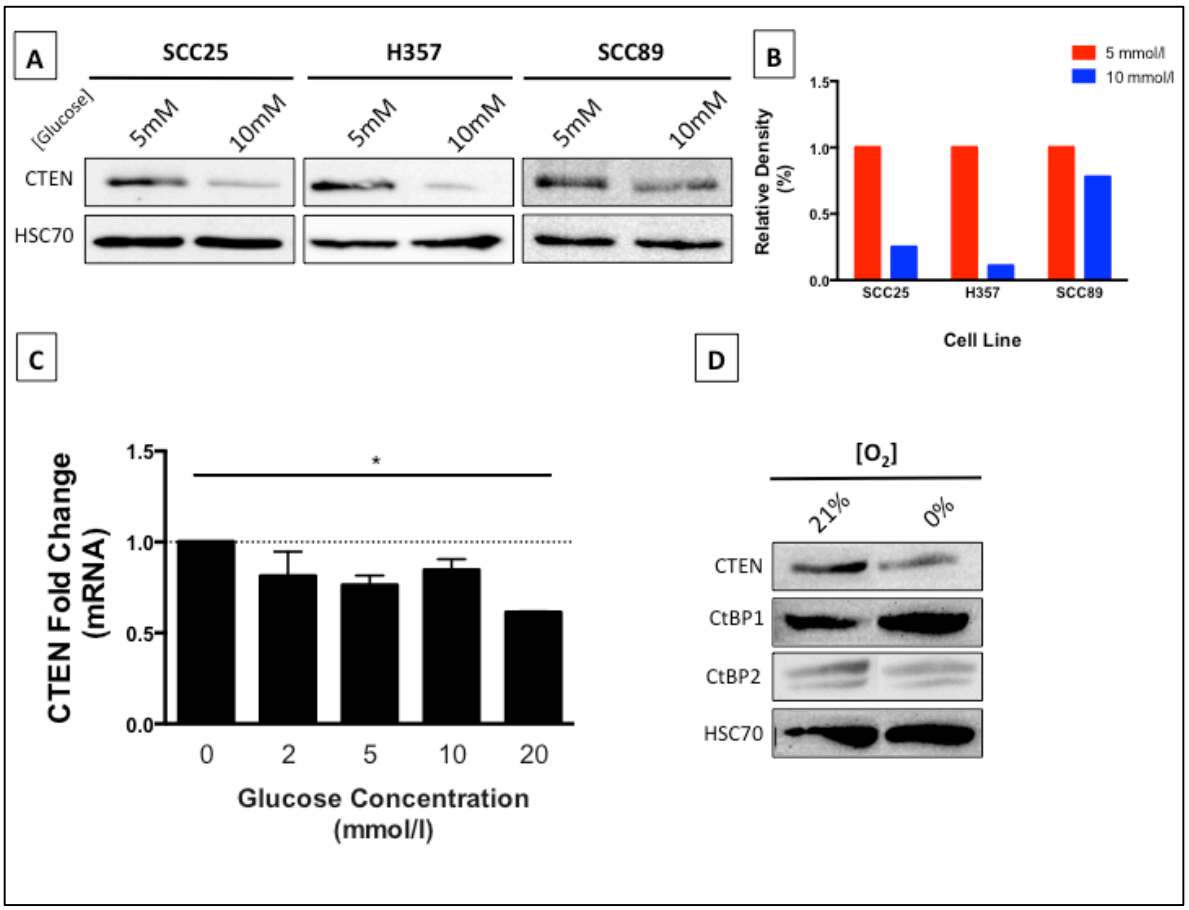

Figure 5-13. CTEN expression is repressed in glycolytic conditions. SCC25 cells were cultured for 48 hours in increasing concentrations of glucose-supplemented media (A, B, C) or hypoxia (D; n=1) in order to stimulate glycolysis. CTEN expression was analysed by Western blotting (A, D) or Real-time Taqman® PCR assay (C). HSC70 was used as a loading control in Western blots and C_T values from PCR replicates were normalised to β-actin control. (B) Western blots from cell line screen in (A) were quantified by densitometry analysis and normalised to loading controls on ImageJ software. (C) Only CTEN mRNA levels comparing 0mmol/l [glucose] to 20mmol/l were statistically significant ($p<0.05$). Representative results are demonstrated.

5.12 CtBP2 is recruited to the CTEN promoter

In order to address whether CtBP2 is directly recruited to the *TNS4* (CTEN) gene promoter, CtBP chromatin immunoprecipitation (ChIP) was performed using chromatin from SCC25 HNSCC cells and either a control IgG or anti-CtBP antibody (Fig. 5-14). The CtBP antibody utilised (Appendix A) is not specific for any particular CtBP monomer but has been previously validated for use in ChIP (M. Chrzan, final PhD thesis). A screen of *TNS4* PCR primer sets identified a fragment proximal to the first exon transcription start site as a likely binding site (Primer 10; Fig. 5-14A). A primer set originally designed for the

E-cadherin (*CDH1*) promoter site (Shi et al., 2003), as recently validated by Chrzan (PhD thesis, 2013), was used as a positive locus control . An internal control of Primer set 1 for CTEN, located furthest from the likely binding site was utilised in further experiments as an internal control and CtBP did not localise to this fragment (Fig. 5-14B), and the negative control IgG ChIP with the CTEN primers also did not yield any signal. Robust CtBP binding was observed with the CTEN promoter region in chromatin from two separate culture batch collections and diluted input chromatin was used for PCR semi-quantification (Fig. 5-14B, left panel), which demonstrated a 26% relative density compared to 1/30 diluted input control (Fig 5-14C, right panel). These findings confirm CtBP2 recruitment to the CTEN promoter and validate the previously observed transcriptional relationship between CTEN and CtBP2. Negative and positive control loci primer pairs for Talin (*TLN1*) as validated previously (Chrzan, PhD thesis, 2013) were also tested using the same chromatin to confirm specificity of the reaction. Sequence details for all primers used, together with graphical representation of the design of the TLN1 primer site is shown in Appendix D.

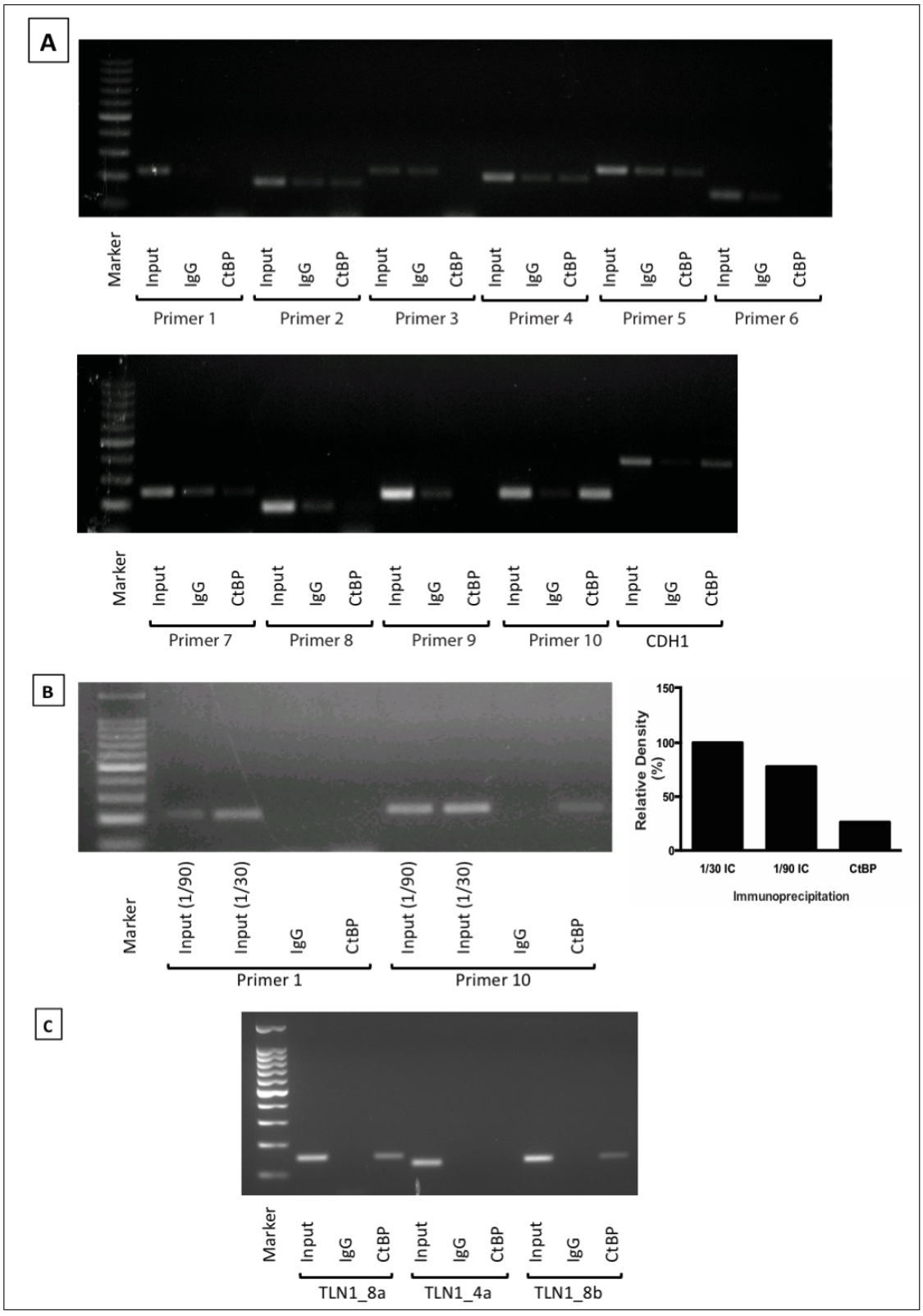

Figure 5-14. CTEN is a transcriptional repression target for CtBP. ChIP assay of the CTEN promoter was performed using chromatin obtained from SCC25 cells. After immunoprecipitation with anti-CtBP or control IgG antibodies, diluted input DNA was amplified by PCR. A, Multiple primer sets spanning the 327bp *TNS4* promoter were screened for likely binding sites, including a negative control (IgG) and positive control (E-cadherin (*CDH1*) promoter) PCR products were electrophoresed in an agarose gel and stained with ethidium bromide. B, Experiment was repeated

with new chromatin from a separate SCC25 batch and diluted range of input controls included for semiquanitification. Primer set 1 was used as an internal negative control due to its location furthest from the likely binding site (left panel). Quantitation of the ChIP results shown in right panel. Experiment shown is representative of 3 independent experiments. C, Talin (*TLN1*) promoter pairs for positive (8a, 8b) and negative (4) controls were used with same chromatin sample to confirm specificity.

5.13 Discussion

After almost a century since Otto Warburg first described a tumour's preference for glycolysis (Warburg et al., 1926), cancer metabolism has been subject to a resurgence of interest. The reasons for this stem from both a clinical and oncology research perspective - observations of the usefulness of ^{18}FDG-PET scanning and the close links discovered between oncogenes and metabolism pathways (Yeung et al., 2008). In addition, new metabolic targets continue to be identified in a variety of tumour types. However, to date there has been sparse research into the metabolic phenotype of HNSCC (Sandulache and Myers, 2012). HNSCC has been shown to be particularly reliant on high rates of glucose uptake and subsequent aerobic glycolysis (Sandulache and Myers, 2012) and clinically FDG uptake, primarily via GLUT-1 receptors, reflects the dynamic glucose metabolism of these tumours (Nakamura et al., 2012). This is likely to be highly clinical relevant as GLUT-1 expression has been shown to correlate with aggressive HNSCC disease (Kunkel et al., 2003; Li et al., 2008; Reisser et al., 1999) and acidification of the microenvironment has also been correlated with reduced 2-year metastasis-free survival (Brizel et al., 2001). The only studies investigating the effects of HPV tumourigenesis on tumour metabolism have been in gynaecological disease (Caneba et al., 2012; Chung et al., 2013; Dier et al., 2014). The availability of real-time flux analysis together with next generation data analysis techniques means that we now have comprehensive research technology to investigate metabolic phenotypes from a number of different perspectives.

Our findings of an increased expression of glycolytic markers in HPV-negative tumours both on immunohistochemistry (IHC), western blotting (MCT1, LDHA) and RNA sequencing (LDHA, LDHB, MCT1, HIFIA and PKM2) were corroborated by our extracellular flux analysis findings confirming a higher rate of glycolysis and glycolytic capacity in HPV-negative cell lines. The reason for this glycolytic preference however is more uncertain;

glycolysis as an energy producing pathway appears highly inefficient with a net gain of 2 ATPs per glucose molecule compared to the 36 ATPs gained from oxidation (Lehninger et al., 1982). We can however point to Vander Heiden's hypothesis (2009) that in the nutrient rich environment of the tumour bed and surrounding vasculature, ATP production is never a limiting factor for tumour growth, and the diversion of glucose into amino acid, fatty acid and nucleotide precursor formation may well explain the selective advantage of the Warburg effect. Indeed our finding of concurrent higher oxygen consumption rates in HPV-negative cell lines is consistent with other studies noting that mitochondrial function is not impaired in the majority of cancer cells (Fantin et al., 2006; Moreno-Sánchez et al., 2007). Furthermore, our RNA sequencing data adds support to this hypothesis by the demonstrated enrichment of a variety of different alternative metabolic pathways in the more glycolytic HPV-negative tumour group including fatty acid, lipid and nucleotide biosynthesis (Fig. 5-9A). Indeed aerobic glycolysis is becoming more appreciated as one aspect of a complex tumour environment (Krupar et al., 2014b) and Curry et al. (2013) proposed two different intra-tumoural compartments based on immunohistochemistry including a proliferative/mitochondrial-rich and non-proliferative/mitochondrial-poor area as well as an extra-tumoural stromal area characterised by sparsity of mitochondria. Although this was in a small patient cohort, this protein analysis of whole tumour sections did enable identification of intra-tumour heterogeneity. An important suggestion from this work was the proposal of a metabolic symbiosis between different compartments within a tumour. Indeed the monocarboxylate transporters were cited as ideal examples of this relationship, having seemingly opposite effects of lactate influx (MCT1) versus efflux (MCT4). Although we failed to observe a reciprocal monocarboxylate transporter RNA expression pattern in these tumours between HPV-negative and HPV-positive groups, the elevated expression of MCT1 in the former is worthy of further examination and will be discussed in Chapter 6.

The finding of increased pyruvate dehydrogenase kinase in an HPV-positive cohort (Fig. 5-6) is an interesting discussion point. The pyruvate dehydrogenase complex occupies a key position at the centre of energy metabolism by promoting the conversion of pyruvate, Coenzyme A (CoA) and NAD^+ into acetyl-CoA, NADH and CO_2 (Zhang et al., 2014). Inhibition of this complex by pyruvate dehydrogenase kinase (PDK) therefore results in a shift of metabolism from OXPHOS to glycolysis. Indeed recent HNSCC cell line

work suggests a level of coordination between OXPHOS, HIF1A and PDK downregulation (Sun et al., 2009). We found higher RNA expression of PDK1, the predominant form of PDK in tumour cells (Roche and Hiromasa, 2007), in the HPV-positive group - inconsistent with our findings of a greater reliance on OXPHOS for energy production in HPV-positive cell lines in the extracellular flux analysis. It is difficult to interpret this result in isolation without knowing the oxygenation state of the primary tumour as it may represent a response to hypoxia in the HPV positive cohort. However we can also hypothesise that it is an adaptive response to the reduced expression of the various other glycolytic marker and effectors, to allow some glycolysis to facilitate biosynthesis and may therefore represent a greater potential therapeutic target in tumours of an HPV-positive origin.

In our analysis of glucose metabolism in HNSCC we have identified not only a glycolytic phenotype in HPV-negative tumours compared to their HPV-positive counterparts, but also a globally altered metabolic profile consistent with the requirements for macromolecule production in rapidly proliferating cells, as well as alterations in other previously uncited metabolic pathways. This is highlighted most clearly in our unsupervised clustering methods and gene ontology analysis. Interestingly our two HPV-positive outliers on heat map representation demonstrate an interesting correlation between tumour and metabolic phenotype. Repeat analysis of both patients showed unique pathological features predominating with a known aggressive subtype of basaloid tumour in one, and unusual keratinising features normally found in HPV-negative tumours in the other. This finding emphasises that a unique metabolic signature is associated with an altered tumour phenotype although from this it is not clear which feature is the driving force for the observed behaviour.

Previous studies have investigated the role of glutaminolysis in tumour cells and our finding of increased expression of glutaminase in the HPV-positive cohort is worthy of further discussion. Glutamine turnover depends on the activity of glutaminase, resulting in glutamate production (Aledo et al., 1994). Glutamine can be used for a variety of purposes within the cell – providing amino groups for purine and pyrimidine bases in proliferating cells, or feeding into the TCA cycle and resulting in lactate production (Eigenbrodt et al.; McKeehan, 1982). In an ovarian cell line, transformation with the E7 oncoprotein resulted in a reduction of glycolysis and an increase in glutaminolysis (Mazurek et al., 2001), in keeping with our *in vitro* and *in vivo* findings in HNSCC. Glutamate, the result of the glutaminolysis reaction, has been shown to suppress T cell

activity *in vitro* (Dröge et al., 1987) and a variety of immune cells exhibit glutamate receptors (Xue and Field, 2011). Our group has already published on the important prognostic information reflected by tumour-infiltrating lymphocyte levels in HPV-positive primary tumours and its relevance in the clinical evaluation of this disease (Ward et al., 2014). Whilst the suppressive effect of lactate on lymphocyte and natural killer cell function is well recognised (Krupar et al., 2014), the activity of glutaminase and levels of subsequent glutamate are alternative candidates for further investigation in HPV-positive HNSCC to assess whether this metabolic pathway is a key regulator of the degree of immune infiltration *in vivo*; this could have important potential for therapeutic applications in this disease either alone or in combination with novel immunomodulatory agents.

Ultimately the classification of metabolic phenotype in HNSCC has important clinical relevance. FDG-PET is now a gold-standard investigation for the diagnosis of new primary and distant metastatic HNSCC as well as post-treatment surveillance and primary component of this imaging is via GLUT1 receptors (Li et al., 2008). As we have demonstrated in a meta-analysis that SUV(max) alone is insufficient to distinguish HPV status in primary tumours, especially given the range of reported metrics and variability of imaging parameters between centres, we would urge avoidance of further proposals of arbitrary cut-off values for a clinical use of PET in predicting HPV-positivity. However, PET/CT standardized uptake value (SUV) measurements have been shown to be reproducible with both diagnostic and prognostic value in HNSCC (Tahari et al., 2014) but with these imaging metrics alone, there have been conflicting reports in the literature about the significance of HPV-related tumours to their glycolytic phenotype. Given the previously discussed implications of glycolysis on tumour progression and invasion, this data adds to the growing evidence that targeting glycolytic pathways may yield more significant value in HPV-negative disease. Indeed the clinical success of FDG PET imaging, perhaps more than any other reason, justifies further research into potential therapeutic potential of HNSCC metabolic targets.

Prospective analyses of HNSCC tumour models indicate that increased tumour lactate levels may be predictive of radioresistance (Quennet et al., 2006) and the increased glycolysis in HPV-negative HNSCC helps explain their increased resistance to this treatment modality. A variety of metabolic targets and enzymes involved in glycolysis have been described and tested *in vitro* (Sandulache and Myers, 2012) but in HNSCC our

findings will help direct future trials to target HPV-negative tumours due to their increased reliance on this metabolic pathway. However, the high respiratory capacity of these cells may help to explain adaptive mechanisms of these tumours and therefore symbiotic combined treatment modalities will likely be required to see significant research successes. Further analysis of metabolic changes in response to some of these inhibitors may help to delineate the reasons for *in vitro* and/or *in vivo* treatment failures as well as identify alternative metabolic pathways that will need to be targeted in combined treatments.

In a review of HNSCC metabolism, Sandulache and Myers (2012) recommended key approaches required to address a significant deficit in the knowledge of tumour cell metabolism. We have comprehensively addressed the first of these recommendations, namely to use protein and genomic techniques to identify specific metabolic alterations in HNSCC. Whilst our initial *in vitro* and *in vivo* results suggested fundamental differences in glucose metabolism between HPV-negative and –positive disease with a prominent glycolytic profile in the former, a wider analysis of metabolism between the two groups revealed a globally altered metabolic profile involving numerous other metabolic and biosynthetic pathways. The detailed analysis of differing metabolic profiles of HPV-negative compared to HPV-positive disease that we have performed forms a sound basis for future research, enabling analysis and identification of future therapeutic targets.

Whilst the effect of a glycolytic phenotype in HNSCC has been associated with poor prognosis, the selective advantage that this confers on tumour cells is less clear. The need for biosynthetic intermediates in rapidly proliferating tumour tissue is suspected to be a key determinant of this glycolytic drive (Kroemer and Pouyssegur, 2008; Lunt and Vander Heiden, 2011) but targeting these pathways in cancer cells without causing significant collateral damage to normal cells is fraught with difficulty and is often cited as a reason for the comparatively slow progress in developing metabolic therapeutics (Pierotti et al., 2012). HNSCC has been shown to be particularly reliant on high rates of glucose uptake and subsequent aerobic glycolysis (Sandulache and Myers, 2012) and clinically FDG uptake, primarily via GLUT-1 receptors, reflects the dynamic glucose metabolism of these tumours (Nakamura et al., 2012). Indeed GLUT-1 expression has been shown to correlate with aggressive HNSCC disease (Kunkel et al., 2003; Li et al., 2008; Reisser et al., 1999).

Given that we have already demonstrated the role of CTEN in supporting tumour growth in HNSCC, we hypothesised a relationship might exist between tumour cell

metabolism and CTEN. CtBPs, in their role as metabolic sensors, are able to act as a unique regulatory switch, activated by NADH binding into a conformational change and dimerisation (Chinnadurai, 2009, 2003; Fjeld et al., 2003; Kumar et al., 2002). Their ability to respond to NADH levels positions them perfectly as a mechanistic link between a tumour's metabolic output and cancer progression. We demonstrated that CTEN is a previously unreported target for transcriptional repression by the metabolic sensor CtBP2. CTEN was found to be consistently upregulated across cell lines following CTBP2 depletion both at the protein and mRNA expression levels, and ChIP analysis confirmed that CtBP was recruited to the CTEN promoter. However although various glycolytic stimuli resulted in the expected repression of CTEN *in vitro*, this relationship failed to be reproduced with historic patient tumour samples. On analysis of our OPSCC dataset, despite not formally examining CtBP2 expression, no significant correlation (inverse or otherwise) between CTEN and Glut1 ($p=0.16$; $r=0.097$) was observed. In the presence of hypoxia or other glycolytic stimulating conditions, CtBPs have already been shown to co-ordinate a wide-reaching transcriptional response including repression of genes involved in 1) cell dynamics and apoptosis, through depletion of proapoptotic genes including Bax and Noxa, as well as stabilisation of the survival kinase AKT by repression of its negative regulator PTEN (Y.-W. Chen et al., 2008; Paliwal et al., 2007; Zhang et al., 2006), 2) tumour cell adherence, through repression of E-cadherin resulting in promotion of cell motility and an EMT phenotypic switch (Paliwal et al., 2012, 2007) and 3) cell cycle inhibitors including the Ink4 family of tumour suppressors. Clearly then the glycolytic regulation of CTEN *in vivo* is more complicated than a direct linear relationship and the functional importance of this relationship *in vitro* must be interpreted with caution.

Further understanding how glycolytic tumours and the Warburg effect favour tumour progression is vitally important for our understanding of the factors regulating aggressive tumour phenotypes. Furthermore, as CtBP-targeting therapeutics are developed, it is vital to anticipate potential knock-on complications following the abrogation of its transcriptional repressive activity. Given our previous evidence of the tumour promoting functions of CTEN, the simultaneous inhibition of both CtBPs and CTEN may have significantly improved tumour-killing effects and theoretically avoid any unwanted tumour promoting effects from the resulting increased expression of CTEN.

Chapter 6: Investigation of a novel MCT-1 inhibitor for the treatment of HNSCC: an *in vitro* study

6.1 Introduction

The Warburg effect in tumour cells is their recognised preference for aerobic glycolysis and we have already demonstrated active glycolysis in both HPV-positive and HPV-negative HNSCC *in vitro* and *in vivo*. The end-point of glycolysis is lactate but anabolic biosynthetic processes for rapidly proliferating cells are also supported whereas OXPHOS results in the full metabolism of glucose into carbon dioxide (Ward and Thompson, 2012). Glutamine catabolism, another hallmark of cancer cells, also results in lactate production through sustaining the TCA cycle (DeBerardinis et al., 2007; DeBerardinis and Cheng, 2010; Son et al., 2013). Many of the oncogenic changes in tumourigenesis such as aberrant PI3K/AKT signalling, MYC and HIF-1α overexpression drive this metabolic reprogramming including increasing GLUT1 expression, LDHA activity as well as activating glycolytic enzymes including hexokinase 2 and 6-phosphofructokinase 1 (Deprez et al., 1997; Gottlob et al., 2001; Kohn et al., 1996)

In glycolytically active cells, including normal muscle and brain cells, as well as cancer cells, lactate homeostasis is a vital component. This process requires specialised transporters known as the monocarboxylic acid transporters, MCT1-4 (Halestrap and Wilson, 2012). MCT1 is expressed in almost all tissues and both MCT1 and MCT4 are both membrane-bound and are classically considered as lactate importers and exporters respectively (Doherty and Cleveland, 2013) although it is likely that the direction of lactate flow depends on specific extracellular factors such as pH, the transmembrane lactate potential, as well as other MCT substrates (Bröer et al., 1998; Dimmer et al., 2000). Whilst acidification of the microenvironment itself is characteristic for tumours and has been proposed as a direct-tumour response to support invasion (Gatenby and Gillies, 2004), lactate is utilised as an oxidative metabolite in many normal cells (e.g. cardiac) or as a substrate for gluconeogenesis (e.g., liver) (Halestrap and Wilson, 2012). However, an excess of lactate build-up and excessive pH changes of the tumour milieu or intracellularly could result in toxicity and therefore the lactate balance maintained by the MCT transporters has been suggested as a potential therapeutic option to target cancer cells. In the previous chapter we noticed an increased expression of MCT1 on RNA sequencing analysis in HPV-negative tumours (Fig. 5-6), despite an increase in HIF1A in the same cohort. Whilst the physiological reason for this expression pattern is not clear, given the recent suggestions that this may represent a reasonable target for a

vulnerability within a cancer cell's metabolic phenotype, we investigated this marker further with both functional and inhibitor investigations.

6.2 Expression of MCT1 on HNSCC TMA

In order to investigate protein level expression of MCT1 and corroborate RNA sequencing findings, we optimised MCT1 antibody for immunohistochemistry and proceeded to stain our OPSCC TMA database (see Table 3-1 for patient demographics; Fig. 6-1A). MCT1 scoring was performed by two blinded raters (KM/JF) as high (moderate/high strength staining) or low (absent/low strength staining) and results collated. This data was then analysed on SPSS (version 22 for Mac, IBM, NY) for association with HPV status and our previous IHC metabolic marker analysis of GLUT1 (Fig 6-1B&D). Kaplan-Meier survival curves were also produced using clinicopathological patient data (Fig 6-1C).

We have previously obtained RNA sequencing data indicating a significantly greater MCT1 expression at the RNA level in HPV-negative HNSCC. This TMA expression data corroborated these findings with a statistically significant greater MCT1 protein expression in the HPV-negative tumours. There was no obvious survival effect of MCT1 score on OPSCC, irrelevant of viral status. However we showed a significant positive correlation between MCT1 and GLUT1 expression, and although the correlation coefficient was weak ($r_s = 0.219$), the association of MCT1 expression level with both HPV-negative tumours and GLUT1 expression suggests that MCT1 expression is being found in the more glycolytic tumours. Given that we have shown HPV-negative cell lines *in vitro* have a higher glycolytic rate, this is a surprising result as MCT1 is classically thought of as a lactate importer, and therefore supporting lactate homeostasis by being expressed on cells favouring energy production through OXPHOS.

A

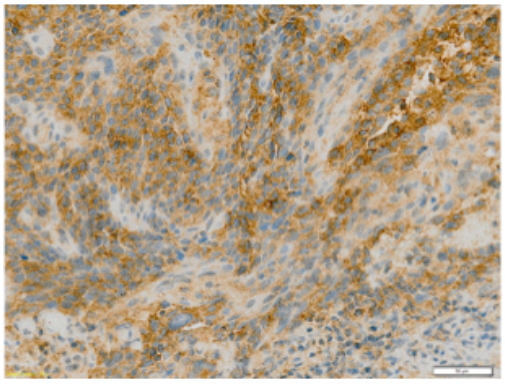

B

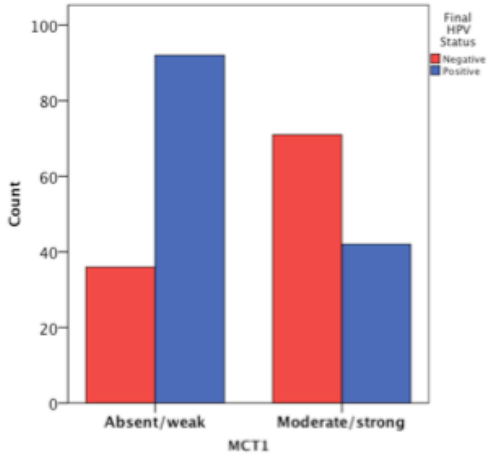

C

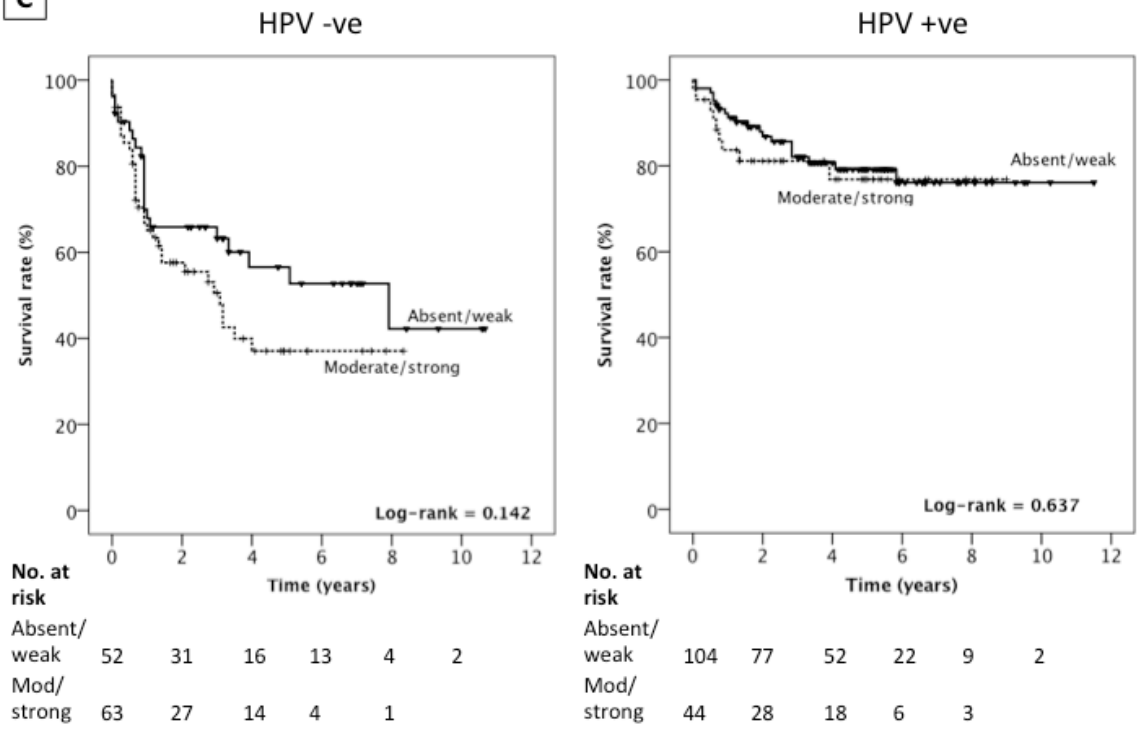

No. at risk						
Absent/weak	52	31	16	13	4	2
Mod/strong	63	27	14	4	1	

No. at risk						
Absent/weak	104	77	52	22	9	2
Mod/strong	44	28	18	6	3	

D

	TMA					
	HPV Status			GLUT1		
	χ^2	Asymp. Sig.	r_s	$\chi 2$	Asymp. Sig.	r_s
MCT1	29.285	<0.0001	-0.349	9.437	0.002	0.219

Figure 6-1. Clinicopathological data for MCT1 scoring in HNSCC TMA. A, Example strong MCT1 following antibody optimisation of a whole tumour section. B, Clustered bar charts of MCT1 scoring by HPV-status indicating larger numbers of high MCT1 expression in the HPV-negative group compared to the HPV-positive group. C, Kaplan-Meier

curves for HPV-negative (left) and HPV-positive OPSCC (right) based on MCT1 expression, scored on immunohistochemistry as low (absent/weak) or high (moderate/high). Numbers of patients at risk by time point are displayed below each graph. No significant correlation was evident between MCT1 expression and disease specific survival in either HPV-negative or HPV-positive disease. D, Test for correlation between MCT1 and HPV status as well as GLUT1 expression. Both chi-squared (χ^2) and Spearman's rank (r_s) statistics are displayed from analysis of immunohistochemistry data. This demonstrated a significant association between MCT1 and GLUT1 expression as well as confirming the association of high MCT1 expression with HPV-negative HNSCC.

6.3 Sensitivity of HNSCC cell lines to AZD3965, a novel MCT1 inhibitor.

We have demonstrated an increased expression of MCT1 at both the protein and RNA level in HPV-negative tumours. Furthermore, published expert reviews have suggested that this target could represent a therapeutic vulnerability for tumours, likely due to disruption of lactate homeostasis (Doherty and Cleveland, 2013). AZD3965 (AstraZeneca, Waltham, MA) is an orally available selective inhibitor of MCT1 with minimal effect on MCT4 which has had success reducing tumour growth and increasing intra-tumour lactate in preclinical trials in lung cancer (Polański et al., 2014) resulting in its introduction into early phase clinical trials.

Highest expression of MCT1 was in the SCC25 HPV-negative cell line and we therefore selected this line in order to determine the appropriate dose of AZD3965 to use in future functional experiments, using a proliferation assay on XCELLigence Real Time analyser as previously described. Serial dilutions from 0.01nM to 1000nM were selected and the culture medium on cell cultures were changed to appropriately diluted AZD3965 for 24 hours prior to the start of the 48-hour proliferation assay (Fig. 6-2A). No effect on SCC25 cell proliferation was observed at compound concentrations of 100nM and below. We also performed a simple count-based proliferation assay with similar results showing no significant effect on cell proliferation at tested concentrations upto and including 100nM (Fig. 6-2C). Therefore to select a range of concentrations to be consistent with previously published use of 8nM for *in vitro* work (Polański et al., 2014), we initially selected two AZD3965 concentrations of 10nM and 100nM and retested these concentrations but including an HPV-positive cell line (SCC2). Once again no significant effect on cell proliferation was observed at these two compound concentrations (Fig. 6-

2B). Further experiments therefore used 10nM AZD3965 as a working concentration for functional assays.

The clonogenic or colony-forming assay is another commonly used to technique to study interventional treatment effects on the proliferation of cancer cell lines. Due to the lack of standardised techniques to analyse clonogenic assays, we utilised a published, validated Image J plugin for automated quantification (Guzmán et al., 2014). This plugin calculates the surface area of colonies as well as an intensity-weighted percentage, which takes the number of cells in each colony into account, and therefore is more representative of cell growth density. In this clonogenic survival analysis we exposed SCC25 and another glycolytic HPV-negative cancer cell line, H357, to both 10nM and 100nM concentrations of AZD3965 for 48 hours prior to plating at 2000 cells/well in 6-well plates (Corning). Colonies were then allowed to grow with fresh medium replacement every 72 hours for a total of 10-14 days and then stained with crystal violet before analysis using ColonyArea plugin (Guzmán et al., 2014) (Fig 6-2D). Inhibition of MCT1 activity resulted in an approximately 50% reduction in colony survival and intensity in SCC25 cells ($P<0.001$). However, no significant effect was seen on H357 cell line indicating a relative resistance to the compound but this was a cell line dependent effect. The difference in effect on cell survival between the XCELLigence assay and the clonogenic assay also indicates that this was an assay specific effect. However, the clonogenic assay is a commonly used technique to assess cell line response to treatment interventions so this data gives us a valid baseline to assess further interventions on these cell lines.

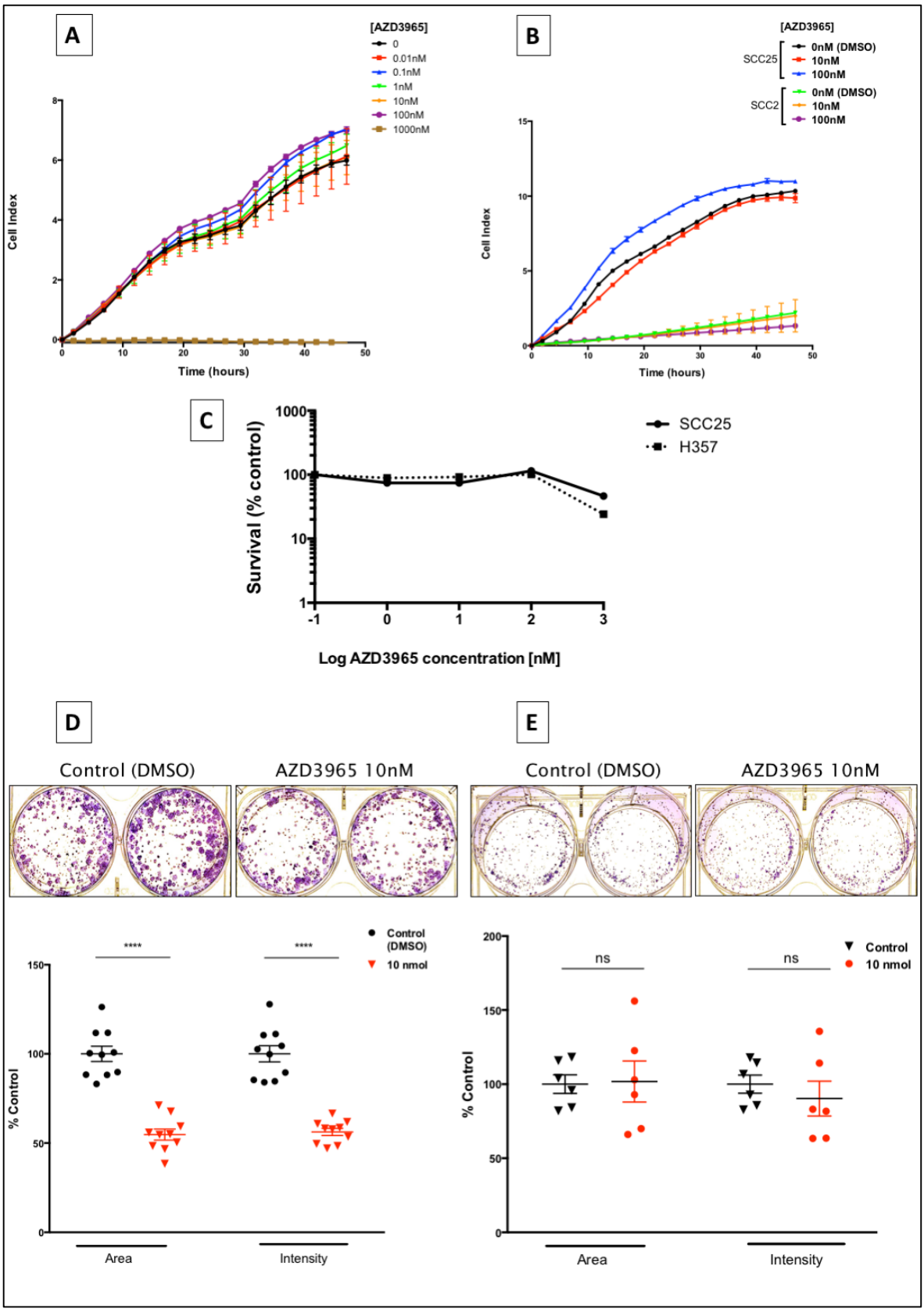

Figure 6-2. Survival effect of AZD3965 on HNSCC cell lines. A, proliferation assay of SCC25 cells was performed on the XCELLigence Real Time Cell Analyser in varying AZD3965 concentration media for 48 hours. No significant effect on cell adhesion and then proliferation was observed in concentrations below 1000nM. B, The experiment was repeated for selected media concentrations of 10nM and 100nM AZD3965,

with inclusion of an HPV-positive cell line, SCC2. Again no significant difference between cell index of different concentrations was observed in either cell line. A DMSO control was included in all experiments as a negative control. Assay results show the mean between two replicate wells with error bars representing standard error. C, A proliferation analysis was repeated using a count based analysis. A 72 hour culture of SCC25 and H357 cells plated at $5x10^4$ in media containing different AZD3965 concentrations was performed and following trypsinisation, final counts were performed on Casy counter (Innovatis AG, UK/Roche Diagnostics GMBH). No significant differences between cell counts at different concentrations were observed until 1000nM was used, with a significant reduction in proliferation at this dose (survival % represented on log scale). Clonogenic assay are represented for SCC25 (D) and H357 (E) and all results were converted to % control well. Almost 50% reduction was observed in both colony area and intensity in SCC25 ($P<0.001$). No significant effect was observed on H357 colony survival. Representative well photographs are displayed. Pooled data from three biological repeats has been presented.

6.4 Metabolic effects of MCT1 inhibition

Tumour metabolism and glycolysis are now being recognised as important mediators of cancer cell phenotype, whether through transcriptional regulation e.g. p53 (Jiang et al., 2011), CtBPs (Postigo and Dean, 1999), or via a direct effect on the tumour microenvironment (Gottfried et al., 2012). Indeed acidification of the tumour microenvironment has been found to correlate with tumour progression in a number of different tumour types (Walenta and Mueller-Klieser, 2004). A lactate shuttle hypothesis has been proposed for how tumour cells control for fluxes in lactate concentration extracellularly, which depends on the distribution of a variable hypoxic and glycolytic cells within the tumour itself (Sonveaux et al., 2008). However despite the initiation of AZD3965 in early phase clinical trials, there is only limited knowledge about the biochemical and metabolic effects of MCT1 inhibition and there have been no studies on its effect in HNSCC.

The Seahorse XF96 Extracellular Flux Analyser (Seahorse Bioscience, North Billericay, MA) was again used to analyse real time metabolic outputs of oxygen consumption rate (OCR) and extracellular acidification rate (ECAR). HPV-negative cell lines SCC25 and H357 were selected due to previously documented increased expression of MCT1 in this HNSCC type. Following 72 hours treatment with AZD3965 (10nM) or DMSO as control, biochemical flux analysis was performed, utilising similar injection compounds as previously to study mitochondrial stress (namely 5mmol/l glucose, oligomycin A and

FCCP or 2-DG), except for the addition of a fourth injection - rotenone and antimycin *A* which act as electron transport inhibitors and therefore completely block respiration (Fig. 6-3). Following completion, all results were normalised to total protein count following Bradford assay analysis to account for any variable cell line proliferation rates.

These results give us important information on the effect of MCT1 inhibition on HPV-negative cell lines. When considering just effect on glycolysis, there appears to be a cell-line dependent effect and MCT1 inhibition in SCC25 results in a dose dependent reduction of glycolytic rate as well as glycolytic capacity. This is mirrored by an increase in mitochondrial respiration in the cell line (Fig. 6-3 A&B). However this pattern is not observed in the H357 cell line, summarised in Fig. 6-3C (full real time flux analysis graph not shown). Interestingly however, despite the variable effects on glycolysis and respiration between cell lines, when analysing paired ECAR-OCR rates in order to plot an energy phenotype profile, this clearly demonstrates the pattern of MCT1 inhibition driving cells into a quiescent phenotype (Fig 6-3D), which supports further investigation of the therapeutic potential of AZD3965.

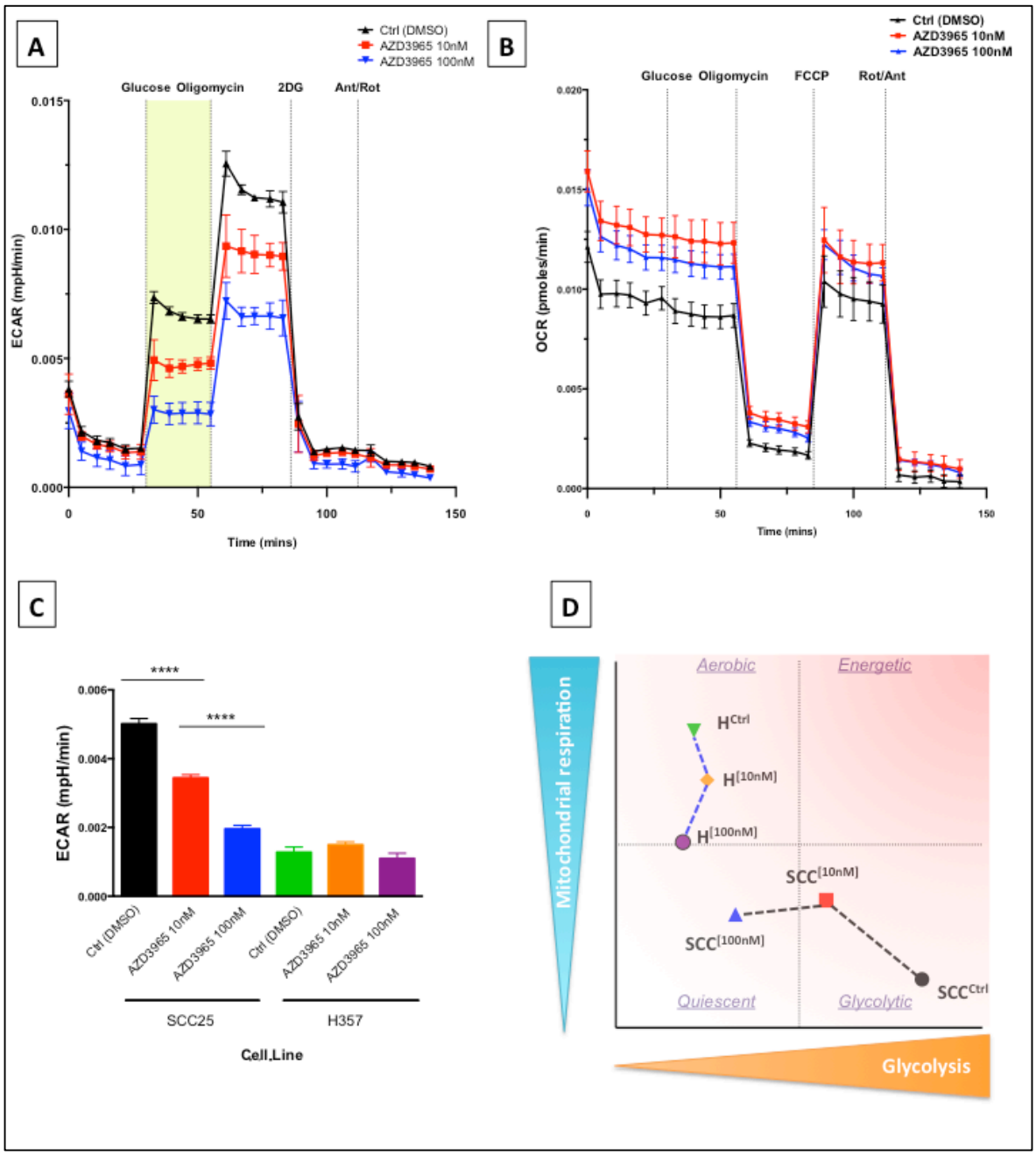

Figure 6-3. Bioenergetic profile of HPV-negative cell lines in response to AZD3965 treatment. The extracellular acidification rate (ECAR; A) and oxygen consumption rate (OCR; B) were measured using an extracellular flux analyser (Seahorse Bioscience) to estimate glycolysis and mitochondrial respiration respectively. Two HPV-negative cell lines (SCC25, H357) were selected and treated with AZD3965 for 72 hours prior to metabolic analysis with 8 replicate wells per condition. Representative data is shown from two biological repeats for SCC25 cell line. Port injections as indicated in (A)&(B) included glucose (5mmol/l), the ATP synthase inhibitor oligomycin A, the mitochondrial uncoupler FCCP or glycolysis inhibitor 2-DG and finally Rotenone/Antimycin A to inhibit the electron transport chain. The shaded area in (A) demonstrates the differential glycolytic response to glucose injection highlighting the differential, dose-sensitive response to MCT1 inhibition. The glycolytic rates have been calculated for each cell line (maximal glycolysis after glucose addition – basal glycolysis) and displayed in (C), showing a cell-line specific effect with significant dose-effect of MCT1 inhibition on impairing glycolysis in SCC25 cells ($P<0.001$). D, A cell energy phenotype profile based on ECAR vs OCR

score for each cell line. This representation allows us to report baseline and maximal mitochondrial respiration and glycolytic activity in the two tested cell lines and plot their profiles. MCT1 inhibition in both cell lines demonstrates a dose-responsive effect of converting HNSCC cell lines into a more quiescent energy phenotype, where neither metabolism pathway is particularly active.

6.5 Effect of AZD3965 on HNSCC invasion

The ability of tumour cells to invade surrounding tissue and ultimately metastasise is a key, persistent hallmark of cancer (Hanahan and Weinberg, 2011, 2000) and therefore the study of *in vitro* cell motility is an important assay for analysing the effects of potential compounds on cancer cell behaviour. This is particularly important in the case of metabolic inhibitors as there is significant evidence in the literature and indeed previously in this thesis that metabolism is fundamentally linked to tumour cell motility.

Furthermore, additions of lactate to cell cultures has been demonstrated to increase cell motility (Walenta et al., 2002) and from the previous section (Fig. 6-3) we have direct evidence that AZD3965 results in a reduction of extracellular acidification and therefore has the potential to modify a cancer cell's interactions with the microenvironment. To study the effect of MCT1 inhibition in physiologically relevant cell invasion, we performed haptotactic Matrigel invasion assays in a range of HPV-negative (SCC25, Detroit 562) and HPV-positive cell lines (SCC2, SCC90). FCS-containing media in the lower well was used as a chemoattractant. In keeping with previous expression data of a high MCT1 expression in HPV-negative cell lines, results demonstrated cell invasion was significantly reduced by MCT1 inhibition in HPV-negative cell lines only ($P<0.0001$ and $P<0.05$ in SCC25 and Detroit 562 respectively).

There is increasing evidence in the literature that extracellular acidity, primarily controlled through lactate, contributes directly to the invasive capability of cancer cells and potentiates their metastatic risk (Silva et al., 2009; Walenta and Mueller-Klieser, 2004). However we have already concluded, at least in SCC25 cells, that AZD3965 treatment results in a reduction in glycolysis and the extracellular acidification rate. Rather than a tumour microenvironment effect *per se*, this therefore suggests that MCT1 inhibition is having a direct effect on the invasive potential of HPV-negative HNSCC cells. We performed organotypic assays in SCC25 cells to examine this effect further and test

whether a similar effect was evident in true tissue substitute 3D models (Fig. 6.4 B-E). The invasion results were replicated here with a reduced overall invasion into the Matrigel/collagen tissue substitute following treatment with AZD3965 ($P<0.01$). There was no significant difference in average tumour island size noted between either group indicating that cell cohesiveness doesn't appear to be affected.

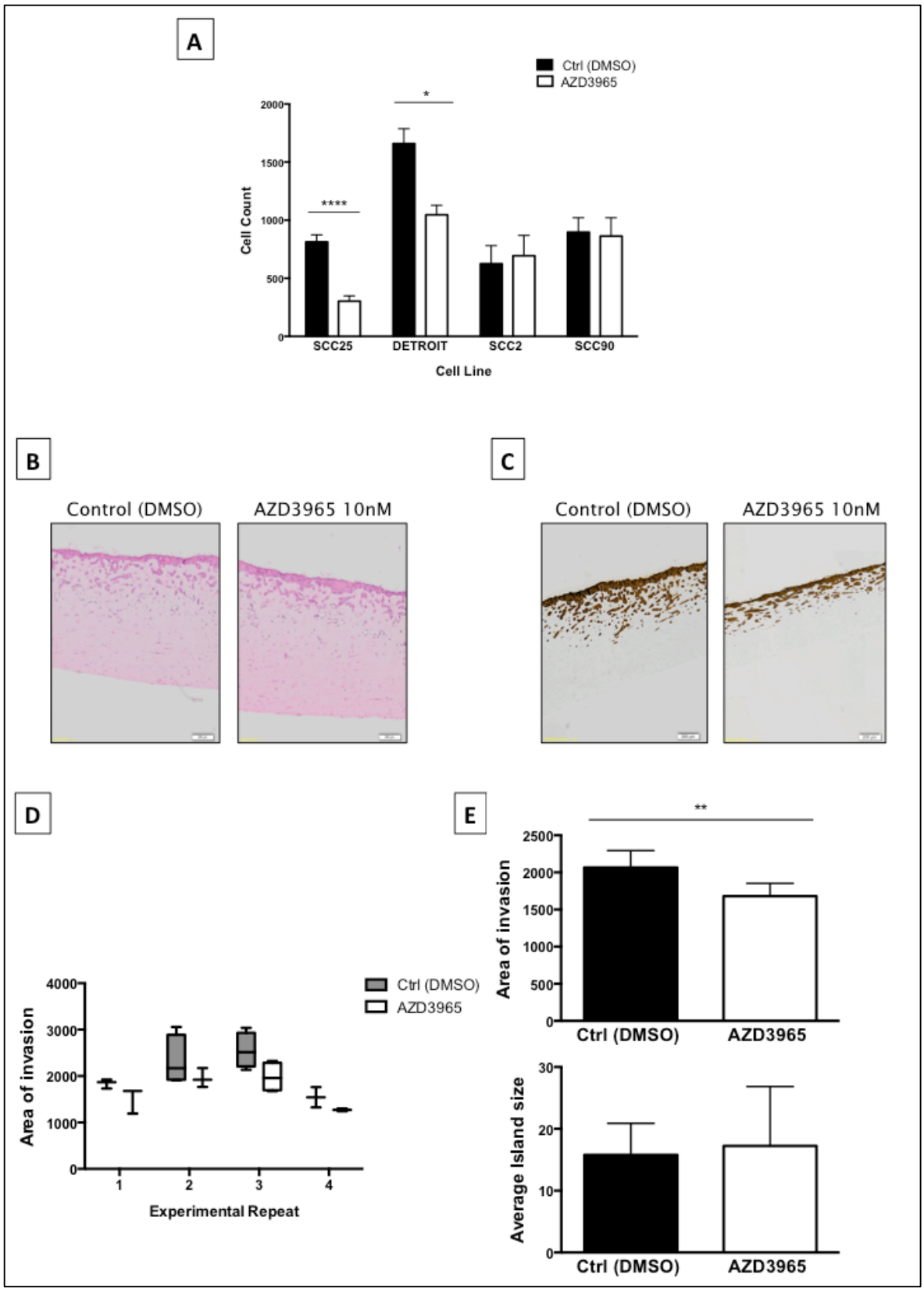

Figure 6-4. Effect of MCT1 inhibition by AZD3965 on tumour cell invasion. A, Invasion assays were performed including HPV-negative (SCC25 and Detroit 562) and HPV-positive (SCC2 and SCC90) cell lines. Cells were treated for 48 hours with 10nM AZD3965 or DMSO as a control and then placed into upper wells in serum-free DMEM media, separated from the inner well filter base by a layer of Matrigel, providing a physical barrier requiring cell invasion for passage to the lower well. 10% FCS-containing media was placed in the lower wells as a chemoattractant and cells were counted

after 72 hours. MCT1 inhibition resulted in reduced cell invasion in HPV-negative cell lines only and representative result is shown (n=3). B-D, Organotypic cultures of SCC25 cells were performed following AZD3965 or DMSO alone treatment and gels were harvested after one week. After fixing, mounting and staining for H&E (B) or pan-cytokeratin (C), slides were examined on a photomicroscope and images captured using dotSlide system (Olympus). Representative images are shown at total 40x magnification. Paired cell invasion area (D) and grouped area (upper panel, E) and average tumour island size (lower panel, E) was analysed using ImageJ software, indicating a significant reduction (P<0.01; Paired T-test) in area of invasion.**

6.6 Effect of AZD3965 on radiation sensitivity

Another advantage of analysing the real-time metabolic flux in cancer cell lines in the ability to predict the effect of combining therapeutic interventions. Indeed therapeutic synergy is receiving significant attention in the literature, especially in the subject area of combining traditional cancer treatment modalities with novel agents e.g. immunotherapy. For example radiosensitivity has been demonstrated to inversely correlate with both glycolytic flux (Lin et al., 2003) and lactate levels (Quennet et al., 2006).

We previously observed a dose-dependent reduction of glycolysis, measured via extracellular acidification rate, following MCT1 inhibition (Fig. 6.3A). We therefore hypothesised that AZD3965 treatment would make SCC25 cells more radiosensitive and took this forward into pilot studies. Two techniques were utilised – both clonogenic survival assays as previously described as well as organotypic cultures. In both techniques, following 48 hours of AZD3965 exposure, cells were exposed to a single 2-Gy dose of γ-rays. For clonogenic assays cells were then plated at 2000/well as previously described where as for organotypic cultures, radiation exposure was performed following cancer cell adhesion to the gel cultures and raising to metal grids so as to eliminate cell adhesion as a confounder. Validation of the effect of radiation exposure was obtained following observation of a small but significant reduction in both control and compound-treated cell invasion following 2 Gy exposure. Furthermore, there was a significant reduction of area of invasion in AZD3965 treated cells over control cells following 2 Gy radiation exposure ($P<0.05$; Fig. 6-5B). No significant change in tumour island size was observed between the two groups (Fig. 6-5C). This evidence supports a radiosensitisation effect of MCT1 inhibition. This hypothesis is further supported by clonogenic assays from two cell

lines where a reduction of colony area is observed at 2Gy in the treated cells (Fig. 6-5 D&E).

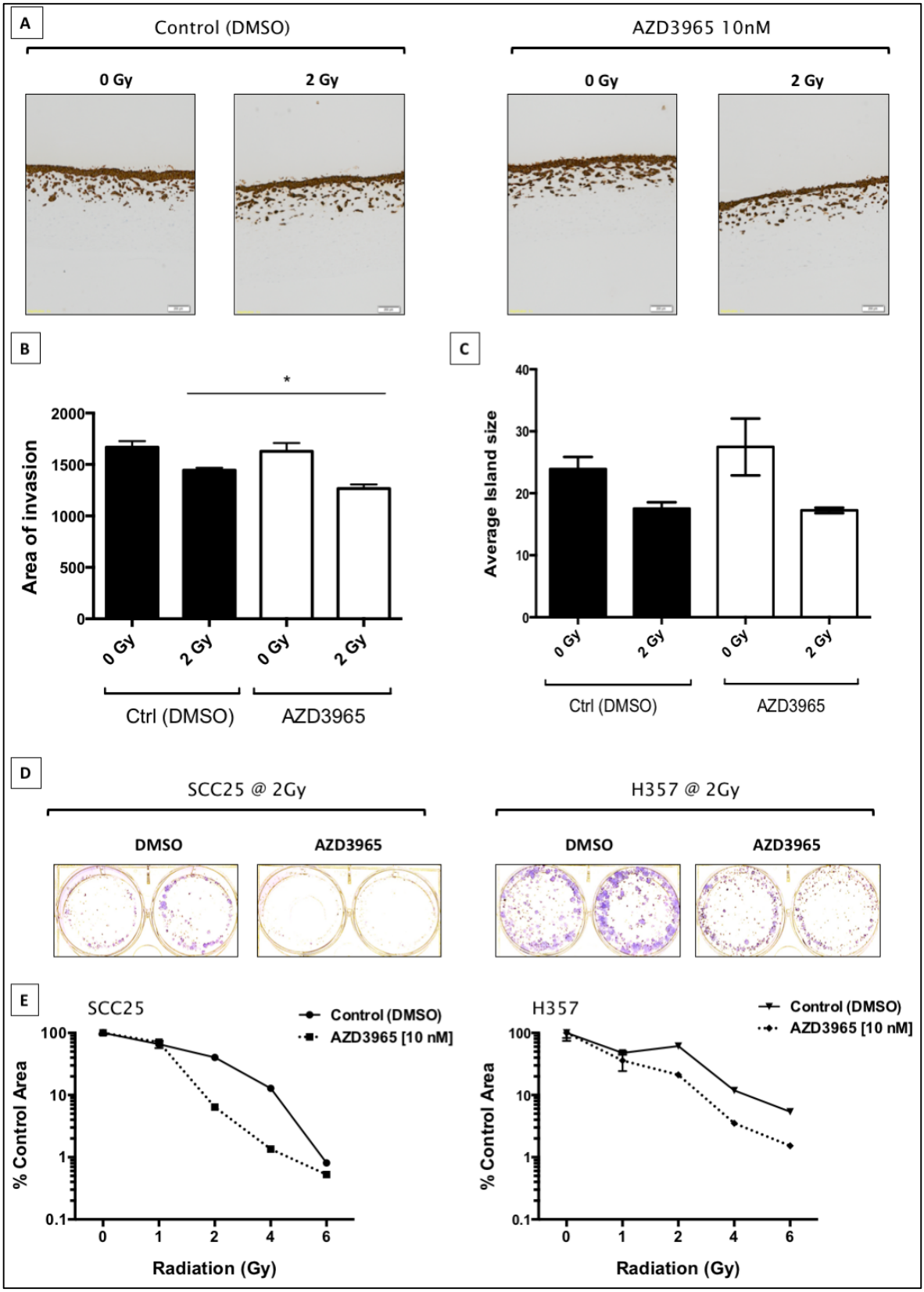

Figure 6-5. Radiosensitisation of SCC25 cells through MCT1 inhibition. A, Organotypic cultures of SCC25 cells were performed following AZD3965 or DMSO alone treatment. After

raising gels to metal grids for the assay culture, test gels were exposed to one 2-Gy dose of γ-rays before return to incubator culture. Gels were harvested after one week, fixed, mounted and stained for pan-cytokeratin as per standard protocol. Slides were examined on a photomicroscope and images captured using dotSlide system (Olympus). Representative images are shown at total 40x magnification. Cell invasion area (B) and average tumour island size (C) was analysed using Image J software, indicating a significant reduction in average area of invasion when comparing Ctrl vs AZD3965 after 2 Gy exposure (*P<0.05; Student's T-test). Area of invasion was also significantly reduced in both test conditions following 2 Gy exposure compared to their 0 Gy counterpart. D, E, Clonogenic assays are represented for SCC25 and H357 with representative well photographs shown. Well area analysis was performed utilising ColonyArea plugin on Image J (Guzmán et al., 2014) and results were converted to % control well for accurate comparison (represented on log scale). Representative well photographs are displayed from this pilot work, representing 2 biological repeats in SCC25, and a single experiment in H357.

6.7 Discussion

The monocarboxylate transporters (MCT) are responsible for the shuttling of lactate between intra- and extra-cellular compartments in tumours and MCT1 and MCT4 are the family members implicated in tumour metabolism (Sonveaux et al., 2008). Although previously considered a lactate importer, the widely expressed MCT1 has in fact demonstrated bi-directionality (Halestrap and Meredith, 2004) which may help to explain some of the variable results on cell metabolism from MCT1 inhibition in the literature. For example, in various cancer cell lines Bola et al. (2014) demonstrated that AZD3965 resulted in an increase in glycolysis and glycolytic enzymes, whereas Doherty et al (2014) found that MCT1 inhibition rapidly abrogated glycolytic function. It is this delicate lactate homeostasis that is likely of critical importance to a tumour's growth and behaviour and the concentration gradient of this molecule is likely the key determining factor in overall net movement (Halestrap and Price, 1999). Limit lactate export and the reduction in intracellular pH could have a dramatic effect inhibiting cell proliferation promoting growth arrest (Le Floch et al., 2011). Reduce lactate import and you cut off the energy supply to those cells who are using it as a substrate for OXPHOS, but also acidify the tumour microenvironment which may promote tumour invasion and metastasis (Rofstad et al., 2006). Indeed Sonveaux et al (2008) provided their summary evidence of a lactate shuttle system where a more hypoxic, and therefore glycolytic cell can be

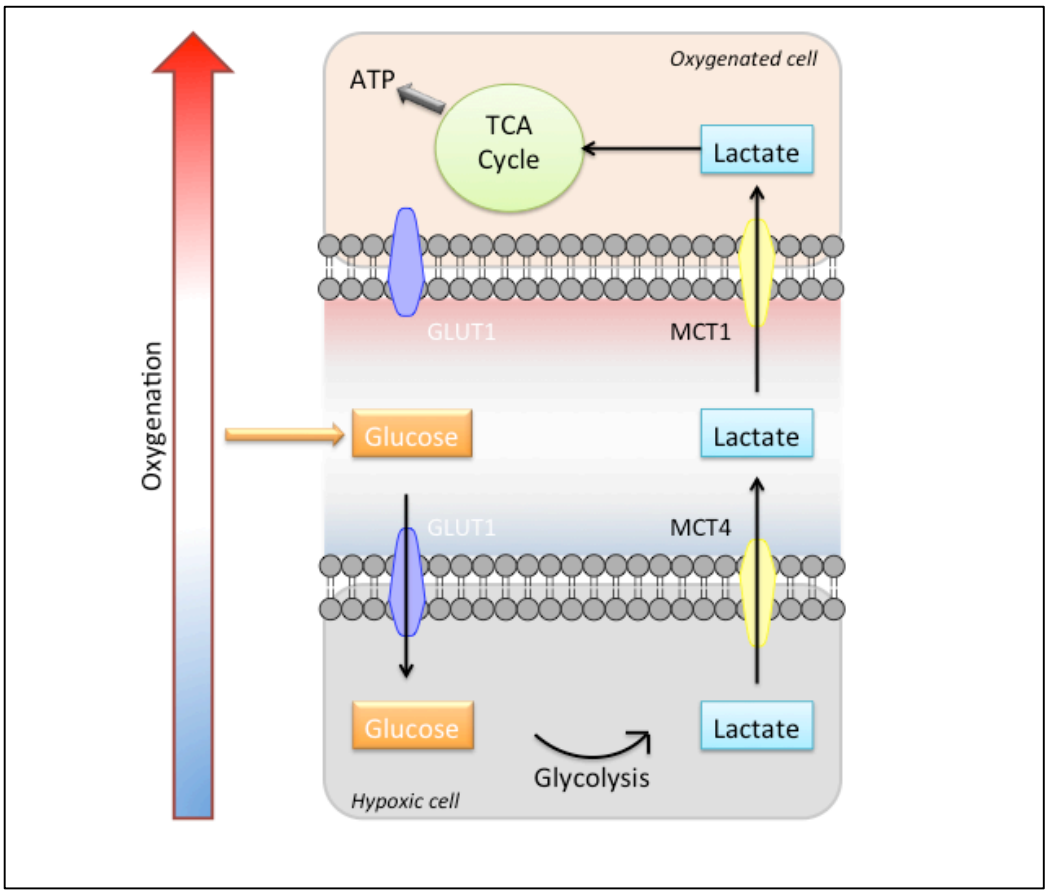

Figure 6-6. Proposed lactate shuttle between tumour cells in a two-compartment model. Hypoxic cells can export glycolysis-derived lactate by membrane-bound MCT4. This lactate represents a potential source of energy and can be imported via MCT1 expressed on well-oxygenated cells and used to produce ATP. Adapted from Porporato et al. (2011).

exported by MCT4, which can then be imported via MCT1 by oxidative cells that can use lactate as an energy source (Fig 6-6).

The last decade has also seen a rapid rise in our understanding of the influence a tumour stroma has on a primary tumour's characteristics and there have been numerous attempts to expand this understanding into metabolism. Thus the tumour stroma is likely to also impact on this lactate homeostasis and provide a symbiotic relationship between key stromal components e.g. fibroblasts and the cancer cells themselves (Bola et al., 2014). Considering all the different cells therefore that inhibition of a metabolic transporter is likely to impact upon, it is therefore vital that comprehensive pre-clinical studies on new compounds are performed to fully understand the metabolic consequences of manipulation in cancer cell types of interest, and identify effects of both potential good and harm from therapeutic targeting.

Following presentation of clinical MCT1 relevance, we have presented a range of *in vitro* work demonstrating the sensitivity, metabolic effects and potential therapeutic potential of MCT1 inhibition in HNSCC.

Unlike clinical survival and prognostic data previously published for tumours of the breast (Pinheiro et al., 2010), ovary (Chen et al., 2010), stomach (Pinheiro et al., 2009) and colon (Pinheiro et al., 2008), we found no evidence of association between MCT1 expression and disease-specific survival in HNSCC patients. However this analysis did support our protein and RNA expression data of a large skew of high expression in HPV-negative tumours and therefore provided a strong rationale to test further functional analysis in this tumour subgroup. In addition, this distribution together with the finding of a weak association of MCT1 with GLUT1 expression would fit with a hypothesis of this receptor being distributed more prominently within glycolytic tumours. At first glance this does appear contrary to published models (Sonveaux et al., 2008). There are potentially two explanations for this pattern: a feedback response to MCT4 expression or a prominent lactate efflux role. As MCT1 is hypothesised to be involved in a lactate homeostatic mechanism, it is possible that MCT1 is upregulated in a feedback response driven initially by a glycolytically-driven MCT4 upregulation. Therefore MCT1 upregulation avoids the imbalance of an unrestricted MCT4 efflux of lactate, potentially resulting in cytotoxicity from an extreme pH. We do not currently have data on MCT4 expression in HNSCC but co-localisation analysis in tumour specimens would be required to examine this further. However, it may be a cancer-type specific observation, where MCT1 bidirectionality plays a more prominent role. In this hypothesis, the large lactate gradient across the cell membrane from active glycolysis may upregulate and revert MCT1 activity to a lactate efflux role. Furthermore, our real time flux analysis data is consistent with this hypothesis, where MCT inhibition is resulting in a dose-dependent reduction of the extracellular acidification rate and we can therefore surmise that lactate efflux is reducing. Indeed this hypothesis ties together the functional results observed in SCC25 cells from MCT1 inhibition. A reduction in intracellular pH would also help explain the cell survival effects on SCC25 observed in clonogenic assays, as well as potentially explain the reduced invasion observed in the more physiologically relevant assays performed.

In addition to these interesting findings on the resulting pH changes from MCT1 inhibition, the cell energy phenotype profile presented from extracellular flux analysis provides a strong rationale for continuing to investigate MCT1 inhibition as a therapeutic

option (Fig. 6-3D). In the two cell lines presented, this energy profile indicates that for cells demonstrating differing metabolic rates for energy production, MCT1 inhibition response results in driving down of the predominant energy-producing pathway in that cell line. This functional view of the response to MCT1 inhibition demonstrates a shift of the metabolism profile across cell lines to a quiescent cell phenotype. This implies that blocking of MCT1 lactate transport preferentially occurs in the dominant directional lactate movement in any particular cell line e.g. lactate efflux in glycolytic cells, influx in OXPHOS-dominant cells. This effect would be highly desirable for both direct effects on tumour growth, as well as synergistic combinations with other potential treatments and suggests that MCT1 targeting for treatment would not rely on more specific investigations of inherent glycolytic parameters in any given tumour.

We proceeded to demonstrate the ability of AZD3965 to sensitise cells to radiotherapy *in vitro* and show that combined treatment produced a significant effect on cancer cell survival and invasion compared to radiation alone. This is an effect that has previously been observed on *in vivo* studies in combination treatment (Bola et al., 2014). Clinically HPV-negative tumours tend to be less radiosensitive than their HPV-positive counterparts, and a number of trials in radiosensitisation strategies are now underway. Previous studies have demonstrated that specific inhibition of glycolysis can result in increased radiosensitivity (Lin et al., 2003) and following our direct illustration of the glycolysis reduction resulting from MCT1 inhibition, we performed early studies looking at this potential role for AZD3965 in therapeutic combination treatment. Experimental repeats were limited and therefore we must draw caution in definitive conclusions from these experiments. However, two different assay techniques appeared to reduce the survival and invasion of HPV-negative cell lines *in vitro*, which would be in keeping with our metabolic hypothesis.

In conclusion, AZD3965 is a novel MCT1 inhibitor, which has shown promise in early phase clinical trials and is orally bioavailable. We have presented the first work in HNSCC of the potential of MCT1 inhibition and provided a rationale based on biochemical findings of its potential mechanism, as well as identifying HPV-negative tumours as the preferential targeting group for potential inclusion in any future clinical trial. Whilst monotherapy treatment on HNSCC cells with our *in vitro* studies show some modest beneficial treatment effects, the demonstrated alteration of the biochemical profile of cells following MCT1 inhibition provides a strong rationale for combined synergistic

therapy in future clinical trials. AZD3965 has demonstrated a favourable safety profile to this point and we therefore strongly support further clinical investigations into the use of this compound in novel therapeutic strategies.

Chapter 7: Conclusions

7.1 Key points

We have investigated the role of the focal adhesion adaptor protein CTEN, and investigated its role in HNSCC. Through discovery of a novel link to a tumour cells glycolytic profile, we have gone on to provide a comprehensive analysis of HNSCC metabolism in both HPV-negative and HPV-positive disease. Finally we have tested a novel compound targeting an important cell membrane transporter in HNSCC that may affect the lactate shuttle, important for HNSCC tumours *in vivo*.

Key findings can be summarised as follows:

- CTEN is widely expressed in HNSCC cell lines and in oropharyngeal tumours, showing the most significant correlation with reduced survival in HPV-positive disease and, more broadly, those treated with non-surgical modalities (chemotherapy/radiotherapy).
- Absence of CTEN expression results in reduction of tumour behaviour in HNSCC cell lines including reduced motility, invasion, suspension culture proliferation and organotypic invasion. CTEN confers a survival effect on HNSCC cells, enabling apoptosis resistance in response to a variety of stimuli.
- CTEN appears to be involved in a signalling role in HNSCC cells, notably in the TGF-β pathway that may have a functional importance not only to the tumour microenvironment, but also to the apoptotic pathways. This latter biological link has clinical relevance whereby CTEN may be a marker of radiosensitivity, allowed de-escalation in the treatment of HPV-positive disease, or a therapeutic target to reduce radio-resistance.
- CTEN is a previously unreported target for transcriptional repression by the metabolic sensor CtBP2
- HPV-negative and HPV-positive disease have distinct metabolic profiles involving a number of biochemical pathways, with further investigation of glucose metabolism demonstrating HPV-negative cells overall to be more metabolically active but more reliant on glycolysis for their maintenance bioenergetic requirements.
- Targeting of MCT1 in HPV-negative tumours *in vitro* has demonstrated an important functional role for this transporter in HNSCC cell metabolism that may be therapeutically attractive as a target in either mono- or combined-systemic therapy.

7.2 Summary discussion and future work

Tensins are proteins that on a cellular level seems to be ideally positioned to facilitate the progression of an oncogenic phenotype: as focal adhesion adaptor proteins they play integral roles in modifying a cell's migratory phenotype, the multi-domain structure permits binding capabilities to multiple ligands including signalling molecules and integrins and the presence of an actin binding region permits the linkage between the cytoskeleton and ECM (Auger et al., 1996; Lo et al., 1994). The focal adhesion complex together with associated integrins, or 'adhesome', has received a significant amount of interest in the literature in the past decade with the realisation that the number of involved adaptor proteins and binding partners have been significantly underestimated and the most recent survey found 42 potential β-integrin-tail-binding adaptor proteins (Legate and Fässler, 2009). These generally fall into structural proteins, scaffolding sites for additional binding proteins, and signalling proteins. The importance of Tensins to the complex as a whole resides in the fact that they can partake in all these roles and their close proximity and binding capability to the β-tail of integrins provides a further level of control on both cell behaviour and interactions with the extracellular environment. Indeed the identification of competitive Tensin or Talin binding to β- integrins at the NPxY site as a form of regulatory switch provides further evidence of the key role of these proteins in determining a cell's phenotype (Legate and Fässler, 2009).

CTEN in particular is receiving considerable recent interest in the cancer literature, and has shown potential as a tumour marker. Although descriptions of biological mechanisms are scarce, CTEN appears to promote tumourigenesis and is associated with aggressive disease in a significant number of different tumour types and the demonstrated biological functions indicate that it is likely actively involved in regulation of tumour development (Lo, 2014). In the present study we have significantly expanded the knowledge base of CTEN biology in functional studies and provided evidence for an expanded role for CTEN in a complex signalling role involving TGF-β activation, changes in surface integrin expression and the apoptosis pathway, the latter potentially key to its tumour-promoting role.

We have presented evidence that CTEN may have a perinuclear location associated with Golgi at least at early stages of cell adhesion and whilst this protein may well be recruited to fibrillar adhesions later in the cell adhesion cycle, the presence of a Src

homology 2 (SH2) domain and a phosphotyrosine binding domain (PTB) in its structure means it has an ideal structure to recruit other adaptor proteins and facilitate intracellular signalling pathways, as well as communicating with the extracellular environment through focal adhesions and β-integrin tails through NPxY motif ligands (Chen and Lo, 2003).

The 2011 hallmarks of cancer cite 'invasion & metastasis' as one of the core properties of a tumour (Hanahan and Weinberg, 2011) and with current literature this is where CTEN would have been positioned. Indeed we have provided supporting evidence of its ability to promote motile and invasive cell behaviour by studying HNSCC cells in its forced absence. However we propose that CTEN has an important functional role in other hallmark processes including 'resisting cell death' (Chapter 3 & 4) as well as involvement as a target in 'deregulating cellular energetics' (Chapter 5). It is perhaps our finding of a role for CTEN in apoptosis that has the most interesting research and therapeutic clinical potential in HNSCC. We have already demonstrated the clinical relevance of CTEN expression in a large head and neck tumour database, and demonstrated the highly significant correlation between CTEN expression and reduced disease-specific survival, most notably in radiotherapy-treated patients. It will be important to corroborate these findings in a second validation tumour database. Our advanced pilot work has suggested that CTEN is involved in promoting cell survival through a TGFβ-dependent pathway. Interestingly, whilst TGF-β has been recognised to induce apoptosis in a variety of cell types, the biological mechanism remains poorly defined, although likely involves a number of death receptors and kinases e.g. FAS (Meulmeester and Ten Dijke, 2011). It is however the presence of a pro-apoptotic profile that has the most interesting clinical relevance, and the level of CTEN expression may represent a promising upstream marker of the activity of this pathway. Whilst the effective mechanism of radiation therapy involves induction of a number of different forms of cell death including autophagy and senescence (Verheij, 2008), apoptosis is a major mechanism through which this treatment modality achieves its therapeutic effect (Dewey et al., 1995). As such there are a number of clinical research strategies currently in progress testing agents that silence genes coding for anti-apoptotic proteins (Wong, 2011). Due to the restricted expression of CTEN in normal human tissue, a similar silencing targeting strategy has potential and, unlike some of the current genes under investigation, would potentially also combine an anti-invasive effect in addition to the apoptosis-promoting mechanism. Treatment de-

escalation specifically in HPV-positive HNSCC is of significant research interest at the current time due to the recognised serious adverse short and long-term effects of chemo- and radiotherapy. Conversely whilst HPV-positive HNSCC shows a significantly better outlook than its HPV-negative counterpart, much effort is now being focussed on an 'intermediate' risk group of patients, often smokers, in whom present with a significantly more aggressive disease pattern. Any potential biomarker that may help identify this group is of paramount importance (Ang et al., 2010) and, subsequent to any positive validation study, a cohort study on patients undergoing chemo-radiotherapy treatment with prospective investigation of tumoural CTEN expression should be expedited. Similarly any agent enabling a dose-reduction in radiotherapy treatment would be a highly desirable treatment option and we propose CTEN worthy of further targeting research for this reason.

The discovery of a biological link between CTEN and a key metabolic sensor has given us a unique insight into tumour cell metabolism and how this can affect tumour cell behaviour. Whilst the final metabolically induced phenotype of a tumour cell behaviour likely depends on a complex transcriptional response to available oxygen, nutrients and biochemical intermediates, elucidating individual transcriptional targets in this response helps us understand the factors involved in influencing the final phenotype. It has also enabled us to investigate more clearly the metabolic differences between HPV-negative and HPV-positive disease. This is a diagnostic distinction that is of fundamental clinical importance yet the generic pan-disease use of glycolytic imaging in the form of FDG-PET in widespread clinical practice demonstrates one example of how we have not yet exploited metabolic differences between virally and non-virally derived HNSCC for diagnostic or therapeutic advantages. Whilst we have reviewed and concluded that SUV(max) scores alone from FDG-PET imaging are insufficient to determine HPV-status, HNSCC as a disease is an ideal candidate for advancing tumour metabolism-based treatment. The recent TCGA genomic categorisation study on HNSCC found a mutation rate of 86% in non-viral related HNSCC (Lawrence et al., 2015) and in HPV-positive disease, the actions of the oncoproteins, predominantly E6, promotes rapid p53 degradation (Huibregtse et al., 1993; Mammas et al., 2008) which is not only an important mechanism behind HPV oncogenic potential, but also has a profound effect on cell metabolism due to p53's ability to invoke a global transcriptional response regulating

glycolysis, mitochondrial respiration, glutaminolysis and regulation of cell growth via interaction with the mTOR pathway (Maddocks and Vousden, 2011).

Tumours are highly glycolytic on PET imaging and, although few in number, metabolic targeting studies with 2-deoxy-D-glucose has been shown to potentiate cisplatin's antitumour effects on tumour cell proliferation and survival, as well as inhibit the growth of HNSCC xenografts (Andrean L Simons et al., 2007; Andrean L. Simons et al., 2007). We have provided evidence for one example of how tumour metabolism can be targeted to affect cancer cell behaviour and survival, through blocking MCT1 activity. The family of MCTs are involved in both lactate influx and efflux across the cell membrane, helping to closely control lactate flux and resulting extracellular pH. Through blocking their activity, it is easy to understand how the tumour microenvironment will be significantly affected, and we have provided a strong scientific rationale on why HPV-negative patients would be more suitable to this form of treatment. The fact is that despite MCT1's recent emergence as a cancer target (Bola et al., 2014), its mechanism of action and relationship with the other MCT family members remains unclear. By demonstrating a significant change in the glycolytic-OXPHOS biodynamics in tumour cells after MCT1 disruption, we have provided evidence that disruption of lactate shuttling, likely involved in a highly regulated symbiotic relationship between cells of differing metabolic state, results in a profound global shift of tumour cells towards a less bioenergetically active state. In turn this offers numerous potential opportunities for symbiotic treatment combinations. However, manipulating tumour metabolism must be investigated with caution; the lactate import function of MCT1 has actually been shown to result in a less aggressive gene expression profile in some tumours (J. L.-Y. Chen et al., 2008) but early results for MCT1 inhibition are promising (Bola et al., 2014). If our *in vitro* study results with MCT1 inhibition can be replicated with *in vivo* experiments, we would propose consideration of planning for a window study to observe for any potential synergistic combination treatment strategy in HPV-negative HNSCC patients.

For each of the 500,000 new patients presenting with HNSCC each year, both new management strategies for targeted therapy and new antitumour agents are urgently required (Le Tourneau et al., 2007). In order for these novel molecular targeting therapies to be realised, we must fully understand the biological mechanisms behind disease progression and we have presented both *in vitro* and *in vivo* data exploring novel aspects of HNSCC disease. After almost a century of metabolism research since Otto Warburg's

first experiments, we now be on the cusp of using the results of his pioneering experiments for therapeutic benefit .

Appendices

Appendix A

Media and buffers

- **Tissue culture**

Phosphate buffered saline (PBS), 10x

NaCl	80g
KCl	2.5g
Na_2HPO_4	2.5g
KH_2PO_4	2.5g

Made up to 1 litre with distilled H_2O

10% DMEM

DMEM (PAA)

10% heat irradiated fetal bovine serum (Biosera)

2mM L-Glutamine (PAA)

10% RPMI

RPMO 1640

10% heat irradiated fetal bovine serum (Biosera)

2mM L-Glutamine (PAA)

SCC25 Media

DMEM (PAA): Hams F12 (1:1)

10% heat irradiated fetal bovine serum (Biosera)

2mM L-Glutamine (PAA)

MLEC Medium

10% DMEM as above

400μg/ml Geneticine

Keratinocyte growth medium (KGM)

A-MEM (Gibco)

10% heat irradiated fetal bovine serum (Biosera)

2mM L-Glutamine (PAA)

1.8x10-4M adenine (Sigma)

0.5mg/ml hydrocortisone (Sigma)

10ng/ml epidermal growth factor (Sigma)

- **Western Blotting**

SDS-polyacrylamide gels

Resolving gels (15ml)	8%	10%
Distilled water (ml)	6.9	5.9
30% acrylamide mix (ml)	4	5
1.5M Tris (pH 8.8) (ml)	3.8	3.8
10% SDS (µl)	150	150
10% ammonium persulphate (APS) (µl)	150	150
TEMED (µl)	9	6

Stacking gel (4ml)

Distilled water (ml)	2.7
30% acrylamide mix (ml)	670
1.5M Tris (pH 6.8) (ml)	500
10% SDS (µl)	40
10% APS (µl)	40
TEMED (µl)	4

Western blotting running buffer (5x) (2L)

Tris base	30g
Glycine	144g
SDS	10g

Distilled water to 2 litres

Western blotting transfer buffer (5x) (2L)

Tris base	58g
Glycine	290g
SDS	10g
Distilled water to 2 litres	

NP40 Lysis Buffer

1M Tris pH 7.4	1ml
10% NP40	1ml
0.5M EDTA	100µl
0.5M EGTA	100µl
5M NaCl	100µl
500mM NaF	100µl

100X PIC (protease inhibitor cocktail (Calbiochem Protease Inhibitor Cocktail Set 1)	100µl
Distilled water	7.5ml

Western blot blocking buffer (50ml)

10% Tween 20	0.5ml
Marvel skimmed milk powder	2.5g
PBS to 50ml	

Western blot washing buffer (1L)

10% Tween	10ml
PBS	1L
5x Laemmli	
625mM Tris ph 6.8	
6% SDS	
15% Glycerol (100%)	
0.009% Bromphenol-blue	

- **Flow cytometry**

FACS Buffer

For 1L

10xPBS	100ml
0.5M EDTA	8ml
6.5% NaN3	1ml
BSA	10g
Add distilled water to volume	1L

Antibodies

Primary antibody	**Species**	**Supplier**	**IHC/IF dilution**	**WB/FC dilution**
HSC70	Mouse	Santa Cruz		1:10,000
Active caspase-3	Rabbit	Abcam		1ug/ml
β1 (P5D2)	Mouse	Abcam		1:1000
CD29/β1 (APC)	Mouse	Biolegend		5µl/test
CD61/ β3 (FITC)	Mouse	Biolegend		5µl/test
β6 (PE)	Mouse	R&D systems		10µl/10^6 cells
Talin-1 (TLN1) (8d4)	Mouse	Abcam		1:2000
TNS1	Rabbit	C/o Dr. S Hafizi (UoP in-house, polyclonal)	1:200	1:500
TNS3	Rabbit	C/o Dr. S Hafizi (UoP in-house, polyclonal)	1:200	1:500
TNS3	Rabbit	C/o Dr. S Hafizi (UoP in-house, polyclonal)	1:200	1:500

TNS3	Rabbit	Abcam		1/1000
Tensin 4/CTEN MAb (Clone 684524)	Mouse	R&D systems	IHC 1:200	WB 1 µg/mL

Inhibitors, reagents and blocking antibodies

Reagent	**Manufacturer**	**Concentration**
Human TGF-β1	Sigma-Aldrich	100-2000pg/ml
Human recombinant TGFβ1-latency-associated peptide (TGF-β1 LAP)	Sigma-Aldrich	0.5µg/ml
63G9 (αvβ6 blocking antibody)	Biogen Idec	20µg/ml
P5D2 (β1 blocking antibody)	Abcam	10µg/ml
ALK5 (TGF-β RI kinase inhibitor)	Calbiochem	1µg/ml

siRNA

siRNA	Manufacturer	Serial/catalogue number	Concentration (nM)
Silencer negative control	Applied Biosystems	AM4635	10-30
αvβ6	Thermo Scientific/Dharmacon	L-00812-00	100
TNS3 (Flexitube)	Qiagen	GS64759	5
TNS4 (CTEN)	Life Technologies	4392421	30
CtBP1 (stock)	Qiagen	Custom*	30
CtBP1 GeneSolution pool	Qiagen	1027416	30
CtBP2 (stock)	Qiagen	Custom**	30
CtBP2 GeneSolution pool	Qiagen	1027416	30

* Target mRNA sequence (CtBP1): 5'-ACGACUUCACCGUCAAGCAdTdT-3'
3'-dTdTUGCUGAAGUGGCAGUUCGU-5'
** Target mRNA sequence (CtBP2): 5'-ACGACUUCACCGUCAAGCAdTdT-3'
3'-dTdTUGCUGAAGUGGCAGUUCGU-5'

shRNA

Sequences	Tube ID	Species Specificity (human, mouse, rat)
GAGCAACGGAAGTGGCAGAAGTACTGCAA	TL300896A / TL300896A	H,M
CCAGTGTTCTTACTACACCACGGAAGGCT	TL300896B / TL300896B	H
ACACGAAGCAGCAGTGAGAGCCTCATCTT	TL300896C / TL300896C	H
CTCTGACTGATGTCCAGAGGAAGGTGTTT	TL300896D / TL300896D	H

PCR Reagents/Primers

Reagent	Manufacturer	Catalogue Number/Assay id
qScript™ cDNA SuperMix	VWR/Quanta	QUNT95118-250
PerfeCTa® qPCR FastMix II®,	VWR/Quanta	733-1177
Taqman gene assay - TNS3 (FAM)	Lifetechnologies	Hs00224228_m1
Taqman gene assay – TNS4 (FAM)	Lifetechnologies	Hs00262662_m1
Taqman gene assay – ITGB1	Lifetechnologies	Hs00559595_m1

Taqman gene assay – ITGB6	Lifetechnologies	Hs00982345_m1
Taqman gene assay – ACTA2	Lifetechnologies	Hs00426835_g1
Taqman gene assay – COL1A1	Lifetechnologies	Hs00164004_m1
Taqman gene assay – FN1	Lifetechnologies	Hs00365052_m1
ACTB (beta actin) Endogenous Control (VIC)	Lifetechnologies	4326315E

E6/E7 primers (courtesy of K. Moutasim)

Oligo Name	Sequences	Tube ID
Spliced E6-E7 (F)	ACTGCGACGTGAGATCATCAAGAAC	HA07506821
Spliced Eg-E7 (R)	TCTGAGAACAGATGGGGCACACA	HA07506822

Appendix B

siRNA optimisation

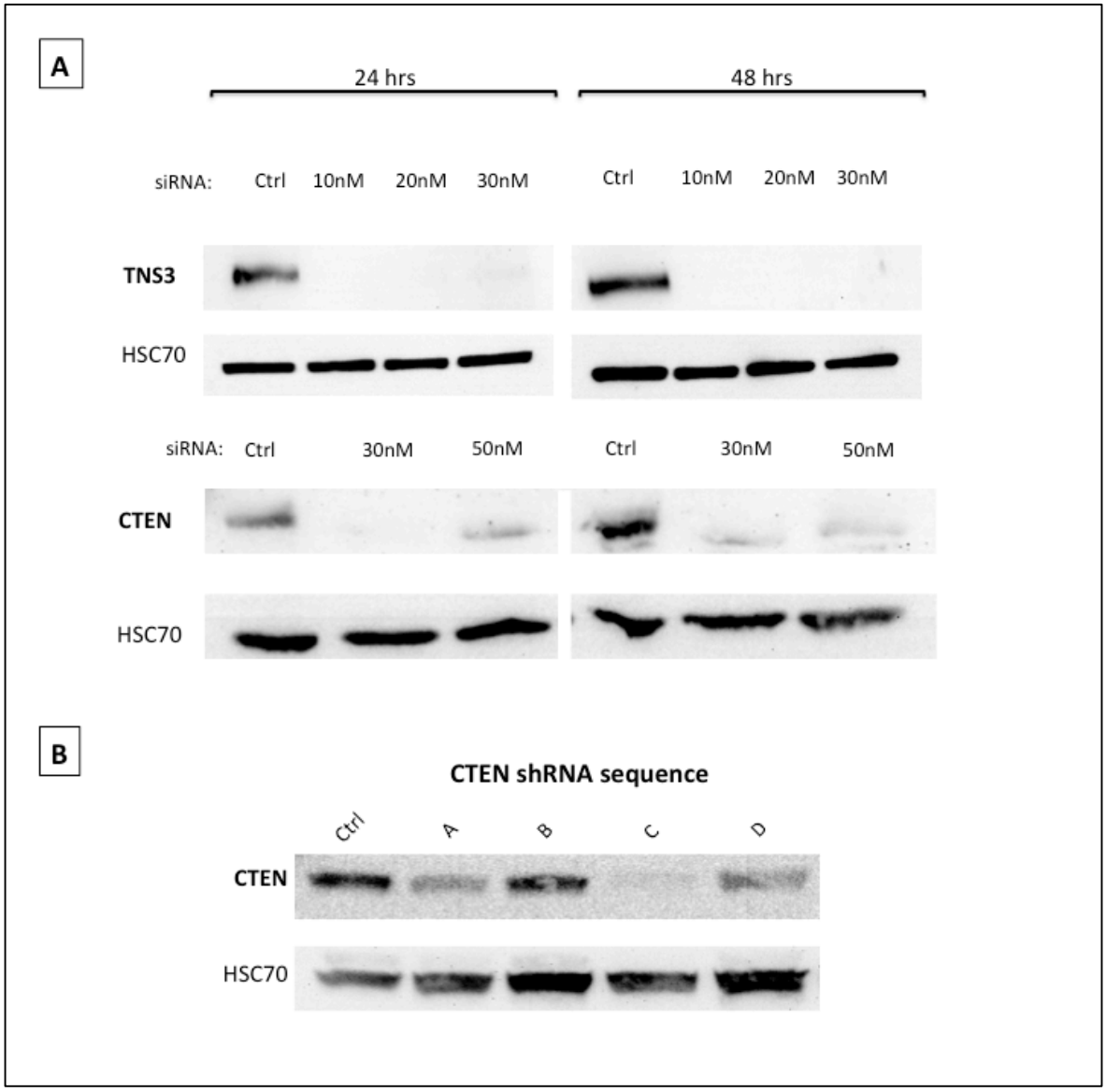

Figure 7-1. Transfection optimisation of Tensin siRNA. A, SCC25 cells were plated at 5 x 10^4 cells/well and transfected with either Control (Ctrl), Tensin-3 (TNS3) siRNA or Cten siRNA. siRNA concentrations of 30 and 50nM were tested with Cten siRNA, and an additional concentration of 10nM in Tensin-3 siRNA. Cells were then lysed at 24 or 48 hours post transfection and Western blot performed. Significant knockdown is observed in both Tensins at 24 hours in all concentrations (an additional 10nM was tested with Cten siRNA but knockdown was insufficient (data not shown)). 10nM siRNA for TNS3 and 30nM for CTEN was therefore chosen as suitable concentrations for all functional assays with setting up of these assays performed at 24 hours post transfection. B, to produce a stable CTEN knockdown cell line,

human shRNA lentiviral particles (4 unique 29mer target-specific shRNA sequences labelled A-D, 1 scrambled control (Ctrl)) were purchased from Origene. SCC25 cells were seeded at $6x10^5$/ $25cm^2$ flask and following overnight incubation, medium in each flask was replaced with 3mls of the virus particle mixture comprising: DMEM, 10% FCS, 1% L-Glutamine, 8 µg/ml Polybrene® and viral particles at a MOI (multiplicity of infection) of 2. Transduction units (TU/ml) for each sequence were supplied on purchase to enable accurate MOI calculation. Puromcyin-containing medium was used for colony selection to obtained pooled culture. Gene silencing was confirmed by examination of protein levels with Western blotting and from this result, shRNA batch C was chose for functional experiments. HSC70 was used as a loading control.

Appendix C

Confirmation of siRNA knockdown of CTEN and RNA quality analysis prior to performance of RNA sequencing

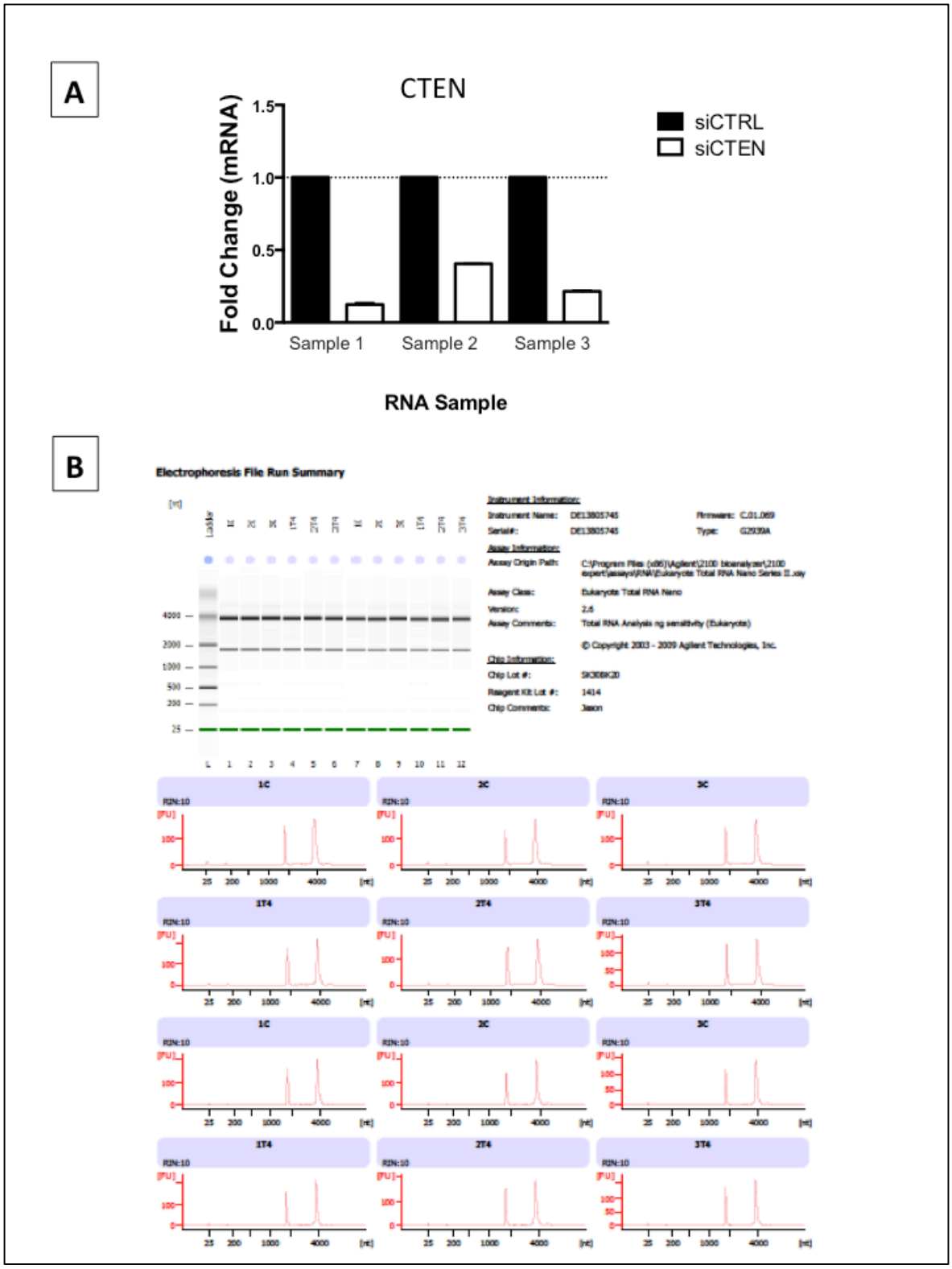

Figure 7-2. Pre-processing and quality assessment of RNA for RNA sequencing analysis. A, Three time- and batch-independent SCC25 cell culture populations were treated with either Ctrl siRNA or CTEN siRNA and collected at 48 hours post-transfection. RNA was extracted with the RNAeasy Kit (Qiagen) according to manufacturer instructions. Extracted RNA was re-suspended in RNAse–free water and then quantified on a spectrophotometer. Real-time Taqman® PCR assay of CTEN target was performed to confirm knockdown at RNA level across cell lines. Results were normalised to a β-actin control. B, RNA quality was determined using Bioanalyser analysis (Agilent Technologies Inc.) to obtain RNA integrity numbers prior to downstream processing.

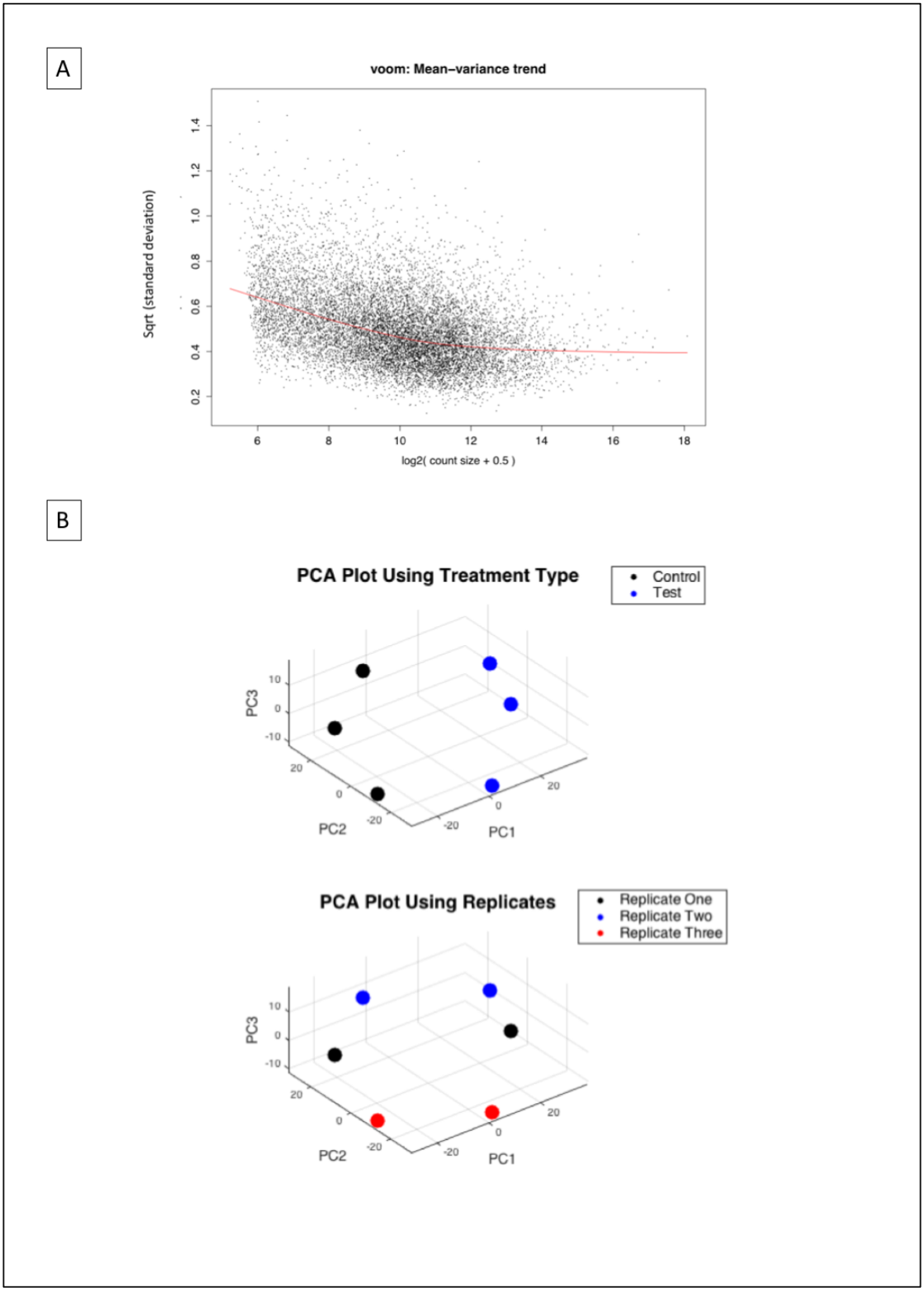

Figure 7-3. A, voom mean-variance modelling. Plot represents gene-wise square-root residual standard deviations versus average log count. Gene-wise means and variances are represented by black points and a LOWESS trend has been drawn, demonstrating moderate-level biological variation. B, 3-dimensional plot showing the first, second and third principal components (PC1, PC2 and PC3 respectively).

Appendix C

MCODE NETWORK ANALYSIS OF CTEN KNOCKDOWN CELLS (siRNA)

Parameters:

Network Scoring:

Include Loops: false Degree Cutoff: 2

Cluster Finding:

Node Score Cutoff: 0.2 Haircut: true Fluff: false K-Core: 2 Max. Depth from Seed: 100

UP-REGULATED GENES

Cluster	Score (Density*#Nodes)	Nodes	Edges	Node IDs (Decreasing M-CODE Network Collection Score
1	9.308	27	137	RND3, PTGS2, STK4, FN1, SEC24B, DUSP5, CHST15, GOLGA4, HNRNPUL1, DYRK2, ZFHX3, CUC4, RBM15B, TFPI2, ASH1L, RBPJ, JAG1, AKAP12, JIPK1, NID1, QKI, LCOR, ADAM19, CYP27B1, CSF2, ATE1, EVA1A,
2	8.15	41	185	MARCKS, LAMC1, TGFBR3, EGR1, FAM171A1, SRPK2, IL10RB, EPHB6, BASP1, CHPF, ROX, TRIB2, SS18L1, ULK1, ATF2, PTPRE, EGR2, TFAP2C, SULT1B1, EMP2, CDK14, SAR1B, BCL11B, ANO10, TAOK1, CCNI, DRAM1, IL11, FRMD4A, SEMA4F, RAB15, ZMAT3, BTRC, DLX2. GJB2, WNT5B, ANKRD50, ELOVL7, NAV1, SLC41A1, ZNF469
3	7.143	15	63	ITGA5, IL6, MMP9, NEK7, F2R, LOX, EDNRA, CREB5, INGBA, HAS2, PTHLH, TGFB2, TNC, SH3PXD2A, ACVR1C
4	6.667	7	25	GFPT2, PLAUR, SPARC, CHSY1, CD55, PLAU, PAPPA
5	6.043	47	147	DNMT1, CDKN3, GLO1, YWHAH, ATP6AP1, SS1B, AKAP8, UHX1, DUSP4, CCNG2, HOMER1, RHOB, DSP, RIT1, TGFB1, VGLL4, PANK3, IL24, PAQR3, USP15, MAPK3, NFYA, CLDND1, POLR3E, LRRC8B, MFSD6, GRB10, SLC7A2, KDELC1, PLEKHM1, PRRC2B, ZFAND6, OLFML, FZD10, FAM135A, HS6ST1, SPOPL, TMEM150A, SPRY4, MICALCL, NTSDC2, C4orf32, ZNF92, SHISA2, C7orf41, ZNF518B, SFT2D3
6	5.333	22	60	TOP1, CEP170, MARCKSL1, TLN1, MED15, PTBP3, EGR3, ATP1B1, IL6ST, ALCAM, TMEM115, HIPK3, IQSEC1, PHLDA1, ARG2, RTF1, PTPN21, CPNE2, TMEM87B, ARHGAP31, SETD7, CACHD1

DOWN-REGULATED GENES

Cluster	Score (Density*#Nodes)	Nodes	Edges	Node IDs
1	31.097	32	551	IFIH, BST2, IRF9, STAT1, HERC6, IFI35, MX2, OAS3, USP18, IRF7, EIF2AK2, XAF1, IFIT5, OAS1, IFI44, ISG15, MX1, RSAD2, IFI44L, TRIM22, RARRES3, IFIT3, OASL, TRANK1, IFIT1, OAS2, APOL3, IFIT2, DDX60, HERC5, RTP4, GBP4

Figure 7-4. MCODE clusters. In addition to a network analysis, we also performed an MCODE clustering algorithm (Bader and Hogue, 2003) **which detected a total of 8 and 4 clusters in the up-regulated and down-regulated DEG networks. Using a cut off of clusters containing >10 nodes and a minimum MCODE score of 5.0, only 6 in the former and 1 clusters in the latter were selected and these are displayed**

Appendix D

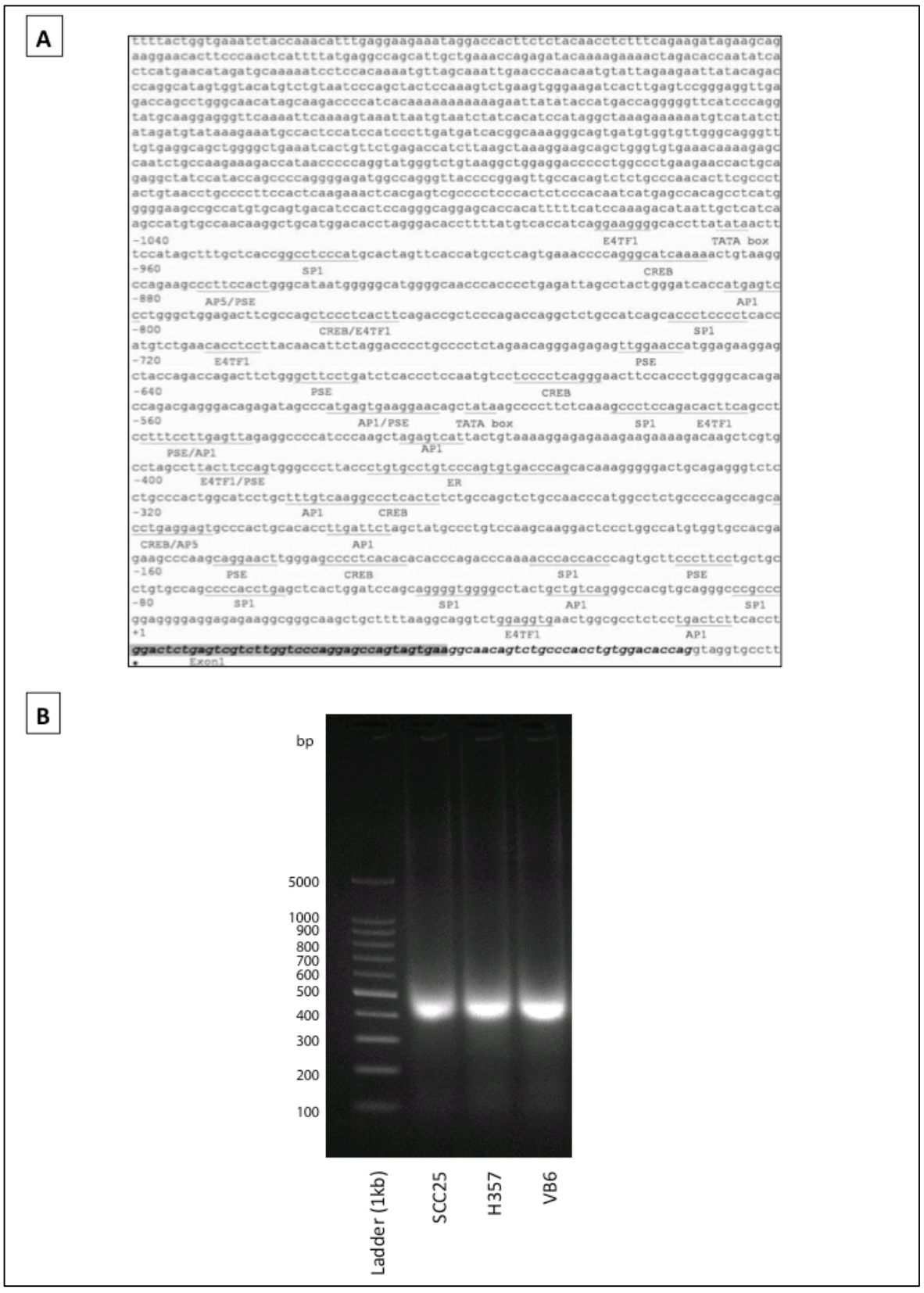

Figure 7-5. Pre-ChIP optimisation. A, DNA sequence of the 5' end of the human CTEN promoter, reproduced from Chen et al (2013). A 2-kb sequence upstream of exon 1 as indicated is shown. About 2-kb human genomic sequence 5' upstream of CTEN

exon 1 (bold italic) is listed. Sequential overlapping sequences were utilised for PCR primer design (Chen et al., 2013). B, chromatin was prepared using the MAGnify system according to the manufacturer's protocol with a few modifications as listed in Methods section. Following focussed-ultrasonication at Intensity 3.5, microtip, 5x15 seconds on, 20 seconds off, DNA size was examined on included cell lines on a 2% agarose gel prior to snap freezing at -70°C storage. Chromatin preparation steps performed together with Ms Abbie Mead.

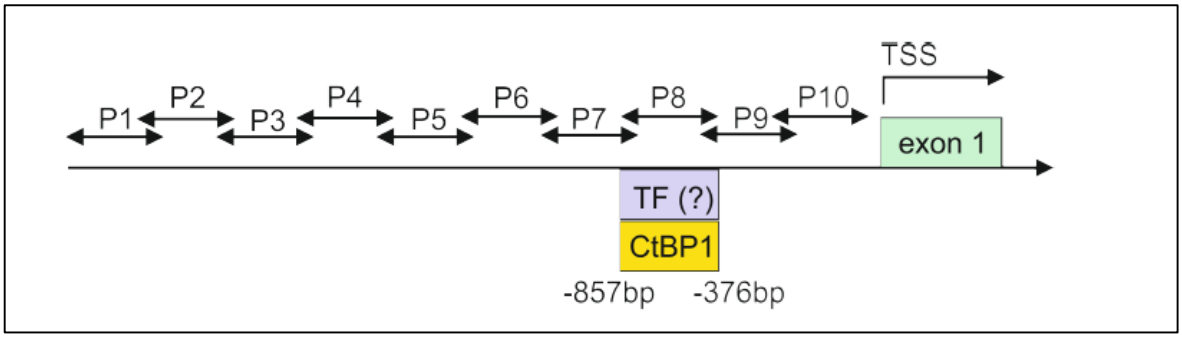

Figure 7-6. Model of CtBP interaction with TLN1 promoter, reproduced from Rucka et al, 2014.

Gene	Oligo name	Sequence (5' -> 3')
TLN1	8a Forward (8aF)	GGGAGTAGGTGTGGTCATGG
	8a Reverse (8aR)	GGTCAAGGCCTGTTCATTGG
	8b Forward (8bF)	ACCCCAACCTACCTCAGAAAG
	8b Reverse (8bR)	ATGGAGCTGGAATTGGATGC
CDH1	Forward	CCCATAACCCACCTAGACCC
	Reverse	CTGATTGGCTGAGGGTTCAC

CTEN	P1 Forward	CACACACCCAGACCCAAAAC
	P1 Reverse	CAGAGTCCAGGTGAAGAGTC
	P2 Forward	CACACCTTGATTCTAGCTATGC
	P2 Reverse	GGATCCAGTGAGCTCAGGTG
	P3 Forward	AAGAAGAAAAGACAAGCTCGTG
	P3 Reverse	ATAGCTAGAATCAAGGTGTGCA
	P4 Forward	TCTGAACACCTCCTTACAACAT
	P4 Reverse	ATAGCTGTTCCTTCACTCATGG
	P5 Forward	CTAGTTCACCATGCCTCAGT
	P5 Reverse	ATGTTGTAAGGAGGTGTTCAGA
	P6 Forward	TCCAAAGACATAATTGCTCATCA
	P6 Reverse	CTGAGGCATGGTGAACTAGT
	P7 Forward	GTGTGAAACAAAAGAGCCAATC
	P7 Reverse	CTCATGATTGTGGGAGAGTGG
	P8 Forward	ATAAAGAAATGCCACTCCATCC
	P8 Reverse	GTTATGGTCTTTGTTGGCAGAT
	P9 Forward	AAAGTCTGAAGTGGGAAGATCA
	P9 Reverse	GGATGGAGTGGCATTTGTTTAT
	P10 Forward	AGATAGAAGCAGAAGGAACACT
	P10 Reverse	TGATCTTCCCACTTCAGACTTT

Figure 7-7. Sequence details for primers used in PCR reactions. Codes in brackets represent label codes used in main thesis body figures.

Appendix E

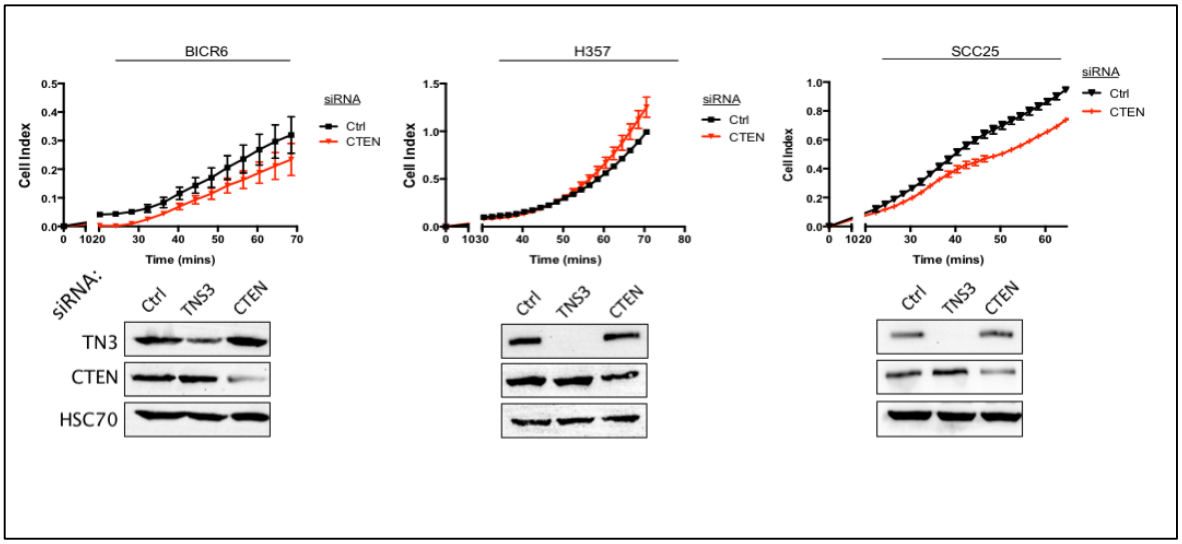

Figure 7-8. CTEN expression affects cell adhesion in a cell line dependent manner. Adhesion assays performed on XCELLigence Real Time Cell Analyser using wells coated with either latency associated peptide (LAP; 0.5µg/ml), or bovine serum albumin (BSA; 0.1%) as a control to monitor non-specific adhesion (data not shown) and the experiment continued until this control showed an adhesive response. No significant alteration in adhesion was observed across all cell lines.

Appendix F

Mycoplasma PCR protocol

PCR

Reaction detects Mycoplasma by amplification of 16S-23S spacer regions in rRNA operons. Sequences below are common to 14 different species of Mycoplasma; primers purchased from Sigma.

Fwd1	ACT CCT ACG GGA GGC AGC AGT A
Fwd2	CTT AAA GGA ATT GAC GGG AAC CCG
Rev	TGC ACC ATC TGT CAC TCT GTT AAC CTC

1st Round – Band at 720bp

Sample DNA/Supernatant (1μl)	1μl
Forward Primer 1 (100pmol/μl)	1μl
Reverse Primer (100pmol/μl)	1μl
Formamide	0.3μl
Master Mix*	Make up to 20μl (16.7μl)

Mega Mix-Blue; #2MMB-5; Microzone Limited

Cycling Conditions

95°C x 30s

35 cycles: 95°C x 30s, 55°C x 30s, 72°C x 1 min, 72°C x 1 min

Make a **1% gel**, run 10μl of the PCR product at **120V** for **20 mins**.

2nd Round – Band at 145bpm

1st Round PCR Product	1μl
Forward Primer 2 (100pmol/μl)	1μl
Reverse Primer (100pmol/μl)	1 μl
Master Mix	17μl

Same cycling conditions as above

Make a **1% gel**, run 10μl of the PCR product at **120V** for **20 mins**.

Bibliography

Abe, M., Harpel, J.G., Metz, C.N., Nunes, I., Loskutoff, D.J., Rifkin, D.B., 1994. An assay for transforming growth factor-beta using cells transfected with a plasminogen activator inhibitor-1 promoter-luciferase construct. Anal. Biochem. 216, 276–284.

Al-Ghamdi, S., Albasri, A., Cachat, J., Ibrahem, S., Muhammad, B.A., Jackson, D., Nateri, A.S., Kindle, K.B., Ilyas, M., 2011. Cten Is Targeted by Kras Signalling to Regulate Cell Motility in the Colon and Pancreas. PLoS One 6, 8.

Al-Ghamdi, S., Cachat, J., Albasri, A., Ahmed, M., Jackson, D., Zaitoun, A., Guppy, N., Otto, W.R., Alison, M.R., Kindle, K.B., Ilyas, M., 2013. C-terminal tensin-like gene functions as an oncogene and promotes cell motility in pancreatic cancer. Pancreas 42, 135–40.

Albasri, A., Aleskandarany, M., Benhasouna, A., Powe, D.G., Ellis, I.O., Ilyas, M., Green, A.R., 2011a. CTEN (C-terminal tensin-like), a novel oncogene overexpressed in invasive breast carcinoma of poor prognosis. Breast Cancer Res. Treat. 126, 47–54.

Albasri, A., Seth, R., Jackson, D., Benhasouna, A., Crook, S., Nateri, S., Chapman, R., Ilyas, M., 2009. C-terminal Tensin-like (CTEN) is an oncogene which alters cell motility possibly through repression of E-cadherin in colorectal cancer 57–65.

Albasri, A., Al-Ghamdi, S., Fadhil, W., Aleskandarany, M., Liao, Y.-C., Jackson, D., Lobo, D.N., Lo, S.H., Kumari, R., Durrant, L., Watson, S., Kindle, K.B., Ilyas, M., 2011b. Cten signals through integrin-linked kinase (ILK) and may promote metastasis in colorectal cancer. Oncogene 30, 2997–3002.

Aledo, J.C., Segura, J.A., Medina, M.A., Alonso, F.J., Núñez de Castro, I., Márquez, J., 1994. Phosphate-activated glutaminase expression during tumor development. FEBS Lett. 341, 39–42.

Alexandrova, A.Y., Arnold, K., Schaub, S., Vasiliev, J.M., Meister, J.J., Bershadsky, A.D., Verkhovsky, A.B., 2008. Comparative dynamics of retrograde actin flow and focal adhesions: Formation of nascent adhesions triggers transition from fast to slow flow. PLoS One 3.

Allal, A.S., 2002. Standardized Uptake Value of 2-[18F] Fluoro-2-Deoxy-D-Glucose in Predicting Outcome in Head and Neck Carcinomas Treated by Radiotherapy With or

Without Chemotherapy. J. Clin. Oncol. 20, 1398–1404.

Anders, S., Huber, W., 2010. Differential expression analysis for sequence count data. Genome Biol. 11, R106.

Anders, S., Pyl, P.T., Huber, W., 2014. HTSeq - A Python framework to work with high-throughput sequencing data. Bioinformatics 31, 166–9.

Ang, K.K., Harris, J., Wheeler, R., Weber, R., Rosenthal, D.I., Nguyen-Tân, P.F., Westra, W.H., Chung, C.H., Jordan, R.C., Lu, C., Kim, H., Axelrod, R., Silverman, C.C., Redmond, K.P., Gillison, M.L., 2010. Human papillomavirus and survival of patients with oropharyngeal cancer. N. Engl. J. Med. 363, 24–35.

Annes, J.P., Munger, J.S., Rifkin, D.B., 2003. Making sense of latent TGFbeta activation. J. Cell Sci. 116, 217–24.

Annes, J.P., Rifkin, D.B., Munger, J.S., 2002. The integrin alphaVbeta6 binds and activates latent TGFbeta3. FEBS Lett. 511, 65–68.

Arihiro, K., Kaneko, M., Fujii, S., Inai, K., Yokosaki, Y., 2000. Significance of alpha 9 beta 1 and alpha v beta 6 integrin expression in breast carcinoma. Breast cancer 7, 19–26.

Auger, K.R., Songyang, Z., Lo, S.H., Roberts, T.M., Chen, L.B., 1996. Platelet-derived growth factor-induced formation of tensin and phosphoinositide 3-kinase complexes. J. Biol. Chem. 271, 23452–23457.

Bacac, M., Stamenkovic, I., 2008. Metastatic cancer cell. Annu. Rev. Pathol. 3, 221–47.

Bader, G.D., Hogue, C.W. V, 2003. An automated method for finding molecular complexes in large protein interaction networks. BMC Bioinformatics 4, 2.

Bakker, B.M., Overkamp, K.M., Van Maris, A.J.A., Kötter, P., Luttik, M.A.H., Van Dijken, J.P., Pronk, J.T., 2001. Stoichiometry and compartmentation of NADH metabolism in Saccharomyces cerevisiae, in: FEMS Microbiology Reviews. pp. 15–37.

Ballestrem, C., Hinz, B., Imhof, B.A., Wehrle-Haller, B., 2001. Marching at the front and dragging behind: Differential αVβ3-integrin turnover regulates focal adhesion behavior. J. Cell Biol. 155, 1319–1332.

Barbacid, M., 1987. ras genes. Annu. Rev. Biochem. 56, 779–827.

Barbieri, I., Pensa, S., Pannellini, T., Quaglino, E., Maritano, D., Demaria, M., Voster, A., Turkson, J., Cavallo, F., Watson, C.J., Provero, P., Musiani, P., Poli, V., 2010. Constitutively active Stat3 enhances neu-mediated migration and metastasis in mammary tumors via upregulation of Cten. Cancer Res. 70, 2558–2567.

Baschnagel, A.M., Wobb, J.L., Dilworth, J.T., Williams, L., Eskandari, M., Wu, D., Pruetz,

B.L., Wilson, G.D., 2015. The association of (18)F-FDG PET and glucose metabolism biomarkers GLUT1 and HK2 in p16 positive and negative head and neck squamous cell carcinomas. Radiother. Oncol. 117, 118–24.

Batlle, E., Sancho, E., Francí, C., Domínguez, D., Monfar, M., Baulida, J., García De Herreros, A., 2000. The transcription factor snail is a repressor of E-cadherin gene expression in epithelial tumour cells. Nat. Cell Biol. 2, 84–89.

Batlle, R., Alba-Castellón, L., Loubat-Casanovas, J., Armenteros, E., Francí, C., Stanisavljevic, J., Banderas, R., Martin-Caballero, J., Bonilla, F., Baulida, J., Casal, J.I., Gridley, T., de Herreros, a G., 2012. Snail1 controls TGF-β responsiveness and differentiation of mesenchymal stem cells. Oncogene 1–9.

Bauer, J.A., Trask, D.K., Kumar, B., Los, G., Castro, J., Lee, J.S.-J., Chen, J., Wang, S., Bradford, C.R., Carey, T.E., 2005. Reversal of cisplatin resistance with a BH3 mimetic, (-)-gossypol, in head and neck cancer cells: role of wild-type p53 and Bcl-xL. Mol. Cancer Ther. 4, 1096–104.

Bauer, K., Mierke, C., Behrens, J., 2007. Expression profiling reveals genes associated with transendothelial migration of tumor cells: a functional role for alphavbeta3 integrin. Int. J. Cancer 121, 1910–8.

Baum, O., Hlushchuk, R., Forster, A., Greiner, R., Clézardin, P., Zhao, Y., Djonov, V., Gruber, G., 2007. Increased invasive potential and up-regulation of MMP-2 in MDA-MB-231 breast cancer cells expressing the beta3 integrin subunit. Int. J. Oncol. 30, 325–32.

Baysal, B.E., Ferrell, R.E., Willett-Brozick, J.E., Lawrence, E.C., Myssiorek, D., Bosch, A., van der Mey, A., Taschner, P.E., Rubinstein, W.S., Myers, E.N., Richard, C.W., Cornelisse, C.J., Devilee, P., Devlin, B., 2000. Mutations in SDHD, a mitochondrial complex II gene, in hereditary paraganglioma. Science 287, 848–51.

Bensaad, K., Cheung, E.C., Vousden, K.H., 2009. Modulation of intracellular ROS levels by TIGAR controls autophagy. EMBO J. 28, 3015–26.

Bensaad, K., Tsuruta, A., Selak, M.A., Vidal, M.N.C., Nakano, K., Bartrons, R., Gottlieb, E., Vousden, K.H., 2006. TIGAR, a p53-inducible regulator of glycolysis and apoptosis. Cell 126, 107–20.

Bergman, L.M., Blaydes, J.P., 2006. C-terminal binding proteins: Emerging roles in cell survival and tumorigenesis. Apoptosis an Int. J. Program. cell death 11, 879–888.

Birts, C.N., Nijjar, S.K., Mardle, C. a., Hoakwie, F., Duriez, P.J., Blaydes, J.P., Tavassoli, A.,

2013. A cyclic peptide inhibitor of C-terminal binding protein dimerization links metabolism with mitotic fidelity in breast cancer cells. Chem. Sci. 4.

Blobe, G.C., Schiemann, W.P., Lodish, H.F., 2000. Role of transforming growth factor beta in human disease. N. Engl. J. Med. 342, 1350–1358.

Bola, B.M., Chadwick, A.L., Michopoulos, F., Blount, K.G., Telfer, B.A., Williams, K.J., Smith, P.D., Critchlow, S.E., Stratford, I.J., 2014. Inhibition of monocarboxylate transporter-1 (MCT1) by AZD3965 enhances radiosensitivity by reducing lactate transport. Mol. Cancer Ther. 13, 2805–16.

Bova, R., McGuinness, J., 2007. Hoarseness: A guide to voice disorders. Med. Today 8, 38–45.

Bova, R.J., Quinn, D.I., Nankervis, J.S., Cole, I.E., Sheridan, B.F., Jensen, M.J., Morgan, G.J., Hughes, C.J., Sutherland, R.L., 1999. Cyclin D1 and p16INK4A expression predict reduced survival in carcinoma of the anterior tongue. Clin. Cancer Res. 5, 2810–9.

Boyd, J.M., Subramanian, T., Schaeper, U., La Regina, M., Bayley, S., Chinnadurai, G., 1993. A region in the C-terminus of adenovirus 2/5 E1a protein is required for association with a cellular phosphoprotein and important for the negative modulation of T24-ras mediated transformation, tumorigenesis and metastasis. EMBO J. 12, 469–78.

Breuss, J.M., Gallo, J., DeLisser, H.M., Klimanskaya, I. V, Folkesson, H.G., Pittet, J.F., Nishimura, S.L., Aldape, K., Landers, D. V, Carpenter, W., 1995. Expression of the beta 6 integrin subunit in development, neoplasia and tissue repair suggests a role in epithelial remodeling. J. Cell Sci. 108(6), 2241–2251.

Brizel, D.M., Schroeder, T., Scher, R.L., Walenta, S., Clough, R.W., Dewhirst, M.W., Mueller-Klieser, W., 2001. Elevated tumor lactate concentrations predict for an increased risk of metastases in head-and-neck cancer. Int. J. Radiat. Oncol. Biol. Phys. 51, 349–53.

Brockstein, B., Haraf, D.J., Rademaker, A.W., Kies, M.S., Stenson, K.M., Rosen, F., Mittal, B.B., Pelzer, H., Fung, B.B., Witt, M.E., Wenig, B., Portugal, L., Weichselbaum, R.W., Vokes, E.E., 2004. Patterns of failure, prognostic factors and survival in locoregionally advanced head and neck cancer treated with concomitant chemoradiotherapy: A 9-year, 337-patient, multi-institutional experience. Ann. Oncol. 15, 1179–1186.

Bröer, S., Schneider, H.P., Bröer, A., Rahman, B., Hamprecht, B., Deitmer, J.W., 1998. Characterization of the monocarboxylate transporter 1 expressed in Xenopus laevis

oocytes by changes in cytosolic pH. Biochem. J. 333(1), 167–74.

Brooks, J.T.S., Elvidge, G.P., Glenny, L., Gleadle, J.M., Liu, C., Ragoussis, J., Smith, T.G., Talbot, N.P., Winchester, L., Maxwell, P.H., Robbins, P.A., 2009. Variations within oxygen-regulated gene expression in humans. J. Appl. Physiol. 106, 212–20.

Burridge, K., Fath, K., Kelly, T., Nuckolls, G., Turner, C., 1988. Focal adhesions: transmembrane junctions between the extracellular matrix and the cytoskeleton. Annu. Rev. Cell Biol. 4, 487–525.

Burrows, N., Resch, J., Cowen, R.L., von Wasielewski, R., Hoang-Vu, C., West, C.M., Williams, K.J., Brabant, G., 2010. Expression of hypoxia-inducible factor 1 alpha in thyroid carcinomas. Endocr. Relat. Cancer 17, 61–72.

Cadoni, G., Boccia, S., Petrelli, L., Di Giannantonio, P., Arzani, D., Giorgio, a, De Feo, E., Pandolfini, M., Gallì, P., Paludetti, G., Ricciardi, G., 2012. A review of genetic epidemiology of head and neck cancer related to polymorphisms in metabolic genes, cell cycle control and alcohol metabolism. Acta Otorhinolaryngol. Ital. 32, 1–11.

Cairns, R. a, Harris, I.S., Mak, T.W., 2011. Regulation of cancer cell metabolism. Nat. Rev. Cancer 11, 85–95.

Calderwood, D.A., Fujioka, Y., De Pereda, J.M., Garcia-Alvarez, B., Nakamoto, T., Margolis, B., McGlade, C.J., Liddington, R.C., Ginsberg, M.H., 2003. Integrin beta cytoplasmic domain interactions with phosphotyrosine-binding domains: a structural prototype for diversity in integrin signaling. Proc Natl Acad Sci USA 100, 2272–2277.

Calderwood, D.A., Zent, R., Grant, R., Rees, D.J., Hynes, R.O., Ginsberg, M.H., 1999. The Talin head domain binds to integrin beta subunit cytoplasmic tails and regulates integrin activation. J. Biol. Chem. 274, 28071–4.

Campbell, I.D., Humphries, M.J., 2011. Integrin structure, activation, and interactions. Cold Spring Harb. Perspect. Biol. 1;3(3)

Caneba, C. a, Bellance, N., Yang, L., Pabst, L., Nagrath, D., 2012. Pyruvate uptake is increased in highly invasive ovarian cancer cells under anoikis conditions for anaplerosis, mitochondrial function, and migration. Am. J. Physiol. Endocrinol. Metab. 303, E1036-52.

Cao, X., Voss, C., Zhao, B., Kaneko, T., Li, S.S.-C., 2012. Differential regulation of the activity of deleted in liver cancer 1 (DLC1) by tensins controls cell migration and transformation. Proc. Natl. Acad. Sci. U. S. A. 109, 1455–60.

Cardesa, A., Nadal, A., 2011. Carcinoma of the head and neck in the HPV era. Acta

Dermatovenerol. Alp. Panonica. Adriat. 20, 161–73.

Castellano, E., Downward, J., 2011. RAS Interaction with PI3K: More Than Just Another Effector Pathway. Genes Cancer 2, 261–74.

Chan, L.-K., Chiu, Y.-T., Sze, K.M.-F., Ng, I.O.-L., 2015. Tensin4 is up-regulated by EGF-induced ERK1/2 activity and promotes cell proliferation and migration in hepatocellular carcinoma. Oncotarget 6, 20964–76.

Chan, L.-K., Ko, F.C.F., Ng, I.O.-L., Yam, J.W.P., 2009. Deleted in liver cancer 1 (DLC1) utilizes a novel binding site for Tensin2 PTB domain interaction and is required for tumor-suppressive function. PLoS One 4, e5572.

Chen, H., Duncan, I.C., Bozorgchami, H., Lo, S.H., 2002. Tensin1 and a previously undocumented family member, tensin2, positively regulate cell migration. Proc. Natl. Acad. Sci. U. S. A. 99, 733–738.

Chen, H., Ishii, A., Wong, W.K., Chen, L.B., Lo, S.H., 2000. Molecular characterization of human tensin. Biochem. J. 351 Pt 2, 403–411.

Chen, H., Lo, S.H., 2003. and Src homology domain 2 1045, 1039–1045.

Chen, H., Wang, L., Beretov, J., Hao, J., Xiao, W., Li, Y., 2010. Co-expression of CD147/EMMPRIN with monocarboxylate transporters and multiple drug resistance proteins is associated with epithelial ovarian cancer progression. Clin. Exp. Metastasis 27, 557–69.

Chen, J., Bardes, E.E., Aronow, B.J., Jegga, A.G., 2009. ToppGene Suite for gene list enrichment analysis and candidate gene prioritization. Nucleic Acids Res. 37, W305-11.

Chen, J.L.-Y., Lucas, J.E., Schroeder, T., Mori, S., Wu, J., Nevins, J., Dewhirst, M., West, M., Chi, J.-T., 2008. The genomic analysis of lactic acidosis and acidosis response in human cancers. PLoS Genet. 4, e1000293.

Chen, N.-T., Kuwabara, Y., Conley, C., Liao, Y.-C., Hong, S.-Y., Chen, M., Shih, Y.-P., Chen, H.-W., Hsieh, F., Lo, S.H., 2013. Phylogenetic analysis, expression patterns, and transcriptional regulation of human CTEN gene. Gene 520, 90–7.

Chen, Y.-W., Paliwal, S., Draheim, K., Grossman, S.R., Lewis, B.C., 2008. p19Arf inhibits the invasion of hepatocellular carcinoma cells by binding to C-terminal binding protein. Cancer Res. 68, 476–482.

Chen, Y., Satoh, T., Sasatomi, E., Miyazaki, K., Tokunaga, O., 2001. Critical role of type IV collagens in the growth of bile duct carcinoma. In vivo and in vitro studies. Pathol.

Res. Pract. 197, 585–96.

Chiang, M.-K., Liao, Y.-C., Kuwabara, Y., Lo, S.H., 2005. Inactivation of tensin3 in mice results in growth retardation and postnatal lethality. Dev. Biol. 279, 368–77.

Chinnadurai, G., 2009. The transcriptional corepressor CtBP: a foe of multiple tumor suppressors. Cancer Res. 69, 731–4.

Chinnadurai, G., 2003. CtBP family proteins: more than transcriptional corepressors. Bioessays 25, 9–12.

Chinnadurai, G., 2002. CtBP, an Unconventional Transcriptional Corepressor in Development and Oncogenesis. Mol. Cell 9, 213–224.

Chinnadurai, G., Lania, L., Majello, B., De Luca, P., 2007. Transcriptional regulation by C-terminal binding proteins. Int. J. Biochem. Cell Biol. 39, 1593–607.

Chipuk, J.E., Bhat, M., Hsing, A.Y., Ma, J., Danielpour, D., 2001. Bcl-xL Blocks Transforming Growth Factor-β1-induced Apoptosis by Inhibiting Cytochrome c Release and not by Directly Antagonizing Apaf-1-dependent Caspase Activation in Prostate Epithelial Cells. J. Biol. Chem. 276, 26614–26621.

Cho, A.-R., Uchio-Yamada, K., Torigai, T., Miyamoto, T., Miyoshi, I., Matsuda, J., Kurosawa, T., Kon, Y., Asano, A., Sasaki, N., Agui, T., 2006. Deficiency of the tensin2 gene in the ICGN mouse: an animal model for congenital nephrotic syndrome. Mamm. genome Off. J. Int. Mamm. Genome Soc. 17, 407–416.

Christofk, H.R., Vander Heiden, M.G., Harris, M.H., Ramanathan, A., Gerszten, R.E., Wei, R., Fleming, M.D., Schreiber, S.L., Cantley, L.C., 2008. The M2 splice isoform of pyruvate kinase is important for cancer metabolism and tumour growth. Nature 452, 230–3.

Chung, C.H., Zhang, Q., Kong, C.S., Harris, J., Fertig, E.J., Harari, P.M., Wang, D., Redmond, K.P., Shenouda, G., Trotti, A., Raben, D., Gillison, M.L., Jordan, R.C., Le, Q.-T., 2014. p16 protein expression and human papillomavirus status as prognostic biomarkers of nonoropharyngeal head and neck squamous cell carcinoma. J. Clin. Oncol. 32, 3930–8.

Chung, Y.L., Nagy, E., Zietkowski, D., Payne, G.S., Phillips, D.H., DeSouza, N.M., 2013. Molecular and metabolic consequences following E6 transfection in an isogenic ovarian cell line (A2780) pair. Cell. Physiol. Biochem. 32, 1460–1472.

Clainche, C.L.E., Carlier, M., 2008. Regulation of Actin Assembly Associated With Protrusion and Adhesion in Cell Migration 489–513.

Clark, J., Jeffery, C.C., Zhang, H., Cooper, T., O'Connell, D.A., Harris, J., Seikaly, H., Biron, V.L., 2015. Correlation of PET-CT nodal SUVmax with p16 positivity in oropharyngeal squamous cell carcinoma. J. Otolaryngol. Head Neck Surg. 44, 37.

Clark, R.A., Ashcroft, G.S., Spencer, M.J., Larjava, H., Ferguson, M.W., 1996. Re-epithelialization of normal human excisional wounds is associated with a switch from alpha v beta 5 to alpha v beta 6 integrins. Br. J. Dermatol. 135, 46–51.

Condeelis, J., Singer, R.H., Segall, J.E., 2005. The great escape: when cancer cells hijack the genes for chemotaxis and motility. Annu. Rev. Cell Dev. Biol. 21, 695–718.

Coughlan, L., Vallath, S., Saha, A., Flak, M., McNeish, I.A., Vassaux, G., Marshall, J.F., Hart, I.R., Thomas, G.J., 2009. In vivo retargeting of adenovirus type 5 to alphavbeta6 integrin results in reduced hepatotoxicity and improved tumor uptake following systemic delivery. J. Virol. 83, 6416–6428.

Cox, E.A., Huttenlocher, A., 1998. Regulation of Integrin-Mediated Adhesion During Cell Migration 419, 412–419.

Critchley, D.R., 2000. Focal adhesions - the cytoskeletal connection. Curr. Opin. Cell Biol. 12, 133–9.

Croft, D., Mundo, A.F., Haw, R., Milacic, M., Weiser, J., Wu, G., Caudy, M., Garapati, P., Gillespie, M., Kamdar, M.R., Jassal, B., Jupe, S., Matthews, L., May, B., Palatnik, S., Rothfels, K., Shamovsky, V., Song, H., Williams, M., Birney, E., Hermjakob, H., Stein, L., D'Eustachio, P., 2014. The Reactome pathway knowledgebase. Nucleic Acids Res. 42, D472-7.

Curry, J.M., Sprandio, J., Cognetti, D., Luginbuhl, A., Bar-ad, V., Pribitkin, E., Tuluc, M., 2014a. Tumor Microenvironment in Head and Neck Squamous Cell Carcinoma. Semin. Oncol. 41, 217–234.

Curry, J.M., Tuluc, M., Whitaker-Menezes, D., Ames, J.A., Anantharaman, A., Butera, A., Leiby, B., Cognetti, D.M., Sotgia, F., Lisanti, M.P., Martinez-Outschoorn, U.E., 2013. Cancer metabolism, stemness and tumor recurrence: MCT1 and MCT4 are functional biomarkers of metabolic symbiosis in head and neck cancer. Cell Cycle 12, 1371–84.

D'Alessandro, A., Zolla, L., 2012. Metabolomics and cancer drug discovery: let the cells do the talking. Drug Discov. Today 17, 3–9.

Danen, E.H., Ten Berge, P.J., Van Muijen, G.N., Van 't Hof-Grootenboer, A.E., Bröcker, E.B., Ruiter, D.J., 1994. Emergence of α5β1 fibronectin- and αvβ3 vitronectin-receptor expression in melanocytic tumour progression. Histopathology 24, 249–56.

Davison, J.M., Ozonoff, A., Imsande, H.M., Grillone, G.A., Subramaniam, R.M., 2010. Squamous cell carcinoma of the palatine tonsils: FDG standardized uptake value ratio as a biomarker to differentiate tonsillar carcinoma from physiologic uptake. Radiology 255, 578–85.

De Wever, O., Demetter, P., Mareel, M., Bracke, M., 2008. Stromal myofibroblasts are drivers of invasive cancer growth. Int. J. Cancer 123, 2229–38.

DeBerardinis, R.J., Cheng, T., 2010. Q's next: the diverse functions of glutamine in metabolism, cell biology and cancer. Oncogene 29, 313–324.

DeBerardinis, R.J., Mancuso, A., Daikhin, E., Nissim, I., Yudkoff, M., Wehrli, S., Thompson, C.B., 2007. Beyond aerobic glycolysis: transformed cells can engage in glutamine metabolism that exceeds the requirement for protein and nucleotide synthesis. Proc. Natl. Acad. Sci. U. S. A. 104, 19345–50.

Dell' Antone, P., 2012. Energy metabolism in cancer cells: how to explain the Warburg and Crabtree effects? Med. Hypotheses 79, 388–92.

Demeure, M.J., Damsky, C.H., Elfman, F., Goretzki, P.E., Wong, M.G., Clark, O.H.,. Invasion by cultured human follicular thyroid cancer correlates with increased beta 1 integrins and production of proteases. World J. Surg. 16, 770–6.

Deng, Y., Deng, H., Liu, J., Han, G., Malkoski, S., Liu, B., Zhao, R., Wang, X.-J., Zhang, Q., 2012. Transcriptional down-regulation of Brca1 and E-cadherin by CtBP1 in breast cancer. Mol. Carcinog. 51, 500–7.

Deng, Y., Liu, J., Han, G., Lu, S.-L., Wang, S.-Y., Malkoski, S., Tan, A.C., Deng, C., Wang, X.-J., Zhang, Q., 2010. Redox-dependent Brca1 transcriptional regulation by an NADH-sensor CtBP1. Oncogene 29, 6603–8.

Denko, N.C., 2008. Hypoxia, HIF1 and glucose metabolism in the solid tumour. Nat. Rev. Cancer 8, 705–713.

Deprez, J., Vertommen, D., Alessi, D.R., Hue, L., Rider, M.H., 1997. Phosphorylation and activation of heart 6-phosphofructo-2-kinase by protein kinase B and other protein kinases of the insulin signaling cascades. J. Biol. Chem. 272, 17269–75.

Desgrosellier, J.S., Cheresh, D.A., 2010. Integrins in cancer: biological implications and therapeutic opportunities. Nat. Rev. Cancer 10, 9–22.

Dewey, W., Ling, C., Mayn, R., 1995. Radiation-induced apoptosis: relevance to radiotherapy. Int. J. Radiat. Oncol. Biol. Phys. 33, 781–796.

Dhani, N., Lohse, I., Foltz, W., Cao, P.-J., Hedley, D.W., 2014. Estimating tumour volume in

a primary orthotopic mouse model of human pancreatic cancer using rapid acquisition magnetic resonance imaging | Journal - Annals of Cancer Research. Ann. Cancer Res. 1, Retrieved from http://www.vipoa.org/cancer.

Di, L.-J., Byun, J.S., Wong, M.M., Wakano, C., Taylor, T., Bilke, S., Baek, S., Hunter, K., Yang, H., Lee, M., Zvosec, C., Khramtsova, G., Cheng, F., Perou, C.M., Miller, C.R., Raab, R., Olopade, O.I., Gardner, K., 2013. Genome-wide profiles of CtBP link metabolism with genome stability and epithelial reprogramming in breast cancer. Nat. Commun. 4, 1449.

Di, L., Fernandez, A., Siervi, A. De, 2010. Transcriptional regulation of BRCA1 expression by a metabolic switch. Nat. Struct. Mol. Biol. 17, 1406–1413.

Dickens, P., Srivastava, G., Loke, S.L., Larkin, S., 1991. Human papillomavirus 6, 11, and 16 in laryngeal papillomas. J. Pathol. 165, 243–6.

Dier, U., Shin, D.-H., Hemachandra, L.P.M.P., Uusitalo, L.M., Hempel, N., 2014. Bioenergetic analysis of ovarian cancer cell lines: profiling of histological subtypes and identification of a mitochondria-defective cell line. PLoS One 9, e98479.

Dimmer, K.S., Friedrich, B., Lang, F., Deitmer, J.W., Bröer, S., 2000. The low-affinity monocarboxylate transporter MCT4 is adapted to the export of lactate in highly glycolytic cells. Biochem. J. 350(1), 219–27.

Doherty, J.R., Cleveland, J.L., 2013. Targeting lactate metabolism for cancer therapeutics. J. Clin. Invest. 123, 3685–92.

Doherty, J.R., Yang, C., Scott, K.E.N., Cameron, M.D., Fallahi, M., Li, W., Hall, M.A., Amelio, A.L., Mishra, J.K., Li, F., Tortosa, M., Genau, H.M., Rounbehler, R.J., Lu, Y., Dang, C. V, Kumar, K.G., Butler, A.A., Bannister, T.D., Hooper, A.T., Unsal-Kacmaz, K., Roush, W.R., Cleveland, J.L., 2014. Blocking lactate export by inhibiting the Myc target MCT1 Disables glycolysis and glutathione synthesis. Cancer Res. 74, 908–20.

Dröge, W., Eck, H.-P., Betzler, M., Nä her, H., 1987. Elevated plasma glutamate levels in colorectal carcinoma patients and in patients with acquired immunodeficiency syndrome (AIDS). Immunobiology 174, 473–479.

Duray, A., Lacremans, D., Demoulin, S., Delvenne, P., Saussez, S., 2014. Prognosis of HPV-positive head and neck cancers: implication of smoking and immunosuppression. Adv. Cell. Mol. Otolaryngol. 2.

Durkin, M.E., Yuan, B.-Z., Zhou, X., Zimonjic, D.B., Lowy, D.R., Thorgeirsson, S.S., Popescu, N.C., 2007. DLC-1:a Rho GTPase-activating protein and tumour suppressor. J. Cell.

Mol. Med. 11, 1185–1207.

Edington, K.G., Loughran, O.P., Berry, I.J., Parkinson, E.K., 1995. Cellular immortality: a late event in the progression of human squamous cell carcinoma of the head and neck associated with p53 alteration and a high frequency of allele loss. Mol. Carcinog. 13, 254–65.

Eigenbrodt, E., Kallinowski, F., Ott, M., Mazurek, S., Vaupel, P.,. Pyruvate kinase and the interaction of amino acid and carbohydrate metabolism in solid tumors. Anticancer Res. 18, 3267–74.

Elayadi, A.N., Samli, K.N., Prudkin, L., Liu, Y.H., Bian, A., Xie, X.J., Wistuba, I.I., Roth, J.A., McGujire, M.J., Brown, K.C., 2007. A peptide selected by biopanning identifies the integrin αvβ6 as a prognostic biomarker for nonsmall cell lung cancer. Cancer Res. 67, 5889–5895.

Eyden, B., 2005. The myofibroblast: a study of normal, reactive and neoplastic tissues, with an emphasis on ultrastructure. Part 1--normal and reactive cells. J. Submicrosc. Cytol. Pathol. 37, 109–204.

Fakhry, C., Westra, W.H., Li, S., Cmelak, A., Ridge, J.A., Pinto, H., Forastiere, A., Gillison, M.L., 2008. Improved survival of patients with human papillomavirus-positive head and neck squamous cell carcinoma in a prospective clinical trial. J. Natl. Cancer Inst. 100, 261–9.

Fantin, V.R., St-Pierre, J., Leder, P., 2006. Attenuation of LDH-A expression uncovers a link between glycolysis, mitochondrial physiology, and tumor maintenance. Cancer Cell 9, 425–434.

Farhan, H., Wendeler, M.W., Mitrovic, S., Fava, E., Silberberg, Y., Sharan, R., Zerial, M., Hauri, H.-P., 2010. MAPK signaling to the early secretory pathway revealed by kinase/phosphatase functional screening. J. Cell Biol. 189, 997–1011.

Felding-Habermann, B., 2003. Integrin adhesion receptors in tumor metastasis. Clin. Exp. Metastasis 20, 203–13.

Felding-Habermann, B., O'Toole, T.E., Smith, J.W., Fransvea, E., Ruggeri, Z.M., Ginsberg, M.H., Hughes, P.E., Pampori, N., Shattil, S.J., Saven, A., Mueller, B.M., 2001. Integrin activation controls metastasis in human breast cancer. Proc. Natl. Acad. Sci. U. S. A. 98, 1853–8.

Ferlay, J., Soerjomataram, I., Ervik, M., Dikshit, R., Eser, S., Mathers, C., Rebelo, M., Parkin, D.M., Forman, D., Gray F. Globocan 2012 v1.0, Cancer Incidence and Mortality

Worldwide: IARC CancerBase No. 11 [Internet] Available from: http//globocan.iarc.fr, accessed on 08/2015

Fischer, K., Hoffmann, P., Voelkl, S., Meidenbauer, N., Ammer, J., Edinger, M., Gottfried, E., Schwarz, S., Rothe, G., Hoves, S., Renner, K., Timischl, B., Mackensen, A., Kunz-Schughart, L., Andreesen, R., Krause, S.W., Kreutz, M., 2007. Inhibitory effect of tumor cell-derived lactic acid on human T cells. Blood 109, 3812–9.

Fjeld, C.C., Birdsong, W.T., Goodman, R.H., 2003. Differential binding of NAD+ and NADH allows the transcriptional corepressor carboxyl-terminal binding protein to serve as a metabolic sensor. Proc. Natl. Acad. Sci. U. S. A. 100, 9202–7.

Fogh, J., Fogh, J.M., Orfeo, T., 1977. One hundred and twenty-seven cultured human tumor cell lines producing tumors in nude mice. JNCI 59, 221-226

Fox, C.J., Hammerman, P.S., Thompson, C.B., 2005. Fuel feeds function: energy metabolism and the T-cell response. Nat. Rev. Immunol. 5, 844–52.

Frederick, M.J., Myers, J.N., Agrawal, N., 2013. neck cancer 35, 454–463.

Frisch, S.M., Screaton, R.A., 2001. Anoikis mechanisms. Curr. Opin. Cell Biol. 13, 555–62.

Furusawa, T., Moribe, H., Kondoh, H., Higashi, Y., 1999. Identification of CtBP1 and CtBP2 as corepressors of zinc finger-homeodomain factor deltaEF1. Mol. Cell. Biol. 19, 8581–90.

Gaggioli, C., Hooper, S., Hidalgo-Carcedo, C., Grosse, R., Marshall, J.F., Harrington, K., Sahai, E., 2007. Fibroblast-led collective invasion of carcinoma cells with differing roles for RhoGTPases in leading and following cells. Nat. Cell Biol. 9, 1392–400.

Galbraith, C.G., Yamada, K.M., Sheetz, M.P., 2002. The relationship between force and focal complex development. J. Cell Biol. 159, 695–705.

Gao, X., Zacharek, A., Grignon, D.J., Sakr, W., Powell, I.J., Porter, A.T., Honn, K. V, 1995. Localization of potential tumor suppressor loci to a < 2 Mb region on chromosome 17q in human prostate cancer. Oncogene 11, 1241–1247.

Gatenby, R.A., Gillies, R.J., 2008. A microenvironmental model of carcinogenesis. Nat. Rev. Cancer 8, 56–61.

Gatenby, R. a, Gillies, R.J., 2004. Why do cancers have high aerobic glycolysis? Nat. Rev. Cancer 4, 891–9.

Gebäck, T., Schulz, M.M.P., Koumoutsakos, P., Detmar, M., 2009. TScratch: a novel and simple software tool for automated analysis of monolayer wound healing assays. Biotechniques 46, 265–74.

Geiger, B., Yamada, K.M., 2011. Molecular architecture and function of matrix adhesions. Cold Spring Harb. Perspect. Biol. 3, 1–21.

Giampieri, S., Manning, C., Hooper, S., Jones, L., Hill, C.S., Sahai, E., 2009. Localized and reversible TGFbeta signalling switches breast cancer cells from cohesive to single cell motility. Nat. Cell Biol. 11, 1287–96.

Gleizes, P.E., Munger, J.S., Nunes, I., Harpel, J.G., Mazzieri, R., Noguera, I., Rifkin, D.B., 1997. TGF-beta latency: biological significance and mechanisms of activation. Stem Cells 15, 190–197.

Gong, L.-B., Luo, X.-L., Liu, S.-Y., Tao, D.-D., Gong, J.-P., Hu, J.-B., 2007. [Correlations of GRIM-19 and its target gene product STAT3 to malignancy of human colorectal carcinoma]. Ai Zheng 26, 683–7.

Gottfried, E., Kreutz, M., Mackensen, A., 2012. Tumor metabolism as modulator of immune response and tumor progression. Semin. Cancer Biol. 22, 335–41.

Gottlob, K., Majewski, N., Kennedy, S., Kandel, E., Robey, R.B., Hay, N., 2001. Inhibition of early apoptotic events by Akt/PKB is dependent on the first committed step of glycolysis and mitochondrial hexokinase. Genes Dev. 15, 1406–18.

Grooteclaes, M., Deveraux, Q., Hildebrand, J., Zhang, Q., Goodman, R.H., Frisch, S.M., 2003. C-terminal-binding protein corepresses epithelial and proapoptotic gene expression programs. Proc. Natl. Acad. Sci. U. S. A. 100, 4568–4573.

Grooteclaes, M.L., Frisch, S.M., 2000. Evidence for a function of CtBP in epithelial gene regulation and anoikis. Oncogene 19, 3823–8.

Grünert, S., Jechlinger, M., Beug, H., 2003. Diverse cellular and molecular mechanisms contribute to epithelial plasticity and metastasis. Nat. Rev. Mol. Cell Biol. 4, 657–665.

Guan, C., Shi, H., Wang, H., Zhang, J., Ni, W., Chen, B., Hou, S., Yang, X., Shen, A., Ni, R., 2013. CtBP2 contributes to malignant development of human esophageal squamous cell carcinoma by regulation of p16INK4A. J. Cell. Biochem. 114, 1343–54.

Guzmán, C., Bagga, M., Kaur, A., Westermarck, J., Abankwa, D., 2014. ColonyArea: an ImageJ plugin to automatically quantify colony formation in clonogenic assays. PLoS One 9, e92444.

Halestrap, A.P., Meredith, D., 2004. The SLC16 gene family-from monocarboxylate transporters (MCTs) to aromatic amino acid transporters and beyond. Pflugers Arch. 447, 619–628.

Halestrap, A.P., Price, N.T., 1999. The proton-linked monocarboxylate transporter (MCT)

family: structure, function and regulation. Biochem. J. 343 Pt 2, 281–99.

Halestrap, A.P., Wilson, M.C., 2012. Critical Review The Monocarboxylate Transporter Family — Role and Regulation 64, 109–119.

Hamidi, S., Salo, T., Kainulainen, T., Epstein, J., Lerner, K., Larjava, H., 2000. Expression of alpha(v)beta6 integrin in oral leukoplakia. Br. J. Cancer 82, 1433–1440.

Hammarstedt, L., Lindquist, D., Dahlstrand, H., Romanitan, M., Dahlgren, L.O., Joneberg, J., Creson, N., Lindholm, J., Ye, W., Dalianis, T., Munck-Wikland, E., 2006. Human papillomavirus as a risk factor for the increase in incidence of tonsillar cancer. Int. J. Cancer 119, 2620–3.

Hanahan, D., Weinberg, R.A., 2011. Hallmarks of cancer: the next generation. Cell 144, 646–674.

Hanahan, D., Weinberg, R.A., 2000. The Hallmarks of Cancer. Cell 100, 57–70.

Hazelbag, S., Kenter, G.G., Gorter, A., Dreef, E.J., Koopman, L.A., Violette, S.M., Weinreb, P.H., Fleuren, G.J., 2007. Overexpression of the alpha v beta 6 integrin in cervical squamous cell carcinoma is a prognostic factor for decreased survival. J. Pathol. 212, 316–324.

Hazelbag, S., Kenter, G.G., Gorter, A., Fleuren, G.J., 2004. Prognostic relevance of TGF-beta1 and PAI-1 in cervical cancer. Int. J. Cancer 112, 1020–1028.

Heiden, M. Vander, 2009. Understanding the Warburg Effect: The Metabolic Requirements of Cell Proliferation. Science 324, 1029–1033.

Heldin, N.E., Westermark, B., 1991. The molecular biology of the human anaplastic thyroid carcinoma cell. Thyroidology 3, 127–31.

Hewitt, C., Wilson, P., McGlinn, E., MacFarlane, G., Papageorgiou, A., Woodwards, R.T.M., Sloan, P., Gollin, S.M., Paterson, I., Parkinson, K.K., Read, A.P., Thakker, N., 2004. DLC1 is unlikely to be a primary target for deletions on chromosome arm 8p22 in head and neck squamous cell carcinoma. Cancer Lett. 209, 207–13.

Hildebrand, J.D., Soriano, P., 2002. Overlapping and unique roles for C-terminal binding protein 1 (CtBP1) and CtBP2 during mouse development. Mol. Cell. Biol. 22, 5296–5307.

Hong, S.-Y., Shih, Y.-P., Li, T., Carraway, K.L., Lo, S.H., 2013. CTEN prolongs signaling by EGFR through reducing its ligand-induced degradation. Cancer Res. 73, 5266–76.

Horiguchi, M., Koyanagi, S., Okamoto, A., Suzuki, S.O., Matsunaga, N., Ohdo, S., 2012. Stress-regulated transcription factor ATF4 promotes neoplastic transformation by

suppressing expression of the INK4a/ARF cell senescence factors. Cancer Res. 72, 395–401.

Hosotani, R., Kawaguchi, M., Masui, T., Koshiba, T., Ida, J., Fujimoto, K., Wada, M., Doi, R., Imamura, M., 2002. Expression of integrin alphaVbeta3 in pancreatic carcinoma: relation to MMP-2 activation and lymph node metastasis. Pancreas 25, e30-5.

Hu, D., Zhou, J., Wang, F., Shi, H., Li, Y., Li, B., 2015. HPV-16 E6/E7 promotes cell migration and invasion in cervical cancer via regulating cadherin switch in vitro and in vivo. Arch. Gynecol. Obstet. 292, 1345–54.

Huang, S., Ingber, D.E., 1999. The structural and mechanical complexity of cell-growth control. Nat. Cell Biol. 1, E131-8.

Huber, M.A., Kraut, N., Beug, H., 2005. Molecular requirements for epithelial-mesenchymal transition during tumor progression. Curr. Opin. Cell Biol. 17, 548–58.

Hughes, S.J., Nambu, Y., Soldes, O.S., Hamstra, D., Rehemtulla, A., Iannettoni, M.D., Orringer, M.B., Beer, D.G., 1997. Fas/APO-1 (CD95) is not translocated to the cell membrane in esophageal adenocarcinoma. Cancer Res. 57, 5571–8.

Huibregtse, J.M., Scheffner, M., Howley, P.M., 1993. Localization of the E6-AP regions that direct human papillomavirus E6 binding, association with p53, and ubiquitination of associated proteins. Mol. Cell. Biol. 13, 4918–27.

Hung, S.-Y., Shih, Y.-P., Chen, M., Lo, S.H., 2014. Up-regulated cten by FGF2 contributes to FGF2-mediated cell migration. Mol. Carcinog. 53, 787–92.

Huttenlocher, A., Ginsberg, M.H., Horwitz, A.F., 1996. Modulation of cell migration by integrin-mediated cytoskeletal linkages and ligand-binding affinity. J. Cell Biol. 134, 1551–62.

Huttenlocher, A., Horwitz, A.R., 2011. Integrins in cell migration. Cold Spring Harb. Perspect. Biol. 3, a005074.

Hynes, R.O., 2002. Integrins: bidirectional, allosteric signaling machines. Cell 110, 673–687.

Hynes, R.O., 1992. Integrins: versatility, modulation, and signaling in cell adhesion. Cell 69, 11–25.

Imsande, H.M., Davison, J.M., Truong, M.T., Devaiah, A.K., Mercier, G.A., Ozonoff, A.J., Subramaniam, R.M., 2011. Use of 18F-FDG PET/CT as a predictive biomarker of outcome in patients with head-and-neck non-squamous cell carcinoma. AJR. Am. J. Roentgenol. 197, 976–80.

Inman, G., 2011. Switching TGFβ from a tumor suppressor to a tumor promoter. Curr Opin Genet Dev 21, 93–9.

Inokuchi, H., Kodaira, T., Tachibana, H., Nakamura, T., Tomita, N., Nakahara, R., Takada, A., Mizoguchi, N., Tamaki, T., Fuwa, N., 2011. Clinical usefulness of [18F] fluoro-2-deoxy-D-glucose uptake in 178 head-and-neck cancer patients with nodal metastasis treated with definitive chemoradiotherapy: consideration of its prognostic value and ability to provide guidance for optimal selection . Int. J. Radiat. Oncol. Biol. Phys. 79, 747–55.

Isles, M.G., McConkey, C., Mehanna, H.M., 2008. A systematic review and meta-analysis of the role of positron emission tomography in the follow up of head and neck squamous cell carcinoma following radiotherapy or chemoradiotherapy. Clin. Otolaryngol. 33, 210–22.

Jay, P.Y., Pham, P.A., Wong, S.A., Elson, E.L., 1995. A mechanical function of myosin II in cell motility. J. Cell Sci. 108(1), 387–93.

Jensen, L.J., Kuhn, M., Stark, M., Chaffron, S., Creevey, C., Muller, J., Doerks, T., Julien, P., Roth, A., Simonovic, M., Bork, P., von Mering, C., 2009. STRING 8--a global view on proteins and their functional interactions in 630 organisms. Nucleic Acids Res. 37, D412-6.

Jiang, P., Du, W., Wang, X., Mancuso, A., Gao, X., Wu, M., Yang, X., 2011. p53 regulates biosynthesis through direct inactivation of glucose-6-phosphate dehydrogenase. Nat. Cell Biol. 13, 310–6.

Joo, Y.-H., Yoo, I.-R., Cho, K.-J., Park, J.-O., Nam, I.-C., Kim, M.-S., 2014. Preoperative 18F-FDG PET/CT and high-risk HPV in patients with oropharyngeal squamous cell carcinoma. Head Neck 36, 323–7.

Jose, C., Bellance, N., Rossignol, R., 2011. Choosing between glycolysis and oxidative phosphorylation: a tumor's dilemma? Biochim. Biophys. Acta 1807, 552–61.

Kaddi, C., Wang, M., 2015. Models for Predicting Stage in Head and Neck Squamous Cell Carcinoma using Proteomic and Transcriptomic Data. IEEE J. Biomed. Heal. informatics.

Kalakonda, S., Nallar, S.C., Lindner, D.J., Hu, J., Reddy, S.P., Kalvakolanu, D. V, 2007. Tumor-suppressive activity of the cell death activator GRIM-19 on a constitutively active signal transducer and activator of transcription 3. Cancer Res. 67, 6212–20.

Kalyankrishna, S., Grandis, J.R., 2006. Epidermal growth factor receptor biology in head

and neck cancer. J. Clin. Oncol. 24, 2666–72.

Kaminska, B., Wesolowska, A., Danilkiewicz, M., 2005. TGF beta signalling and its role in tumour pathogenesis. Acta Biochim. Pol. 2005;52(2):329-37

Kato, H., Liao, Z., Mitsios, J. V, Wang, H.-Y., Deryugina, E.I., Varner, J. a, Quigley, J.P., Shattil, S.J., 2012. The primacy of β1 integrin activation in the metastatic cascade. PLoS One 7, e46576.

Katsanis, N., Fisher, E.M., 1998. A novel C-terminal binding protein (CTBP2) is closely related to CTBP1, an adenovirus E1A-binding protein, and maps to human chromosome 21q21.3. Genomics 47, 294–9.

Katz, B.Z., Zohar, M., Teramoto, H., Matsumoto, K., Gutkind, J.S., Lin, D.C., Lin, S., Yamada, K.M., 2000. Tensin can induce JNK and p38 activation. Biochem. Biophys. Res. Commun. 272, 717–20.

Katz, M., Amit, I., Citri, A., Shay, T., Carvalho, S., Lavi, S., Milanezi, F., Lyass, L., Amariglio, N., Jacob-Hirsch, J., Ben-Chetrit, N., Tarcic, G., Lindzen, M., Avraham, R., Liao, Y.-C., Trusk, P., Lyass, A., Rechavi, G., Spector, N.L., Lo, S.H., Schmitt, F., Bacus, S.S., Yarden, Y., 2007. A reciprocal tensin-3-cten switch mediates EGF-driven mammary cell migration. Nat. Cell Biol. 9, 961–9.

Kawashiri, S., Tanaka, A., Noguchi, N., Hase, T., Nakaya, H., Ohara, T., Kato, K., Yamamoto, E., 2009. Significance of stromal desmoplasia and myofibroblast appearance at the invasive front in squamous cell carcinoma of the oral cavity. Head Neck 31, 1346–53.

Kendi, A.T.K., Magliocca, K., Corey, A., Nickleach, D.C., Galt, J., Higgins, K., Beitler, J.J., El-Deiry, M.W., Wadsworth, J.T., Hudgins, P.A., Saba, N.F., Schuster, D.M., 2015. Do 18F-FDG PET/CT parameters in oropharyngeal and oral cavity squamous cell carcinomas indicate HPV status? Clin. Nucl. Med. 40, e196-200.

Kikkawa, H., Kaihou, M., Horaguchi, N., Uchida, T., Imafuku, H., Takiguchi, A., Yamazaki, Y., Koike, C., Kuruto, R., Kakiuchi, T., Tsukada, H., Takada, Y., Matsuura, N., Oku, N., 2002. Role of integrin alpha(v)beta3 in the early phase of liver metastasis: PET and IVM analyses. Clin. Exp. Metastasis 19, 717–25.

Kim, J., Gao, P., Liu, Y.-C., Semenza, G.L., Dang, C. V, 2007. Hypoxia-inducible factor 1 and dysregulated c-Myc cooperatively induce vascular endothelial growth factor and metabolic switches hexokinase 2 and pyruvate dehydrogenase kinase 1. Mol. Cell. Biol. 27, 7381–93.

Kim, J., Gardner, L.B., Dang, C. V., 2005. Oncogenic alterations of metabolism and the

Warburg effect. Drug Discov. Today Dis. Mech. 2, 233–238.

Kim, J., Tchernyshyov, I., Semenza, G.L., Dang, C. V, 2006. HIF-1-mediated expression of pyruvate dehydrogenase kinase: a metabolic switch required for cellular adaptation to hypoxia. Cell Metab. 3, 177–185.

Kim, J.W., Kim, H.S., Kim, I.K., Kim, M.R., Cho, E.Y., Kim, H.K., Lee, J.M., Namkoong, S.E., 1998. Transforming growth factor-beta 1 induces apoptosis through down-regulation of c-myc gene and overexpression of p27Kip1 protein in cervical carcinoma. Gynecol Oncol 69, 230–236.

Kim, S., Grandis, J.R., Rinaldo, A., Takes, R.P., Ferlito, A., 2008. Emerging perspectives in epidermal growth factor receptor targeting in head and neck cancer. Head Neck 30, 667–74.

Kinahan, P.E., Fletcher, J.W., 2010. Positron emission tomography-computed tomography standardized uptake values in clinical practice and assessing response to therapy. Semin. Ultrasound. CT. MR 31, 496–505.

Klemke, R.L., Yebra, M., Bayna, E.M., Cheresh, D.A., 1994. Receptor tyrosine kinase signaling required for integrin alpha v beta 5-directed cell motility but not adhesion on vitronectin. J. Cell Biol. 127, 859–66.

Kohn, A.D., Summers, S.A., Birnbaum, M.J., Roth, R.A., 1996. Expression of a constitutively active Akt Ser/Thr kinase in 3T3-L1 adipocytes stimulates glucose uptake and glucose transporter 4 translocation. J. Biol. Chem. 271, 31372–8.

Koivisto, L., Grenman, R., Heino, J., Larjava, H., 2000. Integrins alpha5beta1, alphavbeta1, and alphavbeta6 collaborate in squamous carcinoma cell spreading and migration on fibronectin. Exp. Cell Res. 255, 10–17.

Kondo, T., Nakazawa, T., Murata, S., Kurebayashi, J., Ezzat, S., Asa, S.L., Katoh, R., 2007. Enhanced B-Raf protein expression is independent of V600E mutant status in thyroid carcinomas. Hum. Pathol. 38, 1810–8.

Kondoh, H., Lleonart, M.E., Gil, J., Wang, J., Degan, P., Peters, G., Martinez, D., Carnero, A., Beach, D., 2005. Glycolytic enzymes can modulate cellular life span. Cancer Res. 65, 177–85.

Kong, C.S., Narasimhan, B., Cao, H., Kwok, S., Erickson, J.P., Koong, A., Pourmand, N., Le, Q.-T., 2009. The relationship between human papillomavirus status and other molecular prognostic markers in head and neck squamous cell carcinomas. Int. J. Radiat. Oncol. Biol. Phys. 74, 553–61.

Koontongkaew, S., 2013. The tumor microenvironment contribution to development, growth, invasion and metastasis of head and neck squamous cell carcinomas. J. Cancer 4, 66–83.

Krejčí, A., 2012. Metabolic sensors and their interplay with cell signalling and transcription. Biochem. Soc. Trans. 40, 311–23.:10.

Kroemer, G., Pouyssegur, J., 2008. Tumor cell metabolism: cancer's Achilles' heel. Cancer Cell 13, 472–482.

Kruiswijk, F., Labuschagne, C.F., Vousden, K.H., 2015. p53 in survival, death and metabolic health: a lifeguard with a licence to kill. Nat. Rev. Mol. Cell Biol. 16, 393–405.

Krupar, R., Robold, K., Gaag, D., Spanier, G., Kreutz, M., Renner, K., Hellerbrand, C., Hofstaedter, F., Bosserhoff, A.K., 2014. Immunologic and metabolic characteristics of HPV-negative and HPV-positive head and neck squamous cell carcinomas are strikingly different. Virchows Arch. 465(3):299-312.

Kumar, V., Carlson, J.E., Ohgi, K.A., Edwards, T.A., Rose, D.W., Escalante, C.R., Rosenfeld, M.G., Aggarwal, A.K., 2002. Transcription corepressor CtBP is an NAD(+)-regulated dehydrogenase. Mol. Cell 10, 857–69.

Kunkel, M., Reichert, T.E., Benz, P., Lehr, H.-A., Jeong, J.-H., Wieand, S., Bartenstein, P., Wagner, W., Whiteside, T.L., 2003. Overexpression of Glut-1 and increased glucose metabolism in tumors are associated with a poor prognosis in patients with oral squamous cell carcinoma. Cancer 97, 1015–24.

Kunz-Schughart, L.A., Knuechel, R., 2002. Tumor-associated fibroblasts (part I): Active stromal participants in tumor development and progression? Histol. Histopathol. 17, 599–621.

Kuppuswamy, M., Vijayalingam, S., Zhao, L.-J., Zhou, Y., Subramanian, T., Ryerse, J., Chinnadurai, G., 2008. Role of the PLDLS-binding cleft region of CtBP1 in recruitment of core and auxiliary components of the corepressor complex. Mol. Cell. Biol. 28, 269–81.

Lafon, C., Mathieu, C., Guerrin, M., Pierre, O., Vidal, S., Valette, A., 1996. Transforming growth factor beta 1-induced apoptosis in human ovarian carcinoma cells: protection by the antioxidant N-acetylcysteine and bcl-2. Cell Growth Differ. 7, 1095–104.

Lai, M.T., Hua, C.H., Tsai, M.H., Wan, L., Lin, Y.J., Chen, C.M., Chiu, I.W., Chan, C., Tsai, F.J., Sheu, J.C.J., 2011. Talin-1 overexpression defines high risk for aggressive oral

squamous cell carcinoma and promotes cancer metastasis. J. Pathol. 224, 367–376.

Lawrence, M.S., Sougnez, C., Lichtenstein, L., Cibulskis, K., Lander, E., Gabriel, S.B., Getz, G., Ally, A., Balasundaram, M., Birol, I., Bowlby, R., Brooks, D., Butterfield, Y.S.N., Carlsen, R., Cheng, D., Chu, A., Dhalla, N., Guin, R., Holt, R.A., Jones, S.J.M., Lee, D., Li, H.I., Marra, M.A., Mayo, M., Moore, R.A., Mungall, A.J., Gordon Robertson, A., Schein, J.E., Sipahimalani, P., Tam, A., Thiessen, N., Wong, T., Protopopov, A., Santoso, N., Lee, S., Parfenov, M., Zhang, J., Mahadeshwar, H.S., Tang, J., Ren, X., Seth, S., Haseley, P., Zeng, D., Yang, L., Xu, A.W., Song, X., Pantazi, A., Bristow, C.A., Hadjipanayis, A., Seidman, J., Chin, L., Park, P.J., Kucherlapati, R., Akbani, R., Casasent, T., Liu, W., Lu, Y., Mills, G., Motter, T., Weinstein, J., Diao, L., Wang, J., Hong Fan, Y., Liu, J., Wang, K., Todd Auman, J., Balu, S., Bodenheimer, T., Buda, E., Neil Hayes, D., Hoadley, K.A., Hoyle, A.P., Jefferys, S.R., Jones, C.D., Kimes, P.K., Liu, Y., Marron, J.S., Meng, S., Mieczkowski, P.A., Mose, L.E., Parker, J.S., Perou, C.M., Prins, J.F., Roach, J., Shi, Y., Simons, J. V., Singh, D., Soloway, M.G., Tan, D., Veluvolu, U., Walter, V., Waring, S., Wilkerson, M.D., Wu, J., Zhao, N., Cherniack, A.D., Hammerman, P.S., Tward, A.D., Sekhar Pedamallu, C., Saksena, G., Jung, J., Ojesina, A.I., Carter, S.L., Zack, T.I., Schumacher, S.E., Beroukhim, R., Freeman, S.S., Meyerson, M., Cho, J., Noble, M.S., DiCara, D., Zhang, H., Heiman, D.I., Gehlenborg, N., Voet, D., Lin, P., Frazer, S., Stojanov, P., Liu, Y., Zou, L., Kim, J., Muzny, D., Doddapaneni, H., Kovar, C., Reid, J., Morton, D., Han, Y., Hale, W., Chao, H., Chang, K., Drummond, J.A., Gibbs, R.A., Kakkar, N., Wheeler, D., Xi, L., Ciriello, G., Ladanyi, M., Lee, W., Ramirez, R., Sander, C., Shen, R., Sinha, R., Weinhold, N., Taylor, B.S., Arman Aksoy, B., Dresdner, G., Gao, J., Gross, B., Jacobsen, A., Reva, B., Schultz, N., Onur Sumer, S., Sun, Y., Chan, T.A., Morris, L.G., Stuart, J., Benz, S., Ng, S., Benz, C., Yau, C., Baylin, S.B., Cope, L., Danilova, L., Herman, J.G., Bootwalla, M., Maglinte, D.T., Laird, P.W., Triche, T., Weisenberger, D.J., Van Den Berg, D.J., Agrawal, N., Bishop, J., Boutros, P.C., Bruce, J.P., Averett Byers, L., Califano, J., Carey, T.E., Chen, Z., Cheng, H., Chiosea, S.I., Cohen, E., Diergaarde, B., Marie Egloff, A., El-Naggar, A.K., Ferris, R.L., Frederick, M.J., Grandis, J.R., Guo, Y., Haddad, R.I., Harris, T., Hui, A.B.Y., Jack Lee, J., Lippman, S.M., Liu, F.-F., McHugh, J.B., Myers, J., Kwok Shing Ng, P., Perez-Ordonez, B., Pickering, C.R., Prystowsky, M., Romkes, M., Saleh, A.D., Sartor, M.A., Seethala, R., Seiwert, T.Y., Si, H., Van Waes, C., Waggott, D.M., Wiznerowicz, M., Yarbrough, W.G., Zhang, J., Zuo, Z., Burnett, K., Crain, D., Gardner, J., Lau, K.,

Mallery, D., Morris, S., Paulauskis, J., Penny, R., Shelton, C., Shelton, T., Sherman, M., Yena, P., Black, A.D., Bowen, J., Frick, J., Gastier-Foster, J.M., Harper, H.A., Leraas, K., Lichtenberg, T.M., Ramirez, N.C., Wise, L., Zmuda, E., Baboud, J., Jensen, M.A., Kahn, A.B., Pihl, T.D., Pot, D.A., Srinivasan, D., Walton, J.S., Wan, Y., Burton, R.A., Davidsen, T., Demchok, J.A., Eley, G., Ferguson, M.L., Mills Shaw, K.R., Ozenberger, B.A., Sheth, M., Sofia, H.J., Tarnuzzer, R., Wang, Z., Yang, L., Claude Zenklusen, J., Saller, C., Tarvin, K., Chen, C., Bollag, R., Weinberger, P., Golusiński, W., Golusiński, P., Ibbs, M., Korski, K., Mackiewicz, A., Suchorska, W., Szybiak, B., Curley, E., Beard, C., Mitchell, C., Sandusky, G., Ahn, J., Khan, Z., Irish, J., Waldron, J., William, W.N., Egea, S., Gomez-Fernandez, C., Herbert, L., Bradford, C.R., Chepeha, D.B., Haddad, A.S., Jones, T.R., Komarck, C.M., Malakh, M., Moyer, J.S., Nguyen, A., Peterson, L.A., Prince, M.E., Rozek, L.S., Taylor, E.G., Walline, H.M., Wolf, G.T., Boice, L., Chera, B.S., Funkhouser, W.K., Gulley, M.L., Hackman, T.G., Hayward, M.C., Huang, M., Kimryn Rathmell, W., Salazar, A.H., Shockley, W.W., Shores, C.G., Thorne, L., Weissler, M.C., Wrenn, S., Zanation, A.M., Brown, B.T., Pham, M., 2015. Comprehensive genomic characterization of head and neck squamous cell carcinomas. Nature 517, 576–582.

Le, Q., Dawson, M.I., Soprano, D.R., Soprano, K.J., 2000. Modulation of retinoic acid receptor function alters the growth inhibitory response of oral SCC cells to retinoids. Oncogene 19, 1457–65.

Le Floch, R., Chiche, J., Marchiq, I., Naiken, T., Naïken, T., Ilc, K., Ilk, K., Murray, C.M., Critchlow, S.E., Roux, D., Simon, M.-P., Pouysségur, J., 2011. CD147 subunit of lactate/H+ symporters MCT1 and hypoxia-inducible MCT4 is critical for energetics and growth of glycolytic tumors. Proc. Natl. Acad. Sci. U. S. A. 108, 16663–8.

Le Tourneau, C., Faivre, S., Siu, L.L., 2007. Molecular targeted therapy of head and neck cancer: review and clinical development challenges. Eur. J. Cancer 43, 2457–66.

Lee, J., Leonard, M., Oliver, T., Ishihara, A., Jacobson, K., 1994. Traction forces generated by locomoting keratocytes. J. Cell Biol. 127, 1957–64.

Leef, G., Thomas, S.M., 2013. Molecular communication between tumor-associated fibroblasts and head and neck squamous cell carcinoma. Oral Oncol. 49, 381–6.

Leemans, C.R., Braakhuis, B.J.M., Brakenhoff, R.H., 2011. The molecular biology of head and neck cancer. Nat. Rev. Cancer 11, 9–22.

Leemans, C.R., Tiwari, R., Nauta, J.J., van der Waal, I., Snow, G.B., 1994. Recurrence at the primary site in head and neck cancer and the significance of neck lymph node

metastases as a prognostic factor. Cancer 73, 187–90.

Legate, K.R., Fässler, R., 2009. Mechanisms that regulate adaptor binding to beta-integrin cytoplasmic tails. J. Cell Sci. 122, 187–98.

Lehninger, A.L., Nelson, D.L., Cox, M.M., others, 1982. Principles of biochemistry, NeuroImage. Worth Publishers New York.

Lévy, P., Bartosch, B., 2015. Metabolic reprogramming: a hallmark of viral oncogenesis. Oncogene. 11;35(32):4155-64

Lewis, B.C., Shim, H., Li, Q., Wu, C.S., Lee, L.A., Maity, A., Dang, C. V, 1997. Identification of putative c-Myc-responsive genes: characterization of rcl, a novel growth-related gene. Mol. Cell. Biol. 17, 4967–78.

Li, H., Handsaker, B., Wysoker, A., Fennell, T., Ruan, J., Homer, N., Marth, G., Abecasis, G., Durbin, R., 2009. The Sequence Alignment/Map format and SAMtools. Bioinformatics 25, 2078–9.

Li, S.-J., Guo, W., Ren, G.-X., Huang, G., Chen, T., Song, S., 2008. Expression of Glut-1 in primary and recurrent head and neck squamous cell carcinomas, and compared with 2-[18F]fluoro-2-deoxy-D-glucose accumulation in positron emission tomography. Br. J. Oral Maxillofac. Surg. 46, 180–6.

Li, Y., Mizokami, A., Izumi, K., Narimoto, K., Shima, T., Zhang, J., Dai, J., Keller, E.T., Namiki, M., 2010. CTEN/tensin 4 expression induces sensitivity to paclitaxel in prostate cancer. Prostate 70, 48–60.

Liao, Y.-C., Chen, N.-T., Shih, Y.-P., Dong, Y., Lo, S.H., 2009. Up-regulation of C-terminal tensin-like molecule promotes the tumorigenicity of colon cancer through β-catenin. Cancer Res 69, 4563–4566.

Liao, Y.-C., Si, L., deVere White, R.W., Lo, S.H., 2007. The phosphotyrosine-independent interaction of DLC-1 and the SH2 domain of cten regulates focal adhesion localization and growth suppression activity of DLC-1. J. Cell Biol. 176, 43–9.

Lin, S.J., Guarente, L., 2003. Nicotinamide adenine dinucleotide, a metabolic regulator of transcription, longevity and disease. Curr. Opin. Cell Biol. 15(2):241-6

Lin, X., Zhang, F., Bradbury, C.M., Kaushal, A., Li, L., Spitz, D.R., Aft, R.L., Gius, D., 2003. 2-Deoxy-D-glucose-induced cytotoxicity and radiosensitization in tumor cells is mediated via disruptions in thiol metabolism. Cancer Res. 63, 3413–7.

Liu, Y., El-Naggar, S., Darling, D.S., Higashi, Y., Dean, D.C., 2008. Zeb1 links epithelial-mesenchymal transition and cellular senescence. Development 135, 579–588.

Lo, S.-S., Lo, S.H., Lo, S.H., 2005. Cleavage of cten by caspase-3 during apoptosis. Oncogene 24, 4311–4314.

Lo, S.H., 2014. C-terminal tensin-like (CTEN): a promising biomarker and target for cancer. Int. J. Biochem. Cell Biol. 51, 150–4.

Lo, S.H., 2004. Tensin. Int. J. Biochem. Cell Biol. 36, 31–34.

Lo, S.H., Janmey, P.A., Hartwig, J.H., Chen, L.B., 1994. Interactions of tensin with actin and identification of its three distinct actin-binding domains. J. Cell Biol. 125, 1067–1075.

Lo, S.H., Lo, T. Bin, 2002. Cten, a COOH-terminal tensin-like protein with prostate restricted expression, is down-regulated in prostate cancer. Cancer Res. 62, 4217–4221.

Lo, S.H., Yu, Q.-C., Degenstein, L., Chen, L.B., Fuchs, E., 1997. Progressive kidney degeneration in mice lacking tensin. J. Cell Biol. 136, 1349–1361.

Loor, R., Nowak, N.J., Manzo, M.L., Douglass, H.O., Chu, T.M., 1982. Use of pancreas-specific antigen in immunodiagnosis of pancreatic cancer. Clin. Lab. Med. 2, 567–78.

Loyo, M., Li, R.J., Bettegowda, C., Pickering, C.R., Frederick, M.J., Myers, J.N., Agrawal, N., 2013. Lessons learned from next-generation sequencing in head and neck cancer. Head Neck 35, 454–63.

Ludbrook, S.B., Barry, S.T., Delves, C.J., Horgan, C.M.T., 2003. The integrin alphavbeta3 is a receptor for the latency-associated peptides of transforming growth factors beta1 and beta3. Biochem. J. 369, 311–8.

Lunt, S.Y., Vander Heiden, M.G., 2011. Aerobic Glycolysis: Meeting the Metabolic Requirements of Cell Proliferation. Annu. Rev. Cell Dev. Biol. 27, 441–464.

Maaten, L. van der, Hinton, G., 2008. Visualizing Data using t-SNE. J. Mach. Learn. Res. 9, 2579–2605.

Machamer, C.E., Ferri, K.F., Kroemer, G., Thornberry, N.A., Lazebnik, Y., Rios, R.M., Bornens, M., Sesso, A., al., et, Lane, J.D., al., et, Shorter, J., Warren, G., Mancini, M., al., et, Chiu, R., al., et, Hicks, S.W., Machamer, C.E., Shorter, J., al., et, Puthenveedu, M.A., Linstedt, A.D., Barr, F.A., al., et, O'Reilly, L.A., al., et, Kumar, S., al., et, Thornberry, N.A., al., et, Lassus, P., al., et, Varfolomeev, E.E., al., et, Sutterlin, C., al., et, Lane, J.D., al., et, 2003. Golgi disassembly in apoptosis: cause or effect? Trends Cell Biol. 13, 279–81.

Maddocks, O.D.K., Vousden, K.H., 2011. Metabolic regulation by p53. J. Mol. Med. (Berl). 89, 237–45.

Maeda, I., Takano, T., Yoshida, H., Matsuzuka, F., Amino, N., Miyauchi, A., 2006. Tensin3 is a novel thyroid-specific gene. J. Mol. Endocrinol. 36, R1-8.

Mammas, I.N., Sourvinos, G., Giannoudis, A., Spandidos, D.A., 2008. Human papilloma virus (HPV) and host cellular interactions. Pathol. Oncol. Res. 14, 345–54.

Mani, S.A., Guo, W., Liao, M., Eaton, E.N., Ayyanan, A., Zhou, A.Y., Brooks, M., Reinhard, F., Zhang, C.C., Shipitsin, M., Campbell, L.L., Polyak, K., Brisken, C., Yang, J., Weinberg, R.A., 2008. The Epithelial-Mesenchymal Transition Generates Cells with Properties of Stem Cells. Cell 133, 704–715.

Margadant, C., Monsuur, H.N., Norman, J.C., Sonnenberg, A., 2011. Mechanisms of integrin activation and trafficking. Curr. Opin. Cell Biol. 23, 607–14.

Marks, P.W., Hendey, B., Maxfield, F.R., 1991. Attachment to fibronectin or vitronectin makes human neutrophil migration sensitive to alterations in cytosolic free calcium concentration. J. Cell Biol. 112, 149–158.

Marsh, D., Dickinson, S., Neill, G.W., Marshall, J.F., Hart, I.R., Thomas, G.J., 2008. v 6 Integrin Promotes the Invasion of Morphoeic Basal Cell Carcinoma through Stromal Modulation. Cancer Res. 68, 3295–3303.

Martin, R.C.W., Fulham, M., Shannon, K.F., Hughes, C., Gao, K., Milross, C., Tin, M.M., Jackson, M., Clifford, A., Boyer, M.J., O'Brien, C.J., 2009. Accuracy of positron emission tomography in the evaluation of patients treated with chemoradiotherapy for mucosal head and neck cancer. Head Neck 31, 244–50.

Martuszewska, D., Ljungberg, B., Johansson, M., Landberg, G., Oslakovic, C., Dahlbäck, B., Hafizi, S., 2009. Tensin3 Is a Negative Regulator of Cell Migration and All Four Tensin Family Members Are Downregulated in Human Kidney Cancer. PLoS One 4, 13.

Marur, S., D'Souza, G., Westra, W.H., Forastiere, A.A., 2010. HPV-associated head and neck cancer: a virus-related cancer epidemic. Lancet. Oncol. 11, 781–9.

Massagué, J., Gomis, R.R., 2006. The logic of TGFbeta signaling. FEBS Lett. 580, 2811–20.

Matthaios, D., Zarogoulidis, P., Balgouranidou, I., Chatzaki, E., Kakolyris, S., 2011. Molecular pathogenesis of pancreatic cancer and clinical perspectives. Oncology 81, 259–72.

Mazurek, S., Zwerschke, W., Jansen-Dürr, P., Eigenbrodt, E., 2001. Effects of the human papilloma virus HPV-16 E7 oncoprotein on glycolysis and glutaminolysis: role of pyruvate kinase type M2 and the glycolytic-enzyme complex. Biochem. J. 356, 247–256.

Mccleverty, C.J., Lin, D.C., Liddington, R.C., 2007. Structure of the PTB domain of tensin1 and a model for its recruitment to fibrillar adhesions 1223–1229.

McKeehan, W.L., 1982. Glycolysis, glutaminolysis and cell proliferation. Cell Biol. Int. Rep. 6, 635–50.

Mellanen, P., Minn, H., Grénman, R., Härkönen, P., 1994. Expression of glucose transporters in head-and-neck tumors. Int. J. Cancer 56, 622–629.

Mendler, A.N., Hu, B., Prinz, P.U., Kreutz, M., Gottfried, E., Noessner, E., 2012. Tumor lactic acidosis suppresses CTL function by inhibition of p38 and JNK/c-Jun activation. Int. J. Cancer 131, 633–40.

Meulmeester, E., Ten Dijke, P., 2011. The dynamic roles of TGF-β in cancer. J. Pathol. 223, 205–218.

Milacic, M., Haw, R., Rothfels, K., Wu, G., Croft, D., Hermjakob, H., D'Eustachio, P., Stein, L., 2012. Annotating cancer variants and anti-cancer therapeutics in reactome. Cancers (Basel). 4, 1180–211.

Miwa, I., Duan, Y.J., Murase, S., Fukatsu, H., Tamura, A., Okuda, J., 1993. Stimulatory effect of phospholipase A2 treatment on glucose utilization in human erythrocytes. Biochim. Biophys. Acta 1175, 174–80.

Moore, K.M., Thomas, G.J., Duffy, S.W., Warwick, J., Gabe, R., Chou, P., Ellis, I.O., Green, A.R., Haider, S., Brouilette, K., Saha, A., Vallath, S., Bowen, R., Chelala, C., Eccles, D., Tapper, W.J., Thompson, A.M., Quinlan, P., Jordan, L., Gillett, C., Brentnall, A., Violette, S., Weinreb, P.H., Kendrew, J., Barry, S.T., Hart, I.R., Jones, J.L., Marshall, J.F., 2014. Therapeutic targeting of integrin αvβ6 in breast cancer. J. Natl. Cancer Inst. 106, dju169-

Moreno-Sánchez, R., Rodríguez-Enríquez, S., Marín-Hernández, A., Saavedra, E., 2007. Energy metabolism in tumor cells. FEBS J. 274, 1393–418.

Morgan, D.O., 1995. Principles of CDK regulation. Nature 374, 131–4.

Mouneimne, G., Brugge, J.S., 2007. Tensins: a new switch in cell migration. Dev. Cell 13, 317–9.

Moustakas, A., Heldin, C.-H., 2012. Induction of epithelial-mesenchymal transition by transforming growth factor β. Semin. Cancer Biol. 22, 446–54.

Moutasim, K., Jenei, V., Sapienza, K., Marsh, D., Weinreb, P., Violette, S., Lewis, M., Marshall, J., Fortune, F., Tilakaratne, W., Hart, I., Thomas, G., 2010. Betel-derived alkaloid up-regulates keratinocyte alphavbeta6 integrin expression and promotes

oral submucous fibrosis. J. Pathol. 223, 366–377.

Mroz, E.A., Baird, A.H., Michaud, W.A., Rocco, J.W., 2008. COOH-terminal binding protein regulates expression of the p16INK4A tumor suppressor and senescence in primary human cells. Cancer Res. 68, 6049–6053.

Mu, Y., Gudey, S.K., Landström, M., 2012. Non-Smad signaling pathways. Cell Tissue Res.

Muharram, G., Sahgal, P., Korpela, T., De Franceschi, N., Kaukonen, R., Clark, K., Tulasne, D., Carpén, O., Ivaska, J., 2014. Tensin-4-dependent MET stabilization is essential for survival and proliferation in carcinoma cells. Dev. Cell 29, 421–36.

Munger, J.S., Huang, X., Kawakatsu, H., Griffiths, M.J., Dalton, S.L., Wu, J., Pittet, J.F., Kaminski, N., Garat, C., Matthay, M.A., Rifkin, D.B., Sheppard, D., 1999. The integrin alpha v beta 6 binds and activates latent TGF beta 1: a mechanism for regulating pulmonary inflammation and fibrosis. Cell 96, 319–328.

Munger, J.S., Sheppard, D., 2011. Integrins , and the Extracellular Matrix 1–17.

Myers, J.N., Holsinger, F.C., Jasser, S.A., Bekele, B.N., Fidler, I.J., 2002. An orthotopic nude mouse model of oral tongue squamous cell carcinoma. Clin. Cancer Res. 8, 293–8.

Nakamura, M., Kitagawa, Y., Yamazaki, Y., Hata, H., Kotsuji, M., Fujibayashi, Y., Okazawa, H., Yonekura, Y., Sano, K., 2012. Increased glucose metabolism by FDG-PET correlates with reduced tumor angiogenesis in oral squamous cell carcinoma. Odontology 100, 87–94.

Nardini, M., Spanò, S., Cericola, C., Pesce, A., Massaro, A., Millo, E., Luini, A., Corda, D., Bolognesi, M., 2003. CtBP/BARS: a dual-function protein involved in transcription co-repression and Golgi membrane fission. EMBO J. 22, 3122–30.

Näsman, A., Attner, P., Hammarstedt, L., Du, J., Eriksson, M., Giraud, G., Ahrlund-Richter, S., Marklund, L., Romanitan, M., Lindquist, D., Ramqvist, T., Lindholm, J., Sparén, P., Ye, W., Dahlstrand, H., Munck-Wikland, E., Dalianis, T., 2009. Incidence of human papillomavirus (HPV) positive tonsillar carcinoma in Stockholm, Sweden: an epidemic of viral-induced carcinoma? Int. J. Cancer 125, 362–6.

Näsman, A., Romanitan, M., Nordfors, C., Grün, N., Johansson, H., Hammarstedt, L., Marklund, L., Munck-Wikland, E., Dalianis, T., Ramqvist, T., 2012. Tumor infiltrating CD8+ and Foxp3+ lymphocytes correlate to clinical outcome and human papillomavirus (HPV) status in tonsillar cancer. PLoS One 7, e38711.

Nip, J., Shibata, H., Loskutoff, D.J., Cheresh, D.A., Brodt, P., 1992. Human melanoma cells derived from lymphatic metastases use integrin alpha v beta 3 to adhere to lymph

node vitronectin. J. Clin. Invest. 90, 1406–1413.

Nogueira, V., Park, Y., Chen, C.C., Xu, P.Z., Chen, M.L., Tonic, I., Unterman, T., Hay, N., 2008. Akt Determines Replicative Senescence and Oxidative or Oncogenic Premature Senescence and Sensitizes Cells to Oxidative Apoptosis. Cancer Cell 14, 458–470.

Numico, G., Russi, E.G., Colantonio, I., Lantermo, R.A., Silvestris, N., Vitiello, R., Comino, A., Abrate, M., Zavattero, C., Melano, A., Merlano, M., 2010. EGFR status and prognosis of patients with locally advanced head and neck cancer treated with chemoradiotherapy. Anticancer Res. 30, 671–6.

Nystrom, M.L., McCulloch, D., Weinreb, P.H., Violette, S.M., Speight, P.M., Marshall, J.F., Hart, I.R., Thomas, G.J., 2006. Cyclooxygenase-2 Inhibition Suppresses v 6 Integrin-Dependent Oral Squamous Carcinoma Invasion. Cancer Res. 66, 10833–10842.

O'Rorke, M.A., Ellison, M. V, Murray, L.J., Moran, M., James, J., Anderson, L.A., 2012. Human papillomavirus related head and neck cancer survival: a systematic review and meta-analysis. Oral Oncol. 48, 1191–201.

Orimo, A., Gupta, P.B., Sgroi, D.C., Arenzana-Seisdedos, F., Delaunay, T., Naeem, R., Carey, V.J., Richardson, A.L., Weinberg, R.A., 2005. Stromal fibroblasts present in invasive human breast carcinomas promote tumor growth and angiogenesis through elevated SDF-1/CXCL12 secretion. Cell 121, 335–48.

Paliwal, S., Ho, N., Parker, D., Grossman, S.R., 2012. CtBP2 Promotes Human Cancer Cell Migration by Transcriptional Activation of Tiam1. Genes cancer 3, 481–90.

Paliwal, S., Kovi, R.C., Nath, B., Chen, Y.-W., Lewis, B.C., Grossman, S.R., 2007. The alternative reading frame tumor suppressor antagonizes hypoxia-induced cancer cell migration via interaction with the COOH-terminal binding protein corepressor. Cancer Res. 67, 9322–9.

Paliwal, S., Pande, S., Kovi, R.C., Sharpless, N.E., Bardeesy, N., Grossman, S.R., 2006. Targeting of C-terminal binding protein (CtBP) by ARF results in p53-independent apoptosis. Mol. Cell. Biol. 26, 2360–2372.

Pasche, B., Knobloch, T., Bian, Y., Liu, J., Phukan, S., Rosman, D., 2005. Somatic acquisition and signaling of TGFBR1*6A in cancer. Jama J. Am. Med. Assoc. 294, 1634–1646.

Patil, A.S., Sable, R.B., Kothari, R.M., 2011. An update on transforming growth factor-β (TGF-β): sources, types, functions and clinical applicability for cartilage/bone healing. J. Cell. Physiol. 226, 3094–103.

Pavlides, S., Whitaker-Menezes, D., Castello-Cros, R., Flomenberg, N., Witkiewicz, A.K.,

Frank, P.G., Casimiro, M.C., Wang, C., Fortina, P., Addya, S., Pestell, R.G., Martinez-Outschoorn, U.E., Sotgia, F., Lisanti, M.P., 2009. The reverse Warburg effect: aerobic glycolysis in cancer associated fibroblasts and the tumor stroma. Cell cycle Georg. Tex 8, 3984–4001.

Pavón, M.A., Parreño, M., Téllez-Gabriel, M., León, X., Arroyo-Solera, I., López, M., Céspedes, M.V., Casanova, I., Gallardo, A., López-Pousa, A., Mangues, M.A., Quer, M., Barnadas, A., Mangues, R., 2015. CKMT1 and NCOA1 expression as a predictor of clinical outcome in patients with advanced-stage head and neck squamous cell carcinoma. Head Neck. 38 Suppl 1:E1392-403

Pedersen, P.L., 2007. Warburg, me and Hexokinase 2: Multiple discoveries of key molecular events underlying one of cancers' most common phenotypes, the 'Warburg Effect', i.e., elevated glycolysis in the presence of oxygen. J. Bioenerg. Biomembr. 39, 211–22.

Peinado, H., Portillo, F., Cano, A., 2004. Transcriptional regulation of cadherins during development and carcinogenesis. Int. J. Dev. Biol. 48, 365–75.

Peterson, W.D., Stulberg, C.S., Simpson, W.F., 1971. A permanent heteroploid human cell line with type B glucose-6-phosphate dehydrogenase. Proc. Soc. Exp. Biol. Med. 136, 1187–91.

Pfeiffer, T., Schuster, S., Bonhoeffer, S., 2001. Cooperation and competition in the evolution of ATP-producing pathways. Science (80-.). 292, 504–507.

Pierotti, M. a, Berrino, F., Gariboldi, M., Melani, C., Mogavero, a, Negri, T., Pasanisi, P., Pilotti, S., 2012. Targeting metabolism for cancer treatment and prevention: metformin, an old drug with multi-faceted effects. Oncogene 1–13.

Pinheiro, C., Albergaria, A., Paredes, J., Sousa, B., Dufloth, R., Vieira, D., Schmitt, F., Baltazar, F., 2010. Monocarboxylate transporter 1 is up-regulated in basal-like breast carcinoma. Histopathology 56, 860–7.

Pinheiro, C., Longatto-Filho, A., Scapulatempo, C., Ferreira, L., Martins, S., Pellerin, L., Rodrigues, M., Alves, V.A.F., Schmitt, F., Baltazar, F., 2008. Increased expression of monocarboxylate transporters 1, 2, and 4 in colorectal carcinomas. Virchows Arch. 452, 139–46.

Pinheiro, C., Longatto-Filho, A., Simões, K., Jacob, C.E., Bresciani, C.J.C., Zilberstein, B., Cecconello, I., Alves, V.A.F., Schmitt, F., Baltazar, F., 2009. The prognostic value of CD147/EMMPRIN is associated with monocarboxylate transporter 1 co-expression in

gastric cancer. Eur. J. Cancer 45, 2418–24.

Polański, R., Hodgkinson, C.L., Fusi, A., Nonaka, D., Smith, P.D., Blackhall, F., Dive, C., Christopher, J., 2014. Activity of the Monocarboxylate Transporter 1 inhibitor AZD3965 in Small Cell Lung Cancer 20, 926–937.

Postigo, A.A., Dean, D.C., 1999. ZEB represses transcription through interaction with the corepressor CtBP. Proc. Natl. Acad. Sci. U. S. A. 96, 6683–8.

Pretscher, D., Distel, L. V, Grabenbauer, G.G., Wittlinger, M., Buettner, M., Niedobitek, G., 2009. Distribution of immune cells in head and neck cancer: CD8+ T-cells and CD20+ B-cells in metastatic lymph nodes are associated with favourable outcome in patients with oro- and hypopharyngeal carcinoma. BMC Cancer 9, 292.

Price, G., Roche, M., Wight, R., Crowther, R., 2010. Profile of head and neck cancers in England: incidence, mortality and survival. Available from: www.ncin.org.**uk**/view?rid=69. [Accessed 03/2015]

Prime, S.S., Nixon, S. V, Crane, I.J., Stone, A., Matthews, J.B., Maitland, N.J., Remnant, L., Powell, S.K., Game, S.M., Scully, C., 1990. The behaviour of human oral squamous cell carcinoma in cell culture. J. Pathol. 160, 259–69.

Principe, D.R., Doll, J.A., Bauer, J., Jung, B., Munshi, H.G., Bartholin, L., Pasche, B., Lee, C., Grippo, P.J., 2014. TGF-β: duality of function between tumor prevention and carcinogenesis. J. Natl. Cancer Inst. 106, djt369.

Qian, X., Li, G., Asmussen, H.K., Asnaghi, L., Vass, W.C., Braverman, R., Yamada, K.M., Popescu, N.C., Papageorge, A.G., Lowy, D.R., 2007. Oncogenic inhibition by a deleted in liver cancer gene requires cooperation between tensin binding and Rho-specific GTPase-activating protein activities. Proc. Natl. Acad. Sci. U. S. A. 104, 9012–7.

Qian, X., Li, G., Vass, W., Papageorge, A., Walker, R.C., Asnaghi, L., J, S.P., Tosato, G., Hunter, K., Douglas R, L., 2009. The tensin-3 protein, including its SH2 domain, is phosphorylated by Src and contributes to tumorigenesis and metastasis 16, 246–258.

Quennet, V., Yaromina, A., Zips, D., Rosner, A., Walenta, S., Baumann, M., Mueller-Klieser, W., 2006. Tumor lactate content predicts for response to fractionated irradiation of human squamous cell carcinomas in nude mice. Radiother. Oncol. 81, 130–5.

Rabinowits, G., Haddad, R.I., 2012. Overcoming resistance to EGFR inhibitor in head and neck cancer: a review of the literature. Oral Oncol. 48, 1085–9.

Rasband, W.S., ImageJ, U. S. National Institutes of Health, Bethesda, Maryland, USA,

http://imagej.nih.gov/ij/, 1997-2016.

Reisser, C., Eichhorn, K., Herold-Mende, C., Born, a I., Bannasch, P., 1999. Expression of facilitative glucose transport proteins during development of squamous cell carcinomas of the head and neck. Int. J. Cancer 80, 194–8.

Ricono, J.M., Huang, M., Barnes, L.A., Lau, S.K., Weis, S.M., Schlaepfer, D.D., Hanks, S.K., Cheresh, D.A., 2009. Specific cross-talk between epidermal growth factor receptor and integrin alphavbeta5 promotes carcinoma cell invasion and metastasis. Cancer Res. 69, 1383–91.

Riedl, S.J., Shi, Y., 2004. Molecular mechanisms of caspase regulation during apoptosis. Nat. Rev. Mol. Cell Biol. 5, 897–907.

Rigo, P., Paulus, P., Kaschten, B.J., Hustinx, R., Bury, T., Jerusalem, G., Benoit, T., Foidart-Willems, J., 1996. Oncological applications of positron emission tomography with fluorine-18 fluorodeoxyglucose. Eur. J. Nucl. Med. 23, 1641–1674.

Ringnér, M., 2008. What is principal component analysis? Nat. Biotechnol. 26, 303–4.

Robey, I.F., Baggett, B.K., Kirkpatrick, N.D., Roe, D.J., Dosescu, J., Sloane, B.F., Hashim, A.I., Morse, D.L., Raghunand, N., Gatenby, R.A., Gillies, R.J., 2009. Bicarbonate increases tumor pH and inhibits spontaneous metastases. Cancer Res. 69, 2260–8.

Robinson, M., Sloan, P., Shaw, R., 2010. Refining the diagnosis of oropharyngeal squamous cell carcinoma using human papillomavirus testing. Oral Oncol. 46, 492–6.

Roche, T.E., Hiromasa, Y., 2007. Pyruvate dehydrogenase kinase regulatory mechanisms and inhibition in treating diabetes, heart ischemia, and cancer. Cell. Mol. Life Sci. 64, 830–49.

Rockett, J.C., Larkin, K., Darnton, S.J., Morris, A.G., Matthews, H.R., 1997. Five newly established oesophageal carcinoma cell lines: phenotypic and immunological characterization. Br. J. Cancer 75, 258–63.

Rofstad, E.K., Mathiesen, B., Kindem, K., Galappathi, K., 2006. Acidic extracellular pH promotes experimental metastasis of human melanoma cells in athymic nude mice. Cancer Res. 66, 6699–707.

Roland, N.J., Paleri, V., 2016. 5th Edition Head and Neck Cancer Multidisciplinary Management Guidelines. Availble from https://bahno.org.uk/wp-content/uploads/2014/03/UK-Head-andCancer-Guidelines-2016.pdf [Accessed 11/2016]

Rosenthal, E., McCrory, A., Talbert, M., Young, G., Murphy-Ullrich, J., Gladson, C., 2004. Elevated expression of TGF-beta1 in head and neck cancer-associated fibroblasts. Mol. Carcinog. 40, 116–21.

Rotnáglová, E., Tachezy, R., Saláková, M., Procházka, B., Košl'abová, E., Veselá, E., Ludvíková, V., Hamšíková, E., Klozar, J., 2011. HPV involvement in tonsillar cancer: prognostic significance and clinically relevant markers. Int. J. Cancer 129, 101–10.

Rottner, K., Hall, A., Small, J. V., 1999. Interplay between Rac and Rho in the control of substrate contact dynamics. Curr. Biol. 9, 640–648.

Ruiz-Lozano, P., Hixon, M.L., Wagner, M.W., Flores, A.I., Ikawa, S., Baldwin, A.S., Chien, K.R., Gualberto, A., 1999. p53 is a transcriptional activator of the muscle-specific phosphoglycerate mutase gene and contributes in vivo to the control of its cardiac expression. Cell Growth Differ. 10, 295–306.

Russell, S., Angell, T., Lechner, M., Liebertz, D., Correa, A., Sinha, U., Kokot, N., Epstein, A., 2013. Immune cell infiltration patterns and survival in head and neck squamous cell carcinoma. Head Neck Oncol. 5, 24.

Sakamoto, S., McCann, R.O., Dhir, R., Kyprianou, N., 2010. Talin1 promotes tumor invasion and metastasis via focal adhesion signaling and anoikis resistance. Cancer Res. 70, 1885–95.

Sakashita, K., Mimori, K., Tanaka, F., Kamohara, Y., Inoue, H., Sawada, T., Hirakawa, K., Mori, M., 2008. Prognostic relevance of Tensin4 expression in human gastric cancer. Ann. Surg. Oncol. 15, 2606–13.

Sánchez-Tilló, E., Lázaro, A., Torrent, R., Cuatrecasas, M., Vaquero, E.C., Castells, A., Engel, P., Postigo, A., 2010. ZEB1 represses E-cadherin and induces an EMT by recruiting the SWI/SNF chromatin-remodeling protein BRG1. Oncogene 29, 3490–3500.

Sánchez-Tilló, E., Siles, L., de Barrios, O., Cuatrecasas, M., Vaquero, E.C., Castells, A., Postigo, A., 2011. Expanding roles of ZEB factors in tumorigenesis and tumor progression. Am. J. Cancer Res. 1, 897–912.

Sandulache, V.C., Myers, J.N., 2012. Altered metabolism in head and neck squamous cell carcinoma: an opportunity for identification of novel biomarkers and drug targets. Head Neck. 282–290.

Sasaki, H., Moriyama, S., Mizuno, K., Yukiue, H., Konishi, A., Yano, M., Kaji, M., Fukai, I., Kiriyama, M., Yamakawa, Y., Fujii, Y., 2003. Cten mRNA expression was correlated with tumor progression in lung cancers. Tumour Biol. J. Int. Soc. Oncodevelopmental

Biol. Med. 40, 271–274.

Schäfer, M., Werner, S., 2008. Cancer as an overhealing wound: an old hypothesis revisited. Nat. Rev. Mol. Cell Biol. 9, 628–38.

Schmitz, F., Königstorfer, A., Südhof, T.C., 2000. RIBEYE, a Component of Synaptic Ribbons. Neuron 28, 857–872.

Semenza, G.L., 2009. Regulation of cancer cell metabolism by hypoxia-inducible factor 1. Semin. Cancer Biol. 19, 12–6.

Semenza, G.L., 2000. HIF-1 and human disease: one highly involved factor. Genes Dev. 14, 1983–91.

Serrano, M., Hannon, G.J., Beach, D., 1993. A new regulatory motif in cell-cycle control causing specific inhibition of cyclin D/CDK4. Nature 366, 704–7.

Sewalt, R.G., Gunster, M.J., van der Vlag, J., Satijn, D.P., Otte, A.P., 1999. C-Terminal binding protein is a transcriptional repressor that interacts with a specific class of vertebrate Polycomb proteins. Mol. Cell. Biol. 19, 777–87.

Sherr, C.J., 1994. G1 phase progression: cycling on cue. Cell 79, 551–5.

Sheu, J.J.-C., Hua, C.-H., Wan, L., Lin, Y.-J., Lai, M.-T., Tseng, H.-C., Jinawath, N., Tsai, M.-H., Chang, N.-W., Lin, C.-F., Lin, C.-C., Hsieh, L.-J., Wang, T.-L., Shih, I.-M., Tsai, F.-J., 2009. Functional genomic analysis identified epidermal growth factor receptor activation as the most common genetic event in oral squamous cell carcinoma. Cancer Res. 69, 2568–76.

Shi, Y., Sawada, J., Sui, G., Affar, E.B., Whetstine, J.R., Lan, F., Ogawa, H., Luke, M.P.-S., Nakatani, Y., Shi, Y., 2003. Coordinated histone modifications mediated by a CtBP co-repressor complex. Nature 422, 735–738.

Shim, H., Dolde, C., Lewis, B.C., Wu, C.S., Dang, G., Jungmann, R.A., Dalla-Favera, R., Dang, C. V, 1997. c-Myc transactivation of LDH-A: implications for tumor metabolism and growth. Proc. Natl. Acad. Sci. U. S. A. 94, 6658–63.

Silva, A.S., Yunes, J.A., Gillies, R.J., Gatenby, R.A., 2009. The potential role of systemic buffers in reducing intratumoral extracellular pH and acid-mediated invasion. Cancer Res. 69, 2677–84.

Simons, A.L., Ahmad, I.M., Mattson, D.M., Dornfeld, K.J., Spitz, D.R., 2007. 2-Deoxy-D-glucose combined with cisplatin enhances cytotoxicity via metabolic oxidative stress in human head and neck cancer cells. Cancer Res. 67, 3364–3370.

Simons, A.L., Fath, M.A., Mattson, D.M., Smith, B.J., Walsh, S.A., Graham, M.M., Hichwa,

R.D., Buatti, J.M., Dornfeld, K., Spitz, D.R., 2007. Enhanced response of human head and neck cancer xenograft tumors to cisplatin combined with 2-deoxy-D-glucose correlates with increased 18F-FDG uptake as determined by PET imaging. Int. J. Radiat. Oncol. Biol. Phys. 69, 1222–30.

Sipos, B., Hahn, D., Carceller, A., Piulats, J., Hedderich, J., Kalthoff, H., Goodman, S.L., Kosmahl, M., Klöppel, G., 2004. Immunohistochemical screening for beta6-integrin subunit expression in adenocarcinomas using a novel monoclonal antibody reveals strong up-regulation in pancreatic ductal adenocarcinomas in vivo and in vitro. Histopathology 45, 226–236.

Sjoestroem, C., Khosravi, S., Zhang, G., Martinka, M., Li, G., 2013. C-terminal tensin-like protein is a novel prognostic marker for primary melanoma patients. PLoS One 8, e80492.

Slaughter, D.P., Southwick, H.W., Smejkal, W., 1953. Field cancerization in oral stratified squamous epithelium; clinical implications of multicentric origin. Cancer 6, 963–8.

Smolková, K., Plecitá-Hlavatá, L., Bellance, N., Benard, G., Rossignol, R., Ježek, P., 2011. Waves of gene regulation suppress and then restore oxidative phosphorylation in cancer cells. Int. J. Biochem. Cell Biol. 43, 950–68.

Son, J., Lyssiotis, C.A., Ying, H., Wang, X., Hua, S., Ligorio, M., Perera, R.M., Ferrone, C.R., Mullarky, E., Shyh-Chang, N., Kang, Y., Fleming, J.B., Bardeesy, N., Asara, J.M., Haigis, M.C., DePinho, R.A., Cantley, L.C., Kimmelman, A.C., 2013. Glutamine supports pancreatic cancer growth through a KRAS-regulated metabolic pathway. Nature 496, 101–5.

Song, J., Chen, C., Raben, D., 2004. Emerging role of EGFR-targeted therapies and radiation in head and neck cancer. Oncology (Williston Park). 18, 1757–67, 1771–2, 1777.

Sonveaux, P., Végran, F., Schroeder, T., Wergin, M.C., Verrax, J., Rabbani, Z.N., De Saedeleer, C.J., Kennedy, K.M., Diepart, C., Jordan, B.F., Kelley, M.J., Gallez, B., Wahl, M.L., Feron, O., Dewhirst, M.W., 2008. Targeting lactate-fueled respiration selectively kills hypoxic tumor cells in mice. J. Clin. Invest. 118, 3930–42.

Spanò, S., Silletta, M.G., Colanzi, A., Alberti, S., Fiucci, G., Valente, C., Fusella, A., Salmona, M., Mironov, A., Luini, A., Corda, D., Spanfò, S., 1999. Molecular cloning and functional characterization of brefeldin A-ADP-ribosylated substrate. A novel protein involved in the maintenance of the Golgi structure. J. Biol. Chem. 274, 17705–10.

Subramaniam, R.M., Truong, M., Peller, P., Sakai, O., Mercier, G., 2010. Fluorodeoxyglucose-positron-emission tomography imaging of head and neck squamous cell cancer. AJNR. Am. J. Neuroradiol. 31, 598–604.

Sun, W., Zhou, S., Chang, S.S., McFate, T., Verma, A., Califano, J.A., 2009. Mitochondrial mutations contribute to HIF1alpha accumulation via increased reactive oxygen species and up-regulated pyruvate dehydrogenease kinase 2 in head and neck squamous cell carcinoma. Clin. Cancer Res. 15, 476–84.

Supek, F., Bošnjak, M., Škunca, N., Šmuc, T., 2011. REVIGO summarizes and visualizes long lists of gene ontology terms. PLoS One 6, e21800.

Syrjänen, S., 2010. The role of human papillomavirus infection in head and neck cancers. Ann. Oncol. 21 Suppl 7, vii243-5.

Szablewski, L., 2013. Expression of glucose transporters in cancers. Biochim. Biophys. Acta 1835, 164–9.

Tahari, A.K., Alluri, K.C., Quon, H., Koch, W., Wahl, R.L., Subramaniam, R.M., 2014. FDG PET/CT imaging of oropharyngeal squamous cell carcinoma: characteristics of human papillomavirus-positive and -negative tumors. Clin. Nucl. Med. 39, 225–31.

Taipale, J., Saharinen, J., Hedman, K., Keski-Oja, J., 1996. Latent transforming growth factor-beta 1 and its binding protein are components of extracellular matrix microfibrils. J Histochem Cytochem 44, 875–89.

Takada, Y., Ye, X., Simon, S., 2007. The integrins. Genome Biol. 8, 215.

Tan, M., Myers, J., Agrawal, N., 2013. Oral cavity and oropharyngeal squamous cell carcinoma genomics. Otolaryngol Clin North Am 46, 545–66.

Tanaka, J., Ogura, T., Sato, H., Hatano, M., 1987. Establishment and biological characterization of an in vitro human cytomegalovirus latency model. Virology 161, 62–72.

Thie, J.A., 2004. Understanding the standardized uptake value, its methods, and implications for usage. J. Nucl. Med. 45, 1431–4.

Thiery, J.P., 2002. Epithelial-mesenchymal transitions in tumour progression. Nat. Rev. Cancer 2, 442–454.

Thiery, J.P., Acloque, H., Huang, R.Y.J., Nieto, M.A., 2009. Epithelial-mesenchymal transitions in development and disease. Cell 139, 871–90.

Thomas, G., Hart, I., Speight, P., Marshall, J., 2002. Binding of TGF-β1 latency-associated peptide (LAP) to αvβ6 integrin modulates behaviour of squamous carcinoma cells.

Br. J. Cancer 87, 859–867.

Thomas, G., Jacobs, K.B., Yeager, M., Kraft, P., Wacholder, S., Orr, N., Yu, K., Chatterjee, N., Welch, R., Hutchinson, A., Crenshaw, A., Cancel-Tassin, G., Staats, B.J., Wang, Z., Gonzalez-Bosquet, J., Fang, J., Deng, X., Berndt, S.I., Calle, E.E., Feigelson, H.S., Thun, M.J., Rodriguez, C., Albanes, D., Virtamo, J., Weinstein, S., Schumacher, F.R., Giovannucci, E., Willett, W.C., Cussenot, O., Valeri, A., Andriole, G.L., Crawford, E.D., Tucker, M., Gerhard, D.S., Fraumeni Jr., J.F., Hoover, R., Hayes, R.B., Hunter, D.J., Chanock, S.J., 2008. Multiple loci identified in a genome-wide association study of prostate cancer. Nat Genet 40, 310–315.

Thomas, G.J., Lewis, M.P., Hart, I.R., Marshall, J.F., Speight, P.M., 2001a. AlphaVbeta6 integrin promotes invasion of squamous carcinoma cells through up-regulation of matrix metalloproteinase-9. Int. J. Cancer 92, 641–50.

Thomas, G.J., Lewis, M.P., Whawell, S.A., Russell, A., Sheppard, D., Hart, I.R., Speight, P.M., Marshall, J.F., 2001b. Expression of the alphavbeta6 integrin promotes migration and invasion in squamous carcinoma cells. J. Invest. Dermatol. 117, 67–73.

Thorpe, H., Akhlaq, M., Jackson, D., Ghamdi, S. Al, Storr, S., Martin, S., Ilyas, M., 2015. Multiple pathways regulate Cten in colorectal cancer without a Tensin switch. Int. J. Exp. Pathol. 96, 362–369.

Thu, K.L., Radulovich, N., Becker-Santos, D.D., Pikor, L.A., Pusic, A., Lockwood, W.W., Lam, W.L., Tsao, M.-S., 2014. SOX15 is a candidate tumor suppressor in pancreatic cancer with a potential role in Wnt/β-catenin signaling. Oncogene 33, 279–88.

Tian, M., Zhang, H., Nakasone, Y., Mogi, K., Endo, K., 2004. Expression of Glut-1 and Glut-3 in untreated oral squamous cell carcinoma compared with FDG accumulation in a PET study. Eur. J. Nucl. Med. Mol. Imaging 31, 5–12.

Tobin, S.W., Brown, M.K., Douville, K., Payne, D.C., Eastman, a, Arrick, B. a, 2001. Inhibition of transforming growth factor beta signaling in MCF-7 cells results in resistance to tumor necrosis factor alpha: a role for Bcl-2. Cell Growth Differ. 12, 109–17.

Tomasek, J.J., Gabbiani, G., Hinz, B., Chaponnier, C., Brown, R.A., 2002. Myofibroblasts and mechano-regulation of connective tissue remodelling. Nat. Rev. Mol. Cell Biol. 3, 349–63.

Trapnell, C., Pachter, L., Salzberg, S.L., 2009. TopHat: discovering splice junctions with RNA-Seq. Bioinformatics 25, 1105–11.

Tripathi, M.K., Misra, S., Khedkar, S. V, Hamilton, N., Irvin-Wilson, C., Sharan, C., Sealy, L., Chaudhuri, G., 2005. Regulation of BRCA2 gene expression by the SLUG repressor protein in human breast cells. J. Biol. Chem. 280, 17163–71.

Urcan, E., Haertel, U., Styllou, M., Hickel, R., Scherthan, H., Reichl, F.X., 2010. Real-time xCELLigence impedance analysis of the cytotoxicity of dental composite components on human gingival fibroblasts. Dent. Mater. 26, 51–8.

Vainshtein, J.M., Spector, M.E., McHugh, J.B., Wong, K.K., Walline, H.M., Byrd, S.A., Komarck, C.M., Ibrahim, M., Stenmark, M.H., Prince, M.E., Bradford, C.R., Wolf, G.T., McLean, S., Worden, F.P., Chepeha, D.B., Carey, T., Eisbruch, A., 2014. Refining risk stratification for locoregional failure after chemoradiotherapy in human papillomavirus-associated oropharyngeal cancer. Oral Oncol. 50, 513–9.

Valcourt, U., Kowanetz, M., Niimi, H., Heldin, C.-H., Moustakas, A., 2005. TGF-beta and the Smad signaling pathway support transcriptomic reprogramming during epithelial-mesenchymal cell transition. Mol. Biol. Cell 16, 1987–2002.

van Waarde, M.A., van Assen, A.J., Kampinga, H.H., Konings, A.W., Vujaskovic, Z., 1997. Quantification of transforming growth factor-beta in biological material using cells transfected with a plasminogen activator inhibitor-1 promoter-luciferase construct. Anal. Biochem. 247, 45–51.

Van Waes, C., Dong Mi Surh, Chen, Z., Kirby, M., Rhim, J.S., Brager, R., Sessions, R.B., Poore, J., Wolf, G.T., Carey, T.E., 1995. Increase in suprabasilar integrin adhesion molecule expression in human epidermal neoplasms accompanies increased proliferation occurring with immortalization and tumor progression. Cancer Res. 55, 5434–5444.

Vaupel, P., 2010. Metabolic microenvironment of tumor cells: a key factor in malignant progression. Exp. Oncol. 32, 125–127.

Verheij, M., 2008. Clinical biomarkers and imaging for radiotherapy-induced cell death. Cancer Metastasis Rev. 27, 471–480.

Vincent, A.S., Phan, T.T., Mukhopadhyay, A., Lim, H.Y., Halliwell, B., Wong, K.P., 2008. Human skin keloid fibroblasts display bioenergetics of cancer cells. J. Invest. Dermatol. 128, 702–9.

Wakefield, L.M., Roberts, A.B., 2002. TGF-beta signaling: positive and negative effects on tumorigenesis. Curr. Opin. Genet. Dev. 12, 22–9.

Walenta, S., Mueller-Klieser, W.F., 2004. Lactate: mirror and motor of tumor malignancy. Semin. Radiat. Oncol. 14, 267–74.

Walenta, S., Schroeder, T., Mueller-Klieser, W., 2002. Metabolic mapping with bioluminescence: basic and clinical relevance. Biomol. Eng. 18, 249–62.

Wan, X., Wang, W., Liu, J., Tong, T., 2014. Estimating the sample mean and standard deviation from the sample size, median, range and/or interquartile range. BMC Med. Res. Methodol. 14, 135.

Wang, D., Müller, S., Amin, A.R.M.R., Huang, D., Su, L., Hu, Z., Rahman, M.A., Nannapaneni, S., Koenig, L., Chen, Z., Tighiouart, M., Shin, D.M., Chen, Z.G., 2012. The pivotal role of integrin β1 in metastasis of head and neck squamous cell carcinoma. Clin. Cancer Res. 18, 4589–99.

Warburg, O., Wind, F., Negelein, E., 1926. Über den Stoffwechsel von Tumoren im Körper. Klin. Wochenschr. 5, 829–832.

Ward, M.J., Thirdborough, S.M., Mellows, T., Riley, C., Harris, S., Suchak, K., Webb, A., Hampton, C., Patel, N.N., Randall, C.J., Cox, H.J., Jogai, S., Primrose, J., Piper, K., Ottensmeier, C.H., King, E. V, Thomas, G.J., 2014. Tumour-infiltrating lymphocytes predict for outcome in HPV-positive oropharyngeal cancer. Br. J. Cancer 110, 489–500.

Ward, P.S., Thompson, C.B., 2012. Metabolic reprogramming: a cancer hallmark even warburg did not anticipate. Cancer Cell 21, 297–308.

Warde-Farley, D., Donaldson, S.L., Comes, O., Zuberi, K., Badrawi, R., Chao, P., Franz, M., Grouios, C., Kazi, F., Lopes, C.T., Maitland, A., Mostafavi, S., Montojo, J., Shao, Q., Wright, G., Bader, G.D., Morris, Q., 2010. The GeneMANIA prediction server: biological network integration for gene prioritization and predicting gene function. Nucleic Acids Res. 38, W214-20.

Wavreille, A.-S., Pei, D., 2007. A chemical approach to the identification of tensin-binding proteins. ACS Chem. Biol. 2, 109–118.

Weis, S.M., Cheresh, D. a, 2011. αV integrins in angiogenesis and cancer. Cold Spring Harb. Perspect. Med. 1, a006478.

Wessels, D., Vawter-Hugart, H., Murray, J., Soll, D.R., 1994. Three-dimensional dynamics of pseudopod formation and the regulation of turning during the motility cycle of Dictyostelium. Cell Motil. Cytoskeleton 27, 1–12.

White, R. a, Malkoski, S.P., Wang, X.-J., 2010. TGFβ signaling in head and neck squamous

cell carcinoma. Oncogene 29, 5437–46.

Williams, B.J., Jones, E., Zhu, X.L., Steele, M.R., Stephenson, R.A., Rohr, L.R., Brothman, A.R., 1996. Evidence for a tumor suppressor gene distal to BRCA1 in prostate cancer. J. Urol. 155, 720–725.

Wise, D.R., DeBerardinis, R.J., Mancuso, A., Sayed, N., Zhang, X.-Y., Pfeiffer, H.K., Nissim, I., Daikhin, E., Yudkoff, M., McMahon, S.B., Thompson, C.B., 2008. Myc regulates a transcriptional program that stimulates mitochondrial glutaminolysis and leads to glutamine addiction. Proc. Natl. Acad. Sci. U. S. A. 105, 18782–7.

Wolf, A., Agnihotri, S., Micallef, J., Mukherjee, J., Sabha, N., Cairns, R., Hawkins, C., Guha, A., 2011. Hexokinase 2 is a key mediator of aerobic glycolysis and promotes tumor growth in human glioblastoma multiforme. J. Exp. Med. 208, 313–26.

Wong, C.-M., Lee, J.M.-F., Ching, Y.-P., Jin, D.-Y., Ng, I.O., 2003. Genetic and epigenetic alterations of DLC-1 gene in hepatocellular carcinoma. Cancer Res. 63, 7646–51.

Wong, R.S.Y., 2011. Apoptosis in cancer: from pathogenesis to treatment. J. Exp. Clin. Cancer Res. 30, 87.

Wurm, C.A., Neumann, D., Lauterbach, M.A., Harke, B., Egner, A., Hell, S.W., Jakobs, S., 2011. Nanoscale distribution of mitochondrial import receptor Tom20 is adjusted to cellular conditions and exhibits an inner-cellular gradient. Proc. Natl. Acad. Sci. U. S. A. 108, 13546–51.

Wyllie, F.S., Lemoine, N.R., Barton, C.M., Dawson, T., Bond, J., Wynford-Thomas, D., 1993. Direct growth stimulation of normal human epithelial cells by mutant p53. Mol. Carcinog. 7, 83–8.

Xie, W., Bharathy, S., Kim, D., Haffty, B., Rimm, D., Reiss, M., 2003. Frequent alterations of Smad signaling in human head and neck squamous cell carcinomas: a tissue microarray analysis. Oncol. Res. 14, 61–73.

Xouri, G., Christian, S., 2010. Origin and function of tumor stroma fibroblasts. Semin. Cell Dev. Biol. 21, 40–6.

Xue, H., Field, C.J., 2011. New role of glutamate as an immunoregulator via glutamate receptors and transporters. Front. Biosci. (Schol. Ed). 3, 1007–20.

Yam, J.W.P., Ko, F.C.F., Chan, C.-Y., Yau, T.-O., Tung, E.K.K., Leung, T.H.-Y., Jin, D.-Y., Ng, I.O.-L., 2006. Tensin2 variant 3 is associated with aggressive tumor behavior in human hepatocellular carcinoma. Hepatology 44, 881–90.

Yamaguchi, H., Condeelis, J., 2007. Regulation of the actin cytoskeleton in cancer cell

migration and invasion. Biochim. Biophys. Acta 1773, 642–52.

Yanagihara, K., Tsumuraya, M., 1992. Transforming growth factor beta 1 induces apoptotic cell death in cultured human gastric carcinoma cells. Cancer Res. 52, 4042–5.

Yeung, S.J., Pan, J., Lee, M.-H., 2008. Roles of p53, MYC and HIF-1 in regulating glycolysis - the seventh hallmark of cancer. Cell. Mol. Life Sci. 65, 3981–3999.

Ying, W., 2008. NAD+/NADH and NADP+/NADPH in cellular functions and cell death: regulation and biological consequences. Antioxid. Redox Signal. 10, 179–206.

Yu, C., Liu, Y., Huang, D., Dai, Y., Cai, G., Sun, J., Xu, T., Tian, Y., Zhang, X., 2011. TGF-β1 mediates epithelial to mesenchymal transition via the TGF-β/Smad pathway in squamous cell carcinoma of the head and neck. Oncol. Rep. 25, 1581–7.

Yuan, B.-Z., Durkin, M.E., Popescu, N.C., 2003. Promoter hypermethylation of DLC-1, a candidate tumor suppressor gene, in several common human cancers. Cancer Genet. Cytogenet. 140, 113–117.

Zaidel-Bar, R., Ballestrem, C., Kam, Z., Geiger, B., 2003. Early molecular events in the assembly of matrix adhesions at the leading edge of migrating cells. J. Cell Sci. 116, 4605–4613.

Zaidel-Bar, R., Cohen, M., Addadi, L., Geiger, B., 2004. Hierarchical assembly of cell-matrix adhesion complexes. Biochem. Soc. Trans. 32, 416–420.

Zamir, E., Katz, B.Z., Aota, S., Yamada, K.M., Geiger, B., Kam, Z., 1999. Molecular diversity of cell-matrix adhesions. J. Cell Sci. 112 (1), 1655–69.

Zavadil, J., Böttinger, E.P., 2005. TGF-beta and epithelial-to-mesenchymal transitions. Oncogene 24, 5764–74.

Zhang, C., Liu, J., Liang, Y., Wu, R., Zhao, Y., Hong, X., Lin, M., Yu, H., Liu, L., Levine, A.J., Hu, W., Feng, Z., 2013. Tumour-associated mutant p53 drives the Warburg effect. Nat. Commun. 4, 2935.

Zhang, I., Branstetter, B.F., Beswick, D.M., Maxwell, J.H., Gooding, W.E., Ferris, R.L., 2011. The benefit of early PET/CT surveillance in HPV-associated head and neck squamous cell carcinoma. Arch. Otolaryngol. Head. Neck Surg. 137, 1106–11.

Zhang, Q., Piston, D.W., Goodman, R.H., 2002. Regulation of corepressor function by nuclear NADH. Science 295, 1895–7.

Zhang, Q., Wang, S.-Y., Nottke, A.C., Rocheleau, J. V, Piston, D.W., Goodman, R.H., 2006. Redox sensor CtBP mediates hypoxia-induced tumor cell migration. Proc. Natl. Acad.

Sci. U. S. A. 103, 9029–9033.

Zhang, S., Hulver, M.W., McMillan, R.P., Cline, M.A., Gilbert, E.R., 2014. The pivotal role of pyruvate dehydrogenase kinases in metabolic flexibility. Nutr. Metab. (Lond). 11, 10.

Zhao, L.-J., Kuppuswamy, M., Vijayalingam, S., Chinnadurai, G., 2009. Interaction of ZEB and histone deacetylase with the PLDLS-binding cleft region of monomeric C-terminal binding protein 2. BMC Mol. Biol. 10, 89.

Zheng, J., 2012. Energy metabolism of cancer: Glycolysis versus oxidative phosphorylation (Review). Oncol. Lett. 4, 1151–1157.

Zwerschke, W., Mazurek, S., Massimi, P., Banks, L., Eigenbrodt, E., Jansen-Dürr, P., 1999. Modulation of type M2 pyruvate kinase activity by the human papillomavirus type 16 E7 oncoprotein. Proc. Natl. Acad. Sci. U. S. A. 96, 1291–6.